Chlorine, Fluorine and Water in the Stratosphere: Chemistry, Transport and Trends based on ACE-FTS measurements

by

Raymond Nassar

A thesis
presented to the University of Waterloo
in fulfillment of the
thesis requirement for the degree of
Doctor of Philosophy
in
Chemistry

Waterloo, Ontario, Canada, 2006

AUTHOR'S DECLARATION

I hereby declare that I am the sole author of this thesis. This is a true copy of the thesis, including any required final revisions, as accepted by my examiners.

I understand that my thesis may be made electronically available to the public.

Abstract

The Atmospheric Chemistry Experiment (ACE) is a satellite mission for remote sensing of the Earth's atmosphere using the solar occultation technique. The primary instrument on this satellite is the Atmospheric Chemistry Experiment Fourier Transform Spectrometer (ACE-FTS). ACE-FTS retrievals are described with a focus on the creation of *a priori* temperature and pressure profiles. ACE-FTS measurements are then used to investigate the chemistry, transport and trends of chlorine, fluorine and water in the stratosphere, leading to an improved understanding of processes affecting both stratospheric ozone depletion and global climate change.

Total chlorine (Cl_{TOT}) in the stratosphere is determined using ACE-FTS measurements of eleven chlorine-containing species, supplemented by both other measurements and models, to determine Cl_{TOT} as a function of altitude in five latitude zones. All resulting Cl_{TOT} profiles are nearly linear, with a slight slope. Mean Cl_{TOT} for 2004 is determined to be 3.65 ppbv for both the northern and southern midlatitudes (with a precision and estimated accuracy of ±0.09 and ±0.13 ppbv, respectively). A slightly lower value of mean Cl_{TOT} is determined for the tropics and slightly higher values at high latitudes. Total fluorine (F_{TOT}) in the stratosphere is also determined primarily from ACE-FTS measurements using a similar approach, resulting in stratospheric F_{TOT} profiles which are nearly linear with mean values ranging from 2.50 to 2.59 ppbv for each latitude zone (with a precision of 0.04-0.07 ppbv and an estimated accuracy of 0.15 ppbv). The observed slopes and pattern of latitudinal variation are evidence of the beginning of a decline in global stratospheric chlorine and of the continuing increase in global stratospheric fluorine levels.

The abundance of water in the stratosphere is investigated for the northern hemisphere midlatitudes in 2004 using ACE-FTS measurements. Potential water is determined as $[H_2O]+2[CH_4]$ and from $[H_2O]$ versus $[CH_4]$ correlations, resulting in a value of 7.14±0.05 ppmv, which is used to determine a value of 3.65±0.15 ppmv for the mean abundance of water entering the stratosphere. Both values are compared directly with historical data from the Atmospheric Trace Molecule Spectroscopy (ATMOS) instrument (1985-1994) and show a negligible change, implying that the increases observed by ATMOS and other long-term measurements from that time period have not continued.

The removal of stratospheric water in the Arctic vortex is investigated using ACE-FTS measurements. Using derived quantities from a meteorological data assimilation, northern hemisphere occultations from early 2004 are classified as vortex, vortex edge or extravortex. $[CH_4]$ versus $[N_2O]$ correlations are used to further classify the extravortex occultations as tropical, subtropical or midlatitude. Comparisons between profiles of $[N_2O]$, $[CH_4]$ and $[H_2O]$ inside and outside the Arctic vortex, give estimates of upper stratospheric and lower mesospheric descent rates, indicating that descent in the winter 2004 Arctic vortex was rapid, with evidence of descent at higher altitudes than in past years.

The dehydration of air in the tropical tropopause layer and mechanisms for the entry of water vapor into the stratosphere are investigated by an analysis of ACE-FTS profiles of temperature, water vapor and $[HDO]/[H_2O]$. Month-to-month comparisons for 2004 and 2005 reveal a clear pattern of seasonal variation and a correlation between minimum temperature and maximum HDO depletion. Further interpretation indicates that the gradual dehydration mechanism accompanied by lofting of ice particles in the tropical troposphere is the most likely explanation for the observed seasonal variation and the shape of the $[HDO]/[H_2O]$ profiles.

Acknowledgments

Isaac Newton once said, "If I have seen further, it is by standing on the shoulders of giants." This quote truly applies to my experience working with the ACE team, who have been so important in making the research described in this thesis possible. Most of all, I think it applies to the relationship that I have had with my supervisor and ACE Mission Scientist, Professor Peter Bernath. I feel very fortunate to have had the opportunity to work with such an accomplished scientist, whose patience, logical approach to problems and knowledge in so many areas of science, make him a model supervisor and an ideal person to lead a scientific satellite mission.

Other members of the ACE team that I would like to thank individually include: Chris Boone, who has done an excellent job on ACE-FTS retrievals and handling the many data processing requests that I have made; Sean McLeod, for helping me to find my way in the confusing world of UNIX, FORTRAN, C and other aspects of computing that I only had a vague understanding of prior to my work on the ACE mission; and Kaley Walker, for her many years of dedication to managing so many of the finer details of the mission. Additionally, I would like to acknowledge the contributions made by Mike Butler, Randall Skelton, Gaëlle Dufour, Keeyoon Sung, Curtis Rinsland, Marty McHugh, Yves Rochon, Gloria Manney, Jim Drummond, Caroline Nowlan, Jack McConnell, Cathy Clerbaux, Piet Coheur and so many others on the ACE science team, whom I have worked with over the years.

Of course, I would also like to thank the Canadian Space Agency (CSA) for providing the primary funding for the ACE mission and I am personally very grateful to both the CSA and the Natural Sciences and Engineering Research Council of Canada (NSERC) for providing scholarship support during the course of my Ph.D.

I would like to thank the members of my advisory committee and thesis committee: Professors Robert LeRoy, Jim Sloan, Nick Westwood, Richard Kelly and Andrew Gettelman, for their comments, suggestions and constructive criticism throughout this process.

Many thanks also go to past and current members of the basement lab including Iouli Gordon, Mike Dick, Jin-Guo Wang, Dejian Fu, Shanshan Yu, Phil Sheridan, Ali Shayesteh, Keith Tereszchuk and others, for making my time at work more enjoyable, although very often less productive.

I would like to thank my family for their support throughout my entire academic career, as well as giving me the space that I needed when I got very busy and saw them less and less. Finally, I thank Kavitha Passaperuma for all of her support, understanding and for just being there. Over the last few years of my Ph.D., she has been my sanctuary from work and has been so important in giving my life a feeling of balance.

Table of Contents

List of Tables

Chapter 2

Chapter 3

Chapter 4

Chapter 5

Chapter 7

List of Figures

Chapter 1

Chapter 2

Chapter 3

Chapter 4

Chapter 5

Chapter 6

Chapter 7

Chapter 1

An Introduction to the ACE Mission and the ACE-FTS

1.1 ACE Mission Overview

The Atmospheric Chemistry Experiment (ACE) also known as SCISAT-1, is a scientific satellite primarily funded and managed by the Canadian Space Agency (CSA). The scientific goals of the ACE mission include: (1) investigating the chemical and dynamical processes that relate to the distribution of ozone in the stratosphere and upper troposphere, (2) exploring the relationship between atmospheric chemistry and climate change, (3) studying the effects of biomass burning on the free troposphere, and (4) measuring aerosols and clouds to reduce the uncertainties in their effects on the global energy balance [*Bernath et al.*, 2005]. The primary instrument onboard the ACE satellite is the ACE-FTS, a high-resolution Fourier transform spectrometer (FTS) which operates in the 2.2-13.3 μm (750-4400 cm^{-1}) range, equipped with a two-channel solar imager operating at 1.02 and 0.525 μm. ACE also contains a dual-grating spectrometer known as MAESTRO (Measurement of Aerosol Extinction in the Stratosphere and Troposphere Retrieved by Occultation) operating in the 285-1030 nm range, and a star-tracker which tracks background stars to aid in the determination of spacecraft orientation.

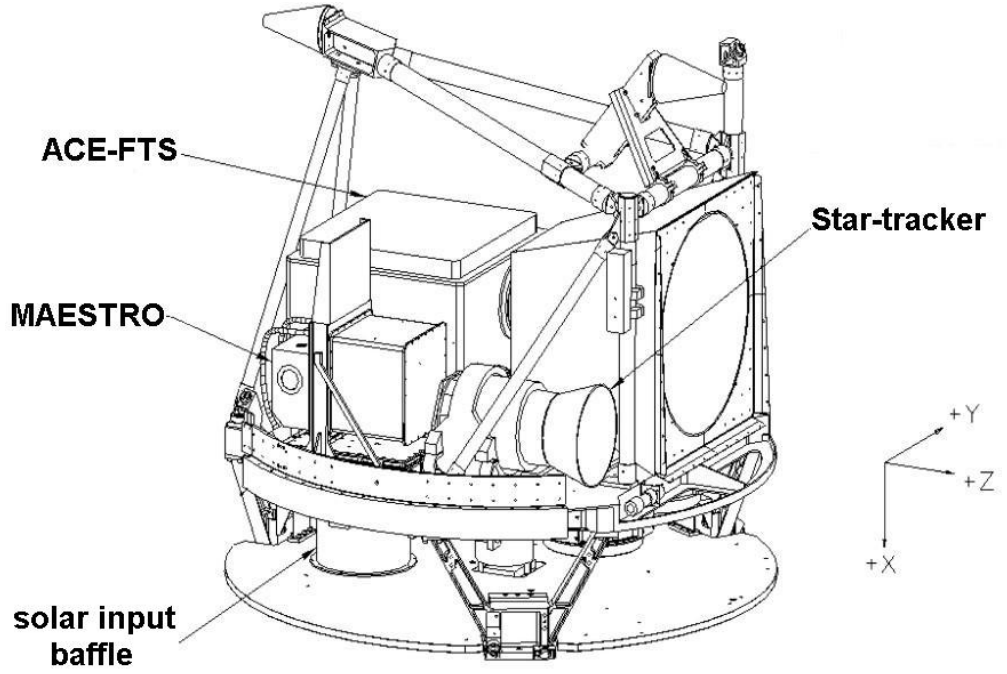

Figure 1-1: The SCISAT-1 or ACE satellite with some important components identified.

The ACE satellite, shown in Figure 1-1, has a mass of approximately 150 kg and was launched by the National Aeronautics and Space Administration (NASA) on August 12, 2003 using a Pegasus-XL rocket. This small, three-stage rocket was dropped from an aircraft at an altitude of ~12 km (39000 feet) off the coast of southern California. The satellite was placed into a circular low-earth orbit with an altitude of ~650 km (orbital radius = 7021.3 km) and an inclination of 74° with respect to the equator, from which it circles the Earth approximately 15 times per day. The ACE-FTS and MAESTRO primarily measure the absorption of solar radiation through the Earth's atmosphere during sunrise or sunset, a technique known as solar occultation (described later). The chosen orbit enables ACE to observe up to 30 occultation events (sunrises or sunsets) in a 24 hour period. This orbit was optimized to achieve a combination of numerous measurements and global coverage with a focus on the middle and high latitudes. The latitude of occultation measurements possible from this highly-inclined orbit essentially repeats itself every year as shown in Figure 1-2.

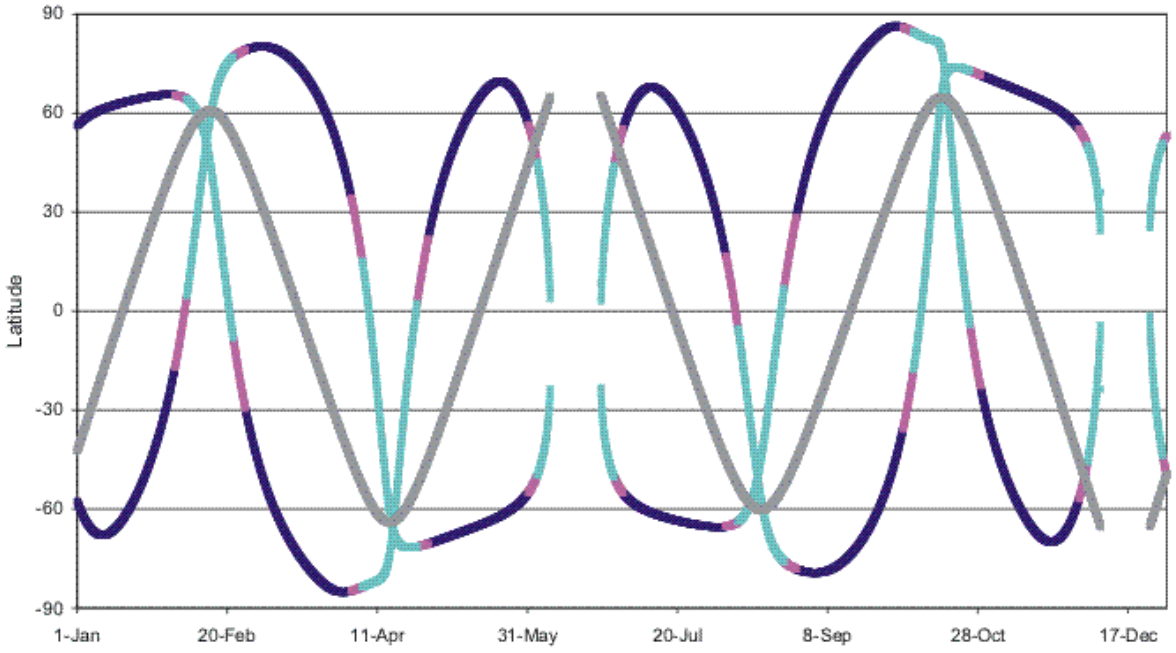

Figure 1-2: The latitude variation in the ACE orbit over one full year. Nearly all occultations shown in dark blue, most occultations shown in violet and less than half of the occultations shown in cyan are measured due to the satellite beta angle (explained later) shown in gray.

The ACE satellite is powered by solar energy and is always oriented with its solar panel in the direction of the Sun, even when the Earth is blocking the Sun from the view of the spacecraft. As ACE orbits the Earth, it rolls at a controlled rate such that the ACE-FTS passive-cooler continuously points to deep space to radiate excess energy and cool the FTS detectors. During an occultation, the ACE instruments observe the Sun through the solar input baffle, which is an

opening in the spacecraft baseplate and solar panel (facing the *x*-direction in Figure 1-1). On each occultation, the ACE-FTS records a series of atmospheric absorption spectra using the Sun as the light source. The portion of the atmosphere sampled in each measurement is referred to as a slant column, which contains contributions from different altitude regions or layers of the atmosphere, as shown in Figure 1-3. The minimum distance between the slant column and the surface of the Earth is the tangent height, which typically decreases by 3-4 km per measurement during a sunset occultation, and increases by the same distance per measurement during a sunrise occultation.

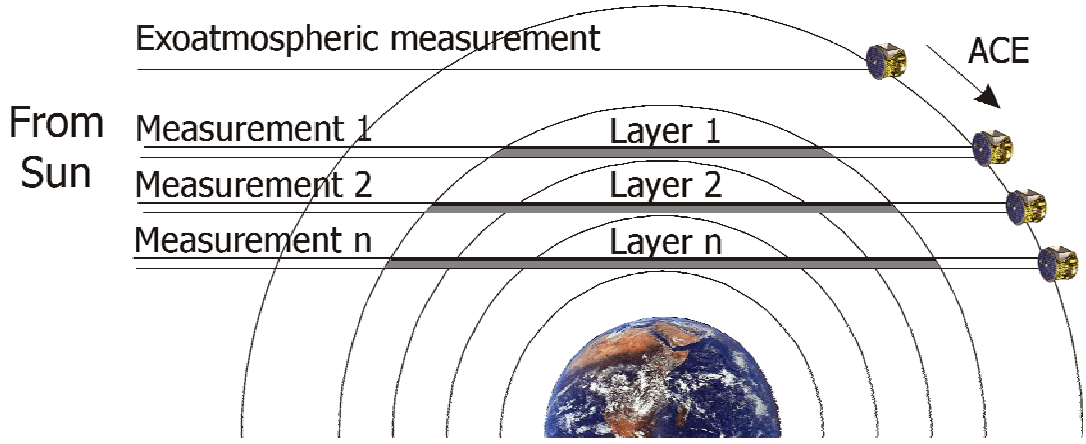

Figure 1-3: A two-dimensional schematic representation depicting the ACE satellite motion while recording spectra during a sunset occultation (distances are not to scale). The shaded areas represent slant columns at a series of tangent heights. The length of a slant column increases with decreasing altitude (spanning approximately 500 km for stratospheric tangent heights) and determines the horizontal resolution of a measurement.

Since the spectrum of each slant column (except for the uppermost) contains contributions from multiple atmospheric layers, as shown in Figure 1-3, obtaining information about each individual layer to create a profile, requires accounting for the contributions to the spectra from other layers. The process for doing this is called inversion and one approach to inverting the slant column measurements involves retrieving values for some quantity (i.e. ozone abundance) from the uppermost layer, subtracting its contribution from the second layer, then subtracting the contribution due to the first and second layer from the next one, and continuing the process for all layers. ACE-FTS retrievals use a better approach known as a *global fit,* in which rather than sequentially retrieving a final value for each layer, as just described, the desired quantity to be retrieved for each layer is represented by a variable and a solution for all layers is determined simultaneously. This is more computer-intensive, but gives smoother profiles and better results overall since it reduces the propagation of errors throughout the retrieval.

An infrared spectrum of solar radiation contains both emission and absorption features due to numerous atomic species (such as sodium, aluminum, magnesium and silicon), as well as some simple molecular species including OH and CO. To remove these features from the atmospheric

spectra, the spectra can be ratioed to a solar spectrum with no atmospheric attenuation, which is referred to as an exoatmospheric spectrum. Prior to ratioing, artifacts that may result from instrument self-emission are removed from both exoatmospheric and atmospheric spectra by subtracting a background emission spectrum of deep space. The ratioed atmospheric spectra are subsequently inverted to profiles of temperature, pressure and molecular abundances. The retrieval of temperature and pressure is carried out first, by fitting measured CO_2 spectral lines to calculated spectral lines from a forward model, in multiple narrow spectral regions (microwindows) through an iterative process beginning with an *a priori* estimate. After retrieving temperature and pressure, the abundances of numerous molecular species are retrieved in a similar manner, with the temperature and pressure fixed. The list of molecular species measured by the ACE-FTS continues to increase, and currently consists of more than 30 species including 14 baseline species (O_3, H_2O, CH_4, N_2O, NO_2, NO, HNO_3, N_2O_5, $ClONO_2$, HCl, CCl_2F_2, CCl_3F, HF, CO), a few other routine species (COF_2, $CHClF_2$, CF_4, CH_3Cl, SF_6 and others) as well as some species designated as *research species*, which are retrieved but are not yet available as an official product (CCl_4, H_2O_2, HO_2NO_2, CCl_2FCClF_2, CH_3CClF_2, ClO, C_2H_2 and many others). Additional details of the ACE-FTS retrieval are given in Chapter 2, including a thorough explanation of ACE *a priori* profiles, but a more complete description of the ACE-FTS retrieval process is given in *Boone et al.* [2005].

ACE occultations are given a designation according to their type (sunrise or sunset) and orbit number since launch, for example, the sunrise in orbit number 3456 is ace.sr3456, and the sunset is ace.ss3456. The angle between the plane of the satellite's orbit track and a vector connecting the center of the Earth to the center of the Sun is known as the beta angle (β). In Figure 1-3, β=0, but in reality, β for ACE measurements varies throughout the year between -65° and +65°. When β=0, the Sun's path during sunrise or sunset is perpendicular to the horizon, from the satellite's point of view, but when β is non-zero, the Sun's path would make an angle with the horizon. High and middle latitude measurements occur over the whole range of β, but measurements over the tropics tend to occur at relatively high β. The larger the magnitude of β, the more time required to complete the measurement of an entire occultation, resulting in a smaller vertical spacing between successive measurements. Over the finite amount of time required to complete the measurement of an occultation, the satellite continues to move along its orbit, which causes a slight change in the latitude and longitude of measurements over the course of an occultation. Therefore, although we refer to a retrieved profile resulting from an occultation as a vertical profile, it is only approximately vertical. Additionally, as sunlight passes through different air densities at different altitudes in Earth's atmosphere, it refracts in the direction of higher density. The refraction also causes an effective deviation from vertical or a change in latitude and longitude for each tangent point measurement, with significant effects for tangent heights below ~40 km. Every ACE occultation has been assigned a reference latitude, longitude and time, based on the calculated unrefracted values at a tangent height of 30 km. A refraction model using the retrieved temperature and pressure determines the latitude, longitude and time of each individual measurement point in an occultation (down to ~4.5 km) when accuracy beyond the reference latitude, longitude and time are required. The larger the β of an occultation, the more deviation

from vertical and the more horizontal smearing of the profile will occur. An occultation with β=0º (ace.sr8560) only spans a horizontal distance of ~56 km over the 4-150 km altitude range, but an occultation with β=60° (ace.ss8930), will span a horizontal distance of ~1400 km over the same altitude range, with most of this change occurring in the north-south direction.

1.2 Fourier Transform Spectrometers

The primary difference between Fourier transform spectrometers and more conventional dispersive spectroscopic instruments is that Fourier transform spectroscopy utilizes a Michelson interferometer rather a prism or grating that disperses light. In a Michelson interferometer, light strikes a beamsplitter which reflects a portion of the light toward one mirror and transmits the remaining light toward another mirror. The light from both mirrors is reflected back to the beamsplitter where it recombines and continues on toward a detector. The superposition of all wavelengths of light (each with an associated intensity) over a desired region plotted versus the optical path difference obtained by precisely varying the position of one or both mirrors results in an interferogram. A mathematical operation known as a Fourier transform (FT) decomposes the interferogram signal back into its component wavelengths and intensities to produce a spectrum. The resolution of this spectrum is primarily limited by the maximum optical path difference (OPD) that can be obtained by varying the relative positions of the mirrors. In other words, an interferometer that can obtain a higher optical path difference during a scan will produce spectra with better resolution, if all other factors are equal.

Acquiring interferograms as raw data, which are Fourier-transformed into spectra, instead of directly recording spectra with a dispersive spectrometer, will typically result in a better signal-to-noise ratio (SNR). In dispersive spectroscopy, a narrow slit is used to restrict the wavelength range of the radiation incident upon the detector, but this greatly reduces the intensity of the radiation as well. Fourier transform spectroscopy allows for the simultaneous observation of all desired wavelengths, so the detector is exposed to a higher intensity of light during a scan. This important advantage of Fourier transform spectroscopy is known as the multiplex advantage or *Fellgett* advantage. It applies if the dominant source of noise is constant regardless of the level of signal incident on the detector, which is typically the case if noise due to the detector or background radiation dominates. In a Fourier transform spectrometer, the quantity of incident radiation which will reach the detector is usually limited by a circular aperture, instead of a slit. Since this aperture transmits a much greater cross-sectional area of light than a slit, the throughput in an FTS greater, so this advantage is referred to as the throughput advantage or *Jacquinot* advantage [*Griffiths and de Haseth*, 1986; *Smith*, 1996]. As a result of these two advantages, a good SNR can often be achieved in the infrared with a short observation time, which makes Fourier transform spectroscopy an excellent technique for remote sensing of Earth's atmosphere.

In addition to the ACE-FTS, other FTS instruments have successfully been used for space-borne atmospheric measurements, including the ATMOS (Atmospheric Trace Molecule Spectroscopy) instrument [*Gunson et al.*, 1996], IMG (the Interferometric Monitor for Greenhouse

gases) [*Kobayashi et al.*, 1999], MIPAS (the Michelson Interferometer for Passive Atmospheric Sounding) [*Endemann et al.*, 1994] and TES (the Tropospheric Emission Spectrometer) [*Beer et al.*, 2001]. Other satellite FTS instruments for atmospheric studies such as IASI (the Infrared Atmospheric Sounding Interferometer) [S*imeoni et al.*, 1997] and GOSAT (the Greenhouse Gas Observing Satellite) [*Hamazaki et al.*, 2004] will be launched in the near future.

1.2.1 The ACE-FTS Design and Specifications

The ACE-FTS was custom-designed and built for the ACE mission by ABB-Bomem of Quebec City. The instrument utilizes a modified Michelson interferometer design (shown in Figure 1-4) with two cube corner mirrors rotating on a central flex pivot to produce the optical path difference for a scan. The cube corner mirrors reflect all incident light rays parallel to their angle of incidence. An end-mirror inside the interferometer reflects the radiation back on itself, effectively doubling the optical path difference. This configuration allows the compact ACE-FTS instrument (with a mass of only ~41 kg and an average power consumption of 37 W) to achieve a maximum OPD of ±25 cm, resulting in relatively high resolution spectra (0.02 cm^{-1} defined as 0.5/OPD) during a 2 second scan. The design is also fully compensated for tilt and shear of both moving and stationary optics inside the interferometer.

The FTS uses two photovoltaic detectors to cover the 2.2 to 13.3 μm (750–4400 cm^{-1}) range. A mercury-cadmium-telluride (MCT) detector is used for the 750-1850 cm^{-1} range and a indium-antimonide (InSb) detector for the 1850-4400 cm^{-1} range. The detectors are aligned with a dichroic element to share the same circular 1.25 mrad field of view (FOV) and are cooled to 80–100 K by pointing the passive radiator attached to the conically-shaped sunshield (shown in Figure 1-1) toward deep space. Pointing is controlled by a suntracker servo-loop, which locks on the Sun center and tracks it while the instrument is taking measurements. The raw interferograms resulting from ACE-FTS measurements are Fourier transformed on the ground to obtain the desired atmospheric spectra [*Bernath et al.*, 2005].

The ACE-FTS is also equipped with a visible-near infrared imager located inside the instrument. The imager operates in two filtered channels of 0.525 and 1.02 μm and provides an important diagnostic for pointing and for detecting the presence of clouds in the FOV. The imager detectors are filtered CMOS (complementary metal-oxide-semiconductor) detector arrays made by Fill Factory of Mechelen, Belgium. The arrays are 256 × 256 pixels, but four adjacent pixels have been binned which effectively reduces the array to 128 × 128 active pixel sensors. This decreases the spatial resolution, but reduces the data rate and the effects of individual pixel sensors that may not be performing properly. The total FOV of the imagers is 30 mrad, which is more than an order of magnitude larger than the FOV of the FTS and larger than the angular diameter of the Sun (~9 mrad). The signal-to-noise-ratio (SNR) in each imager channel is greater than 1000, but the main image suffers from overlap by weak secondary images from optical filters that were not tipped far enough off the optical axis [*Bernath et al.*, 2005].

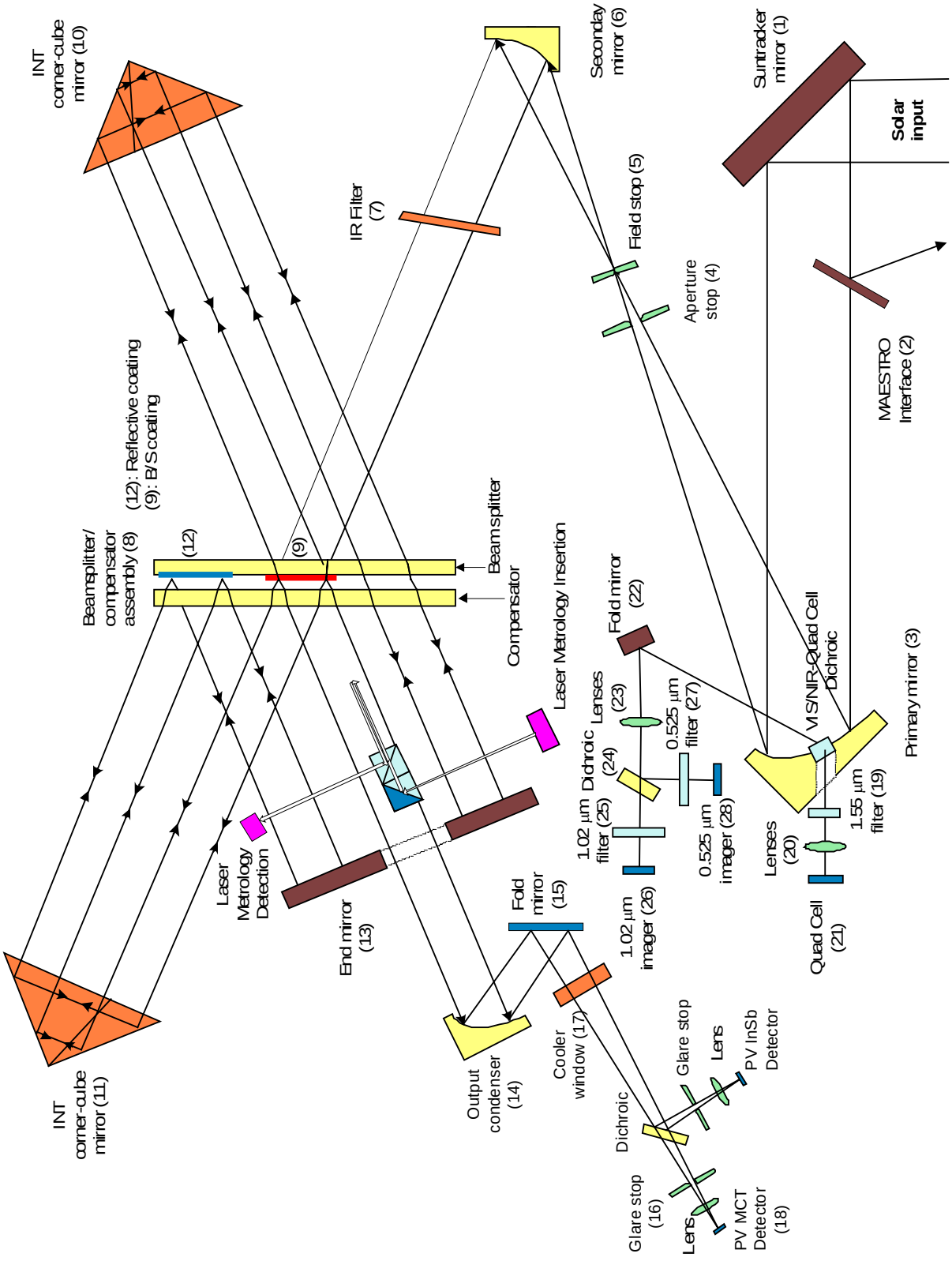

Figure 1-4: The ACE-FTS optical layout, courtesy of ABB-Bomem.

1.2.2 ACE-FTS Pre-Launch Science Characterization Testing

Instruments destined for space-borne measurements require pre-launch characterization of their performance in a simulated space environment. In September 2002, the FTS underwent acceptance tests carried out by ABB Bomem at their facility in Quebec City. From February to March 2003, approximately six weeks were spent testing the ACE-FTS and MAESTRO at the Instrument Calibration Facility (ICF) in the Department of Physics at the University of Toronto. During the Toronto tests, the ACE-FTS and MAESTRO were integrated and tested simultaneously under on-orbit conditions to determine their performance capability with respect to the ACE science goals. Specific objectives of testing were to: (1) Test the performance of the FTS using the passive cooler; (2) Perform gas cell measurements using the FTS and MAESTRO; (3) Carry out complete testing of the solar imager; and (4) Characterize the sun-tracker pointing [*Nassar et al.*, 2003]. Performing these tests therefore required simulating the space environment in a laboratory setting.

The ICF in Toronto, consists of a *Class 10 000* clean-room (an enclosed environment with no more than 10 000 particles larger than 0.5 μm per cubic foot of air) containing a large thermal-vacuum chamber (TVAC). The cylindrical TVAC has a diameter of 2 m and is approximately 5 m long with rounded ends and an optical window on one side. The TVAC can be evacuated to pressures on the order of 10^{-6} Torr with instruments and equipment inside, in order to simulate the extremely low pressures of space. The instruments were mounted to a copy of the spacecraft baseplate and surrounded by a cylindrical copper cold shroud to simulate the low temperature environment of space. To cool the system, liquid nitrogen flowed through a series of thin pipes on the surface of the cold shroud which was wrapped in multi-layer insulation (MLI) to reduce heat loss to the surroundings. The optical input opening of the baseplate was aligned with the TVAC window, and an opening on the cold shroud was aligned with the sunshield of the detector cooler assembly. A cold target was used to simulate deep space for the purpose of testing the passive cooler sub-system. The cold target consisted of a panel with a coolant reservoir behind it, which was filled with liquid nitrogen during the initial cooling stage, but later filled with liquid helium (with a boiling point of 4.2 K at standard pressure) to more closely mimic the ~3 K temperature of deep space. Using this approach, the detectors were cooled to 88 K and maintained at this temperature for extended periods of time while operating the FTS. To simulate solar output in the infrared, the highest temperature commercial hot blackbody (HBB) source available was employed which was capable of operating at 3000ºC, but was limited to approximately 30 minutes at this temperature due to the lifetime of the graphite HBB cavity. In order to measure absorption spectra of individual gases, a gas cell was placed in the optical path and a collimator system was used to direct its radiation into the TVAC [*Nassar et al.*, 2003].

The pre-launch science characterization tests showed that both detectors had high SNR regions ranging from 200:1 to 500:1 for the MCT and 500:1 to 1200:1 for the InSb when test measurements were extrapolated to the operating conditions of space. The SNR over the remainder of the spectral range was not quite as high but exceeded the SNR requirement of 100:1 over nearly

all of this range. Of CO_2 and the 14 baseline species (O_3, H_2O, CH_4, N_2O, NO_2, NO, HNO_3, N_2O_5, $ClONO_2$, HCl, CCl_2F_2, CCl_3F, HF, and CO), all but HF and $ClONO_2$, had at least one microwindow in the high SNR regions with the detectors operating at ~89 K. Typically one would expect the performance of infrared detectors to increase as they are cooled but detector cool-down tests indicated that the opposite occurred due to the build-up of contaminants on the detectors decreasing the signal transmission over time. This was most evident in the ~3000-3500 cm^{-1} range where water ice absorbs strongly, but the effects were seen to a lesser extent over the entire range of both detectors. Despite the problems with ice contamination, there was evidence that the actual sensitivity of the detector was still improving with cooling as it should, and in the ~700-790 cm^{-1} region of the MCT, the improvement in sensitivity exceeded the effect of contamination. Similar results were obtained during the FTS acceptance test carried out by ABB Bomem, and are typical for space instruments with cryogenic detectors.

Detector contamination mainly consists of water vapor which was trapped in porous materials or small cavities in the instruments and MLI, which later condensed on the cold surface of the detectors. Removing the contamination requires temporarily heating the detectors to vaporize the contaminants, allowing them to diffuse away, followed by re-cooling the detectors. A decontamination procedure tested in the Toronto TVAC worked with some temporary success, since immediately after re-cooling the detector performance improved, but the gradual accumulation of contaminants resumed over time. This procedure served as a starting point for the development of an on-orbit decontamination or outgassing scheme mentioned in the next subsection.

1.2.3 ACE-FTS Science Commissioning and On-Orbit Performance

Following the launch of the ACE satellite, a period of commissioning was necessary before routine science operations could begin. The first phase involved limited commissioning of the scientific instruments, as well as commissioning of all other systems external to the scientific payload, known as the *satellite bus*. Once this phase, which lasted approximately four months, was considered complete, science-oriented commissioning activities were undertaken by the science team. The objective of the science phase was to establish command sequences and appropriate instrument settings for operational measurements, as well as to verify and extend the results of the pre-launch science characterization and performance tests. Some key areas of science commissioning included: (1) simultaneous commanding of the ACE-FTS and MAESTRO, (2) optimization of preliminary instrument settings determined during the first phase of commissioning, (3) ACE-FTS and MAESTRO co-registration, suntracker offset and pointing tests; (4) occultation command sequences, and (5) secondary science modes such as ACE-FTS nadir measurements [*Walker et al.*, 2004]. The latter part of science commissioning overlapped with the beginning of ACE-FTS routine measurements. The record of ACE-FTS acceptable measurements begins on February 2, 2004 at ace.ss2551 and continues to the time of this writing (March 2006), although measurements in the period of 17-29 May, 2004 (i.e. ace.ss4108 to ace.sr4281) have errors in the satellite pointing commands which have caused incorrect altitude registration.

ACE-FTS spectra recorded during commissioning were of quite good quality, with a SNR between 300:1 and 450:1 for nearly all of the ~1000-3000 cm^{-1} range of the detectors. For the remainder of the 750-4400 cm^{-1} range, SNR exceeded the target SNR of 100:1 except for a small region on the low wavenumber end of the MCT (750-850 cm^{-1}), the region of ice contamination at approximately 3450-3550 cm^{-1}, and the high wavenumber portion of the InSb detector at greater than 3800 cm^{-1} [*Châteauneuf et al.*, 2004]. Post-commissioning measurements up to late 2005 indicate that ACE-FTS detector performance has improved relative to commissioning and the post-launch early operation phase. The improvements are the result of the successful detector decontamination procedures which have made permanent reductions in detector contamination by outgassing the contaminants to space. The most recent unpublished analysis of changes in detector performance carried out by R. Skelton, appears to indicate that detector performance may have reached or is now nearing its maximum.

1.3 ACE Ground Segment and Data

The data measured by ACE is sent as a microwave transmission from the spacecraft (downlinked) to receivers on the ground. The Canadian Space Agency has facilities to receive the data in St. Hubert, Quebec and Saskatoon, Saskatchewan, but more downlink capability was required to handle all 2 gigabytes of ACE data per day, so additional ground receivers are currently under contract to NASA in Fairbanks, Alaska and to the European Space Agency (ESA) in Kiruna, Sweden. All the data is then transferred to the Mission Operations Center (MOC) in St. Hubert, where it undergoes initial pre-processing before being transferred to the Science Operations Center (SOC), located at the University of Waterloo. The SOC houses the mission data processing server and data archive. All FTS and imager data processing is carried out at the SOC, but MAESTRO processing is done at the University of Toronto. Key members of the ACE science team are stationed at the SOC in Waterloo, and other science team members access the data via the internet from across Canada, the US, Europe and Japan.

The ACE mission concept is based on the ATMOS (Atmospheric Trace Molecule Spectroscopy) instrument [*Gunson et al.*, 1996] that NASA flew four times (1985, 1992, 1993 and 1994) on the Space Shuttle, but the ACE-FTS has been miniaturized by nearly a factor of 10 in mass, power and volume, as compared to ATMOS. With fewer than 400 occultations, ATMOS data has made and continues to make valuable contributions to atmospheric science. The ACE mission had recorded approximately 5000 occultations at the end of its initial 2-year funding period which ended in August 2005. Due to the general demonstrated success of the mission and the lack of any degradation in performance of the spacecraft or instruments, ACE was granted an additional 2-year funding extension and is currently making measurements at a rate of ~6000 occultations per year. If all spacecraft systems continue to perform well, further extensions to the mission are expected.

At the present time, multiple versions of ACE-FTS data exist. ACE-FTS version 1.0 is the initial version which was intended to demonstrate the general capability of the retrievals and determine if retrieval problems existed through inspection of the results and initial validation efforts. This version only included sunset occultations from the beginning of the mission to 1 November 2004. However, some interesting scientific studies were also undertaken with these data, and the findings were published as a collection of 17 separate papers in an ACE special issue of the journal *Geophysical Research Letters*, in June 2005. Version 2.0 was the next data version, and it included both sunrises and sunsets from the start of the mission to 5 December 2004. The version also included many additional species, along with some improvements to the retrieval, but these changes resulted in unphysical oscillations for some individual profiles. Version 2.1 processing was only performed on a subset of the measured occultations, mostly concentrating on Arctic measurements during January to March 2005, and was an experiment in processing the data in near real-time (usually within ~48 hours of measurement). Version 2.2 is the latest version (at the time of this writing) and it contains the most species and spans the entire mission consisting of nearly 10000 occultations by the end of April 2006. Updates to version 2.2 also exist, which have an improved ozone retrieval and include HDO as an official data product. Version 3.0, which will incorporate further improvements and additional species, is expected to begin processing in the summer of 2006.

MAESTRO measures temperature, pressure, ozone, nitrogen dioxide and aerosol/cloud extinction. Although some of these quantities are also measured by the ACE-FTS, the MAESTRO data is complementary since its measurements are made at a lower spectral resolution but a better vertical resolution (1-2 km). The ACE-FTS data, augmented by measurements from MAESTRO and the imager, together provide a wealth of scientific data that is being used to help improve our understanding of processes in the Earth's atmosphere, and will likely continue to be a value resource for researchers in atmospheric science for years to come.

1.4 Overview of Subsequent Chapters

The objective of this chapter was to introduce the ACE mission and the ACE-FTS, as well as to give background information that is relevant to subsequent chapters. The activities described in this introductory chapter were carried out by numerous participants in the ACE mission. In Chapter 2, the ACE-FTS retrieval method will be described with a focus on *a priori* temperature and pressure profiles. The description of *a priori* profiles begins the discussion based on the author's individual work. Chapters 3 through 7 involve the use of ACE-FTS data for scientific studies of the atmosphere, with a large overlap between these studies and the main science objectives of the mission. Each of these chapters begins with some background and the motivation behind studying that specific atmospheric phenomenon. Chapters 3 and 4 are a global inventory of stratospheric chlorine and fluorine, including comparisons to past and current measurements made by other instruments. Chapters 5, 6 and 7 are an analysis of water vapor in the atmosphere, including trends in stratospheric water and its relationship to methane, the loss of stratospheric water vapor via descent in the Arctic vortex and an investigation of the entry of water into the

stratosphere across the tropical tropopause by investigating tropical HDO/H_2O abundance ratios. Chapter 8 brings together these findings by describing the relationship between the different components of this work, and outlines the relevance of this work in the broad field of atmospheric science.

References

Beer, R., T.A. Glavich, D.M. Rider (2001), Tropospheric emission spectrometer for the Earth Observing System's Aura satellite, *Applied Optics*, 40(15), 2356-2367.

Bernath, P.F., C.T. McElroy, M.C. Abrams, C.D. Boone, M. Butler, C. Camy-Peyret, M. Carleer, C. Clerbaux, P.-F. Coheur, R. Colin, P. DeCola, M. De Mazière, J.R. Drummond, D. Dufour, W.F.J. Evans, H. Fast, D. Fussen, K. Gilbert, D.E. Jennings, E.J. Llewellyn, R.P. Lowe, E. Mahieu, J.C. McConnell, M. McHugh, S.D. McLeod, D. Michelangeli, C. Midwinter, R. Nassar, F. Nichitiu, C. Nowlan, C.P. Rinsland, Y.J. Rochon, N. Rowlands, K. Semeniuk, P. Simon, R. Skelton, J.J. Sloan, M.-A. Soucy, K. Strong, P. Tremblay, D. Turnbull, K.A. Walker, I. Walkty, D.A. Wardle, V. Wehrle, R. Zander, J. Zou (2005), Atmospheric Chemistry Experiment (ACE): mission overview, *Geophysical Research Letters*, 32, L15S01.

Boone, C.D., R. Nassar, K.A. Walker, Y. Rochon, S.D. McLeod, C.P. Rinsland, P.F. Bernath. (2005), Retrievals for the Atmospheric Chemistry Experiment Fourier Transform Spectrometer, *Applied Optics*, 44(33) 7218-7231.

Châteauneuf, F., S. Fortin, H. Buijs, M.-A. Soucy (2004), On-orbit performance of the ACE-FTS Instrument, in Proceedings of SPIE-The International Society for Optical Engineering 2004, vol. 5542, Earth Observing systems IX, 166-175, edited by William L. Barnes (Bellingham, WA).

Endemann, M, G. Lange, B. Fladt, (1994) MIPAS for Envisat-1, in Proceedings of SPIE-The International Society for Optical Engineering 1994, vol. 2209, Space Optics 1994: Earth Observation and Astronomy, 36-47, editors G. Cerutti-Maori, P. Roussel (Bellingham, WA).

Gunson, M.R., M.M. Abbas, M.C. Abrams, M. Allen, L.R. Brown, T.L. Brown, A.Y. Chang, A. Goldman, F.W. Irion, L.L. Lowes, E. Mahieu, G.L. Manney, H.A. Michelsen, M.J. Newchurch, C.P. Rinsland, R.J. Salawitch, G.P. Stiller, G.C. Toon, Y.L. Yung, R. Zander (1996), The Atmospheric Trace Molecule Spectroscopy (ATMOS) experiment: Deployment on the ATLAS Space Shuttle missions, *Geophysical Research Letters*, 23(17), 2333-2336.

Griffiths, P.R., J.A. de Haseth (1986), Fourier Transform Infrared Spectrometry, John Wiley and Sons, Toronto.

Hamazaki, T, A. Kuze, K. Kondo (2004), Sensor system for Greenhouse Gas Observing Satellite (GOSAT) in Proceedings of SPIE-The International Society for Optical Engineering 2004, vol. 5543, Infrared Spaceborne Remote Sensing XII, 275-282, edited by William L. Barnes (Bellingham, WA).

Kobayashi, H., A. Shimota, K. Kondo, E. Okumura, Y. Kameda, H. Shimoda, T. Ogawa (1999), Development and evaluation of the interferometric monitor for greenhouse gases: A high-throughput Fourier-transform infrared radiometer for Earth observations, *Applied Optics*, 38(33), 6801-6807.

Nassar, R., C. Boone, K.A. Walker, S.D. McLeod, P.F. Bernath (2003), SCISAT-1: Retrieval algorithms, ACE-FTS testing and the ACE database, in Proceedings of SPIE-The International Society for Optical Engineering 2003, vol. 5151, Earth Observing systems VIII, 173-183, edited by William L. Barnes (Bellingham, WA).

Simeoni, D., C. Singer, G. Chalon (1997), Infrared Atmospheric Sounding Interferometer, *Acta Astronaut.*, 40(2-8), 113-118.

Smith, B.C. (1996), Fundamentals of Fourier Transform Infrared Spectroscopy, CRC Press, New York.

Walker, K.A., J. Zou, F. Nichitiu, K.L. Gilbert, D. Turnbull, C.T. McElroy, W.F.J. Evans, C. Ferguson, E. Puckrin, C. Boone, S.D. McLeod, M. Butler, C. Midwinter, J.R. Drummond, P.F. Bernath (2004), Science Commissioning of the Atmospheric Chemistry Experiment (ACE), in Proceedings of SPIE-The International Society for Optical Engineering 2004, vol. 5542, Earth Observing systems IX, edited by William L. Barnes (Bellingham, WA).

Chapter 2

A Priori Temperature and Pressure Profiles for ACE Retrievals

2.1 Background and Introduction

Earth's atmosphere is comprised of ~78% nitrogen (N_2) and ~21% oxygen (O_2), with the remaining ~1% attributed to argon and numerous trace gas species. The highest atmospheric pressure (and highest density) occurs near the surface of the Earth, then pressures decrease approximately exponentially with altitude. An example of a midlatitude atmospheric temperature profile as a function of the logarithm of pressure is shown in Figure 2.1. Profiles of temperature or other atmospheric quantities are often plotted with the decreasing logarithm of pressure as the vertical co-ordinate since it nearly corresponds to a linear change in altitude as shown in Figure 2-1.

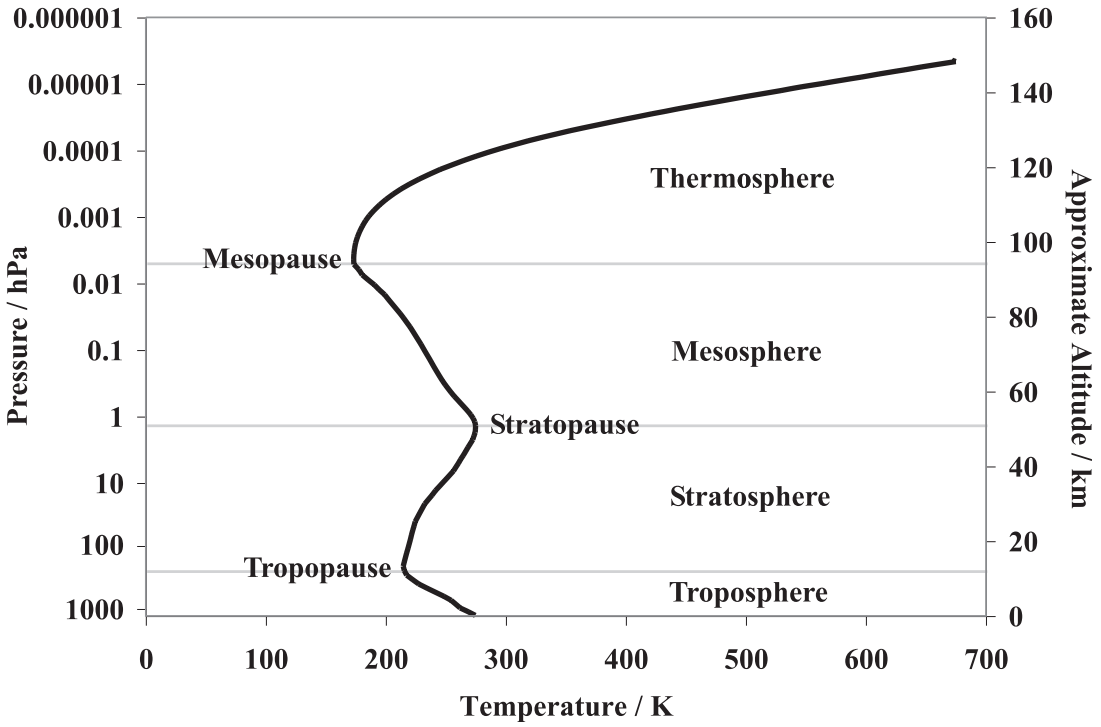

Figure 2-1: An example of a typical midlatitude atmospheric temperature profile. The major regions and temperature inversion points of the atmosphere are labeled.

The shape of a temperature profile arises from the radiative properties of the trace gas constituents that dominate at a given altitude. A typical temperature profile contains three major inversion points. In a simplified description of the atmosphere, it is divided into regions which are bound by the inversions in the temperature profile. The lowest major region is the troposphere, where temperature decreases with altitude from the surface of the Earth to the first inversion known

as the tropopause, which is found at an altitude of ~17 km in the tropics and ~7 km near the poles. Above the tropopause is the stratosphere, where temperature increases with altitude until a second inversion called the stratopause at ~45-55 km. Temperature again decreases with altitude in the mesosphere, which is the region bound by the stratopause and the mesopause at ~80-95 km. Above the mesopause is the thermosphere, where temperature rapidly increases with altitude, although the density in this region is very low. Even in this simplified description, the altitudes of all boundaries are only approximate, since they vary with latitude and season. Furthermore, these boundaries have a finite thickness so they should more properly be thought of as a thin layer, which in the case of the tropopause has multiple definitions for the altitude at which its boundaries begin or end. More rigorous definitions of some of these layers and boundaries will be given throughout this document.

ACE-FTS and MAESTRO measurements are both used for the determination of temperature and pressure profiles. While measurement of the variability of temperature and pressure profiles is of some scientific interest, the primary reason for obtaining these profiles from ACE measurements is that they are necessary for the subsequent determination of atmospheric composition. Due to the large quantity of data that results from a scientific satellite mission like ACE (discussed in the opening chapter), a large degree of automation is required for dealing with data. An automated system has been designed and implemented for the production of *a priori* or initial guess temperature and pressure profiles for ACE retrievals. These profiles have been used in the retrieval of all ACE-FTS temperature and pressure retrievals to date, and continue to be used. They are also being used for the development of MAESTRO temperature and pressure retrievals, and are expected to be implemented in operational MAESTRO retrievals in the future. The *a priori* profiles are created by combining data from a meteorological data assimilation system for the troposphere and lower stratosphere with the output from a thermospheric model for the upper portion of the atmosphere. This chapter contains a very brief outline of general retrieval theory for atmospheric sounding, an outline of the ACE-FTS retrieval method, a description of models used and their required external input, a description of the algorithm for interfacing with the ACE database and combining these datasets to generate *a priori* profiles, as well as discussion of the accuracy and planned improvements to our method.

2.2 General Retrieval Theory

The general idea of a retrieval is to determine the state of a complex system such as the Earth's atmosphere, based on a set of remotely measured quantities. Mathematically, the problem can be expressed as:

$$\mathbf{y} = F(\mathbf{x},\mathbf{b}) + \boldsymbol{\varepsilon}_y \qquad (2.1)$$

where $\mathbf{y}$ is a *measurement vector* with an associated *error vector* $\boldsymbol{\varepsilon}_y$, and F is the *forward model* which is a function of the state of the system described by the *state vector* $\mathbf{x}$ and some *model parameters* $\mathbf{b}$ [*Rodgers*, 1990 and 2000]. The forward model should contain all the physics of the measurement, making use of the model parameters including assumed profiles or any other *a priori*

information. As just one example, if the state vector **x** to be determined was a profile of ozone abundance (i.e. ozone concentrations at a series of altitudes), **y** could be a set of high resolution spectroscopic measurements at different altitudes, in which case **b** would include spectral line intensities corresponding to specific abundances, along with *a priori* temperature profiles and all other required information or assumptions.

Retrieval of the state vector **x** from the measurement vector **y** is commonly referred to as inversion, because it involves a formal inversion of equation 2.1 (i.e. $\mathbf{x} = F^{-1}(\mathbf{y})$). In practice, this is typically carried out by an iterative method in which the forward model attempts to simulate the measurements, beginning with *a priori* information or an initial guess of the state of the system. The observed state is fit to the calculated state using a non-linear least squares procedure in which the residuals are minimized through performing a series of iterations. In the Optimal Estimation Method (OEM) of *Rodgers* [2000], which is perhaps the most common approach used in atmospheric science, the *a priori* is also used as a constraint in determining the final solution. Constraining the retrieved profile using the *a priori* requires an *a priori* covariance matrix specifying the assumed accuracy of the *a priori* data. Information on the recommended relative weighting that should be given to the *a priori* and to the measurements must also be incorporated into the forward model to determine the final result. For current ACE-FTS and MAESTRO retrievals, the *a priori* temperature and pressure profiles described in this chapter are being used as an initial guess only, and not as an *a priori* according to the definition of *Rodgers* [2000], since they do not include an error covariance matrix and are not used to constrain the retrieved profiles.

2.3 ACE-FTS Retrievals

The volume mixing ratio (VMR) of a given species μ^s is defined as the ratio of the number density of the species n^s to the number density of air n^{air} at a given altitude (i.e. $\mu^s = n^s/n^{air}$). VMR is a convenient and widely used parameter for expressing molecular abundance in atmospheric science because absolute quantities such as number density or mass density vary a great deal over a given altitude range due to the approximately exponential decrease in atmospheric pressure with altitude. Temperature T, pressure p and VMR profiles of numerous trace gas species are retrieved from ACE-FTS solar occultation spectra. Only a brief outline of the T and p retrievals will be given here, but a more detailed description is given in *Boone et al.* [2005]. Since accurate pointing knowledge cannot currently be determined from satellite sensor information, tangent height z is also considered an unknown quantity to be determined during the retrieval process. The T and p retrieval is based on carbon dioxide (CO_2) spectral lines because CO_2 has a long atmospheric lifetime and is thus well-mixed, typically giving it a roughly constant VMR for altitudes below ~80 km, the exception being during the polar winters. Therefore, up to 75 km altitude (65 km if greater than 60º latitude), the VMR of CO_2 is calculated from an empirical relationship which accounts for the increase in CO_2 VMR as a function of time. This empirical relationship was originally suggested for the Halogen Occultation Experiment (HALOE) on the NASA Upper Atmospheric Research Satellite (UARS) [*Russell et al.*, 1993]. Above 75 km (65 km if greater than 60º latitude), photodissociation and diffusion cause the VMR of CO_2 to decrease.

A Priori Temperature and Pressure Profiles for ACE Retrievals

T and *p* are retrieved by minimizing the variance between observed ACE-FTS spectra and simulated spectra calculated from a forward model, which contains *a priori T* and *p* data. Rather than analyzing entire spectra, the analysis is carried out for a number of microwindows, which are small portions of the spectra typically 0.2-0.4 cm^{-1} wide, containing CO_2 lines. Both the absolute intensities and the intensity distribution of these lines contain information that can be used to retrieve one or more of the four potential unknowns (*z, p, T* and CO_2 VMR). Different methods are used for retrieving at altitudes above and below 43 km, termed the crossover point.

Below the crossover point down to ~12 km or the lowest measurement, the CO_2 VMR is fixed to the value obtained from an empirical relationship, and tangent height is expressed as a dependent function of *p* and *T* through the hydrostatic equation and the ideal gas law:

$$\frac{1}{\rho}\frac{\partial p}{\partial z} = -g \qquad (2.2)$$

$$p = \rho RT \qquad (2.3)$$

where ρ is the air density, g is the acceleration due to gravity, and R is the gas constant. The absolute intensities of CO_2 lines provide information for retrieving pressure, while the intensity distribution yields information on temperature. Above the crossover and up to 115 km, tangent heights can be reliably calculated from knowledge about the satellite position and orientation in space referred to as ephemeris data. Temperature is again retrieved in this altitude region (43-115 km) while the CO_2 VMR is fixed up to about 70 km and is retrieved above that. Calculating pressures in this altitude region requires only a single unknown parameter, the pressure at the crossover. Pressure at other altitudes in the measurement range can be generated by integration of the hydrostatic equation. For altitudes below ~12 km (or the lowest measurement point), *T* and *p* are fixed to the *a priori* values, and for altitudes above 115 km, *T* and *p* are determined by retaining the shape of the *a priori* profile and scaling it to merge with the retrieval. After determining *T* and *p*, VMRs of numerous trace gases are determined by a fitting a set of microwindows for each species, with *T* and *p* fixed to the retrieved values.

Although interferograms, which are considered *Level 0* data, and spectra, which are considered *Level 1* data, exist on the variable tangent height measurement grid, *a priori* data and the forward model calculations are carried out on a 1-km grid with 150 equally-spaced levels at 0.5, 1.5, 2.5... and 149.5 km altitude. The final ACE-FTS *T, p* and VMR profiles, which comprise *Level 2* data, are available on both the measurement and 1-km grids. Working with data on the 1-km grid is typically more convenient if dealing with multiple profiles or making comparisons with other data.

2.4 Derivation of ACE *A Priori* Temperature and Pressure Profiles

In order to carry out the retrieval according to the process outlined above, *a priori* temperature and pressure knowledge in the form of profiles are required. These profiles are derived by combining meteorological data from the ground to a pressure of 10 hPa (where 1 hPa = 10^{-3} bar = 100 N/m^2) or ~30 km altitude, and model output from ~4 km below the stratopause to 150 km altitude. The detailed method for producing these *a priori* profiles is described in the remainder of this section.

2.4.1 MSIS

The model output comes from the US Naval Research Laboratory Mass Spectrometer Incoherent Scatter Extended model version 2000 (Official Beta Release v2.0), abbreviated as NRL-MSISE-00 [*Picone et al.*, 2002], but more commonly referred to as MSIS, which is the complete acronym for the original version [*Hedin et al.*, 1977a, 1977b]. MSIS is an empirical climatological model that was originally designed for the thermosphere, but subsequent versions were extended to lower altitudes [*Hedin*, 1983, 1987, 1991]. The MSIS thermospheric model resulted from the joining of several incoherent scatter radar data sets providing temperatures at specific latitudes, with several satellite mass spectrometer data sets providing composition on a global basis. Since solar activity and the Earth's magnetism have an influence on the thermosphere, MSIS requires the input of solar flux and geomagnetic data as proxies for the calculation of temperature and molecular densities for a given universal time, day-of-year (DOY) and location. It is capable of calculating the number densities (in cm^{-3}) of He, O, N_2, O_2, Ar, H and N, as well as the total mass density (in g/cm^3) and the atmospheric temperature all at a given altitude.

2.4.1.1 Solar Flux

$F_{10.7}$ is a measure of the flux density of the Sun generated at a radio wavelength of 10.7 cm (~2.80 GHz), as measured by the Dominion Radio Astrophysical Observatory (DRAO) located in Penticton, British Columbia (but measurements were made near Ottawa from 1946-1990). $F_{10.7}$ values are correlated with sunspot number in the sense that both are indicators of solar activity and follow the approximately 11-year solar cycle. The values are given in solar flux units (sfu) in which 1 sfu = 10^{-22} W m^{-2} Hz^{-1}. A very quiet sun will have a value of ~60 sfu, but typical values range from 70-250 sfu. During very rare periods of extreme solar activity, solar flux can reach the 300-700 sfu range. The change in $F_{10.7}$ over time for monthly averages are plotted in *Figure 2-2*.

The DRAO makes measurements of solar flux throughout the day, but reports three standard measurements per day which occur at 17:00, 20:00 and 23:00 UT for most of the year although between November and February when the Sun in Penticton is lower on the horizon, these are made at 18:00, 20:00 and 22:00 UT [*Tapping*, 2004]. The measurements are made using two fully automated radio telescopes called flux monitors.

An archive of $F_{10.7}$ values dating back to 1947, is currently available on the web at *http://www.drao-ofr.hia-iha.nrc-cnrc.gc.ca/icarus/www/archive.html,* but the three daily measurements can be received via an automated email. Typically, two values of $F_{10.7}$ are available for any given measurement time: the observed value and adjusted value. The observed $F_{10.7}$ is the relevant value when concerned with the effects of solar output on the Earth's upper atmosphere, because this is a measure of the flux observed on Earth. The adjusted $F_{10.7}$ is the value relevant when studying the Sun itself, and is obtained by applying a correction to the observed value to account for the difference between the actual Earth-Sun distance and the mean distance of 1 astronomical unit (~150 million km).

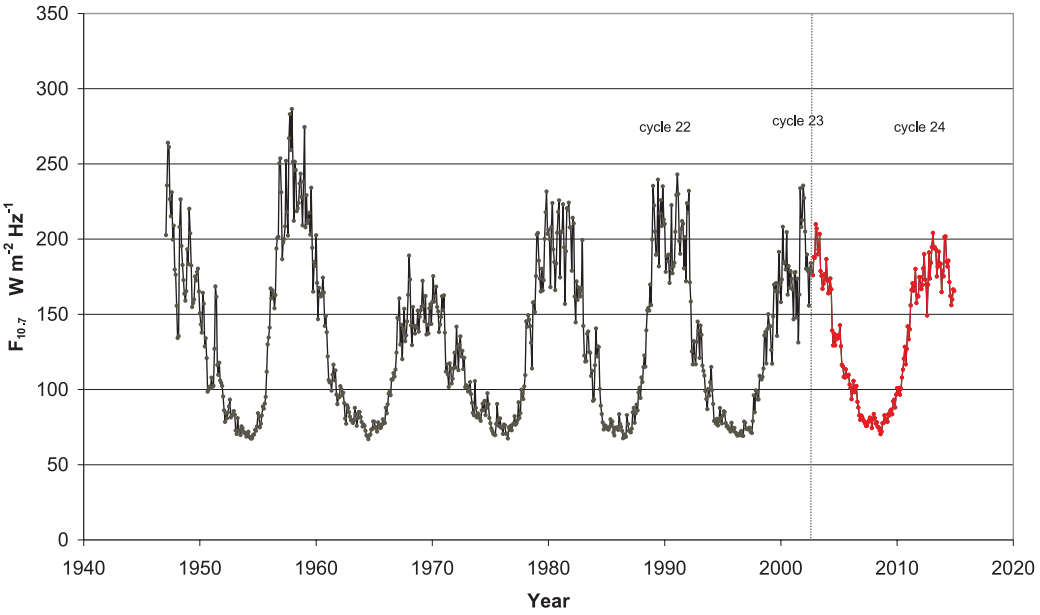

Figure 2-2: The variability of the monthly average $F_{10.7}$ from February 1947 to September 2002. The values after September 2002 (separated by the vertical line) are predicted values.

The input required to run MSIS is the observed $F_{10.7}$ at 20:00 UT for the previous day and an average of $F_{10.7}$ measurements over three solar rotations or 81 days centered on the current day. The 81-day average is somewhat problematic for our purposes, since 40 days of future $F_{10.7}$ data are required in order to run MSIS, but are not available if working in real-time. Problems associated with the 81-day average are described later; however, since the effects of $F_{10.7}$ on the atmosphere are only detectable above 110 km [*Hedin*, 1991], they have only a minor impact on most ACE work.

2.4.1.2 Planetary Geomagnetism

Solar activity alters the Earth's upper atmosphere and magnetic fields such that small changes in the magnetic fields can be detected at the surface of the Earth. MSIS requires a value for the daily

level of planetary geomagnetic activity *Ap*, which is a measure of the frequency and intensity of this magnetic disturbance [*Bartels et al.*, 1939]. A series of steps are required to obtain *Ap* from measurements. The local geomagnetic activity relative to an assumed quiet-day curve is measured at 13 stations across the planet over a three hour period and converted to the *K* index, which uses a scale from 0 to 9 [*Bartels et al.*, 1939]. Eleven of these stations are in the northern hemisphere (48.8-62.5ºN) and two are in the southern hemisphere (45.2 and 50.2ºS). Since the range of variability may differ for different stations, the *Ks* index is used to standardize *K* values between the 13 stations and it further subdivides each number into smaller increments with the *N- No N+* system (where *N* is a number between 0 and 9). The *Kp* index is a planetary average of *Ks* values, and is therefore on the same scale and consists of eight values per day or a value every 3 hours. *Kp* is converted to the linear *ap* scale ranging from 0 to 400 based on a lookup table, which is shown as Table 2-1, then the daily planetary geomagnetic index *Ap* is determined by averaging the eight 3-hourly *ap* values for a given day. Germany's National Research Centre for Geosciences (GeoForschungsZentrum (GFZ) Potsdam) provides an archive of *ap* and *Ap* values dating back to 1932 for anonymous downloading at *ftp://ftp.gfz-potsdam.de/pub/home/obs/kp-ap/wdc/*. The US National Geophysical Data Center (NGDC) provides a very similar archive; however, the ACE mission utilizes the GFZ archive since it is updated twice per month, while the NGDC archive is updated monthly.

Table 2-1: Lookup table for converting between *Kp* and *ap* indices.

Kp	0o	0+	1-	1o	1+	2-	2o	2+	3-	3o	3+	4-	4o	4+
ap	0	2	3	4	5	6	7	9	12	15	18	22	27	32
Kp	5-	5o	5+	6-	6o	6+	7-	7o	7+	8-	8o	8+	9-	9o
ap	39	48	56	67	80	94	111	132	154	179	207	236	300	400

A switch in MSIS allows it to be run with only the *Ap* value or with an array of the following seven *ap* values:

(1) *Ap* index
(2) 3 hour *ap* index for desired time
(3) 3 hour *ap* index for 3 hours before desired time
(4) 3 hour *ap* index for 6 hours before desired time
(5) 3 hour *ap* index for 9 hours before desired time
(6) Average of eight 3 hour *ap* indices from 12 to 33 hours prior to the desired time
(7) Average of eight 3 hour *ap* indices from 36 to 57 hours prior to the desired time

ACE_ap uses the *ap* array, which should give better results than using only *Ap* (the daily average), but verification of this claim is difficult since the effects of *ap* are only seen above 90 km [*Hedin*, 1991], where very few other atmospheric data sets are available for comparison.

2.4.2 GEM

Since the MSIS model is primarily intended for upper atmospheric work, we combine MSIS profiles with meteorological temperature and pressure from GEM to improve the accuracy of our *a priori* profile for the troposphere and lower stratosphere. GEM is the bilingual acronym for "Global Environmental Multi-scale model" in English or "le modèle Global Environnemental Multi-échelle" in French [*Côté et al.*, 1998], produced and run by the Canadian Meteorological Centre (CMC), a division of the Meteorological Service of Canada (MSC). It is a weather forecast data assimilation model for both operational and research purposes with a global grid as well as a variable resolution regional grid located approximately over North America. The exact location of this grid is shown in *Figure 2-3*, which also indicates that the GEM computational poles are rotated with respect to the Earth's geographic poles.

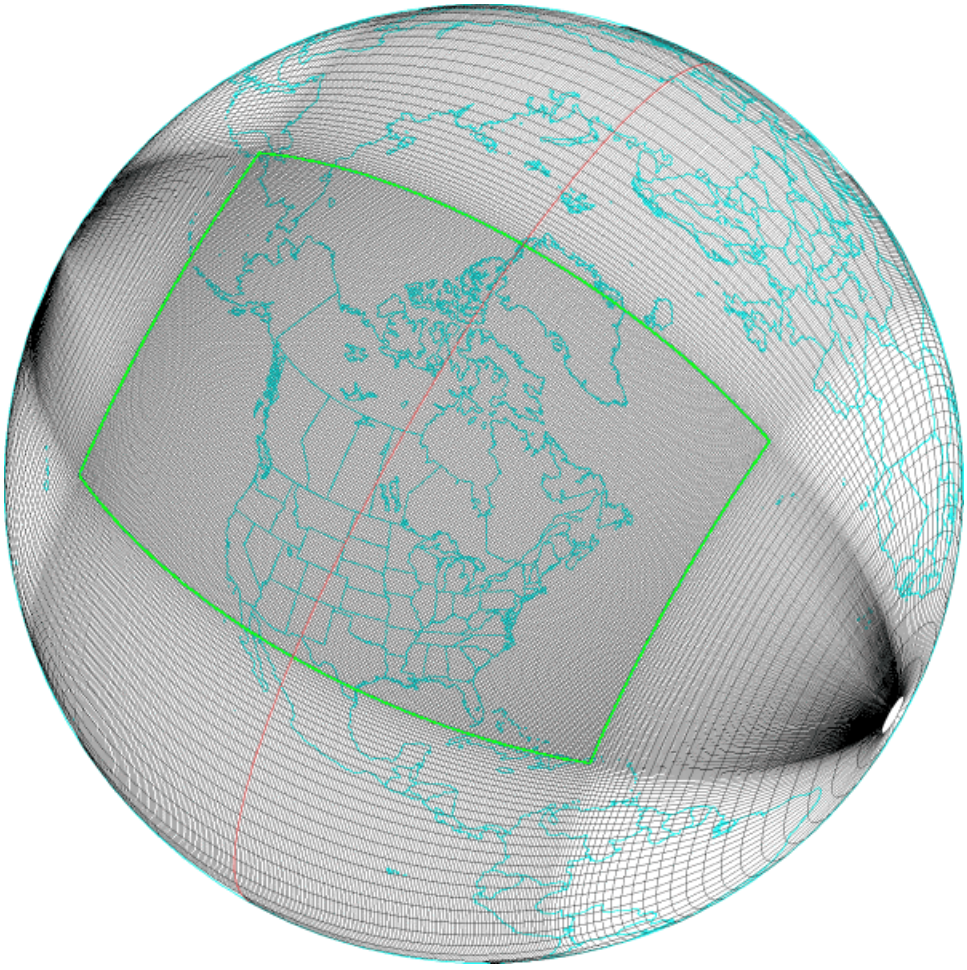

Figure 2-3: The variable-resolution horizontal grid of the currently operational regional configuration of the GEM model.

The model physics incorporated into GEM is beyond the scope of this work; however, Table 2-2 lists some specifications for GEM calculations, indicating that the compromise of the variable resolution regional grid is to favor high local resolution over a limited area, as well as a lower frequency of run times. Both cycles are run using 28 vertical levels known as η-*levels*, with η defined according to:

$$\eta = \frac{p - p_{top}}{p_{surface} - p_{top}} \qquad (2.3)$$

where p is the hydrostatic pressure. The highest level or the lid is currently at 10 hPa (typically 27-32 km altitude); however, the CMC plans to raise this to 1 hPa and eventually 0.1 hPa in a few years time.

Table 2-2: Some GEM global and regional cycle model parameters.

	Global	**Regional**
Time step	2700 s	720 s
Spatial resolution	0.9º (~100 km at the equator)	0.22º (~24 km)
Grid points	401 x 200	270 x 353 (central window)
Vertical η-*levels*	28	28
Model lid	10 hPa	10 hPa
Model run times	00, 06, 12, 18 UT	00, 12 UT

MSC provides GEM temperature and pressure profiles interpolated in both space and time to the reference latitude, longitude and time of ACE measurements for ACE *a priori* profile work. The true measurement locations and times will differ from the reference location and time due to the smearing effect discussed in Chapter 1. The change in location and time over the course of an occultation (smearing) results from the motion of the satellite in orbit and atmospheric refraction. The contribution from orbital motion increases with β and can be calculated with commercial software such as the Satellite Tool Kit (STK). The effects of atmospheric refraction, which have a large influence below ~40 km in altitude, can be accounted for with the refraction model created by K. Gilbert of the ACE Science Team, but with the current approach, this can only be carried out after the retrieval. Therefore, it was decided prior to launch that GEM results would be interpolated by MSC to a single reference location and time, and the hypothetical unrefracted 30-km reference point was arbitrarily selected for this purpose.

Y. Rochon of the Experimental Studies Division of the Air Quality Research Branch (ARQX) of MSC has created an automated system for carrying out the interpolation of GEM output to the reference position and time for the ACE occultations. This is done three times per occultation, referred to as the *forecast* (*prog*), *analysis 1* (*anal_1*) and *analysis 2* (*anal_2*). The

forecast is carried out prior to the ACE occultation, *analysis 1* is the result of a data assimilation (DA) with measurements from a network of radiosondes (described in section 2.5), carried out approximately 6-12 hours after the reference time, and *analysis 2* is the result of a second DA carried out approximately 12-18 hours after the reference time. This is done for both the global mesh and regional mesh model configurations. Whether or not the observation is inside or outside the regional mesh determines which of the global or regional mesh based outputs is identified as the best choice for the profile. The profiles are identified with one of six data types: *anal_reg2*, *anal_reg1*, *anal_glb2*, *anal_glb1*, *prog_glb*, *prog_reg* where *reg* refers to regional and *glb* to global mesh profiles. ARQX puts each of these files on an FTP (file transfer protocol) site, and computers at the SOC typically download the files once per day and write the necessary data to the ACE database.

2.4.3 The ACE Database

The ACE mission will produce several terabytes of data that must be stored and easily accessed. An array of high performance computers at the SOC store the data, which is organized in the form of the ACE database using the PostgreSQL relational database management system software [*Nassar et al.*, 2003]. What is commonly referred to as the ACE database is actually a collection of 20 linked databases, with each database containing one or more tables of data. Each table has a number of columns as fields and a number of rows which are database entries. An example of this structure is shown in *Figure 2-4*.

Solar flux data, planetary geomagnetic data, meteorological data, and *a priori* profiles are stored in the *climatology* database, occultation ephemeris data are stored in the *occultations* database, and retrieved temperature, pressure and VMR profiles are stored in the *level2* database. Some possible data types include *text*, *integer*, *float*, *BLOb* and *timestamptz*. *Text*, *integer* and *float* are straightforward except for the fact that they can be of the array type, if they are followed by '[ ]'. *BLOb* is an abbreviation for Binary Large Object, which is the data type used to store interferograms and spectra. *Timestamptz* is a timestamp with time zone, which is typically set to the International Standards Organization (ISO) format, i.e. "2006-05-05 12:34:56 -07" corresponding to "year-month-day hour:minute:second time zone". This is the most logical and practical date-time format, since sorting can be done easily because the size of increments decreases from left to right as in standard numbers. All times in this document refer to the Universal Time (UT) zone corresponding to +00 (unless otherwise specified), so the time zone will usually be omitted. Utilizing a database approach facilitates searching and sorting data, and also makes automated reading, writing and accessing data much more efficient and easier to maintain than a system of individual files. While a human user can search or modify the database using freeware such as *PG Admin II*, ACE data processing requires automation.

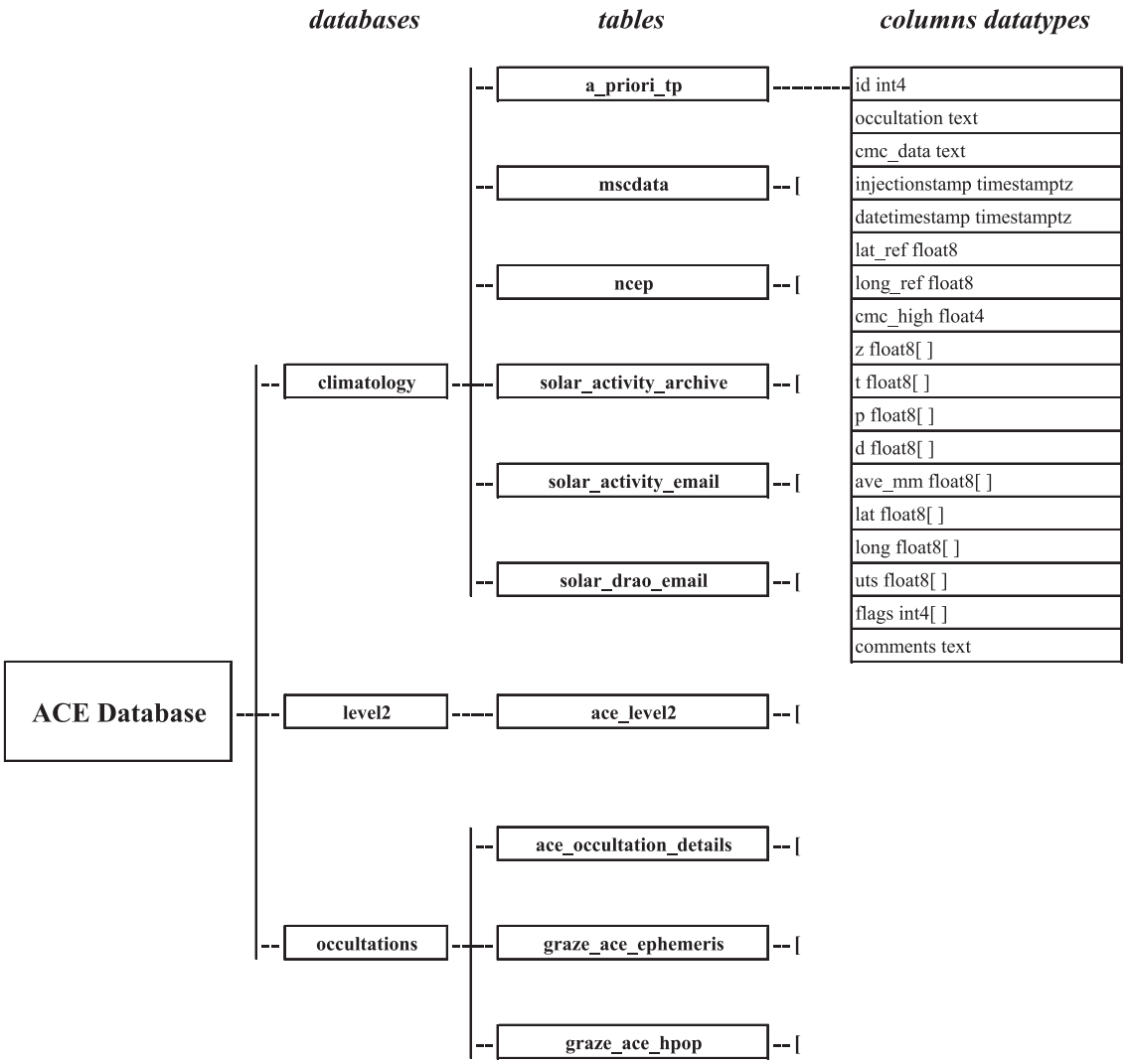

Figure 2-4: Schematic diagram showing some relevant tables to display the structure of the ACE database. The majority of databases and tables are not shown and only the columns and data types for the table *a_priori_tp* have been expanded.

2.4.4 The ACE_ap Software

The process of producing *a priori* profiles is now automated using a program called ACE_ap, which is short for "Atmospheric Chemistry Experiment *a priori*". This program is routinely run as part of Level 1 to 2 processing. When executed, ACE_ap reads the necessary data from the ACE database (tangent positions, solar and geomagnetic data, GEM meteorological profiles), calls MSIS, and produces *a priori* profiles by linearly interpolating between the GEM and MSIS segments. The main ACE_ap outputs are altitude, temperature, pressure, density, average molecular mass, tangent point date, time, latitude, longitude and error flags.

Data from the ATMOS mission was used during pre-launch production and testing of the software, so old versions of the software had the capability of working with ATMOS data, but this capability has been removed in order to streamline and optimize the code, which will reduce confusion for future users who may need to make changes or modifications. The code, which can be found in the Appendix, includes descriptive commenting and write statements which have been commented out, yet retained since they are useful to aid with troubleshooting when necessary. The MSIS code and the bulk of ACE_ap were written in FORTRAN 77 which can not interface directly with the database, and therefore C functions containing PostgreSQL commands were created that are called from the main FORTRAN program. Some C functions and programs for interfacing with the database are listed in Table 2-3.

Table 2-3: C functions and programs used for database interfacing.

C Function or Program	Purpose	File
getap	reads ap data	climatology.c
getfluxes	reads solar flux data	climatology.c
getmsc	reads meteorological data	climatology.c
write_apriori	writes *a priori* data	climatology.c
getapriori_tp	reads *a priori* data	climatology.c
getocc_vec	reads ephemeris data	getorbit_sql.c
drao*	reads DRAO email files and writes DRAO data	drao.c
geoupgfz*	reads GFZ archive files and writes *ap* data	geoupgfz.c

*programs used for archiving, not processing

2.4.4.1 ACE_ap Subroutines

The ACE_ap MAIN program carries out some minimal computations, calls a number of subroutines described in this section, and writes the start and end times of *a priori* production to a log file. Start and end times are determined by the subroutine GMDATETIME which uses the FORTRAN function GMTIME. *Figure 2-5* is a schematic diagram depicting the structure of

ACE_ap algorithm including the multiple subroutines. The subroutines and some functions or programs for interfacing with the database are included in Appendix 1.

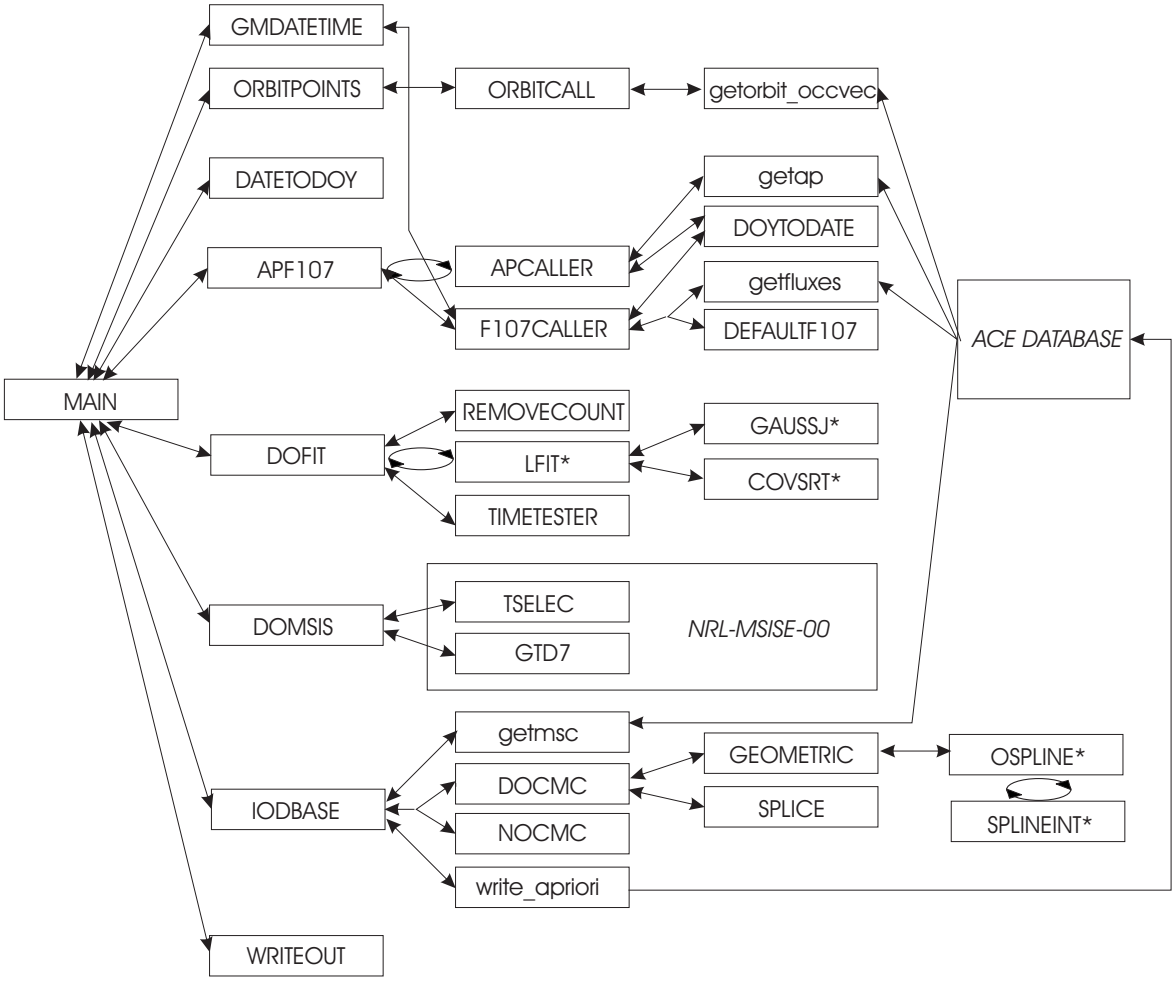

Figure 2-5: Schematic diagram of the ACE_ap algorithm. The uppercase lettering denotes FORTRAN subroutines (*Numerical Recipes* subroutines [*Press et al.*, 1992] are marked with *), the lowercase lettering denotes C functions, the italicized uppercase denote non-program components. The direction of the arrows denotes the direction of dataflow, circular arrows denote loops, and forked arrows denote *if* statements.

The subroutine ORBITPTS reads values for an array of 150 tangent point altitudes, latitudes, longitudes, dates and universal times from the ACE database for a given occultation. The database interface is accomplished using the C function *getocc_vec* which reads from the table *graze_ace_ephemeris*. The positions and times in this table are derived from satellite position by the MOC, ignoring the effects of refraction. In the future, we may move to tangent point positions

and times based on the refraction model, which would require editing the subroutine to direct it to a new table and recompiling, as is done in the absence of MOC data. In the absence of MOC data, ORBITPTS can be redirected to *graze_ace_hpop*, which holds the same information based on a high-precision orbit-propagator calculation carried out with the STK software package.

The subroutine DOFIT fits "time vs. altitude" to a cubic function using the *Numerical Recipes* subroutines LFIT, GAUSSJ, and COVSRT [*Press et al.*, 1992], then evaluates the function on a 1 km grid with 150 grid points at 0.5,1.5, ... and 149.5 km in altitude. DOFIT calls the subroutine REMOVECOUNT which calls TIMETESTER to flag data points that do not fall on the line from the polynomial fit. The threshold distance from the line is set with the parameter *acctest* in the subroutine TIMETESTER and is currently set at 2.75 seconds, but it may be changed in the subroutine REMOVECOUNT. The process is repeated until convergence is achieved, which is often on the first iteration. DOFIT then calls LFIT two additional times to fit "latitude vs. time" and "longitude vs. time". Appropriate conversions are made to deal with equator, prime meridian, dateline, polar and midnight crossings during these fits. Lastly, in addition to the 150 tangent points, the latitude, longitude, date and time for the 30 km reference point are determined.

The subroutines APF107, APCALLER, and F107CALLER use the C functions *getap* and *getfluxes* to read raw values of *ap* and $F_{10.7}$ from the solar and geomagnetic tables in the *climatology* database, then calculate an array of the necessary *ap* values described above, as well as $F_{10.7A}$, the 81-day $F_{10.7}$ average. The subroutine also contains an array of eight 3-hourly *ap* default values (15,15,14,13,14,14,15,15), determined based on rounded monthly average values from January 1932 to January 2002. There is no straightforward way to predict *ap* values; therefore, the default values tend to be quite different from the real *ap* values so they are only used if processing must be done and no *ap* values are available from the archived data or email sources. The subroutine DEFAULTF107 contains default $F_{10.7}$ values (which may also be used to calculate $F_{10.7A}$). These default values are better than the default *ap* values, since $F_{10.7}$ is known to follow the solar cycle as shown in *Figure 2-2*. They were calculated using the monthly average $F_{10.7}$ values from the period of June 1958 to September 2002, covering four 11.09 year (133 month) sunspot cycles. The monthly average $F_{10.7}$ values for the period of October 2002 to November 2013 were then determined using the values from 133, 266, 399, 532 months prior (i.e. averaging corresponding months over the past 4 periods of the 11.09 year sunspot cycle) and for subsequent sunspot cycles the process repeats. These predicted values are shown in *Figure 2-2*, as an extrapolation of the measured values. The values are used as default values if the DRAO email values are not available for calculating $F_{10.7A}$, which requires 40 days of future data. ACE-FTS *Level 2* near-real time processing has used these default values; however, whenever an *a priori* profile is created using an incomplete set of *ap* or *F10.7*, error flags (described later) are used to identify it and it is usually reprocessed in the future.

DATETODOY makes conversions between standard dates and the day-of-year (DOY) where the DOY is 1 for January 1. All leap years between 1947 and 2100 are fully accounted for. DOYTODATE does the conversion in the reverse direction.

DOMSIS calls the model NRL-MSISE-2000 (Official Beta Release v2.0) to calculate number densities, temperature and pressure. It calculates the total number density in (cm^{-3}) at a given altitude by taking the sum of all calculated atomic and molecular number densities at that altitude. The pressure is determined from this total number density using the ideal gas law, and the average molecular mass is also calculated from the total number density as:

$$M^{ave}_i = [4.002602\ n^{He}_i + 15.9994\ n^{O}_i + 2(14.00674)\ n^{N2}_i + 2(15.9994)\ n^{O2}_i + 39.948\ n^{Ar}_i + 1.00794\ n^{H}_i + 14.00674\ n^{N}_i] / n^{Total}_i \quad (2.4)$$

where M^{ave}_i is the average molecular mass and n_i is the number density at level *i*.

In early versions of ACE-FTS retrievals, average molecular mass was assumed constant up to 150 km, but it was determined that temperature and pressure could be retrieved with greater accuracy at high altitudes by using an average molecular mass calculated based on MSIS number densities with the above relationship. The value for average molecular mass essentially anywhere in the lower to middle atmosphere (where N_2 and O_2 dominate), is found to be 28.96 g/mole, but the value begins to decrease due to photodissociation at altitudes above ~65 km. At 150 km, calculated average molecular masses from the first two years of *a priori* runs were in the 22.64-27.63 g/mole range.

IODBASE reads the temperature and pressure versus altitude input from the table *mscdata* in the *climatology* database. These data are the output from the CMC's GEM model on a 1-km altitude grid and are available up to 10 hPa, which corresponds to 26.5 to 31.5 km altitude depending on the latitude and season. After calling the subroutine SPLICE and carrying out its operations, IODBASE writes the output to the table *a_priori_tp* in the *climatology* database.

SPLICE determines the gridpoint nearest to the position of the stratopause by determining the temperature maximum between 40 and 60 km in the MSIS profile. In order to merge or splice the MSIS profiles with the CMC profiles to obtain an accurate *a priori*, MSIS temperature and log pressure profiles are cut off four kilometers below the gridpoint closest to the stratopause and a linear interpolation is applied between the two partial profiles. Smoothing is applied to the upper end of the interpolation in the combined temperature profile, but due to the very nearly linear relationship between altitude and log pressure, smoothing is not used in the pressure profile. Smoothing was not applied where the interpolated data meets the meteorological data because although a smoother profile would result, it would actually decrease the accuracy of the temperature and pressure profile at the upper end of the CMC range. Higher accuracy over this limited range was deemed more important than the appearance of smooth profiles or profiles that appeared correct to the eye but were less representative of true atmospheric conditions. Similarly, other interpolation schemes that produced smooth profiles were rejected since they decrease the use of the CMC data. After calculating temperature and pressure, density is calculated from *p* and *T* using the ideal gas law.

GEOMETRIC changes the geopotential heights given by the CMC to geometric heights. It uses a cubic spline subroutine called OSPLINE and the SPLINT subroutine (but called SPLINEINT here) from Numerical Recipes [*Press et al.*, 1992] to represent the curves and interpolate. GEOMETRIC then replots the data on a 1-km grid. Finally, the data is written to database/file by the subroutine WRITEOUT and the temperature profile can be plotted or used as an *a priori* profile for the ACE-FTS, MAESTRO or a variety of other uses.

2.4.4.2 Compiling and Running

The code for the ACE_ap program is mainly found in the file ACE_ap.F. This file must be complied with MSIS2000.F (the MSIS code), recipes.F (*Numerical Recipes* subroutines) and the ACE library which contains all of the C functions. This is done with the UNIX command:

```
f77 -o ACE_ap ACE_ap.F recipes.F MSIS2000.F -L../acelib -R../acelib -lace
```

Recompiling the program should only be necessary if changes must be made. Following any changes, the new program must be saved using Concurrent Versions System (CVS) software. CVS is a powerful open source tool for code maintenance, which enables a user to commit new versions of a program to a repository which tracks the changes over time.

To run the program it must be called as "ACE_ap ace.ss1234" where ace.ss1234 means ACE sunset number 1234. As mentioned earlier, this is presently done routinely during automated processing, but can be done from the command line or in batches by using the shell command "sh filename" where the filename is the name of a file containing a list of occultations. The input CMC data, output data filename and the splice range are derived from the occultation. When the program is executed and runs to completion, output is written to the table *a_priori_tp* in the *climatology* database.

2.4.4.3 ACE_ap Output and Error Flags

A set of ten error flags (Table 2-4) is written to the *a_priroi_tp* table to be used as a diagnostic for the quality of the profile produced. If the error flag array of an *a priori* profiles contains only zeros, the profile was processed with no known issues. Profiles with some nonzero values are most likely still sufficient, but lack some input data and could potentially be improved for later runs.

Table 2-4: Current *a priori* error flag codes.

Flag number - name	Value	Description
1 - Occultation Format	-1	Occultation not recognized
	0	Occultation recognized
2 - Date	-1	Invalid date
	0	Valid date
3 - Solar Flux	0	Full 81-day F107 average (only possible during post-processing)
	1	Real time processing (incomplete future F107 data for 81-day average)
	2	Have F107 (missing some, but enough for average)
	3	Missing F107 (but enough for average)
	4	Have F107 (but not enough for average, used default)
	5	Missing F107 (not enough for average, used default)
4 - *ap*	0	Complete ap data taken from archives
	1	ap data for one or more days from email not archive (necessary for near real time processing)
	5	No ap data available for one or more of the desired days, used default
5 - MSC Profile version	-1	No CMC profile available, MSIS used for full range or zeroes written out
	0	Appropriate CMC profile used
	1	Analysis 1 (6-12 hr) used instead of 2 (12-18 hr)
	2	Forecast profile used instead of analysis 2
	4	Global profile used rather than regional
6 - MSC Profile properties	0	Meteorological data passes "cold point"
	1	Meteorological data does not reach "cold point"
7 - blank	0	
8 - blank	0	
9 - blank	0	
10 - Other	0	Standard processing values
	1	Used current day F10.7 rather than previous day

2.5 *A Priori* Accuracy and Comparisons

The accuracy and precision of the current ACE-FTS and MAESTRO temperature and pressure retrievals do not depend strongly on the accuracy of the *a priori* profile because it is not used to constrain the retrieval, as would be the case if the Optimal Estimation Method (OEM) [*Rodgers*, 2000] were applied. Even without using OEM, it is useful to characterize the error associated with our *a priori* profiles. At the current time, no universal temperature standard exists to determine the absolute accuracy of our *a priori* profiles; however, comparisons can be made to radiosonde measurements or some external data sources such as the European Centre for Medium Range Weather Forecasting (ECMWF) and US National Center for Environmental Predication (NCEP). Additionally, internal comparisons to the ACE-FTS retrieved profiles can also yield valuable information.

Historically, the GEM temperature data has been validated by comparison with radiosondes in the Global Climate Observation System (GCOS), formerly the WMO Network (*J. Morneau*, private communication, 2005). GCOS is a network containing 161 stations which carry out the radiosonde measurements. A radiosonde is a balloon-borne instrument platform with radio transmitting capabilities used for measuring a number of atmospheric properties including temperature, humidity and pressure, versus height. Temperature is typically measured with a resistance thermistor, which is a white ceramic-covered metallic rod with a diameter of approximately 0.7 mm and length of no more than 2 cm. To increase contact with the air, the thermistor is located on an outrigger, extended a distance from the outside of the instrument package. The electrical resistance of this rod changes with a change in the air temperature. (A brief description of radiosondes, can currently be found at: http://www.aos.wisc.edu/~hopkins/wx-inst/wxi-raob.htm.)

Since GEM mainly operates on a pressure grid, the errors in temperature and height were determined relative to radiosonde measurements, which yielded typical errors of less than 2 K and 0.1 km for the surface up to 10 hPa (*J. Morneau*, private communication, 2005). When converting to an altitude grid, the typical equivalent error in pressure is estimated to be less than 2%.

2.5.1 NCEP and ECMWF Data

The US National Center for Environmental Prediction (NCEP) produces profiles of pressure versus temperature from the surface to an altitude equivalent to 0.4 hPa and the European Centre for Medium Range Weather Forecasting (ECMWF) produces a similar product from the surface to 1 hPa. These are very useful for external comparisons with our *a priori* profiles and retrievals.

NCEP data includes daily global profiles of temperature, pressure and altitude at 12:00 UT. The NCEP model output is provided on a pressure grid with 18 levels at 1000, 850, 700, 500, 400, 300, 250, 200, 150, 100, 70, 50, 30, 10, 5, 2, 1 and 0.4 hPa, and a horizontal resolution of 2.5º. Access to the NCEP data was provided by M. McHugh of GATS Inc., who is a member of the

ACE Science Team and is actively involved with retrieval software for the HALOE instrument on UARS and the SABER instrument on the TIMED satellite. He has provided software to interpolate between NCEP grid points for ACE occultation locations, but no reasonable interpolation in time could be carried out since the profiles are daily. The C^{++} program *ingest_ncep* is used to interpolate the NCEP data to our occultation point and write the profile to the *ncep* table in the *climatology* database. The C program *readncep* is used to read the data from the database and write it to a file for the purpose of plotting.

The ACE science team has very limited access to ECMWF profiles, which are available on a pressure grid containing 21 levels at 1000, 925, 850, 700, 500, 400, 300, 250, 200, 150, 100, 70, 50, 30, 20, 10, 7, 5, 3, 2 and 1 hPa. A few of these profiles have been acquired and utilized manually. Although ECMWF is commonly regarded as the world standard, any improvement in accuracy over NCEP is negligible for our purposes; therefore, we have primarily compared with NCEP data for which we have complete access, and only used ECMWF data in a few cases for additional confirmation.

2.5.2 Comparisons with NCEP and ECMWF

Figure 2-6 indicates that from the surface to almost 10 hPa, the *a priori* profile, NCEP profile and ECMWF profile are nearly indistinguishable for tropical occultations such as ace.ss2551 (2004-02-02-04:21, 18.46ºS, 146ºW) in the South Pacific. The ACE-FTS version 2.2 retrieved profile, which is fixed to the *a priori* up to 14.5 km (144 hPa) in this case, is also in excellent agreement with the *a priori*. Beginning just below 10 hPa, there is a small offset between the *a priori* and the other three profiles. This offset spans the two uppermost points in the CMC profile, the full interpolation region, and the lower end of the MSIS region. It appears to result from the height of the MSIS stratopause, which is lower than in the other three profiles, with a slightly higher temperature at the two uppermost points in the CMC profile adding to the effect. The oscillations in the mesosphere in the ACE-FTS retrieval are not predicted by the *a priori*. These oscillations are most likely real and result from *gravity waves* perturbing the temperature profile. Atmospheric gravity waves are oscillations in temperature, pressure and density that result when a stably stratified region of the atmosphere is perturbed. *Lee waves,* for example, are a type of gravity wave created when horizontal motion forces air over a large mountain range, resulting in a vertical force which can cause oscillations in the stratified air above. With a vertical resolution of 3-4 km, ACE-FTS measurements may be too undersampled to accurately determine the structure of these oscillations, so the pattern retrieved may not be entirely correct, but it is indicative of the presence of these waves. The *a priori* profile uses MSIS for the mesosphere, and since MSIS is simply a climatological model (i.e. it is based on the average conditions or climate), it is not designed to predict temperature fluctuations resulting from gravity waves. Overall, this comparisons illustrates that the good agreement between the ACE-FTS retrieval with NCEP and ECMWF indicates that minor inaccuracies in the *a priori* do not prevent the ACE-FTS retrieval from obtaining the correct temperature profile.

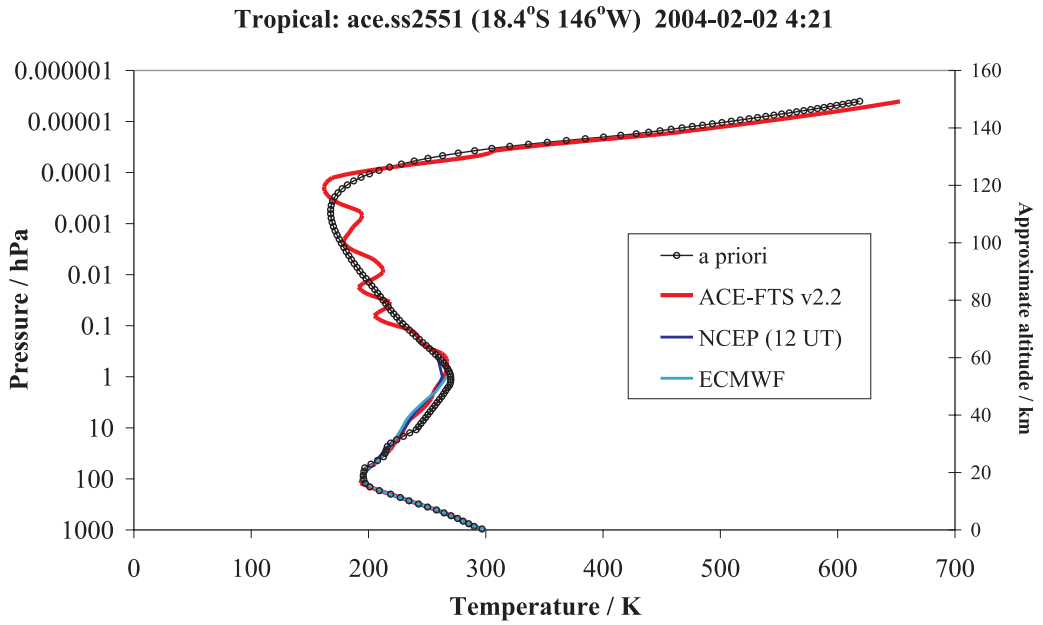

***Figure 2-6*:** Comparison between the ACE *a priori*, the ACE-FTS v2.2 retrieval, NCEP and ECMWF pressure vs. temperature profiles for a tropical occultation.

Figure 2-7 shows the ACE-FTS version 2.2 springtime midlatitude profile for ace.sr9276 (2005-05-03-10:13, 41.35ºN, 78.4ºW) which is close to Waterloo, Ontario, Canada. The retrieval is fixed to this profile up to 11.5 km (205 hPa) in this case. The agreement between the *a priori*, the retrieval and NCEP is excellent up to the lower stratosphere. All profiles show a broad temperature minimum with both the upper and lower temperature inversions coincident among datasets. Once again, the retrieval and NCEP are slightly offset from the *a priori* in the upper stratosphere. The offset begins above 10 hPa in this case, and can be fully attributed to a high stratopause temperature predicted by MSIS. Gravity waves have also caused some fluctuations in the mesopause region that were not predicted by MSIS, as expected.

Figure 2-8 illustrates temperature profiles for the third occultation, ace.ss2842 (2004-02-21-21:05, 76.56ºN, 118ºW), which is a high latitude winter occultation near the MSC Eureka meteorological station in the Canadian high Arctic. Using externally-derived meteorological products provided to the ACE mission, it has been determined that this occultation includes ACE measurements of an air mass inside the Arctic vortex. Vortices are cold, isolated regions of the stratosphere that typically form over the poles [*Nassar et al.*, 2005]. These disturbances can form as early as autumn, strengthen during the polar winter, and break up in the spring, as described in Chapter 6.

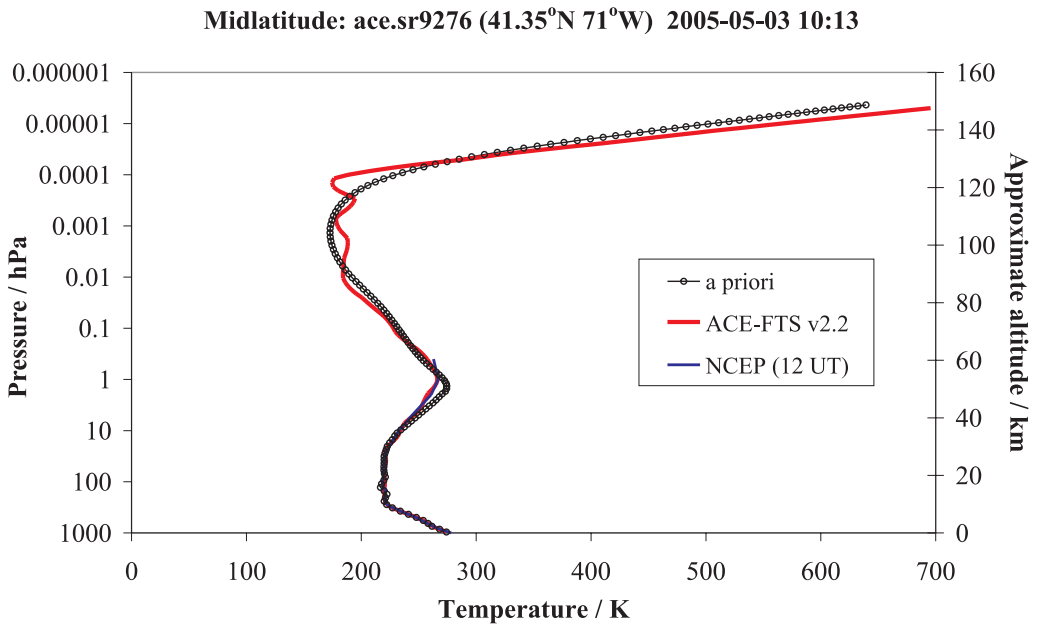

Figure 2-7: Comparison between the ACE *a priori*, the ACE-FTS v2.2 retrieval and NCEP pressure vs. temperature profiles for a midlatitude occultation.

The large discrepancy above 10 hPa between the retrieved profile and the *a priori* in Figure 2-8 is the result of problems with both MSIS and the CMC data. The original MSIS model was designed for the thermosphere, and subsequent versions were then extended to lower in the atmosphere. The accuracy of the extension in the stratosphere is expected to be poor, especially in the case of high latitude winter occultations. The temperature profiles of these occultations are greatly influenced by the size and strength of the polar vortex if it is present, and in early 2004 the Arctic upper stratospheric vortex was the strongest on record since regular observations began [*Manney et al.*, 2005]. For extreme cases such as ace.ss2842, a climatological model like MSIS will usually fail. The problem with the CMC data is not one of inaccuracy, but rather the limited height range available. When the CMC temperature profile has a positive lapse rate (-dT/dz) at 10 hPa, i.e. temperature is still decreasing with altitude, then interpolation joins the upper end of the CMC profile to the MSIS profile and applies smoothing at the MSIS end, as usual. However, when the quality of the data is poor at both ends of the interpolation scheme, the result of a direct interpolation will obviously be poor as well. Greater effort could have been devoted to replicating the true temperature profile, but any method of doing this would introduce a set of complicated assumptions about what the profile should indeed look like. Since the range of variability of vortex temperature profiles is large and we are not using the *a priori* to constrain the retrieval, it was decided that the simple approach would suffice; however, profiles which are likely to have this problem are flagged.

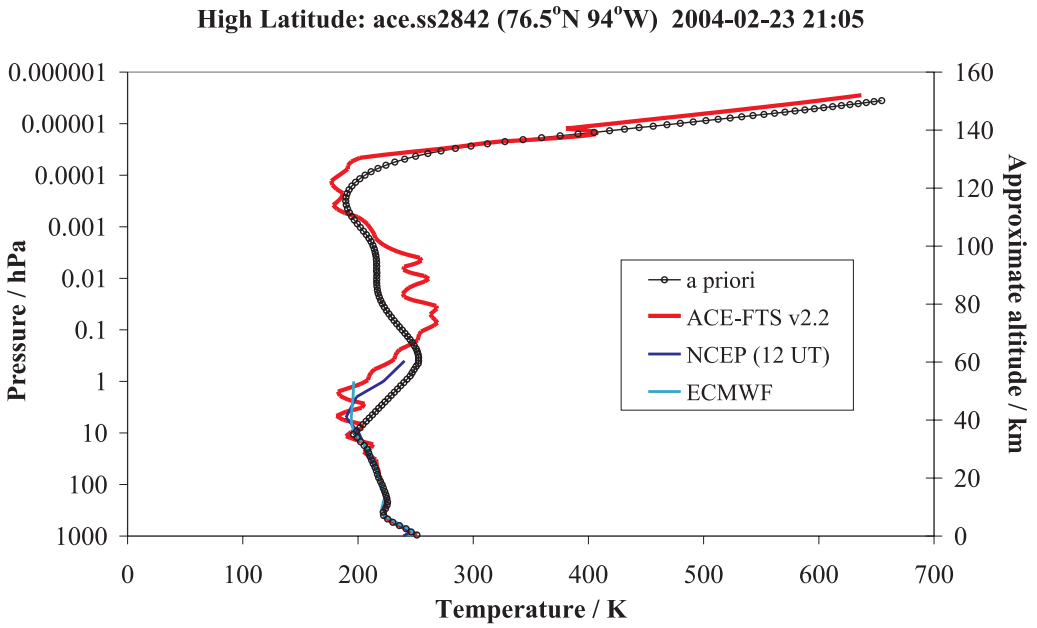

Figure 2-8: Comparison between the ACE *a priori*, the ACE-FTS v2.2 retrieval, NCEP and ECMWF pressure vs. temperature profiles for a high latitude occultation.

Understanding the criteria for flagging, requires some clarification regarding vertical temperature structure and regions of the atmosphere. As Figures 2-8 and 2-9 show, the position of the tropopause cannot be clearly defined by the temperature minimum as in the simple definition. The correct definition of the tropopause according to the World Meteorological Organization (WMO) is the point where the lapse rate (-dT/dz) is less than 2 K/km for a vertical range of more than 2 km [*World Meteorological Organization*, 1957]. In the tropics, this is sometimes referred to as the *lapse-rate tropopause* while the temperature minimum is referred to as the *cold-point tropopause*. In Figures 2-8 and 2-9, a lapse rate tropopause appears as the minor inversion beginning at 6.5 km (between 1000 and 100 hPa) and a temperature minimum at 36.5 km (between 10 hPa and 1 hPa). This minimum is well into the stratosphere; hence it can be referred to simply as the *cold point*. If the cold point is above the range of the CMC profiles, the *a priori* profiles are expected to differ significantly from the true temperature profile and are flagged, such that flag number 6 has a value of 1 (outlined in Table 2-4).

Although MSIS is expected to be better in the mesosphere than in the stratosphere or troposphere, a sizeable discrepancy still exists in the mesosphere between the *a priori* and the retrieval (*Figure 2-8*). This may also be a result of the uncharacteristically strong Arctic vortex causing abnormal conditions in the lower mesosphere [*Nassar et al.*, 2005], but further study would be required to confirm this.

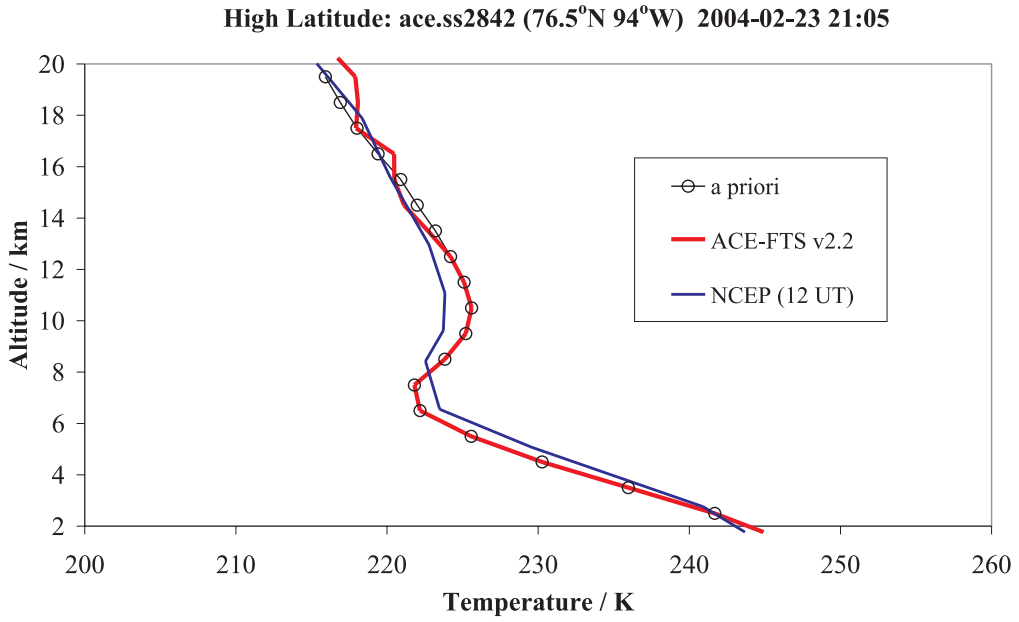

Figure 2-9: A closer view of the tropopause for ace.ss2842.

2.5.3 Extensive Comparisons Between *A Priori* Profiles and ACE-FTS Retrievals

ACE-FTS retrievals can be used to infer some information about the accuracy of the *a priori* profiles; however, the retrieved profiles themselves do not contain uncertainties for temperature or pressure and are still undergoing an extensive validation effort. One important reason for the comparison between *a priori* profiles and retrievals is that they span nearly the same altitude range, unlike NCEP or ECMWF profiles or radiosonde measurements which only cover the lower atmosphere. Since so few good data sources are available above the upper stratosphere, it is still instructive to compare *a priori* profiles to the retrievals over the 12-100 km range even prior to the completion of validation. Some known issues with the retrieval above 100 km remain, must eventually be corrected. Therefore, the *a priori* profiles are likely more accurate than current retrievals in the 100-150 km range, and with no reliable and readily available source to compare with the *a priori* profiles at this altitude, the range will not be discussed further at the current time.

Comparison of a large number of temperature profiles shown in Figures 2-9 to 2-11, indicates that the *a priori* deviation from the ACE-FTS retrieval varies with altitude and latitude range. For the purposes of these comparisons, occultations were divided into tropical (30ºN-30ºS), midlatitude (30-60ºN or 30-60ºS) and high latitude or polar (60-90ºN or 60-90ºS) based on their reference latitude. The differences in temperature were determined as $T_{a\ priori}$ - $T_{\text{retrieval}}$ and the percent difference in pressure was calculated as:

$$\sigma P = \frac{(P_{a\ \ priori} - P_{retrieval})}{\frac{1}{2}(P_{a\ \ priori} + P_{retrieval})} \times 100\% \qquad (2.5)$$

The mean difference in temperature and the mean percent difference in pressure were taken as indicators of systematic biases and are shown in the difference plots as a black line. A quantitative breakdown of these differences is given in Table 2-5. For all latitude zones, the difference in profiles above ~100 km can be attributed more to the retrieval than the *a priori* (as mentioned earlier), so the 100-150 km altitude range will essentially be ignored here, but has been retained in the figures for illustrative purposes.

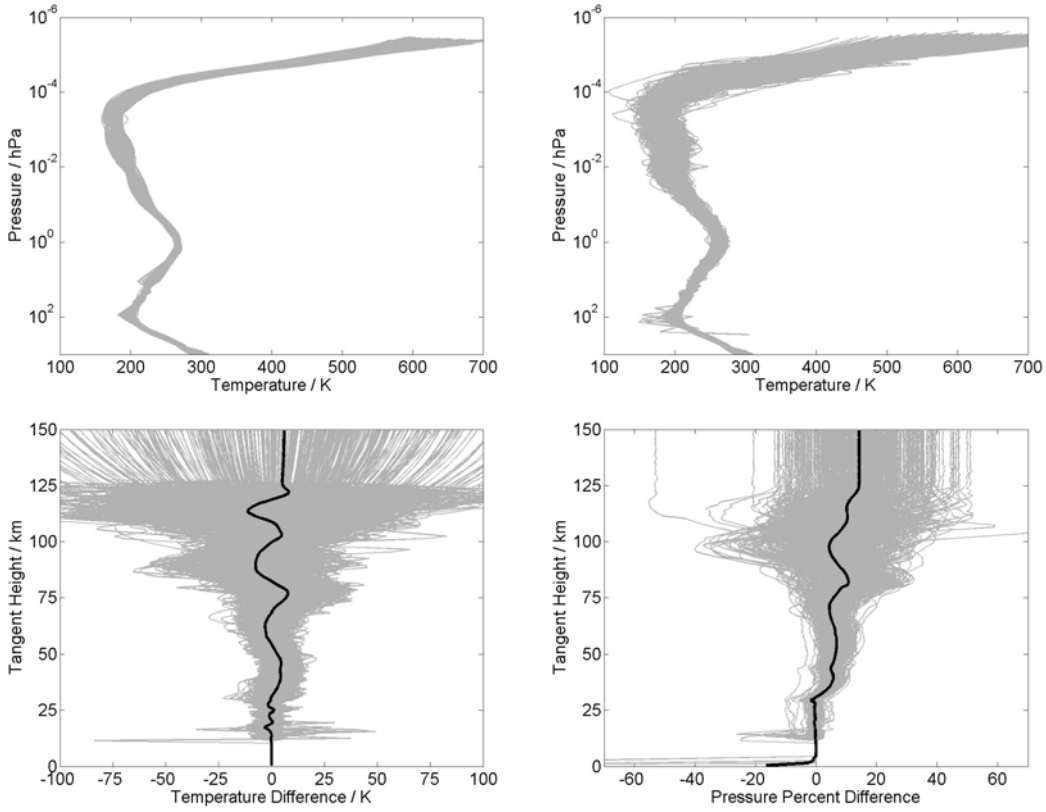

Figure 2-10: 463 Tropical profiles - *a priori* (top left), retrieved (top right), temperature difference (bottom left) and the pressure percent difference (bottom right).

The differences in the tropical profiles are relatively small below 30 km, with typical random differences of about 2 K or 2% in pressure. A few outliers in the 10-20 km range are most likely due to anomalous retrieved profiles due to tropical clouds. (The offset seen in the pressure percent difference below 2 km is due to the absence of values for pressure at altitudes below the surface elevation.) In the upper stratosphere the random differences become slightly larger and significantly larger again in the mesosphere due to the gravity-wave-induced oscillations in the

profiles that MSIS cannot predict, as seen earlier. A small systematic offset in pressure also appears in the mesosphere. At the mesopause and above, temperature differences continue to increase but pressure percent differences do not. Above 125 km, the temperature and pressure profiles from the ACE-FTS retrievals are fixed to the *a priori* profiles with an offset applied, as evidenced by a reduction in randomness seen in both temperature difference and pressure difference profiles.

The differences in the midlatitude profiles are comparable below 30 km but slightly larger than with the tropical profiles at higher altitudes. A few outliers in the ACE-FTS retrieval have corresponding outliers in the temperature and pressure differences. Some of the higher midlatitude winter profiles in this set behave very much like the polar winter profiles and exhibit problems just above 10 hPa or about 30 km.

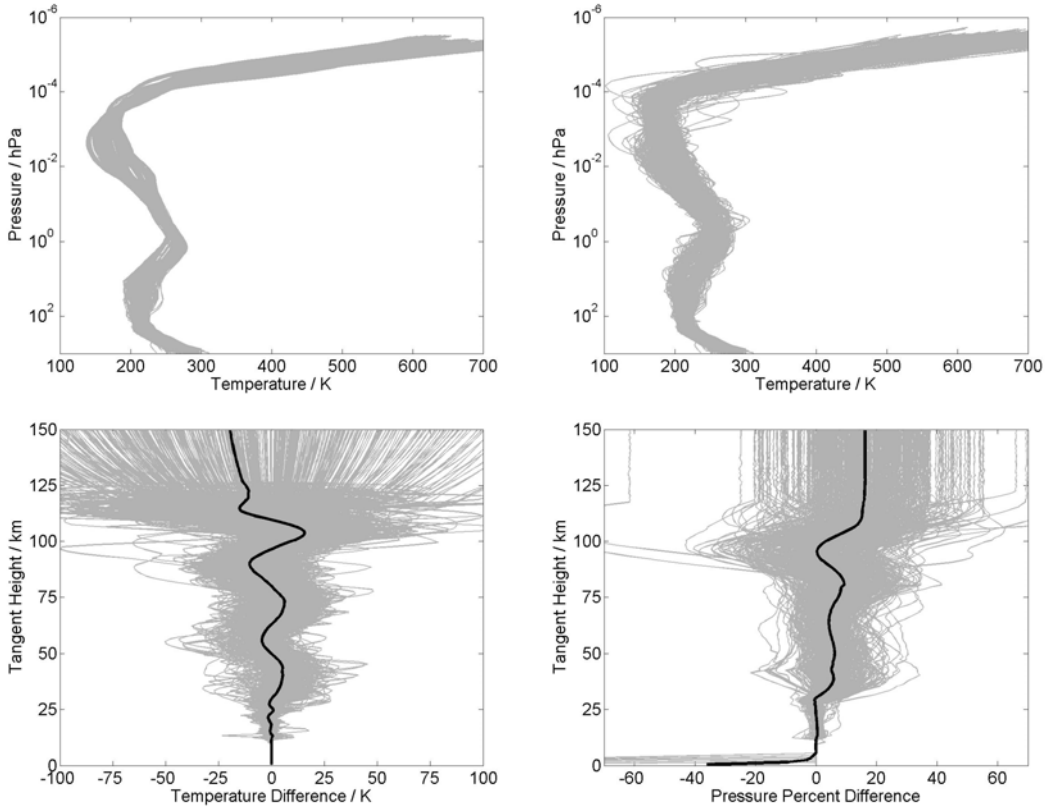

Figure 2-11: 500 Midlatitude profiles - *a priori* (top left), retrieved (top right), temperature difference (bottom left) and the pressure percent difference (bottom right).

Winter high latitude or polar profiles exhibit problems above the 10 hPa point where MSIS is unreliable and CMC data are not available, as was the case for ace.ss2842 (Figures 2-8 and 2-9). The most problematic range spans about 10-75 km in which typical systematic temperature differences are about 15 K or as high as 50 K in extreme cases, and typical pressure percent

difference are about 20% or as high as 60% in extreme cases. At very high altitudes, the *a priori* profiles have a negative systematic temperature difference and a small positive systematic percent pressure difference.

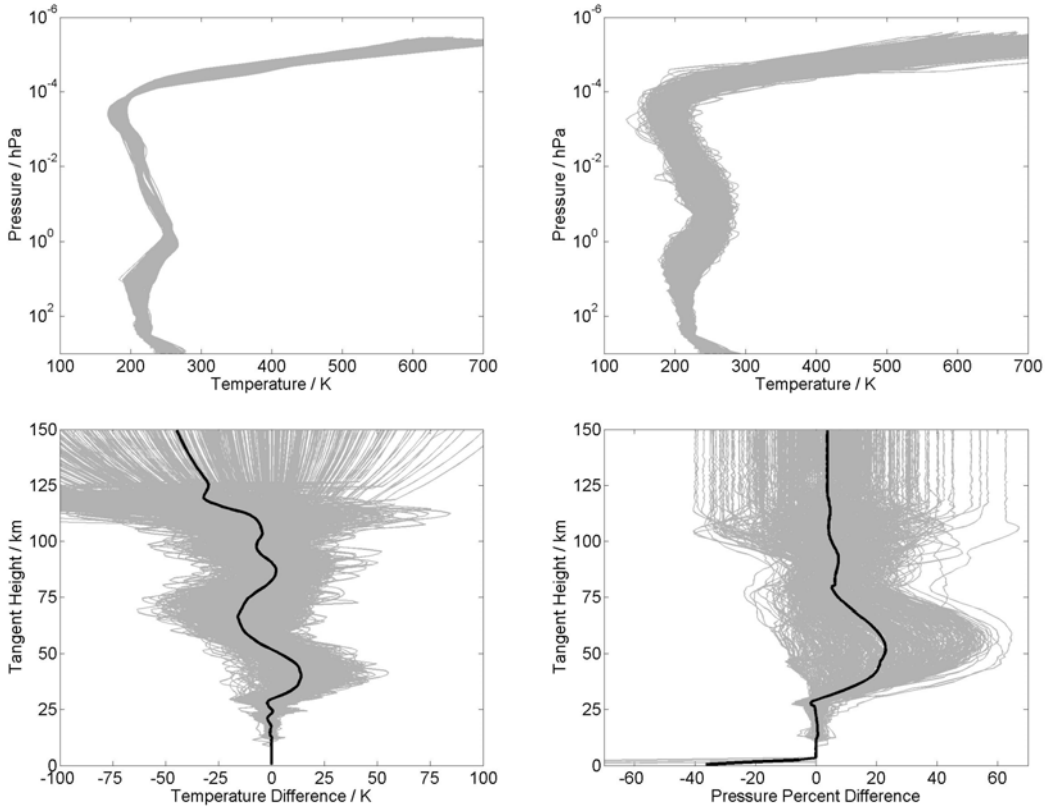

Figure 2-12: 500 High latitude profiles - *a priori* (top left), retrieved (top right), temperature difference (bottom left) and the pressure percent difference (bottom right).

2.5.4 Best Estimates of Overall Accuracy

According to the analysis carried out in previous subsections, estimates were made of the uncertainty in ACE *a priori* temperature and pressure profiles. As in the previous subsections, errors were estimated for ranges of altitudes and latitudes. The estimates for the 100-150 km region are much lower than the differences between the *a priori* profiles and ACE-FTS retrieved profiles because the retrievals have known issues at these altitudes causing some irregularities. It does not make sense to accept these retrieved profiles as correct for determining our error budget. These errors are a starting point for the use of creating *a priori* profiles for OEM or other methods that require errors on the *a priori* profiles, but further development work and validation in conjunction with development and validation of ACE-FTS retrievals are needed before a true *a priori* covariance matrix can be derived.

Table 2-5: Estimates of accuracy in the pressure (σP) and temperature (σT) of *a priori* profiles for tropical, midlatitude and high latitude profiles in the specified altitude ranges.

Latitude Range		**Tropical**	**Midlatitude**	**High latitude**
		30ºS - 30ºN	30-60ºS or 30-60ºN	> 60ºN or > 60ºS
Number of profiles		463	500	500
100-150 km	σT	30 K	30 K	30 K
	σP	25%	25%	25%
70-100 km	σT	30 K	30 K	35 K
	σP	25%	25%	25%
10hPa -70 km	σT	10 K	20 K	40 K
	σP	10%	15%	50%
below 10 hPa	σT	2 K	2 K	2 K
	σP	2%	2%	2%

2.5.5 Improving Accuracy and Future Work

The current ACE *a priori* temperature and pressure profiles provide a sufficiently good initial guess for the retrievals by the ACE-FTS, as evidenced by the success of these retrievals to date. Neither the ACE-FTS nor MAESTRO use the *a priori* as a constraint in the retrieval process, but it is still useful to examine the accuracy of the *a priori* in order to determine ways to improve it. More accurate *a priori* profiles should theoretically require less time for the *T* and *p* retrieval to converge. ACE-FTS *T* and *p* retrievals use a much larger proportion of processing time than all VMR retrievals combined; therefore, improving accuracy in the *a priori T* and *p* profiles could largely reduce the average processing time for a retrieval.

This work has shown that MSIS has difficulty with winter high latitude profiles in the upper stratosphere and that an alternative to MSIS for this region is desirable, but GEM data does not currently go above the 10 hPa point. In the future, the CMC plans to raise the upper limit of GEM from 10 hPa (~30 km) to 1 hPa (~ 50 km) or even 0.1 hPa (~68 km). Incorporating this into our work would produce a large improvement to *a priori* profiles in the middle to upper stratosphere, especially for winter high latitude profiles. An improvement in the *a priori* may also improve retrieved profiles from high latitude winter occultations which are scientifically very important, but it is more probable that the retrieved result would not change much, although it would require fewer iterations. Therefore, increasing the upper altitude limit on GEM data could result in a significant reduction in average processing time.

In some cases, weaknesses in the *a priori* profiles are a direct result of limitations to the models used. For example, MSIS documentation states that it suffers from poor accuracy during periods of high solar activity (defined as greater than 240 sfu) [*Picone et al.*, 2002], but in reality this is of minor importance for our work. Solar flux predominantly effects higher altitudes with

only very minor effects below 120 km altitude, as evidenced by comparing *a priori* profiles created based on a complete set of $F_{10.7}$ data (81 days) and the same profiles based on default solar flux data. No change was found below 100 km using the default data, with changes of less than 0.2 K below 110 km, less than 2 K below 120 km and less than 20 K below 150 km.

Furthermore, as a climatological model, MSIS does not incorporate gravity waves into the computation of temperature. Gravity waves are considered the main cause of oscillations observed throughout the mesosphere in ACE-FTS retrievals, resulting in discrepancies between the *a priori* and retrievals. For issues such as these, very little can be done aside from switching to another model, but other models will likely have other problems. Few (if any) real alternatives exist, as evidenced by the fact that MSIS 2000 is also being used for HALOE *a priori* profiles and older versions of MSIS were used for ATMOS *a priori* profiles.

It would be possible to make a minor improvement to ACE *a priori* profiles in the lower atmosphere, below ~40 km in altitude. This arises from the fact that the MSIS portion of the profile currently uses the predicted latitude, longitude and time arrays, ignoring the effects of atmospheric refraction, which are significant below ~40 km. The CMC portion of the profile, simply uses the unrefracted 30 km reference altitude. More accurate co-ordinates for MSIS and an array of co-ordinates for CMC interpolation based on output of the refraction model would result in improved accuracy for the *a priori* in a region where much of the ACE-FTS retrieval is actually fixed. Implementation would be simple for the *a priori,* since it would only require changing the table used in the *getorbit_occvec* function and the table used by the CMC for their interpolation of GEM data. However, the refraction model requires spacecraft co-ordinates as well as values for atmospheric temperature, pressure and tangent heights which are all quantities derived from the retrieval, therefore under the current setup, the refraction model is run after *Level 1 to 2* processing. To supply the refracted co-ordinates to ACE_ap would require first running ACE_ap with the current configuration, retrieving the needed quantities, running the refraction model, rerunning ACE_ap with the new co-ordinates, then rerunning the retrieval and refraction model. The loop as described would require considerable processing power and it is unlikely that it would be implemented in the near future, but it may be possible to base the refraction model on the *a priori* values and bypass the initial retrieval which is the most compute-intensive step. Furthermore, since data is continually being reprocessed, and will likely be reprocessed even after the mission has ceased, earlier versions of the retrieved parameters could be fed into the loop.

As mentioned earlier, ACE-FTS and MAESTRO retrievals are not constrained by the *a priori* as in OEM, so complete knowledge of the accuracy of the *a priori* is not required. OEM has both advantages and disadvantages over the approach used for ACE-FTS retrievals, which will not be discussed here. However, one key advantage of OEM is the resulting error vector to accompany the state vector, whereas at the present time ACE-FTS retrievals do not estimate absolute accuracy. OEM or some equivalent method for determining absolute accuracy may be used in the future, in which case the accuracy of *a priori* profiles and knowledge of the *a priori T* and *p* uncertainties will be more important.

References

Andrews, D.G. (2000), An Introduction to Atmospheric Physics, Cambridge University Press, Cambridge.

Bartels, J., N.H. Heck, and H.F. Johnston (1939), The three-hour-range index measuring geomagnetic activity, *J. Geophys. Res.,* 44, 411-454.

Boone, C.D., R. Nassar, K.A. Walker, Y. Rochon, S.D. McLeod, C.P. Rinsland, P.F. Bernath. (2005), Retrievals for the Atmospheric Chemistry Experiment Fourier Transform Spectrometer. *Applied Optics*, 44(33) 7218-7231.

Brown, L.R., C.B. Farmer, C.P. Rinsland, R. Zander (1992), "Remote Sensing of the Atmosphere by High Resolution Infrared Absorption Spectroscopy", in Spectroscopy of the Earth's Atmosphere and Interstellar Medium, N.K. Rao and A. Weber (editors), Academic Press Inc., Toronto.

Côté, J., S. Gravel, A. Méthot, A. Patoine, M. Roch, A. Stainforth. (1998), The Operational CMC-MRB Global Environmental Multiscale (GEM) Model. Part I: Design Considerations and formulation. *Monthly Weather Review*, 126(6), 1373.

Côté, J., J.-C. Desmarais, S. Gravel, A. Méthot, A. Patoine, M. Roch, A. Stainforth. (1998), The Operational CMC-MRB Global Environmental Multiscale (GEM) Model. Part II: Results. *Monthly Weather Review*, 126(6), 1397.

Gauthier, P., C. Charette, L. Fillion, P. Koclas, S. Laroche. (1999), Implementation of a 3D Variational Data Assimilation System at the Canadian Meteorological Centre. Part I: The Global Analysis, *Atmosphere-Ocean*, 37(2), 103-156.

Hedin, A.E. (1991), Extension of the MSIS Thermospheric Model into the middle and lower atmosphere, *J. Geophys. Res.*, 96 (A2) 1159-1172.

Hedin, A.E. (1987), MSIS-86 Thermospheric Model, *J. Geophys. Res.*, 92 (A5) 4649-4662.

Hedin, A.E. (1983), A Revised Model Based on Mass Spectrometer and Incoherent Scatter Data: MSIS-83, *J. Geophys. Res.*, 88 (A12) 10170-10188.

Hedin, A.E., J.E. Sala, J.V. Evans, C.A. Reber, G.P. Newton, N.W. Spencer, D.C. Kayser, D. Alcaydé, P. Bauer, L. Cogger, J.P. McClure (1977), A Global Thermospheric Model Based on Mass Spectrometer and Incoherent Scatter Data MSIS 1. N_2 Density and Temperature, *J. Geophys. Res.*, 82 (16) 2139-2147.

Hedin, A.E., C.A. Reber, G.P. Newton, N.W. Spencer, H.C. Brinton, H.G. Mayr (1977), A Global Thermospheric Model Based on Mass Spectrometer and Incoherent Scatter Data MSIS 2. Composition, *J. Geophys. Res.*, 82 (16) 2148-2156.

Laroche, S., P. Gauthier, J. St-James, J. Morneau (1999), Implementation of a 3D Variational Data Assimilation System at the Canadian Meteorological Centre. Part II: The Regional Analysis, *Atmosphere-Ocean*, 37(3), 281-307.

Manney, G.L., K. Krüger, J.L. Sabutis, S.A. Sena, S. Pawson (2005), The remarkable 2003-2004 winter and other recent warm winters in the Arctic stratosphere since the late 1990s, *J. Geophys. Res.*, 110, D04107.

Mayaud, P.N. (1980), Derivation, Meaning, and Use of Geomagnetic Indices, *Geophys. Monogr. Ser., Vol. 22*, AGU, Washington, D.C.

Menvielle, M., A. Berthelier (1991), The *K*-derived planetary indices: description and availability, *Rev. Geophys., 29*, 415-432. and Correction: Ibid., 30, 91, (1992).

Nassar, R., K.A. Walker, C. Boone, S.D. McLeod, P.F. Bernath. SCISAT-1: Retrieval Algorithms, ACE-FTS Testing and the ACE Database. Proceedings of SPIE, vol. 5151, Earth Observing Systems VII, edited by W. L. Barnes (SPIE, Bellingham, WA, 2003) pp 173-183.

Nassar, R., P.F. Bernath, C.D. Boone, G.L. Manney, S.D. McLeod, C.P. Rinsland, R. Skelton, K.A. Walker (2005), ACE-FTS measurements across the edge of the winter 2004 Arctic vortex. *Geophys. Res. Lett.*, 32, L15S05.

Picone, J.M., A.E. Hedin, D.P. Drob, A.C. Aikin (2002), NRLMSISE-00 empirical model of the atmosphere: Statistical comparisons and scientific issues, *J. Geophys. Res.,* 107(A12) 1468.

Press, W. H., S.A. Teukolsky, W.T. Vetterling, B.P. Flannery (1992), Numerical Recipes in FORTRAN: The Art of Scientific Computing, 2nd ed., Cambridge University Press, New York.

Rodgers, C.D (1990), Characterization and Error Analysis of Profiles Retrieved From Remote Sounding Measurements, *J. Geophys. Res.*, 95(D5), 5587-5595.

Rodgers, Clive D (2000), Inverse Methods for Atmospheric Sounding: Theory and Practice. World Scientific, River Edge, New Jersey.

Russell, J.M. III, L.L. Gordley, J.H. Park, S.R. Drayson, D.H. Hesketh, R.J. Cicerone, A.F. Tuck, J.E. Frederick, J.E. Harries, P.J. Crutzen (1993), The Halogen Occultation Experiment, *J. Geophys. Res.*, 98, 10777-10797.

Tapping, Ken (2004), Dominion Radio Astrophysical Observatory, private communication and http://www.drao-ofr.hia-iha.nrc-cnrc.gc.ca/icarus/www/about.html.

Tapping, K.F., B. DeTracey (1990), The origin of the 10.7 cm flux, *Solar Physics*, 127(2), 321-32.

Tapping, K.F., D.P. Charrois (1994), Limits to the accuracy of the 10.7 cm flux, *Solar Physics*, 150, 305-315.

World Meteorology Organization (1957), Meteorology - A three-dimensional science: Second session of the commission for aerology, *WMO Bulletin*, vol. IV, no. 4, pp. 134-138.

Chapter 3

A Global Inventory of Stratospheric Chlorine

3.1 Introduction

Atmospheric profiles of ozone typically exhibit a peak in the mid-stratosphere, with their general shape resulting from the Chapman cycle [*Chapman*, 1930]:

$$O_2 + h\nu \rightarrow O + O \qquad (3.1)$$
$$O + O_2 + M \rightarrow O_3 + M \qquad (3.2)$$

$$O + O_3 \rightarrow 2O_2 \qquad (3.3)$$
$$O_3 + h\nu \rightarrow O_2 + O \qquad (3.4)$$

However, natural catalytic cycles involving active chlorine, bromine, hydrogen and nitrogen (ClO_x, BrO_x, HO_x, and NO_x) are also involved in the destruction of ozone, resulting in lower levels of ozone than would occur if the Chapman cycle were the only mechanism for ozone destruction. Over the past few decades, the emission of certain anthropogenic compounds has been causing additional destruction of stratospheric ozone, especially in the polar regions.

Since the discovery of large ozone losses over Antarctica by *Farman et al.* [1985], as well as evidence of ozone depletion over the Arctic and more populated areas at lower latitudes, stratospheric ozone depletion has been recognized as a problem warranting serious scientific investigation. The majority of ozone decline is related to the anthropogenic emission of organic chlorine and bromine compounds. The principal organic chlorine compounds, including chlorofluorcarbons (CFCs), hydrochlorofluorocarbons (HCFCs), halons and others, are chemically very stable in the troposphere where they behave as greenhouse gases, contributing to global climate change. These long-lived compounds are transported to the stratosphere and subsequently distributed through the Brewer-Dobson circulation [*Brewer*, 1949], in which tropospheric air ascends across the tropical tropopause then moves poleward at midlatitudes throughout the stratosphere. In the stratosphere, these halogenated species are photolysed by UV radiation or broken down by reaction with radicals such as $O(^1D)$, OH and Cl. As a result, chlorine monoxide (ClO) is formed which can destroy ozone via the catalytic cycle [*Molina and Rowland*, 1974; *Stolarski and Cicerone*, 1974]:

$$ClO + O \rightarrow Cl + O_2 \qquad (3.5)$$
$$Cl + O_3 \rightarrow ClO + O_2 \qquad (3.6)$$
$$\text{Net: } O + O_3 \rightarrow 2O_2 \qquad (3.7)$$

In the polar springtime when temperatures are very low, the modified catalytic cycle [*Molina and Molina*, 1987] which does not require oxygen atoms is the dominant cause of ozone destruction:

$$2\,(Cl + O_3 \rightarrow ClO + O_2) \quad (3.8)$$
$$ClO + ClO \rightarrow ClOOCl \quad (3.9)$$
$$ClOOCl + h\nu \rightarrow Cl + ClOO \quad (3.10)$$
$$ClOO + M \rightarrow Cl + O_2 + M \quad (3.11)$$
$$\text{Net: } 2O_3 \rightarrow 3O_2 \quad (3.12)$$

Additionally, cycles involving chlorine and other species such as bromine compounds are also of importance:

$$ClO + BrO \rightarrow Br + Cl + O_2 \quad (3.13)$$
$$Cl + O_3 \rightarrow ClO + O_2 \quad (3.14)$$
$$Br + O_3 \rightarrow BrO + O_2 \quad (3.15)$$
$$\text{Net: } 2O_3 \rightarrow 3O_2 \quad (3.16)$$

Each of these catalytic cycles repeats numerous times before undergoing an alternate pathway leading to conversion to a reservoir compound such as chlorine nitrate ($ClONO_2$) or hydrogen chloride (HCl). However, heterogeneous reactions on the surface of polar stratospheric clouds (PSCs) can cause temporary chlorine reservoir species such as $ClONO_2$ and HCl to react, forming active chlorine (ClO_x = Cl, ClO, and ClOOCl) and enabling the catalytic destruction of ozone. Catalytic cycles involving ClO_x are considered the primary cause of stratospheric ozone decline because the large increase in chlorine-containing compounds in the stratosphere as a result of anthropogenic emissions has greatly enhanced these cycles.

The *Montreal Protocol on Substances that Deplete the Ozone Layer* is a treaty adopted in 1987 by the international community to control the emission of substances that contribute to ozone depletion. It has been strengthened further in later years through numerous amendments. Essentially all of the most destructive ozone depleting substances such as CCl_4, CH_3CCl_3, CFCs and halons are now banned under the Montreal Protocol and its amendments. The banned compounds were largely replaced by HCFCs, which typically have shorter tropospheric lifetimes and lower ozone depleting potentials (ODPs) than CFCs, although these are also being phased out and replaced with hydrofluorocarbons (HFCs) which do not contain chlorine.

Prior to the widespread use of these ozone depleting gases only a few decades ago, total chlorine (Cl_{TOT}) in the stratosphere was equal to the natural background level of about 0.6 ppbv (parts per billion by volume) primarily due to CH_3Cl emissions from tropical plants and biomass burning, as well as algae and phytoplankton in the oceans [*WMO, 2003*]. Observations indicate that mean stratospheric Cl_{TOT} reached 3.70±0.20 ppbv around 1997 [*Sen et al.*, 1999] and has recently begun a slow decline [*Anderson et al.*, 2000; *Mahieu et al.*, 2004] as a result of the emission restrictions required by the Montreal Protocol and its amendments, but the exact date and the volume mixing ratio (VMR) of the maximum in stratospheric Cl_{TOT} are somewhat ill-defined

[*Waugh et al.*, 2001]. Most modeling studies predict that global stratospheric ozone should fully recover shortly after stratospheric chlorine declines to 2.0 ppbv [WMO, 1999; *Prather et al.*, 1990, 1996], but predictions of the date that chlorine will reach this level range from 2040 to 2070 [*Engel et al.*, 2002]. Some studies [*Austin et al.*, 1992; *Shindell et al.*, 1998] suggest that in the future, the convergence of multiple factors such as decreased stratospheric temperatures related to climate change and increased levels of stratospheric water (which have been measured in recent years, although they are not fully understood [*Oltmans et al.*, 2000; *Rosenlof et al.*, 2001; *Nedoluha et al.*, 2003; *Nassar et al.*, 2005a]) would lead to elevated levels of PSCs. This indicates that unless climate change and stratospheric chlorine are controlled simultaneously, the recovery of the Antarctic ozone layer could be delayed and the possibility of a future Arctic ozone 'hole' can not be completely ruled out [*Austin et al.*, 1992; *Shindell et al.*, 1998; *Shindell and Grewe*, 2001]. In a comparison of a number of chemistry-climate models carried out by *Austin et al.* [2002], most models did not predict a future Arctic ozone 'hole', but the larger range of predicted Arctic ozone scenarios in comparison to the Antarctic, highlights the difficulty in predicting the evolution of Arctic ozone with current models.

Until there is more certainty regarding the recovery of global stratospheric ozone, it will remain necessary to monitor ozone levels and make continual measurements of the species that contribute to stratospheric chlorine. There are currently a variety of different instruments being used to measure chlorinated species in the atmosphere using *in situ* techniques from the ground or aircraft, or remote sensing methods from the ground, aircraft, balloons or space-based platforms. *Zander et al.* [1992, 1996] determined mean stratospheric Cl_{TOT} values of 2.58±0.10 ppbv in 1985 and 3.53±0.10 ppbv in 1994 for northern hemisphere midlatitudes, primarily using measurements from the Atmospheric Trace Molecule Spectroscopy (ATMOS) instrument which flew four times on the NASA Space Shuttle (1985, 1992, 1993 and 1994). Similarly, a value of 3.70±0.20 ppbv was determined based on measurements by the balloon-borne MkIV interferometer during the Arctic summer of 1997 [*Sen et al.*, 1999]. Both of these are high-resolution infrared FTS instruments which are capable of measuring a large number of chlorinated species. The determination of total chlorine from their measurements was made by summing the chlorine contributions from all significant individual species averaged over a range of stratospheric altitudes. A similar approach was used during the Stratospheric Aerosol and Gas Experiment (SAGE) III Ozone Loss and Validation Experiment (SOLVE) campaign, in which air samples were collected from a NASA ER-2 aircraft between 10 and 21 km altitude in the 2000 Arctic winter [*Schauffler et al.*, 2003]. Laboratory analysis of the air samples gave individual VMR profiles of 15 chlorine-containing species and summing these profiles yielded a Cl_{TOT} value of about 3.6 ppbv.

HALOE on UARS has produced a record of total inorganic chlorine (Cl_y) from 1991 to 2005 based on measured values of HCl at 55 km [*Russell et al.*, 1996b; *Anderson et al.*, 2000], but has now been retired. According to the HALOE method, at 55 km altitude the ratio HCl/Cl_y is 0.93 at the equator and 0.95 at high latitudes, so measurements of HCl at a given latitude are divided by this ratio to obtain Cl_y, which has often been used as an approximation for Cl_{TOT}. *Russell et al.* [1996b] state that HCl/Cl_{TOT} is less than 1 mostly due to $CHClF_2$ (HCFC-22), one of the few

organic chlorine species known to exist in the upper stratosphere in significant amounts at that time [*Weisenstein et al.*, 1992; *Rummukainen et al.*, 1996; *Coheur et al.*, 2003]. HALOE determined Cl_y values of 3.3±0.33 ppbv in June 1995 [*Russell et al.*, 1996b] and over 3.5 ppbv in 2000 [*Anderson et al.*, 2000] which indicate that HALOE Cl_y are somewhat lower than ClTOT determined by ATMOS or MkIV at a similar time.

Although ground-based measurements provide less global coverage than satellites, a large number of sites make measurements of chlorine-containing species, which together make an important contribution to assessing chlorine levels in the atmosphere and their temporal evolution. Some of the most important sets of ground-based measurements come from the Atmospheric Lifetime Experiment, the Global Atmospheric Gases Experiment and the Advanced Global Atmospheric Gases Experiment (ALE/GAGE/AGAGE) [*Prinn et al.*, 2000], the National Oceanic and Atmospheric Administration Climate Monitoring and Diagnostics Laboratory (NOAA/CMDL) measurements [*Montzka et al.*, 1999] and the Network for the Detection of Stratospheric Change (NDSC) [*Rinsland et al.*, 2003], which has recently been renamed the Network for the Detection of Atmospheric Composition Change (NDACC). The *in situ* ALE/GAGE/AGAGE and NOAA/CMDL measurements both indicate declining levels of tropospheric chlorine, largely driven by declines in CH_3CCl_3 and CCl_4 [*Prinn et al.*, 2000]. The NDSC solar absorption measurements are used to infer total column amounts of a number of species, including HCl and $ClONO_2$. These measurements indicate that Cl_y in the lower stratosphere has been decreasing very slowly (-0.7 ±0.3%/yr, 1σ) since it peaked in late 1996 [*Mahieu et al.*, 2004].

Comparisons between measurement sets and industry-reported levels of source gas production and emission with modeling studies of chemistry and transport helps to obtain a complete understanding of the distribution and composition of chlorine species in the stratosphere, which aids in making accurate predictions about ozone recovery. In the present work, stratospheric Cl_{TOT} is calculated by taking the sum of the chlorine contribution from VMR profiles of individual chlorine-containing species measured by the Atmospheric Chemistry Experiment Fourier Transform Spectrometer (ACE-FTS), supplemented by profiles of species measured by other instruments or, in some cases, calculated profiles. Separate daytime Cl_{TOT} profiles are determined separately in five latitude zones (60-82ºN, 30-60ºN, 30ºS-30ºN, 30-60ºS and 60-82ºS) during the period of February 2004 to January 2005 inclusive. Cl_{TOT} profiles are then averaged over a range of stratospheric altitudes to obtain a value for mean stratospheric Cl_{TOT}, as in *Zander et al*. [1992, 1996]. The results of this global inventory of stratospheric chlorine can be used for comparing with other measurements as well as reported emission inventories, for assessing the effectiveness of the Montreal Protocol and for incorporating into models to predict the eventual date of recovery of the ozone layer.

3.2 Method for the Determination of Total Stratospheric Chlorine

The method for the determination of stratospheric Cl_{TOT} in this work is similar to the method of *Zander et al.* [1992, 1996] based on the sum of all significant chlorine-containing species in the

stratosphere. In the present work, total organic chlorine CCl_y, total inorganic chlorine Cl_y, and total chlorine Cl_{TOT} as a function of altitude were determined using the following summations:

$$CCl_y = 4[CCl_4] +3[CCl_3F] +2[CCl_2F_2] +[CH_3Cl] +[CHClF_2] +3[CCl_2FCClF_2] +[CH_3CClF_2] +3[\mathit{CH_3CCl_3}] + \mathit{minor\ species} \quad (3.17)$$

$$Cl_y = [HCl] +[ClONO_2] +[COClF] +[\mathit{ClO}] +2[\mathit{ClOOCl}] + [\mathit{HOCl}] +2[\mathit{COCl_2}] \quad (3.18)$$

$$Cl_{TOT} = CCl_y + Cl_y \quad (3.19)$$

CCl_y includes the source gases which comprise most of the chlorine in the troposphere and lower stratosphere. Figure 3-1 shows an example of the component profiles of CCl_y at southern midlatitudes. Cl_y consists of reservoir species and short-lived species, which dominate in the middle and upper stratosphere. Most major species in this inventory were measured by the ACE-FTS, although species shown above in italics are primarily based on data from other sources including both measurements and models. The detailed methods for obtaining profiles of all species are described in the following sections.

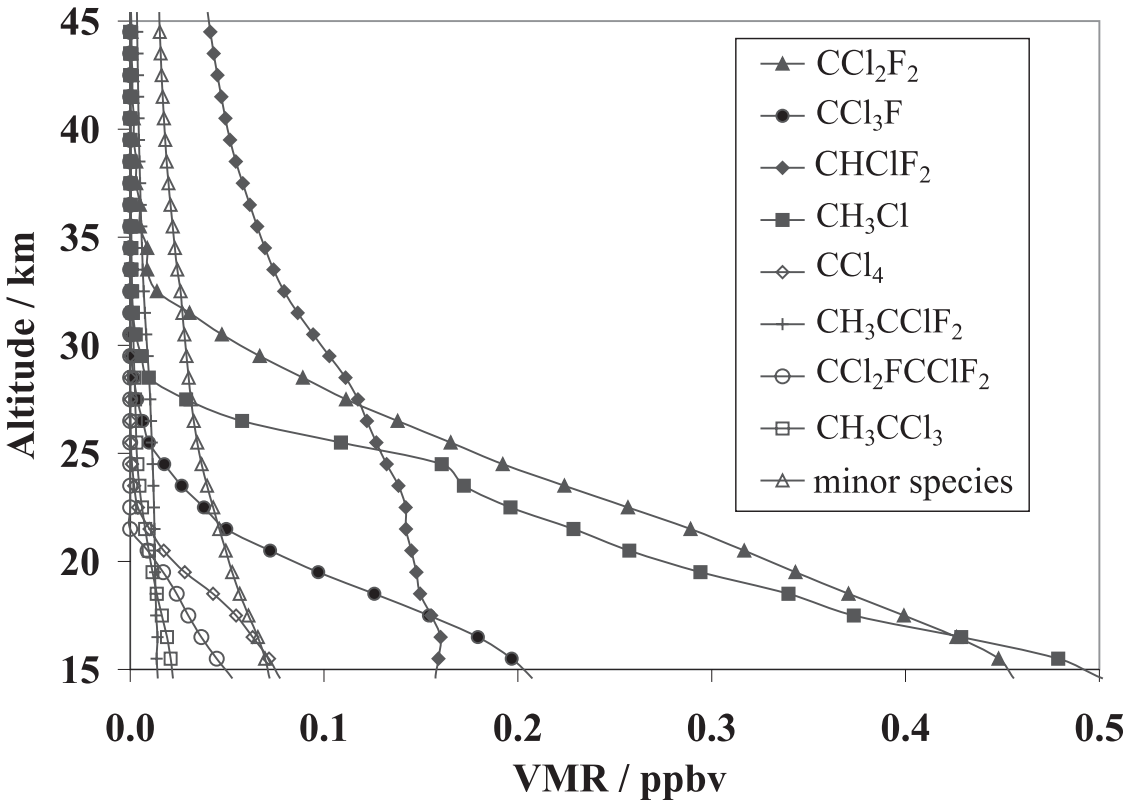

Figure 3-1: Averaged organic chlorine profiles for southern midlatitudes in 2004. Most organic chlorine species, with the exception of $CHClF_2$ (HCFC-22) are negligible above ~35 km altitude.

3.3 Chlorine-containing Species Retrieved from ACE-FTS Spectra

The altitude ranges of the microwindows used for all ACE-FTS retrieved chlorine species and the acceptable altitude range used to determine the ACE-FTS average profiles are shown in Table 3-1. In many cases, the spectral contribution from known interfering species including O_3, CH_4, H_2O, HDO and others were accounted for during the retrieval process. ACE-FTS retrieved VMR profiles are not constrained by the *a priori*; however, above the retrieval range, the *a priori* profile is scaled based on the values retrieved at the two highest points [*Boone et al.*, 2005]. If necessary, a more reliable method was found for extending individual mean VMR profiles above the retrieval range, as described later.

Since profiles of $ClONO_2$ and ClO exhibit diurnal variation, day and night profiles should not be averaged together, especially if these species are not necessarily measured at coincident locations and times. Using the longitude (λ, ranging from -180º to +180º) and universal time (UT) in hours for the reference tangent point of each occultation, local times (LT) were determined using:

$$LT = UT + (24/360)\,\lambda \quad (3.20)$$

The above equation gives the LT relative to the stated UT calendar day, so 24 hours were added or subtracted accordingly (to values less than zero or greater than 24, respectively) to determine the standard local time (SLT) relative to the diurnal cycle. It should be noted that although all ACE occultations are labeled as sunrise or sunset as seen from orbit, outside of the tropics, this label is not necessarily indicative of whether it is a sunrise or sunset at the measurement location; however, since ACE measurements only occur at twilight, measurements before local noon are sunrises and measurements after local noon are sunsets. For this chlorine inventory, only measurements taken at local sunset have been used, giving the daytime composition of the stratosphere and thus facilitating direct comparison to the ATMOS chlorine budgets [*Zander et al.*, 1992, 1996].

Table 3-2 lists the number of ACE-FTS profiles averaged for each latitude zone; however, profiles with an unphysical shape (such as noise spikes or oscillations) were discarded as outliers, so the actual number for a given species is typically lower. In addition, some profiles are also missing one or more points at the upper and/or lower end of the altitude ranges in Table 3-1, as a result of variation in the tangent heights of ACE-FTS measurements prior to interpolation to the standard grid [*Boone et al.*, 2005]. Approximately the first year of ACE-FTS measurements (February 2004 to January 2005 inclusive) was averaged to determine values for 2004, while attempting to account for seasonal variations; however, the limited coverage provided by the ACE orbit often results in periods of more than a month where no measurements are made for some latitude zones.

Table 3-1: Microwindows for chlorine species retrieved from ACE-FTS measurements.

Species	Total Range (km)	Microwindow		
		Center (cm^{-1})	Width (cm^{-1})	Range (km)
HCl	8.5 - 56.5	2701.26	0.30	8.5 - 35.5
		2703.03	0.30	35.5 - 46.5
		2727.77	0.40	8.5 - 44.5
		2751.97	0.30	47.5 - 54.5
		2775.75	0.30	40.5 - 56.5
		2798.95	0.35	51.5 - 56.5
		2819.48	0.30	20.5 - 53.5
		2821.47	0.30	18.5 - 56.5
		2841.63	0.40	20.5 - 49.5
		2843.67	0.30	15.5 - 56.5
		2865.16	0.26	38.5 - 56.5
		2906.30	0.30	45.5 - 56.5
		2923.57	0.50	20.5 - 47.5
		2923.73	0.30	44.5 - 49.5
		2925.90	0.30	17.5 - 56.5
		2942.67	0.40	15.5 - 53.5
		2944.95	0.30	10.5 - 56.5
		2961.00	0.40	25.5 - 47.5
		2963.11	0.50	8.5 - 56.5
		2981.00	0.50	40.5 - 56.5
		2995.88	0.30	45.5 - 50.5
		2998.14	0.30	52.5 - 56.5
$ClONO_2$	12.5 - 34.5	780.15	0.60	12.5 - 19.5
		1202.86	0.50	12.5 - 17.5
		1292.60	1.60	18.5 - 34.5
		1728.28	0.50	12.5 - 17.5
COClF [a]	17/19 - 30	1860.35	0.70	17/19 – 30
		1862.55	1.30	17/19 – 30
		1864.30	0.60	17/19 – 30
		1865.45	1.10	17/19 – 30
		1866.80	0.40	17/19 – 30
		1868.80	0.60	17/19 – 30
		1870.575	0.35	17/19 – 30
		1874.95	0.90	17/19 – 30
ClO [b]	12.5 - 24.5	823.475	5.00	11.5 - 29.5
		828.475	5.00	11.5 - 29.5
		833.475	5.00	11.5 - 29.5
		838.475	5.00	11.5 - 29.5
		843.475	5.00	11.5 - 29.5
CH_3Cl	9.5 - 24.5	2966.50	0.40	9.5 - 24.5
		2966.90	0.40	9.5 - 24.5
		2967.30	0.70	9.5 - 24.5
CCl_4	8.5 - 22.5	799.85	11.00	8.5 - 22.5
CCl_3F (CFC-11)	5.5 - 21.5	842.50	25.00	5.5 - 21.5
CCl_2F_2 (CFC-12)	6.5 - 27.5	922.00	4.00	6.5 - 27.5
		1161.00	1.20	12.5 - 24.5
$CHClF_2$ (HCFC-22)	5.5 - 24.5	809.30	1.10	5.5 - 14.5
		820.85	0.70	5.5 - 11.5
		829.03	0.50	5.5 - 24.5
CCl_2FClF_2 (CFC-113)	7.5 - 16.5	817.50	25.00	7.5 - 16.5
CH_3CClF_2 (HCFC-142b)	8.5 - 18.5	1134.50	4.00	8.5 - 18.5
		1193.60	3.60	8.5 - 18.5

[a] Special circumstances for the retrieval of COClF are outlined in the text.
[b] ACE-FTS ClO retrieval only used for southern high latitudes over a reduced altitude range.

Table 3-2: Number of profiles averaged for each latitude range between February 2004 and January 2005 inclusive.

	Maximum ACE-FTS profiles	**Odin SMR ClO profiles**
Northern high latitudes (60-82ºN)	63	72
Northern midlatitudes (30-60ºN)	131	58
Tropics (30ºS-30ºN)	170	157
Southern midlatitudes (30-60ºS)	180	22
Southern high latitudes (60-82ºS)	135	38

3.3.1 Organic Species: CH_3Cl, CCl_3F, CCl_2F_2, CCl_2FClF_2, CH_3CClF_2, CCl_4 and $CHClF_2$

Profiles of methyl chloride (CH_3Cl), CFC-11 (CCl_3F), CFC-12 (CCl_2F_2), and HCFC-22 ($CHClF_2$) were retrieved using the ACE-FTS version 2.2 retrieval algorithm which is described in *Boone et al.* [2005]. CFC-113 (CCl_2FClF_2), HCFC-142b (CH_3CClF_2) and carbon tetrachloride (CCl_4) were specially retrieved for this work. The ACE-FTS retrievals of CCl_2FClF_2 and CH_3CClF_2 used in this work are the first retrievals of these two species from space-borne measurements [*Dufour et al.*, 2005].

In the troposphere and lower stratosphere CCl_y species dominate Cl_{TOT}, with the largest contributions from CH_3Cl (the only significant natural source of organic chlorine), CCl_2F_2, and CCl_3F. From the surface up to the middle stratosphere, CCl_2F_2 with two chlorine atoms, makes the largest contribution to Cl_{TOT} of all CCl_y species. $CHClF_2$ (HCFC-22) is only the fourth largest organic chlorine species in the upper troposphere, but in the middle and upper stratosphere it is long-lived and is the dominant CCl_y species.

The ATMOS and MkIV chlorine budgets [*Zander et al.*, 1992, 1996; *Sen et al.*, 1999] did not include $CHClF_2$ in the upper stratosphere because its VMR was below their detection limits; however, *Weisenstein et al.* [1992] have shown that it exists in the upper stratosphere in significant quantities. Their modeled value in the upper stratosphere was based on the surface value in 1985, but in a more recent work by *Coheur et al.* [2003], a profile of $CHClF_2$ is determined with the global three dimensional chemical transport model SCTM-1 [*Rummukainen et al.*, 1996]. The SCTM-1 model output for 1 January 2000, 00:00 UT, at 45ºN, 90ºE is shown in Figure 3-2. This profile was scaled by a factor of 1.062 based on a comparison of ACE-FTS average midlatitude measured value of $CHClF_2$ in 2004 and their modeled value from 2000 at 19.5 km. The profile was very similar to (yet much smoother than) the retrieved northern and southern midlatitude profiles over the 17.5-24.5 km range. The scaled profile was grafted onto both midlatitude profiles above the range of ACE-FTS retrievals (beginning at 25.5 km). For northern high latitudes, the scaled midlatitude profile was shifted down by 5 km before grafting it to the ACE-FTS measurements. The need for this shift results from descent in the winter Arctic vortex [*Nassar et al*, 2005] contributing to the annual average profile for northern high latitudes. The southern high latitude profile showed much more descent than the north, so it was necessary to shift the midlatitude profile down by 10 km to coincide with the ACE-FTS measurements. Similarly, an upward by 10

km was required to coincide with the ACE-FTS tropical measurements. These ACE-FTS profiles and the scaled and shifted SCTM-1 profiles are shown in Figure 3-2. The application of shifts to the $CHClF_2$ profiles depending on their latitude is qualitatively consistent with the latitudinal distribution of $CHClF_2$ in 1985 modeled by *Weisenstein et al*. [1992], although their model results showed a more symmetrical relationship between the northern and southern hemispheres. While some of the hemispheric asymmetry in the measured high latitude profiles is likely real, much of it can be attributed to the lack of complete seasonal coverage at high latitudes due to the ACE orbit and the exclusion of local sunrises.

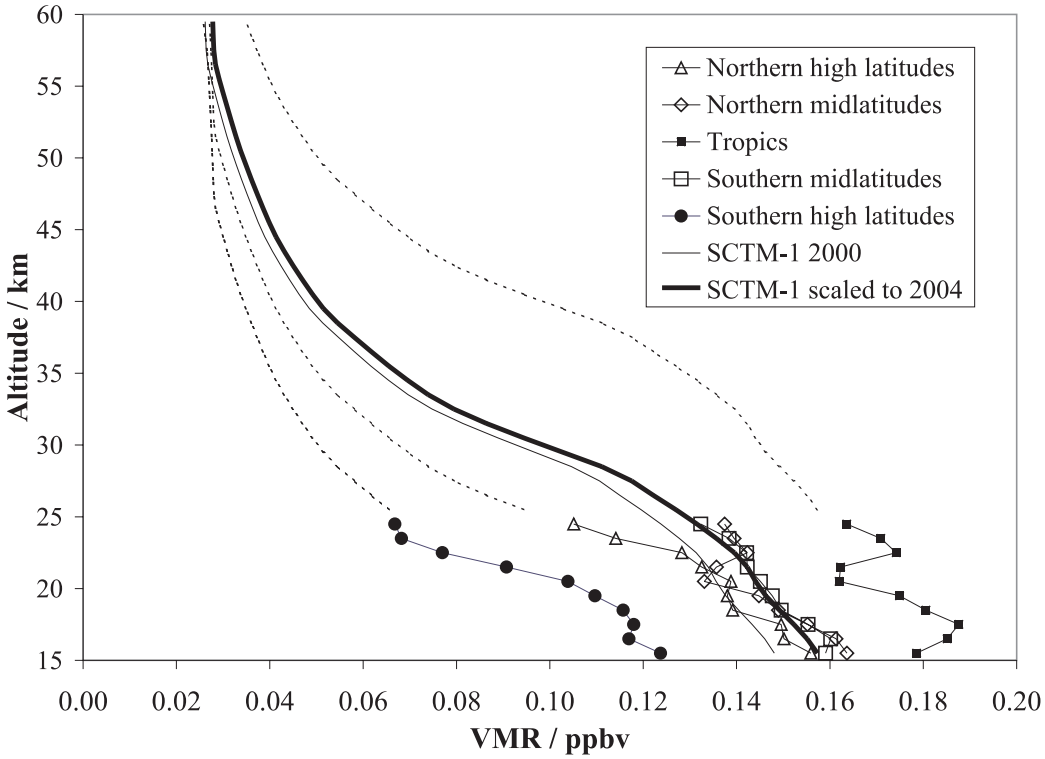

Figure 3-2: $CHClF_2$ (HCFC-22) profiles in the stratosphere: the SCTM-1 model for 45ºN in 2000 (thin line), the SCTM-1 profile scaled to 2004 (thick line) and the ACE-FTS measured values in each latitude range. The scaled and shifted SCTM-1 profiles for extending the ACE-FTS measurements to higher altitudes are shown as dotted lines.

3.3.2 Inorganic Species: HCl, $ClONO_2$, COClF and ClO

HCl exhibits a nearly constant increase with altitude throughout the stratosphere. It is the dominant chlorine species in the middle and upper stratosphere, representing about 96-98% of total chlorine at 55 km. The profile of $ClONO_2$ approximates a Gaussian distribution with a peak ranging from 23.5 km at southern high latitudes to 28.5 km in the tropics. At its peak, $ClONO_2$ typically accounts for ~25% of the chlorine budget. The profiles of HCl and $ClONO_2$ were taken from ACE-FTS version 2.2 data.

COClF results from the breakdown of CCl_3F, so it has a peak in the lower to middle stratosphere [*Kaye et al.*, 1991]. Retrievals of COClF involving averaged ACE-FTS spectra have produced some promising early results [*Rinsland et al.*, 2006]; however, a routine operational retrieval has not been developed at the time of this writing. The tropical and midlatitude COClF profiles in this work were based on the *Rinsland et al.* [2006] retrieval using ACE-FTS measurements. The lower altitude limit for COClF in those retrievals is 19 km for tropical occultations and 17 km for midlatitudes, while the upper altitude limit is 30 km. Their dates and latitude zones were similar but did not exactly match the zones used for other species in this work. In spite of this discrepancy, a tropical COClF profile was included based on the 20ºS-20ºN zone and both the northern and southern midlatitude profiles were based on the 30ºN-50ºN zone, using occultations spanning 2004 to 2005. The signal-to-noise ratio for COClF is low and since the peak VMR value decreases with latitude, a high latitude profile for COClF was not retrieved in *Rinsland et al.* [2006], so high latitude profiles were based on the model results of *Kaye et al.* [1991] scaled to 2004 based on the change in stratospheric abundance of CCl_3F [*WMO*, 2003].

The production of COClF modeled by *Kaye et al.* [1991] is based on the thermodynamic assumption that in CFCs, all C-Cl bonds break before C-F bonds and for HCFCs, C-H bonds break first, followed by C-Cl bonds, then C-F bonds. This implies that CCl_2F_2 will break down to form COF_2 and that CCl_3F will break down to form COClF as follows:

$$CCl_3F + h\nu \rightarrow CCl_2F + Cl \qquad (3.21)$$
$$CCl_2F + O_2 + M \rightarrow CCl_2FO_2 + M \qquad (3.22)$$
$$CCl_2FO_2 + NO \rightarrow CCl_2FO + NO_2 \qquad (3.23)$$
$$CCl_2FO + O_2 \rightarrow COClF + ClOO \qquad (3.24)$$
$$COClF + h\nu \rightarrow Cl + COF \qquad (3.25)$$

The removal of COClF by $O(^1D)$ was also accounted for in the work by *Kaye et al.* [1991], as they modeled COClF at a range of latitudes and different times of the year in 1989. COClF only makes a small contribution to Cl_{TOT}, with a peak in the profile of ~0.10 ppbv in the tropics (less than 3% of Cl_{TOT} at that altitude), ~0.05 ppbv at midlatitudes and ~0.02 ppbv at high latitudes, so its accuracy has a small impact on Cl_{TOT}, but in the future, it would be desirable to carry out a routine operational ACE-FTS COClF retrieval, as was done for other species.

ClO has a single peak in the upper stratosphere for most seasons and latitudes but is enhanced in the winter polar vortices causing a second highly-variable peak in the lower stratosphere. In the upper stratosphere, it can comprise close to 20% of Cl_{TOT}. Since the signal-to-noise ratio for ClO in ACE-FTS spectra is usually very low, most of the ClO measurements used in this work are from the Sub-Millimeter Receiver (SMR) [*Urban et al.*, 2005] on the Odin satellite [*Murtagh et al.*, 2002], just as *Zander et al.* [1996] used ClO measurements from the Millimeter-wave Atmospheric Sounder (MAS) [*Hartmann et al.*, 1996; *Aellig et al.*, 1996] for the ATMOS chlorine budget. Version 1.2 SMR ClO profiles were obtained for the period of February 2004 to

January 2005 inclusive, to match the temporal range of the ACE-FTS measurements. From the SMR dataset, only measurements with a solar zenith angle between 88-92º and made during local sunset were chosen. The latitudes for the SMR data were selected to match the ACE-FTS mean latitudes in the five latitude zones, 71±2º for high latitudes, 45±1º for midlatitudes and 15±2º for the tropics (assuming symmetry about the equator). Since all ACE-FTS southern high latitude daytime measurements occurred during the southern hemisphere winter months, SMR ClO profiles were selected for this date range rather than using data with full seasonal coverage.

The SMR profiles were interpolated to the ACE-FTS 1-km grid using a cubic spline interpolation, then averaged in each latitude zone. The number of SMR profiles included in each average is shown in Table 3-2. Profiles with unphysical shapes were discarded as outliers, as was done with the ACE-FTS data. In a few cases, an unphysical increase in SMR ClO profiles above 51.5 km was manually removed, but this is above the range of altitude considered in the calculation of stratospheric Cl_{TOT}. This lower mesospheric increase has recently been identified as an artifact in version 1.2 of the SMR data and has apparently been corrected in SMR version 2.0 data (*D.P. Murtagh*, private communication, 2006).

At southern high latitudes in the 12.5-24.5 km range, strong ClO enhancement was measured by the ACE-FTS. Since lower stratospheric ClO enhancement is extremely variable, these measurements have been used so that the ClO profiles are properly matched to those of other species. The ACE-FTS ClO retrievals are somewhat noisy but averaging 119 southern high latitude profiles produced a smooth result. Weak ClO enhancement is observed for northern high latitudes, but since the signal-to-noise ratio is still low, the SMR profiles were used rather than ACE-FTS measurements in this altitude range.

3.4 Chlorine-containing Species Not Measured by the ACE-FTS

Some species that contribute to stratospheric chlorine were not measured by the ACE-FTS, so they have been included in this inventory based on measurements by other instruments, model values or estimates as described in the following subsections.

3.4.1 Organic Species: CH_3CCl_3 and Minor CFCs, HCFCs and Halons

CH_3CCl_3 and a number of minor organic chlorine species make a small contribution to Cl_{TOT} in the stratosphere. Measurements from the SOLVE campaign [*Schauffler et al.*, 2003] were used to estimate profiles of CH_3CCl_3, $CClF_2CClF_2$ (CFC-114), CCl_2FCF_3 (CFC-114a) CCl_2FCF_3 (CFC-115), CH_3CCl_2F (HCFC-141b) and $CBrClF_2$ (Halon-1211). Empirical equations for the SOLVE VMR profiles of the chlorine contribution from these species were provided on an N_2O scale [*Schauffler et al.*, 2003], as shown in Figure 3-3. These were converted to an altitude scale using ACE-FTS retrieved mean N_2O profiles from each of the five latitude zones then the profiles of each chlorine-containing species were multiplied by a scale factor to account for the changes in abundance which occurred between 2000 and 2004. Scaling was carried out using the ratio

between the 2004 to 2000 surface values in Table 1-16 of *WMO* [2003]. The profiles should theoretically scale without significant changes to their shapes since their stratospheric VMRs were increasing or decreasing at an approximately constant rate in 2000 which was at least 4 years before (or after) the year of maximum VMR for any of these species.

The SOLVE profiles were only valid over the 50-315 ppbv N_2O range [*Schauffler et al.*, 2003], where 50 ppbv corresponds to an altitude of ~23.5 km at southern high latitudes and ~39.5 km in the tropics. CFC-114a and Halon-1211 were negligible above this altitude. The HCFC-141b and CFC-115 profiles appeared satisfactory above this altitude range, each with only a small contribution in the upper stratosphere. Since CH_3CCl_3 is expected to completely break down in the stratosphere [*Weisenstein et al.*, 1992], the CH_3CCl_3 profiles were manually extrapolated to smoothly reach zero VMR above the measured altitude range.

At 17.5 km in altitude, CH_3CCl_3 contributes between 0.015 ppbv chlorine at southern high latitudes and 0.08 ppbv chlorine in the tropics (0.4-2.2% respectively). The combined total chlorine contribution from the other species at 17.5 km is 0.04 ppbv at southern high latitude and 0.08 ppbv in the tropics and decreases to just over 0.01 ppbv at the top of the stratosphere, with the largest contributions from the minor species due to CFC-114 and HCFC-141b. When all of these species are combined, their contribution to Cl_{TOT} is significant, but errors of 20-30% on any individual species would make a very small change to Cl_{TOT}; therefore, although an accurate estimate of profiles for each of these minor species was sought, it is not critical to main objective of this chapter.

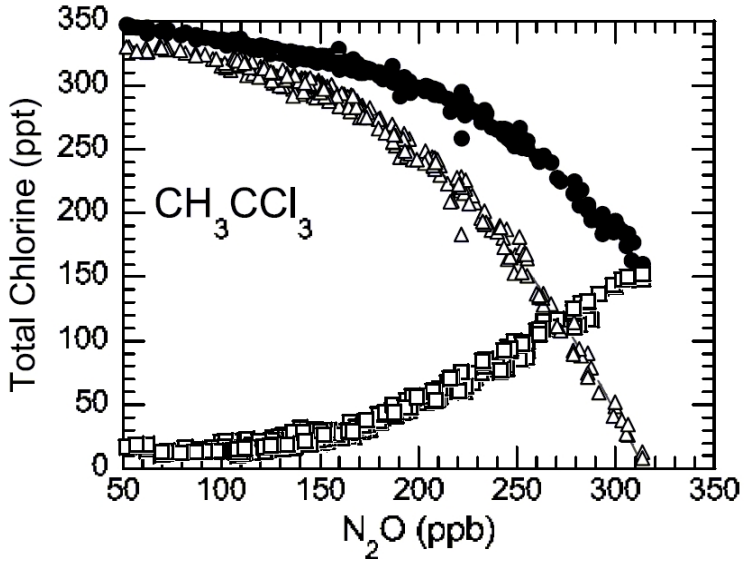

***Figure 3-3*:** The organic chlorine contribution from CH_3CCl_3 (open squares) from measurements of SOLVE samples, the calculated inorganic chlorine contribution (open triangles), and calculated expected total chlorine contribution (solid circles) relative to N_2O mixing ratios. This figure was reproduced directly from *Schauffler et al.* [2003].

3.4.2 Inorganic Species: HOCl, $COCl_2$ and ClOOCl

Efforts to retrieve HOCl from ACE-FTS spectra are in progress; however, *von Clarmann et al.* [2006] have retrieved HOCl from MIPAS spectra, so these profiles are the basis for the HOCl profiles in this chorine inventory. Since their work indicates that HOCl exhibits a small diurnal variation, and the selected ACE-FTS measurements are at sunset, a day-night average of their profiles has been used which was manually extrapolated to 54 km to obtain a smooth transition to zero, since the actual profiles abruptly end at 50 km. The work of *von Clarmann et al.* [2006] indicates latitudinal variation in HOCl with the altitude of the maximum 2.2±0.3 km lower for the 45ºN-45ºS latitude zone than for the more poleward latitudes of 45-90º in each hemisphere. This is a 2.2 km shift for a change in mean latitude from 22.5º to 67.5º, or 0.0488 km per degree. To account for latitudinal variability in both the altitude and value of the maximum VMR, scale factors and shifts were applied to the mean (day-night) 30ºN profile. The resulting HOCl profiles make a maximum contribution to Cl_{TOT} of 0.192 ppbv (~5.3%) at 35.5 km for the tropics, 0.167 ppbv (~4.6%) at 36.5 km for midlatitudes, and 0.098 ppbv (~2.6%) at 37.5 km for high latitudes.

The retrieval of phosgene ($COCl_2$) from ACE-FTS spectra has not yet been attempted. It is very difficult to retrieve because its spectral lines are buried in the stronger spectrum of CCl_3F. $COCl_2$ was not included in the chlorine budgets based on ATMOS [*Zander et al.*, 1992, 1996] or MkIV measurements [*Sen et al.*, 1999]; however, it has since been successfully retrieved from MkIV balloon-borne infrared solar occultation spectra by *Toon et al.*, [2001]. A line of best fit was drawn through the MkIV points in the 6-30 km range measured between September 1992 and March 2000. The $COCl_2$ profile was included directly (without scaling or shifting) in each of the five latitude zones since no clear latitudinal shift can be determined from the data, and only a very small temporal change would be expected from this species which makes only a very minor contribution to total stratospheric chlorine (a maximum of ~0.065 ppbv Cl at 20 km).

The ClO dimer (ClOOCl) only occurs in significant quantities in the polar vortices, where it exists in equilibrium with ClO. Although no known remote measurements of ClOOCl were found, *Stimpfle et al.* [2004] have made *in situ* measurements in the Arctic vortex from a NASA ER-2 aircraft during the SOLVE/THESEO-2000 campaign. More recently, *von Hobe et al.* [2005] made *in situ* aircraft measurements during the SOLVE II/VINTERSOL-EUPLEX and ENVISAT validation campaigns using the HALOX instrument. The measurements by *Stimpfle et al.* [2004] confirm the basic mechanism for loss and production of ClOOCl (equations 3.22-3.24) but indicate some uncertainty in the rate constants.

$$ClO + ClO + M \xrightarrow{k^{prod}} ClOOCl + M \qquad (3.26)$$

$$ClOOCl \xrightarrow{j} ClO + ClO \qquad (3.27)$$

$$ClOOCl + M \xrightarrow{k^{loss}} ClO + ClO + M \qquad (3.28)$$

Using these reactions and solving the rate law, a relationship for the expected ClOOCl profile can be determined from the profile of ClO and the appropriate values of the rate constants for ClOOCl production (k^{prod}), loss by thermal decomposition (k^{loss}) and loss by photolytic decomposition (j).

$$\frac{d[ClOOCl]}{dt} = k^{prod}[ClO]^2[M] - j[ClOOCl] - k^{loss}[M][ClOOCl] = 0 \quad (3.29)$$

$$k^{prod}[ClO]^2[M] = (j + k^{loss}[M])[ClOOCl] \quad (3.30)$$

$$K_{eq} = \frac{[ClOOCl]}{[ClO]^2} = \frac{k^{prod}[M]}{j + k^{loss}[M]} \quad (3.31)$$

Stimpfle et al. [2004] recommend combinations of the above three rate constants that give results consistent with their observations. The value of the photolysis rate constant (j) used here, is the value determined in *Stimpfle et al.* [2004] based on cross sections determined by *Burkholder et al.* [1990] shown in *Stimpfle et al.* [2004] as a function of solar zenith angle (SZA). Since all ACE-FTS measurements occur at a SZA of 90º, a value of $j = 4.4 \times 10^{-4}$ s^{-1} at a SZA = 90º was used in this work. k^{loss} is determined from the empirical equation $k^{loss}(T) = 9.81 \times 10^{-7} \exp(-7980/T)$ $molecules^{-1}$ cm^3 s^{-1} from *Nickolaisen et al.* [1994] and $k^{prod}(T) = 1.49 \times 10^{-32} (T/300)^{-4.50}$ $molecules^{-2}$ cm^6 s^{-1} from *Bloss et al.* [2001]. (The uncertainties for both rate constants have been ignored in this approximation of the ClOOCl concentration.)

Using the above rate constants, the ratio $k^{prod}[M]/(j + k^{loss}[M])$ was then calculated using ACE-FTS retrieved values of temperature and density for each high latitude profile. Since ACE-FTS individual ClO profiles tend to be noisy, the ratio of constants for each profile was applied to the averaged ClO profile to calculate ClOOCl profiles. From the individual ClOOCl profiles, an average profile is calculated over the altitude range of 12.5-26.5 km where ClO enhancement is observed at high latitudes in each hemisphere.

3.5 Results

Mean profiles for each latitude zone of all chlorine containing species in the previous section are given in Appendix 2. The chlorine contribution based on species measured by the ACE-FTS varies with altitude, although for the northern midlatitudes at 17.5 km where CCl_y dominates, 87% of the chlorine comes from species measured by the ACE-FTS. The percentage gradually decreases to 80% between 37.5-40.5 km, then gradually increases up to almost 98% above 54.5 km, where nearly all chlorine is contained in HCl. Figure 3-4 shows profiles of CCl_y, HCl, $ClONO_2$, ClO, and a combined profile for the chlorine contribution from HOCl, $COCl_2$, COClF and ClOOCl, between 15 and 55 km altitude. It indicates that total chlorine is nearly constant throughout this altitude range. *Zander et al.* [1996] determined mean Cl_{TOT} by averaging all points in the 16.4-50.2 km

altitude range which was intended to span the stratosphere for the northern midlatitudes or subtropics in November. The positions of the tropopause and stratopause exhibit large seasonal and latitudinal variations such that the lapse rate definition of the tropopause recommended by the WMO often places the tropopause as low as ~6-8 km during winter near the poles. In this work, mean stratospheric Cl_{TOT} for each latitude zone was based on points between 17.5 km and 50.5 km altitude, which are close to the positions of the local minima and maxima in mean ACE-FTS temperature profiles. One can argue that this altitude range is too high, therefore, not the best representation of the stratosphere for high latitudes, but it was chosen in part to avoid the large deviation from linearity seen in the Cl_{TOT} profile at southern high latitudes, which will be discussed later.

Stratospheric Cl_{TOT} values for 2004 are shown in Table 3-3 and the mean Cl_{TOT} values are shown in Table 3-4. The method of error determination used by *Zander et al.* [1996] based on the standard deviation of points over a given altitude range was adopted here and should give a reasonable estimate of the precision of mean Cl_{TOT}. Propagating the uncertainty on each species to obtain the uncertainty on total chlorine would largely overestimate the overall uncertainty because the variability in any given species is mostly a result of conversion to another species. Furthermore, it is difficult to make accurate estimates of the uncertainty for the modeled data. Perhaps the best simple estimate of the absolute uncertainty on Cl_{TOT} can be made based on the uncertainty of HCl at high altitudes, where it is the dominant contributor to Cl_{TOT}. The retrieval of HCl utilized spectroscopic parameters from the HITRAN 2004 database [*Rothman et al.*, 2005]. The HCl line intensities in HITRAN that lie in the microwindows shown in Table 3-1, have uncertainties in the 1-2% range, which translates to a maximum of 0.08 ppbv. The uncertainty contribution to the VMR of HCl from the retrieval of pressure and temperature is also estimated to be about 2% or about 0.08 ppbv. An additional source of uncertainty for the HCl retrieval comes from the precision of the fit, which reaches a maximum at high altitudes, although this random error is reduced by averaging multiple profiles. The 1σ error contribution from the precision of the fit for the southern midlatitude mean profile, which had the highest number of profiles used to determine its mean, is only 0.003 ppbv at 18 km, and increases to 0.04 ppbv (or 1.1%) at 50 km, while for the northern high latitude mean profile, which used the fewest profiles, the precision is 0.06 ppbv (or 1.7%) at 50 km. Combining these three sources of error gives an accuracy of 0.12-0.13 ppbv for HCl at 50 km, which includes both a systematic and random component. This value can be used to estimate the accuracy of the Cl_{TOT} values. Since HCl comprises 93% of Cl_{TOT} at 50 km (at midlatitudes), scaling the error would give an accuracy of 0.13-0.14 ppbv for Cl_{TOT}, which is equivalent to less than 4% of mean Cl_{TOT}. This uncertainty is smaller than the estimated precision from random variability in the HCl mean values at 50 km, but slightly greater than the variability of 0.09 ppbv in the midlatitude Cl_{TOT} profile over the 17.5-50.5 km range. Although the variability in the Cl_{TOT} profiles in some other latitude zones was larger than at midlatitudes, the accuracy should be comparable.

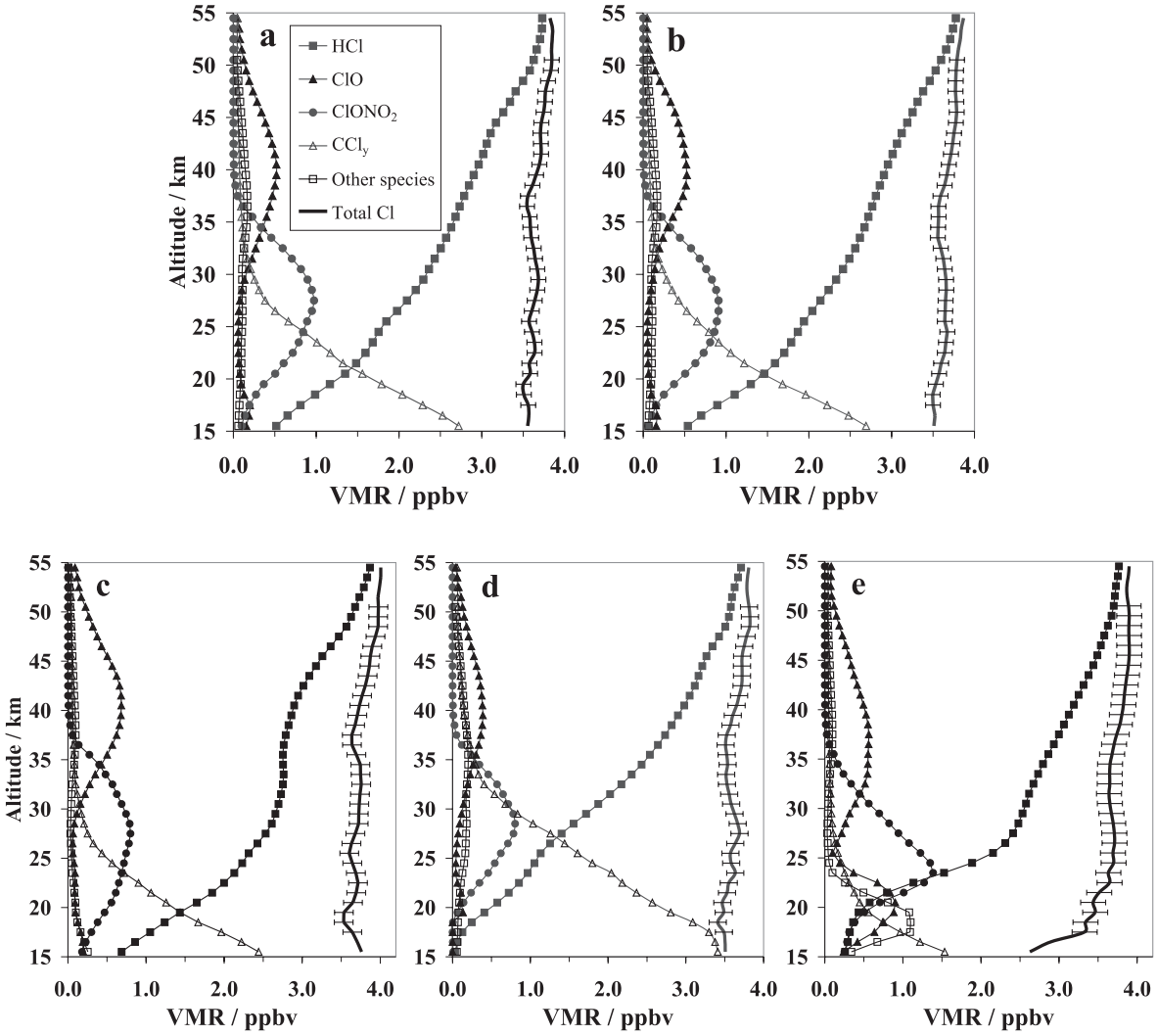

***Figure 3-4*:** Stratospheric chlorine inventories for 2004: (a) northern midlatitudes (30-60ºN), (b) southern midlatitudes (30-60ºS), (c) northern high latitudes (60-82ºN), (d) tropics (30ºS-30ºN), and (e) southern high latitudes (60-82ºS), showing VMR profiles for HCl (shaded squares), ClO (shaded triangles), $ClONO_2$ (shaded circles), the combined chlorine contribution from CCl_y (open triangles) and the combined chlorine contribution from "Other species" comprised of HOCl, COClF, $COCl_2$, and ClOOCl (open squares) and Cl_{TOT} (thick line). Error bars indicating the 1σ precision are included on the total chlorine profiles for the 17.5-50.5 km range.

***Table 3-3*:** Cl_{TOT} as a function of altitude from 17.5 to 50.5 km in five latitude zones for the period of February 2004 to January 2005 inclusive.

Altitude / km	Total Chlorine / ppbv				
	60-82ºN	**30-60ºN**	**30ºS-30ºN**	**30-60ºS**	**60-82ºS**
17.5	3.64	3.56	3.49	3.50	3.33
18.5	3.53	3.51	3.41	3.50	3.34
19.5	3.53	3.50	3.49	3.53	3.46
20.5	3.65	3.58	3.47	3.57	3.44
21.5	3.69	3.57	3.53	3.60	3.51
22.5	3.71	3.64	3.55	3.64	3.65
23.5	3.69	3.63	3.64	3.65	3.63
24.5	3.64	3.61	3.58	3.67	3.70
25.5	3.60	3.57	3.57	3.64	3.69
26.5	3.63	3.60	3.64	3.65	3.71
27.5	3.68	3.64	3.69	3.65	3.71
28.5	3.72	3.67	3.67	3.66	3.69
29.5	3.72	3.68	3.63	3.66	3.67
30.5	3.73	3.67	3.58	3.64	3.65
31.5	3.74	3.64	3.56	3.62	3.64
32.5	3.76	3.63	3.53	3.59	3.65
33.5	3.75	3.60	3.52	3.56	3.65
34.5	3.74	3.59	3.54	3.56	3.65
35.5	3.69	3.58	3.53	3.57	3.68
36.5	3.64	3.55	3.51	3.56	3.70
37.5	3.63	3.56	3.53	3.59	3.74
38.5	3.68	3.61	3.57	3.64	3.78
39.5	3.71	3.65	3.60	3.67	3.80
40.5	3.73	3.69	3.65	3.69	3.82
41.5	3.77	3.72	3.68	3.72	3.84
42.5	3.81	3.71	3.72	3.74	3.85
43.5	3.84	3.71	3.72	3.75	3.87
44.5	3.86	3.72	3.72	3.77	3.89
45.5	3.87	3.75	3.72	3.78	3.90
46.5	3.90	3.76	3.75	3.78	3.90
47.5	3.94	3.77	3.78	3.77	3.89
48.5	3.97	3.80	3.82	3.77	3.89
49.5	3.97	3.83	3.82	3.78	3.90
50.5	3.98	3.84	3.81	3.79	3.89

If the points in the 17.5-50.5 km altitude range are fit to a straight line, in all cases, they yield a slight positive slope in ppbv/km. These slopes and the associated 1σ precision on each slope, as a result of the fit, are also shown in Table 3-4 and discussed in the next section. No estimate of the absolute accuracy on the slopes has been made.

***Table 3-4*:** Mean total chlorine with 1σ precision and the slope (ppbv/km) with 1σ standard precision for the points from 17.5-50.5 km altitude in five latitude zones.

	Mean Cl_{TOT} (ppbv)	**slope (ppbv/km)**
Northern high latitudes (60-82ºN)	3.74 ± 0.12	0.010 ± 0.001
Northern midlatitudes (30-60ºN)	3.65 ± 0.09	0.007 ± 0.001
Tropics (30ºS-30ºN)	3.62 ± 0.11	0.009 ± 0.001
Southern midlatitudes (30-60ºS)	3.65 ± 0.09	0.007 ± 0.001
Southern high latitudes (60-82ºS)	3.71 ± 0.16	0.014 ± 0.001

3.6 Discussion

A principal improvement of the present chlorine inventory with respect to most earlier studies is that the ACE-FTS measures a large number of species relative to other satellite instruments but also provides better global coverage than aircraft, balloon or ground-based measurements. The altitude coverage and vertical resolution of the ACE-FTS measurements are also better than those of ground-based measurements; however, the small number of measurements per day is a significant disadvantage of solar occultation relative to other observation techniques. ACE is often lacking measurements in a particular latitude zone for periods of one month or more. In this work, roughly fifty percent of measurements were also neglected in order to avoid averaging over diurnal variability. The seasonal distribution of ACE profiles used at some latitudes means that ACE and SMR coincidences do not occur frequently enough to properly match profile by profile and annually averaged ACE-FTS profiles have simply been matched with those of SMR (which obtains better seasonal and global coverage), except at southern high latitudes, where only profiles from the same time period were used so that ClO and other species would be properly anti-correlated with respect to seasonal variability.

The missing chlorine indicated by the deviation from linearity in the southern high latitude Cl_{TOT} profile from ~15-21 km may be the result of some HCl or other chlorine species dissolved or frozen in PSCs, since this inventory was only dealing with measurements of species in the gas phase, but this explanation has not been verified quantitatively. Some portion of the low altitude deviation may also result from the calculated value of ClOOCl, either due to the amplification of errors in ClO affecting the ClOOCl value or errors in the rate constants. Although the values of these rate constants used were those suggested by *Stimpfle et al.* [2004], which give ClOOCl values that compare well with *in situ* measurements, *Von Hobe et al.* [2005], *Berthet et al.* [2005] and *Boakes et al.* [2005] all show that the correct values for these rate constants and the resulting equilibrium constant are still the subject of debate. The revised value of K_{eq} suggested by *Boakes et al.* [2005] indicates that ClOOCl may be more abundant than prior studies suggest, which would reduce the deviation from linearity in the southern hemisphere high latitude Cl_{TOT} profile. Smaller deviations from a straight line in total chlorine profiles may be related to very short-lived (VSL) species such as CH_2Cl_2, $CHCl_3$, and C_2Cl_4; or transient species such as Cl, Cl_2, and OClO which have not been included in this inventory, but may also make a small contribution. For example, daytime OClO can contribute approximately 0.010 ppbv [*Canty et al.*, 2005] to Cl_{TOT} at certain altitudes near the poles.

The slopes in Table 3-4 can primarily be attributed to changes in chlorine VMR which occur during the lag time necessary for transport, with a higher value of total chlorine in older air at higher altitudes indicating that the stratospheric peak in total chlorine has already past. This result is qualitatively consistent with the lowest total chlorine values occurring in the tropics and the highest at high latitudes due to the Brewer-Dobson circulation. Although the direction these slopes are reasonable, the absolute accuracy of the slopes is likely low and a proper quantitative check of their validity would require modeling of stratospheric transport.

This chlorine inventory has shown that near the stratopause, HCl accounts for the majority of Cl_{TOT}. The Earth Observing System Microwave Limb Sounder (EOS-MLS) is a second generation MLS instrument on the NASA Aura satellite that was launched in July 2004 and measures a variety of atmospheric species including HCl. Comparisons have been made between the EOS-MLS (version 1.5) and ACE-FTS HCl data (version 2.1) by *Froidevaux et al.* [2006a]. Based on 623 near-coincident profiles, the agreement between the two instruments was typically much better than 5% from 100 hPa to about 1 hPa, above which point ACE-FTS values appear about 5-8% higher. More recent comparisons between MLS and ACE-FTS version 2.2 data using 1019 coincident profiles, give a similar result (Figure 3-5), indicating perhaps even better agreement in the middle and lower stratosphere. Possible causes for a slightly larger difference at high altitudes are currently under investigation.

McHugh et al. [2005] found that ACE-FTS HCl (version 1.0) abundances are 10 to 20% larger than those from HALOE, based on a more limited sampling of 32 coincident profiles, mostly in July 2004. MLS HCl values are also high relative to HALOE by about 0.2 to 0.4 ppbv (~10 to 15%) for roughly the same time period and latitudes used in the ACE-FTS and MLS comparisons [*Froidevaux et al.*, 2006a]. The absolute accuracy of HALOE HCl reported by *Russell et al.* [1996b] is 12-24% depending on altitude, so given this wide margin of error, ACE-FTS and MLS results can be considered consistent with those of HALOE. The exact cause of the systematic difference with HALOE is not yet known, but there were early indications that HALOE HCl measurements were low relative to other observations [*Russell et al.*, 1996a, 1996b], as well as evidence from more recent comparisons [*Barret et al.*, 2005]. It is possible that both the ACE-FTS and MLS HCl measurements are slightly high, but it is unlikely that they are the sole cause of the large difference with respect to HALOE.

The most important implication of a difference in HCl values is the effect it will have on Cl_{TOT}. *Froidevaux et al.* [2006b] have derived a value of 3.65 ppbv for near-global Cl_{TOT} for August 2004 based on MLS measurements of HCl from 0.7-0.1 hPa. Their value compares extremely well with both ACE-FTS midlatitude values of 3.65 ppbv in 2004, further reinforcing the good agreement between these two instruments. Since the discrepancy between MLS and ACE appears limited to altitudes above 1 hPa or approximately 45 km at midlatitudes (~48 km in the tropics or ~42 km for the polar winter), high-biased ACE-FTS values of HCl would cause a small error in the determination of tropical mean Cl_{TOT}, but a more significant error at higher latitudes, all

of which are based on the 17.5-50.5 km range. By determining mean Cl_{TOT} using a reduced altitude range of 20.5-39.5 km, values of 3.69±0.05, 3.61±0.04, 3.57±0.06, 3.62±0.04, and 3.67±0.08 ppbv are obtained for northern high latitudes, northern midlatitudes, tropics, southern midlatitudes, and southern high latitudes, respectively (where the uncertainty is the 1σ precision from 20.5-39.5 km altitude). These values are all slightly lower than those determined using the wider altitude range.

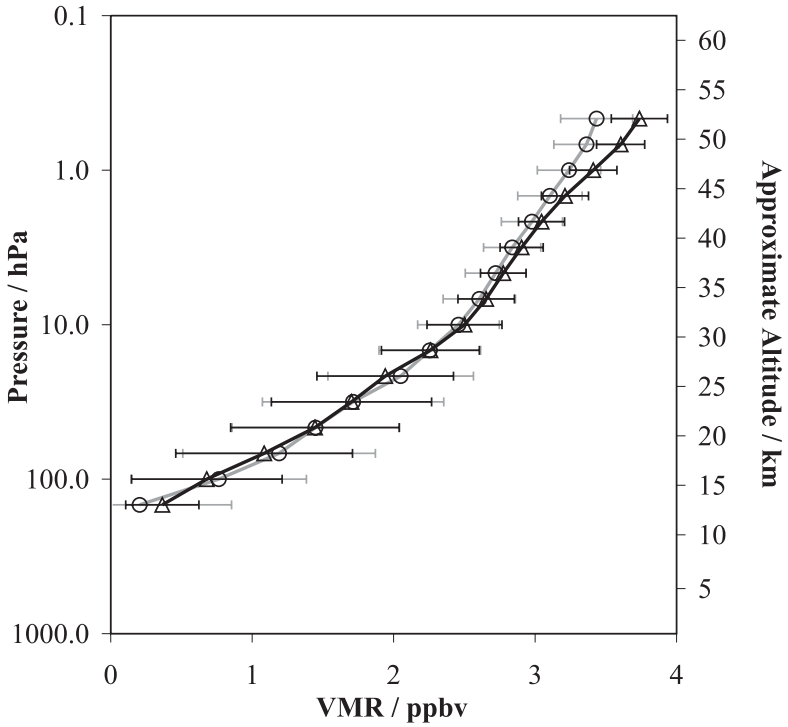

***Figure 3-5*:** A comparison showing average HCl profiles based on MLS (circles, gray line) and ACE-FTS (triangles, black line) coincidences. 1019 coincidences from the period of August 2004 to 31 January 2005 were used, although at the upper and lower ends of the altitude range fewer profiles are included in the average. The criteria for coincidences are measurements within 1° latitude, 8° longitude and 12 hours. This comparison includes both ACE-FTS sunrise and sunset occultations, with all ACE-FTS data interpolated to the MLS vertical pressure grid. The error bars indicate the 1σ variability for each set of data.

Previous chlorine inventories often neglected CCl_y in the upper stratosphere [*Zander et al.*, 1992 and 1996; *Sen et al.*, 1999], thus assuming Cl_{TOT} was equal to Cl_y at high altitudes. Dividing the HALOE 2004 globally-averaged HCl value at 55 km of 3.13 ppbv (*J. Anderson, private communication, 2006*) by the HCl/Cl_y ratios (0.93-0.95) results in Cl_y estimates of ~3.29-3.37 ppbv. The difference between ACE-FTS mean Cl_{TOT} values and HALOE Cl_y values is larger than the contribution from CCl_y at 55 km, which is expected to be less than 0.06 ppbv. From this work, based on *Weisenstein et al.* [1992], *Coheur et al.* [2003] and additional knowledge of source gas trends and lifetimes [*WMO*, 2003], one can estimate a value of HCl/Cl_{TOT} near 55 km altitude, since HCFC-22 accounts for about 1% (0.027-0.040 ppbv) of Cl_{TOT} and a contribution of only

about 0.5% (0.019-0.023 ppbv) is due to other organic chlorine gases mainly CFC-114, CFC-115, HCFC-142b. Inorganic chlorine species that may contribute to Cl_{TOT} at this altitude include ClO, HOCl and Cl. It is difficult to determine accurate values of the contributions from these species, although a reasonable estimate would attribute the largest contribution (~0.07 pbbv at high latitudes) to ClO. Unfortunately, the version of SMR ClO measurements used here, did not appear reliable at this altitude. These estimates imply that HCl may comprise as much as ~98-99% of Cl_y or ~96-98% of Cl_{TOT} at 55 km, in contrast to the above values used by others.

When using HCl at 55 km to determine stratospheric Cl_y, it is rarely emphasized that 55 km is actually in the lower mesosphere, not the stratosphere. Thus, relating the Cl_y value at 55 km to Cl_{TOT} in the stratosphere is complicated both by CCl_y and by the presence of slightly sloped stratospheric Cl_{TOT} profiles as determined in this work. Small changes in Cl_{TOT} associated with the slope, coupled with differences attributable to CCl_y, should all be considered in very accurate comparisons of HALOE Cl_y values with ATMOS, MkIV, SOLVE and ACE-FTS Cl_{TOT} values. While there is a good theoretical foundation for slightly sloped stratospheric Cl_{TOT} profiles, the present uncertainty in many parameters prevents a quantitative treatment of the slope or its use in a meaningful quantitative comparison such as the one mentioned above. However, it does imply that prior to the peak in upper stratospheric chlorine, Cl_{TOT} at 55 km should be slightly less than a true stratospheric value (below ~50 km), and after the peak it should be slightly more, which adds to the discrepancy between ACE-FTS and HALOE values.

Ideally, a technique or combination of techniques that could accurately measure all relevant chlorine species over a large altitude range, would provide the most reliable approach to determining stratospheric Cl_{TOT} or Cl_y. While eleven important chlorine species have been retrieved from ACE-FTS measurements in this work, some key species are still missing, thus ACE-FTS data can only provide a partial solution at the current time, but the results obtained in this work are significant in the sense that if stratospheric Cl_{TOT} in 2004 was indeed as high as determined here, it may take longer for it to decline to a safe level of 2.0 ppbv, which could mean a delay in the expected date of the recovery of stratospheric ozone.

3.7 Summary and Conclusions

A global inventory of stratospheric chlorine has been created which includes all significant inorganic and organic chlorine species in five latitude zones during the period of February 2004 to January 2005 inclusive, based on measurements by the ACE-FTS supplemented by measurements by other instruments and model results. The sum of all significant chlorine species at each altitude nearly makes a straight line, with a slight positive slope (ppbv/km). The average of these points in the 17.5-50.5 km altitude range is used to determine mean stratospheric Cl_{TOT} for each latitude zone yielding values of 3.62±0.11 ppbv for the tropics, 3.65±0.09 ppbv for both the northern and southern midlatitudes, 3.74±0.12 ppbv for the northern high latitudes, and 3.71±0.16 ppbv for the southern high latitudes (where the uncertainty given is the 1σ precision for points between 17.5-50.5 km and the estimated accuracy is 0.13-0.14 ppbv). Both the latitudinal variation and the

slopes can be interpreted as evidence that stratospheric Cl_{TOT} is now declining, but the accuracy of the slopes does not permit quantitative conclusions.

HCl is the principal component of high altitude Cl_{TOT}, and ACE-FTS and MLS HCl measurements agree very well up to 1 hPa (or ~45 km altitude). Due to the possibility that ACE-FTS HCl values above this range are biased high, an alternate set of mean Cl_{TOT} values based only on the 20.5-39.5 km altitude range were determined for the five latitude zones. These values are 0.03-0.06 ppbv lower than those based on the wider altitude range. ACE-FTS or MLS measurements and historical ATMOS or MkIV measurements, all yield higher HCl values than HALOE, which translate to larger inferred stratospheric Cl_{TOT} (or Cl_y) than obtained using HALOE data. The cause of this discrepancy cannot be determined at present. In spite of these higher stratospheric chlorine values, the latitudinal variation in mean Cl_{TOT} and Cl_{TOT} slopes obtained in this work, as well as a comparison of mean Cl_{TOT} values to past ATMOS and MkIV measurements, all indicate that stratospheric Cl_{TOT} is now decreasing, which reinforces previous work that has shown the success of the Montreal Protocol and its amendments at controlling and reducing chlorine levels. However, the high values of stratospheric Cl_{TOT} may be an indication that it will take longer than previously expected for Cl_{TOT} to decline to a safe level, potentially causing a delay in the expected date of ozone recovery.

References

Aellig, C.P., N. Kampfer, C. Rudin, R.M. Bevilacqua, W. Degenhardt, P. Hartogh, C. Jarchow, K. Künzi, J.J. Olivero, C. Croskey, J.W. Waters, H.A. Michelsen (1996), Latitudinal distribution of upper stratospheric ClO as derived from space-borne microwave spectroscopy, *Geophys. Res. Lett.*, 23(17), 2321-2324.

Anderson, J., J.M. Russell III, Long Term Changes of HCl and HF as Observed by HALOE, (2004) in Ozone, Vol. I, Proceedings of the XX Quadrennial Ozone Symposium, Kos, Greece, 1-8 June 2004, Editor C.S. Zerefos, Extended Abstract #363, (also http://www.qos2004.gr/abstract4.php).

Anderson, J., J.M. Russell III, S. Solomon, L.E. Deaver (2000), Halogen Occultation Experiment confirmation of stratospheric chlorine decreases in accordance with the Montreal Protocol, *J. Geophys. Res.*, 105(D4), 4483-4490.

Austin, J., N. Butchart, K. Shine (1992), Possibility of an Arctic ozone hole in a doubled-CO_2 climate, *Nature*, 360, 221-225.

Austin, J., D. Shindell, S.R. Beagley, C. Brūhl, M. Dameris, E. Manzini, T. Nagashima, P. Newman, S. Pawson, G. Pitari, E. Rozanov, C. Schnadt, T.G. Shepherd (2002), Uncertainties and assessments of chemistry-climate models of the stratosphere, *Atmospheric Chemistry and Physics Discussions*, 2, 1035-1096.

Barret, B., D. Hurtmans, M. Carleer, M. De Mazière, E. Mahieu, P.-F. Coheur (2005), Line narrowing effect on the retrieval of HF and HCl vertical profiles from ground-based FTIR measurements, *Journal of Quantitative Spectroscopy and Radiative Transfer*, 95(4), 499-519.

Bernath, P.F., C.T. McElroy, M.C. Abrams, C.D. Boone, M. Butler, C. Camy-Peyret, M. Carleer, C. Clerbaux, P.-F. Coheur, R. Colin, P. DeCola, M. De Mazière, J.R. Drummond, D. Dufour, W.F.J. Evans, H. Fast, D. Fussen, K. Gilbert, D.E. Jennings, E.J. Llewellyn, R.P. Lowe, E. Mahieu, J.C. McConnell, M. McHugh, S.D. McLeod, D. Michelangeli, C. Midwinter, R. Nassar, F. Nichitiu, C. Nowlan, C.P. Rinsland, Y.J. Rochon, N. Rowlands, K. Semeniuk, P. Simon, R. Skelton, J.J. Sloan, M.-A. Soucy, K. Strong, P. Tremblay, D. Turnbull, K.A. Walker, I. Walkty, D.A. Wardle, V. Wehrle, R. Zander, J. Zou (2005), Atmospheric Chemistry Experiment (ACE): mission overview. *Geophys. Res. Lett.*, 32, L15S01.

Berthet, G., P. Ricaud, F. Lefèvre, E. Le Flochmoën, J. Urban, B. Barret, N. Lautié, E. Dupuy, J. De La Noë, D. Murtagh (2005), Nighttime chlorine monoxide observations by the Odin satellite and implications for the ClO/Cl_2O_2 equilibrium, *Geophys. Res. Lett.*, 32, L11812.

Bloss, W.J., S.L. Nickolaisen, R.J. Salawitch, R.R. Friedl, S.P. Sander (2001), Kinetics of the ClO Self-reaction and 210 nm Absorption Cross Section of the ClO Dimer, *J. Phys. Chem.*, 105, 11226-11239.

Boakes, G., W.H.H. Mok, D.M. Rowley (2005), Kinetic studies of the ClO + ClO association reaction as a function of temperature and pressure, *Phys. Chem. Chem. Phys.*, 7, 4102-4113.

Boone, C.D., R. Nassar, K.A. Walker, Y. Rochon, S.D. McLeod, C.P. Rinsland, P.F. Bernath (2005), Retrievals for the Atmospheric Chemistry Experiment Fourier Transform Spectrometer, *Applied Optics*, 44(33), 7218-7231.

Burkholder, J.B., J.J. Orlando, C.J. Howard (1990), Ultraviolet absorption cross sections of the Cl_2O_2 between 210 and 410 nm, *J. Phys. Chem.*, 94, 687-695.

Brewer, A.W. (1949), Evidence for a world circulation provided by the measurements of helium and water vapor distribution in the stratosphere, *Quarterly Journal of the Royal Meteorological Society*, 75, 351.

Canty, T., E.D. Rivière, R.J. Salawitch, G. Berthet, J.-B. Renard, K. Pfeilsticker, M. Dorf, A. Butz, H. Bösch, R.M. Stimpfle, D.M. Wilmouth, E.C. Richard, D.W. Fahey, P.J. Popp, M.R. Schoeberl, L.R. Lait, T.P. Bui (2005), Nighttime OClO in the winter Arctic vortex, *J. Geophys. Res.*, 110 D01301.

Chapman, S. (1930), On ozone and atomic oxygen in the upper atmosphere, *Phil. Mag.*, 10, 369.

Coheur, P.F., C. Clerbaux, R. Colin (2003), Spectroscopic measurements of halocarbons and hydrohalocarbons by satellite-borne remote sensors, *J. Geophys. Res.*, 108(D4), 4130.

Dufour, G., C.D. Boone, P.F. Bernath (2005), First measurements of CFC-113 and HCFC-142b from space using ACE-FTS infrared spectra, *Geophys. Res. Lett.*, 32, L15S09.

Engel, A., M. Strunk, M. Müller, H.-P. Haase, C. Poss, I. Levin, U. Schmidt (2002), Temporal development of total chlorine in the high-latitude stratosphere based on reference distributions of mean age derived from CO_2 and SF_6, *J. Geophys. Res.*, 107(D12), 4136.

Farman, J.C., B.G. Gardiner, J.D. Shanklin (1985), Large losses of total ozone in Antarctica reveal seasonal ClO_x/NO_x interaction, *Nature*, 315, 207-210.

Froidevaux, L., N.J. Livesey, W.G. Read, Y.B. Jiang, C. Jimenez, M.J. Filipiak, M.J. Schwartz, M.L. Santee, H.C. Pumphrey, J.H. Jiang, D.L. Wu, G.L. Manney, B.J. Drouin, J.W. Waters, E.J. Fetzer, P.F. Bernath, C.D. Boone, K.A. Walker, K.W. Jucks, G.C. Toon, J.J. Margitan, B. Sen, C.R. Webster, L.E. Christensen, J.W. Elkins, E. Atlas, R.A. Lueb, R. Hendershot (2006a), Early Validation Analyses of Atmospheric Profiles from EOS MLS on the Aura Satellite, *IEEE Transactions on Geoscience and Remote Sensing*, in press.

Foridevaux, L., N.J. Livesey, W.G. Read, R.J. Salawitch, J.W. Waters, B. Drouin, I.A. Mackenzie, H.C. Pumphrey, P. Bernath, C. Boone, R. Nassar, S. Montzka, J. Elkins, D. Cunnold, D. Waugh (2006b), Decreases in upper atmospheric chlorine*, Geophys. Res. Lett.,* submitted*.*

Hartmann, G.K., R.M Bevilacqua, P.R. Schwartz, N. Kampfer, K.F. Künzi, C.P. Aellig, A. Berg, W. Boogaerts. B.J. Connor, C.L. Croskey, M. Daehler, W. Degenhardt, H.D. Dicken, D. Goldizen, D. Kriebel, J. Langen, A. Loidl, J.J. Olivero, T.A. Pauls, S.E. Pauliafito, M.L. Richards, C. Rudin, J.J. Tsou, W.B. Watman, G. Umlauft, R. Zwick (1996), Measurements of O_3, H_2O and ClO in the middle atmosphere using the millimeter-wave atmospheric sounder (MAS), *Geophys. Res. Lett.*, 23(17), 2313-2316.

Kaye, J.A., A.R. Douglass, C.H. Jackman, R.S. Stolarski (1991), Two-Dimensional Model Calculation of Fluorine-Containing Reservoir Species in the Stratosphere, *J. Geophys. Res.,* 96(D7), 12865-12881.

Mahieu, E., P. Duchatelet, R. Zander, P. Demoulin, C. Servais, C.P. Rinsland, M.P. Chipperfield, M. De Mazière (2004), The evolution of inorganic chlorine above the Jungfraujoch station: An update, in *Ozone, Vol. II, Proceedings of the XX Quadrennial Ozone Symposium, Kos, Greece, 1-8 June 2004*, Editor C.S. Zerefos, pp. 997-998, (also http://www.qos2004.gr/abstract4.php).

McHugh, M., B. Magill, K.A. Walker, C.D. Boone, P.F. Bernath, and J.M. Russell III (2005), Comparison of atmospheric retrievals from ACE and HALOE, *Geophys. Res. Lett.*, 32, L15S10.

Molina M.J., F.S. Rowland (1974), Stratospheric sink for chlorofluoromethanes: Chlorine atom-catalysed destruction of ozone, Nature, 249, 810-812.

Molina, L.T., M.J. Molina (1987), Production of Cl_2O_2 from the self-reaction of the ClO radical, *J. Phys. Chem.*, 91, 433-436.

Montzka, S.A., J.H. Butler, R.C. Myers, T.M. Thompson, T.H. Swanson, A.D. Clarke, L.T. Lock, J.W. Elkins (1996), Decline in Tropospheric Abundance of Halogen from Halocarbons: Implications for Stratospheric Ozone Depletion, *Science*, 2272(5266), 1318-1322.

Murtagh, D., U. Frisk, F. Merino, M. Ridal, A. Jonsson, J. Stegman, G. Witt, P. Eriksson, C. Jiménez, G. Megie, J. de la Noë, P. Ricaud, P. Baron, J.R. Pardo, A. Hauchcorne, E.J. Llewellyn, D.A. Degenstein, R.L. Gattinger, N.D. Lloyd, W.F.J. Evans, I.C. McDade, C.S. Haley, C. Sioris, C. von Savigny, B.H. Solheim, J.C. McConnell, K. Strong, E.H. Richardson, G.W. Leppelmeier, E.

Kyrölä, H. Auvinen, L. Oikarinen (2002), An overview of the Odin atmospheric mission, *Can. J. Phys.*, 80, 309-319.

Nassar, R., P.F. Bernath, C.D. Boone, G.L. Manney, S.D. McLeod, C.P. Rinsland, R. Skelton, K.A. Walker (2005a), ACE-FTS measurements across the edge of the winter 2004 Arctic vortex, *Geophys. Res. Lett.*, 32, L15S05.

Nassar, R., P.F. Bernath, C.D. Boone, G.L. Manney, S.D. McLeod, C.P. Rinsland, R. Skelton, K.A. Walker (2005b), Stratospheric abundances of water and methane based on ACE-FTS measurements, *Geophys. Res. Lett.*, 32, L15S04.

Nassar, R., P.F. Bernath, C.D. Boone, C. Clerbaux, P.F. Coheur, G. Dufour, L. Froidevaux, E. Mahieu, J.C. McConnell, S.D. McLeod, D.P. Murtagh, C.P. Rinsland, K. Semeniuk, R. Skelton, K.A. Walker, R. Zander (2006), A global inventory of stratospheric chlorine in 2004, *J. Geophys. Res.*, submitted.

Nedoluha, G.E., R.M. Bevilacqua, R.M. Gomez, B.C. Hicks, J.M. Russell III, B.J. Connor (2003), An evaluation of trends in middle atmospheric water vapor as measured by HALOE, WVMS, and POAM, *J. Geophys. Res.*, 108(D13), 4391.

Nickolaisen, S.L., R.R. Friedl, S.P. Sander (1994), Kinetics of the ClO + ClO Reaction: Pressure and Temperature Dependences of the Bimolecular and Termolecular Channels and Thermal Decomposition of Chlorine Peroxide, *J. Phys. Chem.*, 98, 155-169.

Oltmans, S.J., S. Vömel, D.J. Hoffman K.H. Rosenlof, D. Kley (2000), The increase in stratospheric water vapor from balloonborne frostpoint hygrometer measurements at Washington, D.C. and Boulder, Colorado, *Geophys. Res. Lett.*, 27(21), 3453-3456.

Prather, M.J., R.T. Watson (1990), Stratospheric ozone depletion and future levels of atmospheric chlorine and bromine, *Nature*, 344, 729-734.

Prather, M., P. Midgely, F.S. Rowland, R. Stolarski (1996), The ozone layer: the road not taken, *Nature*, 381, 551-554.

Prinn, R.G., R.F. Weiss, P.J. Fraser, P.G. Simmonds, D.M. Cunnold, F.N. Alyea, S. O'Doherty, P. Salameh, B.R. Miller, J. Huang, R.H.J. Wang, D.E. Hartley, C. Harth, L.P. Steele, G. Sturrock, P.M. Midgley, A. McCulloch (2000), A history of chemically and radiatively important gases in air deduced from ALE/GAGE/AGAGE, *J. Geophys. Res.*, 105(D14), 17751–17792.

Rinsland, C.P., E. Mahieu, R. Zander, N.B. Jones, M.P. Chipperfield, A. Goldman, J. Anderson, J.M. Russell III, P. Demoulin, J. Notholt, G.C. Toon, J.-F. Blavier, B. Sen, R. Sussmann, S.W. Wood, A. Meier, D.W.T. Griffith, L.S. Chiou, F.J. Murcray, T.M. Stephen, F. Hase, S. Mikuteit, A. Schulz, T. Blumenstock (2003), Long-term trends of inorganic chlorine from ground-based infrared solar spectra: Past increases and evidence for stabilization, *J. Geophys. Res.*, 108(D8), 4252.

Rinsland, C.P., R. Nassar, C.D. Boone, P.F. Bernath, B. Jelley, L. Chiou, D.K. Weisenstein, G. Dufour, E. Mahieu, R. Zander (2006), Spectroscopic Detection of COClF in the Tropical and Mid-

Latitude Lower Stratosphere from Atmospheric Chemistry Experiment Infrared Spectra: Preliminary Retrievals and Comparison with Previous Measurements and Model Calculations, *Geophys. Res. Lett.*, submitted.

Rosenlof, K.H., S.J. Oltmans, D. Kley, J.M. Russell III, E.W. Chiou, W.P. Chu, D.G. Johnson, K.K. Kelly, H.A. Michelsen, G.E. Nedoluha, E.E. Remsberg, G.C. Toon, M.P. McCormick (2001), Stratospheric water vapor increases over the past half-century, *Geophys. Res. Lett.*, 28(7), 1195-1198.

Rothman, L.S., D. Jacquemart, A. Barbe, D.C. Benner, M. Birk, L.R. Brown, M.R. Carleer, C. Chackerian Jr., K. Chance, L.H. Coudert, V. Dana, V.M. Devi, J.-M. Flaud, R.R. Gamache, A. Goldman, J.-M. Hartmann, K.W. Jucks, A.G. Maki, J.-Y. Mandin, S.T. Massie, J. Orphal, A. Perrin, C.P. Rinsland, M.A.H. Smith, J. Tennyson, R.N. Tolchenov, R.A. Toth, J. Vander Auwera, P. Varanasi, G. Wagner (2005), The HITRAN 2004 molecular spectroscopic database, *Journal of Quantitative Spectroscopy and Radiative Transfer*, 96, 139-204..

Rummukainen, M. (1996), Modeling stratospheric chemistry in a global three-dimensional chemical transport model, SCTM-1: Model development, *Finn. Meteorol. Inst. Contrib., 19*, 206 pages.

Russell, J.M. III, L.E. Deaver, M. Luo, J.H. Park, L.L. Gordley, A.F. Tuck, G.C. Toon, M.R. Gunson, W.A. Traub, D.G. Johnson, K.W. Jucks, D.G. Murcray, R. Zander, I.G. Nolt, C.W. Webster (1996a), Validation of hydrogen chloride measurements made by the Halogen Occultation Experiment from the UARS platform, *J. Geophys. Res.*, 101(D6), 10151-10162.

Russell, J.M. III, M. Luo, R.J. Cicerone, L.E. Deaver (1996b), Satellite confirmation of the dominance of chlorofluorocarbons in the global stratospheric chlorine budget, *Nature*, 379, 526-529.

Schauffler, S.M., E.L. Atlas, S.G. Donnelly, A. Andrews, S.A. Montzka, J.W. Elkins, D.F. Hurst, P.A. Romashkin, G.S. Dutton, V. Stroud (2003), Chlorine budget and partitioning during the Stratospheric Aerosol and Gas Experiment (SAGE) III Ozone Loss and Validation Experiment (SOLVE), *J. Geophys. Res.*, 108(D5), 4173.

Sen, B., G.B. Osterman, R.J. Salawitch, G.C. Toon, J.J. Margitan, J.-F. Blavier, A.Y. Chang, R.D. May, C.R. Webster, R.M. Stimpfle, G.P. Bonne, P.B. Voss, K.K. Perkins, J.G. Anderson, R.C. Cohen, J.W. Elkins, G.S. Dutton, D.F. Hurst, P.A. Romashkin, E.L. Atlas, S.M. Schauffler, M. Loewenstein (1999), The budget and partitioning of stratospheric chlorine during the 1997 Arctic summer, *J. Geophys. Res.*, 104, D21, 26653-26665.

Shindell, D.T., V. Grewe (2002), Separating the influence of halogen and climate changes on ozone recovery in the upper stratosphere, *J. Geophys. Res.*, 107(D12), 4144.

Shindell, D.T., D. Rind, P. Lonergan (1998), Increased polar stratospheric ozone losses and delayed eventual recovery due to increasing greenhouse gas concentrations, *Nature*, 392, 589-592.

Stimpfle, R.M, D.M. Wilmouth, R.J. Salawitch, J.G. Anderson (2004), First measurements of ClOOCl in the stratosphere: The coupling of ClOOCl and ClO in the Arctic polar vortex, *J. Geophys. Res.,* 109, D03301.

Stolarski, R.S., R.J. Cicerone (1974), Stratospheric chlorine: A possible sink for ozone, *Can. J. Chem.*, 52, 1610-1615.

Toon, G.C., J.-F. Blavier, B. Sen, B.J. Drouin (2001), Atmospheric $COCl_2$ measured by solar occultation spectrometry, *Geophys. Res. Lett.,* 28(14) 2835-3838.

Urban, J., N. Lautié, E. Le Flochmoën, C. Jiménez, P. Eriksson, J. de La Noë, E. Dupuy, M. Ekström, L. El Amraoui, U. Frisk, D. Murtagh, M. Olberg, P. Ricaud (2005), Odin/SMR limb observations of stratospheric trace gases: Level 2 processing of ClO, N_2O, HNO_3, and O_3, *J. Geophys. Res.*, 110, D14307.

von Clarmann, T., N. Glatthor, U. Grabowski, M. Höpfner, S. Kellmann, A. Linden, Gizaw Mengistu Tsidu, M. Milz, T. Steck, G. P. Stiller, H. Fischer, B. Funke (2006), Global stratospheric HOCl distributions retrieved from infrared limb emission spectra recorded by the Michelson Interferometer for Passive Atmospheric Sounding (MIPAS), *J. Geophys Res.,* 111, D05311.

Von Hobe, M., J.-U. Grooβ, R. Müller, S. Hrechanyy, U. Winkler, F. Stroh (2005), A re-evaluation of the ClO/Cl_2O_2 equilibrium constant based on stratospheric in-situ observations, *Atmospheric Chemistry and Physics*, 5, 693-702.

Waugh, D.W, D.B. Considine, E.L. Fleming (2001), Is upper stratospheric chlorine decreasing as expected?, *Geophys. Res. Lett.*, 28(7), 1187-1190.

Weisenstein, D.K., M.K.W. Ko, N.-D. Sze (1992), The Chlorine Budget of the Present-Day Atmosphere: A Modeling Study, *J. Geophys. Res.*, 97(D2), 2547-2559.

World Meteorology Organization (1957), Meteorology - A three-dimensional science: Second session of the commission for aerology, *WMO Bulletin*, vol. IV, no. 4, 134-138.

World Meteorological Organization (1999), Scientific Assessment of Ozone Depletion: 1998. Global Ozone Research and Monitoring Project - Report No. 44, Geneva, Switzerland.

World Meteorological Organization (2003), Scientific Assessment of Ozone Depletion: 2002. Global Ozone Research and Monitoring Project - Report No. 47, Geneva, Switzerland.

Zander, R., M.R. Gunson, C.B. Farmer, C.P. Rinsland, F.W. Irion, E. Mahieu (1992), The 1985 Chlorine and Fluorine Inventories in the Stratosphere Based on ATMOS Observations at 30º North Latitude, *J. Atmos. Chem*., 15, 171-186.

Zander, R., E. Mahieu, M.R. Gunson, M.C. Abrams, A.Y. Chang, M. Abbas, C. Aellig, A. Engel, A. Goldman, F.W. Irion, N. Kämpfer, H.A. Michelsen, M.J. Newchurch, C.P. Rinsland, R.J. Salawitch, G.P. Stiller, G.C. Toon (1996), The 1994 northern midlatitude budget of stratospheric chlorine derived from ATMOS/ATLAS-3 observations, *Geophys. Res. Lett.,* 23(17) 2357-2360.

Chapter 4

A Global Inventory of Stratospheric Fluorine

4.1 Introduction

Halogenated gases such as chlorofluorcarbons (CFCs), hydrochlorofluorocarbons (HCFCs) and halons are very stable, with long lifetimes in the troposphere. When these gases are transported to the stratosphere, they dissociate releasing F, Cl and Br radicals. Cl-containing radicals and the much less abundant Br-containing radicals participate in the destruction of ozone via catalytic cycles which have the greatest impact in the springtime polar vortices. In contrast, F radicals quickly react with CH_4 and H_2O producing the stable reservoir molecule HF. The formation of HF prevents fluorine from undergoing similar catalytic cycles [*Stolarski and Rundel*, 1975].

Despite the fact that fluorine does not directly participate in ozone depletion, monitoring of atmospheric fluorine levels is important for a number of reasons: 1) To compare with emission inventories reflecting the quantities of individual species used and emitted that often contain chlorine or bromine; 2) To check the validity of methods for the determination of total stratospheric chlorine which is the main contributor to polar ozone decline; and 3) Fluorinated species in the troposphere behave as greenhouse gases, some species with global warming potentials orders of magnitude larger than CO_2 [*World Meteorological Organization (WMO)*, 2003].

HF is the dominant fluorine species in the middle and upper stratosphere. ATMOS measured HF along with six other fluorine species in 1985, 1992, 1993 and 1994. The 1985 ATMOS measurements were used to create a fluorine inventory for 30ºN, including a profile of total fluorine (F_{TOT}) throughout the stratosphere [*Zander et al.,* 1992]. HALOE measurements of HF at 55 km in altitude between 1991-2005 have been used to calculate total inorganic fluorine (F_y) [*Russell et al.*, 1996; *Anderson et al.*, 2000], which serves as a proxy for F_{TOT}. Since it is very difficult to monitor HF with microwave or infrared emission instruments, the ACE-FTS is only the third space-borne instrument capable of measuring HF, and with ATMOS and HALOE now retired, it is the only one currently making these measurements. It also measures profiles of several other important fluorine-containing molecules, some of which are also unique to the ACE-FTS. The ACE-FTS method for the determination of stratospheric F_{TOT} is similar to the approach employed using measurements by ATMOS [*Zander et al.,* 1992] and the MkIV balloon-borne FTS [*Sen et al.,* 1996], which were based on a summation of the abundances of relevant species.

Perhaps the most important reason for revisiting the fluorine budget is that the partitioning between fluorine-containing gases in the stratosphere is continually changing. As a result of the Montreal Protocol and subsequent amendments, abundances of CFCs and Halons are decreasing, HCFCs are near their predicted maxima, and HFCs are rapidly increasing. ACE-FTS measurements of several fluorine species have been reported in the past (based on v1.0 data) by

Rinsland et al. [2005, 2006a], which combined the ACE-FTS measurements with ATMOS measurements to demonstrate changes in abundances of these species over time. Furthermore, changes in atmospheric composition, improved laboratory spectroscopic data, advances in retrieval methodology and the high signal-to-noise ratio achieved by the ACE-FTS, now make it possible to retrieve some fluorine-containing species which could not be retrieved in the past.

This chapter demonstrates the ACE-FTS method for determining F_{TOT} by creating a near global (82ºS-82ºN) inventory of stratospheric fluorine species in 2004 [*Nassar et al.*, 2006a]. With the absence of other satellite instruments measuring HF, this approach may provide the primary source of stratospheric fluorine abundances in the coming years.

4.2 Method for Determining Total Stratospheric Fluorine

The volume mixing ratios (VMRs) of total inorganic fluorine F_y, total organic fluorine CF_y and total fluorine F_{TOT} at discrete stratospheric altitudes were determined using the summations below, where the square brackets indicate the VMR of a species. For the purpose of this work, F_y and CF_y are defined below, and F_{TOT} is the sum of all significant fluorine species including both F_y and CF_y.

$$F_y = [HF] + 2[COF_2] + [COClF] + 6[SF_6] \quad (4.1)$$

$$CF_y = 4[CF_4] + [CCl_3F] + 2[CCl_2F_2] + 2[CHClF_2] + 3[CCl_2FCClF_2] + 2[CH_3CClF_2] + [CH_2FCF_3] + \textit{minor species} \quad (4.2)$$

$$F_{TOT} = F_y + CF_y \quad (4.3)$$

As in the ACE-FTS global inventory of stratospheric chlorine [*Nassar et al.*, 2006b], mean profiles for each species and the summations (shown above) were determined in five latitudinal zones (60-82ºN, 30-60ºN, 30ºS-30ºN, 30-60ºS and 60-82ºS) over the 17.5-50.5 km range; however, since no fluorine-containing species exhibit major diurnal variations, occultations at all local times could be combined in an average, unlike in the chlorine inventory. Profiles for each species in the above equations (with exception of the *minor species*) were based on ACE-FTS retrieved profiles; although, various methods were used to extend the profiles when they did not span the entire stratosphere. The spectral microwindows and altitude ranges for the retrieval of each species are given in Table 4-1. Figure 4-1 shows an example of average northern midlatitudes profiles for fluorinated species included in this inventory. Brief descriptions of the method for obtaining profiles of each species follow.

Table 4-1: Microwindows for fluorine species retrieved from ACE-FTS measurements. The spectral contributions from interfering species including $H_2{}^{16}O$, $H_2{}^{17}O$, $H_2{}^{18}O$, HDO, N_2O, $^{12}CO_2$, $^{13}CO_2$, O_3 and others were removed as required.

Species	Total Range (km)	Microwindow		
		Center (cm^{-1})	Width (cm^{-1})	Range (km)
HF	12.5 - 59.5	3788.33	0.40	12.5 - 51.5
		3833.71	0.40	18.5 - 54.5
		3877.75	0.35	12.5 - 59.5
		3920.39	0.30	27.5 - 59.5
		4001.03	0.30	12.5 - 59.5
		4038.37	0.45	12.5 - 59.5
		4075.30	0.35	45.5 - 59.5
		4109.94	0.35	25.5 - 49.5
COF_2	12.5-37.5/41.5[a]	1930.18	0.35	12.5-37.5/41.5[a]
		1936.97	0.30	12.5-37.5/41.5[a]
		1937.06	0.30	15.5-37.5/41.5[a]
		1938.26	0.30	30.5-37.5/41.5[a]
		1939.97	0.30	12.5-37.5/41.5[a]
		1949.81	0.30	12.5-37.5/41.5[a]
		1950.70	0.50	12.5-37.5/41.5[a]
		1952.03	1.00	12.5-37.5/41.5[a]
		1953.36	0.30	30.5-37.5/41.5[a]
		1954.17	0.30	20.5-37.5/41.5[a]
COClF [b]	17/19 – 30 [c]	1860.35	0.70	17/19 – 30 [c]
		1862.55	1.30	17/19 – 30 [c]
		1864.30	0.60	17/19 – 30 [c]
		1865.45	1.10	17/19 – 30 [c]
		1866.80	0.40	17/19 – 30 [c]
		1868.80	0.60	17/19 – 30 [c]
		1870.575	0.35	17/19 – 30 [c]
		1874.95	0.90	17/19 – 30 [c]
CF_4	20.5 - 44.5	1283.20	8.00	20.5 - 44.5
CCl_3F (CFC-11)	5.5 - 21.5	842.50	25.00	5.5 - 21.5
CCl_2F_2 (CFC-12)	6.5 - 27.5	922.00	4.00	6.5 - 27.5
		1161.00	1.20	12.5 - 24.5
CCl_2FClF_2 (CFC-113)	7.5 - 16.5	817.50	25.00	7.5 - 16.5
$CHClF_2$ (HCFC-22)	5.5 - 24.5	809.30	1.10	5.5 - 14.5
		820.85	0.70	5.5 - 11.5
		829.03	0.50	5.5 - 24.5
CH_3CClF_2 (HCFC-142b)	8.5 - 18.5	1134.50	4.00	8.5 - 18.5
		1193.60	3.60	8.5 - 18.5
CH_2FCF_3 (HFC-134a)	5.5 - 16.5	1190.00	20.00	5.5 - 16.5
SF_6	7.5 - 30.5	948.50	7.00	7.5 - 30.5

[a] Latitude dependent retrieval range where the retrieval went highest in the tropics and lowest for polar latitudes.

[b] Special circumstances for the retrieval of this species are outlined in the text.

[c] The lower altitude limit for COClF is 19 km for tropical occultations and 17 km for midlatitudes.

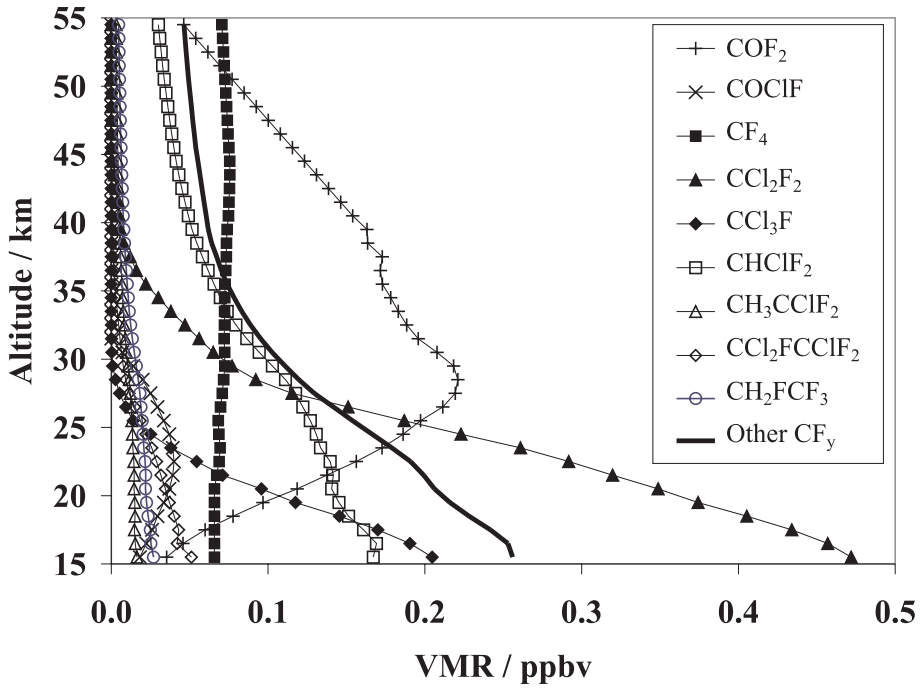

Figure 4-1: Northern midlatitude (30-60°N) profiles of species included in the ACE-FTS fluorine inventory. HF is not shown because its VMR is mostly above 0.5 ppbv and SF_6 is not shown as it occurs at very low levels.

4.2.1 HF, CF_4, CCl_3F (CFC-11) and CCl_2F_2 (CFC-12)

The CCl_3F and CCl_2F_2 data utilized here are from the ACE-FTS version 2.2 dataset. Although HF and CF_4, are included in version 2.2, they were retrieved to higher altitudes specifically for this work. If the retrieval range for a species was below 54.5 km, then above the retrieval range, *a priori* profiles were automatically scaled to produce a similarly-shaped profile using the value at the second highest retrieved point. If this was insufficient, the retrieved profile was manually extrapolated to zero.

4.2.2 COF_2 and COClF

COF_2 is included in version 2.2, but ACE-FTS retrievals were extended to higher altitudes specifically for this work, using a latitude dependent altitude range which is highest in the tropics and lowest near the poles. COF_2 makes a maximum contribution to F_{TOT} in the tropics, where it contributes ~24% at its peak near 39.5 km. A slightly weaker peak is centered at 28.5 km at midlatitudes and at 25.5 km at northern high latitudes. At southern high latitudes, the mean profile has a primary peak at 23.5 km and a secondary peak at 36.5 km. Since COF_2 has only been retrieved up to approximately 40 km from ACE-FTS spectra, the profiles were extended based on

the shape of the tropical profile modeled in *Kaye et al.* [1991], shifted appropriately for the middle and high latitudes.

COClF results from the breakdown of CCl_3F (as described in the previous chapter), so it has a peak in the lower to middle stratosphere. Retrievals of COClF involving averaged ACE-FTS spectra have produced some promising early results [*Rinsland et al.*, 2006b]; however, a routine operational retrieval has not been developed at the time of this writing. The tropical and midlatitude COClF profiles in this work were based the retrieval of *Rinsland et al.* [2006b] using ACE-FTS measurement and the high latitude profiles were based on the model results of *Kaye et al.* [1991], both described in the previous chapter. COClF only makes a small contribution to F_{TOT}, with a peak in the profile of ~0.10 ppbv in the tropics, ~0.05 ppbv at midlatitudes and ~0.02 ppbv at high latitudes, but in the future it would be desirable to carry out a complete ACE-FTS COClF retrieval, as was done for the other species.

4.2.3 $CHClF_2$ (HCFC-22), CCl_2FCClF_2 (CFC-113) and CH_3CClF_2 (HCFC-142b)

The ATMOS and MkIV fluorine budgets [*Zander et al.*, 1992; *Sen et al.*, 1999] did not include $CHClF_2$ in the upper stratosphere; however, according to the modeling work of *Weisenstein et al.* [1992], $CHClF_2$ exists in the upper stratosphere in significant quantities. Retrieved $CHClF_2$ profiles were extended beyond 24.5 km altitude by scaling and shifting the profile from the SCTM-1 model [*Rummukainen et al.*, 1996] for 2000 January 01, 00:00 UT, 45ºN, 90ºE [*Coheur et al.*, 2003], as described in Chapter 3 and *Nassar et al.* [2006b].

CCl_2FCClF_2 and CH_3CClF_2 are not included in version 2.2 or any earlier data versions, but were retrieved for this work and the ACE-FTS stratospheric chlorine inventory [*Nassar et al.*, 2006b]. These two species have not been included in past fluorine inventories. The retrieval of these species was described in *Dufour et al.* [2005] and was the first retrieval of these species from space-based measurements. The chemistry responsible for the break down of CFCs is similar but distinct from that of HCFCs or other classes of species. Therefore, CFC-113, which has a lifetime of 85 years, was extended above 16.5 km by scaling the shape of the profile of CFC-12 which has a lifetime of 100 years, by a factor of 0.099. HCFC-142b, which has a lifetime of 17.9 years, was extended above 18.5 km by scaling the shape of the profile of HCFC-22 which has a lifetime of 12.0 years, by a factor of 0.103. Lifetimes of these species were taken from the 2002 WMO Report [*WMO*, 2003]. The scale factors were determined by taking the global mean values of $[CCl_2FCClF_2]/[CCl_2F_2]$ and $[CH_3CClF_2]/[CHClF_2]$ at the last point prior to the extension, i.e., the highest retrieved point. Since these species rapidly photodissociate in the stratosphere, they make a small contribution to F_{TOT} above the highest altitude point in their respective retrievals.

4.2.4 CH_2FCF_3 (HFC-134a)

HFC-134a is an important CFC-replacement compound. Although it is not an ozone depleting substance, it is a greenhouse gas with a very high radiative efficiency and is becoming a significant

contributor to the fluorine budget as its VMR is rapidly increasing. The retrieval of HFC-134a from ACE-FTS measurements is the first retrieval of this species from space-based measurements. The ability to retrieve HFC-134a (as well as CFC-113 and HCFC-142b) from ACE-FTS measurements was predicted prior to launch [*Coheur et al.*, 2003].

HFC-134a retrievals employed a 20 cm^{-1} wide microwindow centered at 1190 cm^{-1} over an altitude range of 5.5 to 16.5 km. Absorption cross sections for the retrievals were from HITRAN 2004 [*Rothman et al.*, 2005] and are based on the laboratory measurements of *Clerbaux et al.* [1993] and *Nemtchinov and Varanasi* [2004]. Interferences from N_2O and the first four isotopologues of H_2O were accounted for in the retrieval, including two relatively strong lines of the $H_2{}^{16}O$ isotopologue in the window for which the line shapes fit poorly in the troposphere (a general problem for H_2O with ACE-FTS measurements). The fitting weights were therefore set to zero in the vicinity of the two strong H_2O lines.

The retrieved global mean value of HFC-134a at the top of the retrieval range (16.5 km) was 25.0 pptv which is slightly below the predicted surface value of ~27.6 pptv for 2004, which one obtains from the 2000 VMR and growth rates [*WMO*, 2003 (Table 1-12)]. Since no stratospheric profiles of any HFCs were available, the profile was extended to higher altitudes by grafting on an extension with the same shape as the scaled and shifted HCFC-22 profiles. HFC-134a is a relatively long-lived HFC with a lifetime of 14.0 years, which is comparable to the 12.0 year lifetime of HCFC-22. A scale factor of 0.155 was applied to the HCFC-22 profiles based the ratio of the values at 16.5 km.

4.2.5 Minor organic fluorine species

Fifteen other organic fluorine species, listed in Table 4-2, including PFCs, CFCs, HCFCs, HFCs and halons were also included in the calculation of F_{TOT}. These species have low individual VMRs but when combined their contribution is not negligible. Profiles for the different classes of species were determined as follows. Perfluorocarbons (PFCs) are long-lived species with lifetimes of thousands of years; therefore, their profiles are expected to be nearly vertical, resembling the profile of the simplest PFC, CF_4. The PFCs CF_3CF_3, C_3F_8 and *c*-C_4F_8 (a cyclic compound) had a combined surface VMR equivalent to 0.0311 ppbv fluorine; therefore, a profile for their fluorine contribution was simulated by scaling the retrieved CF_4 profile by a factor of 0.41 (0.0311 ppbv divided by the maximum retrieved VMR of CF_4 averaged over the five latitude zones). Profiles of the minor CFCs in Table 4-2 are expected to resemble the shape of the other CFC profiles. Since we have not measured any halons, these were grouped with the CFCs, resulting in a surface contribution equivalent to 0.148 ppbv fluorine, so a profile for the fluorine contribution from the minor CFCs and halons was simulated by scaling the profile of CFC-12 by a factor of 0.28. Profiles of HCFCs and HFCs are assumed to resemble the shape of the HCFC-22 profiles. The minor HCFCs and HFCs had a combined VMR equivalent to 0.107 ppbv fluorine; therefore, profiles for their fluorine contribution were simulated by scaling the HCFC-22 profiles by a factor of 0.58.

Table 4-2: Minor organic fluorine species included in the fluorine budget based on their predicted surface values in Table 1-12 of the 2002 WMO Report [2003]. VMRs are given in parts per trillion by volume (pptv).

Chemical Formula	Industrial Name	VMR	VMR contribution to F_{TOT}
CF_3CF_3	PFC-116	3.32	19.9
C_3F_8	PFC-218	0.3	2.4
c-C_4F_8	PFC-318	1.1	8.8
Total minor PFC Contribution			**31.1**
$CClF_3$	CFC-13	3.5	10.5
$CClF_2CClF_2$	CFC-114	16.4	65.6
CCl_2FCF_3	CFC-114a	1.8	7.2
$CClF_2CF_3$	CFC-115	9.2	46.0
$CBrClF_2$	Halon-1211	4.16	8.32
$CBrF_3$	Halon-1301	3.11	9.33
$CBrF_2CBrF_2$	Halon-2402	0.38	1.52
Total minor CFC and halon contribution			**148.47**
$CHClFCF_3$	HCFC-124	2.7	10.8
CH_3CCl_2F	HCFC-141b	20.9	20.9
CHF_3	HFC-23	19.1	57.3
CHF_2CF_3	HFC-125	2.6	13.0
CH_3CHF_2	HFC-152a	2.5	5.0
Total minor HCFC and HFC contribution			**107.0**

4.2.6 SF_6

ACE-FTS version 2.2 SF_6 had a problem at the high altitude end of the retrieval relating to the *a priori* profile that was used for the atmospheric layers above the highest retrieved altitude. After correcting the problem by using a more realistic *a priori*, SF_6 was re-retrieved for this work, over the 7.5-30.5 km altitude range. Although the maximum mean VMR of SF_6 from ACE-FTS measurements was only 0.00661 ppbv at 7.5 km in the tropics, with six fluorine atoms, this is equivalent to 0.04 ppbv fluorine. *Sen et al.* [1996], *Patra et al.* [1997] and *Burgess et al.* [2004] all report stratospheric SF_6 profiles, while in *Zander et al.* [1992], SF_6 decreased to zero near 20 km. According to *Ravishankara et al.* [1993] and *Morris et al.* [1995], SF_6 has a long lifetime in the stratosphere and is decomposed by UV absorption and electron reactions in the mesosphere. The *Patra et al.* [1997] results are the most consistent with a long stratospheric lifetime and decomposition beginning at the stratopause but the slope of the *Burgess et al.* [2004] profile most resembles the ACE-FTS results in the lower stratosphere. A more recent paper by *Burgess et al.* [2006] shows SF_6 profiles with a shape similar to their earlier work. Therefore, the ACE-FTS SF_6 profiles were extrapolated based on a combination of the *Patra et al.* [1997] and *Burgess et al.* [2004] profiles, beginning near 30.5 km altitude and smoothly decreasing to zero at 49.5 km for the midlatitudes. In the tropics and high latitudes, a vertical shift was applied to the midlatitude

extrapolation so that it coincided with the measured portion of the profile. ACE-FTS retrieved SF_6 profiles and their extensions are shown in Figure 4-2.

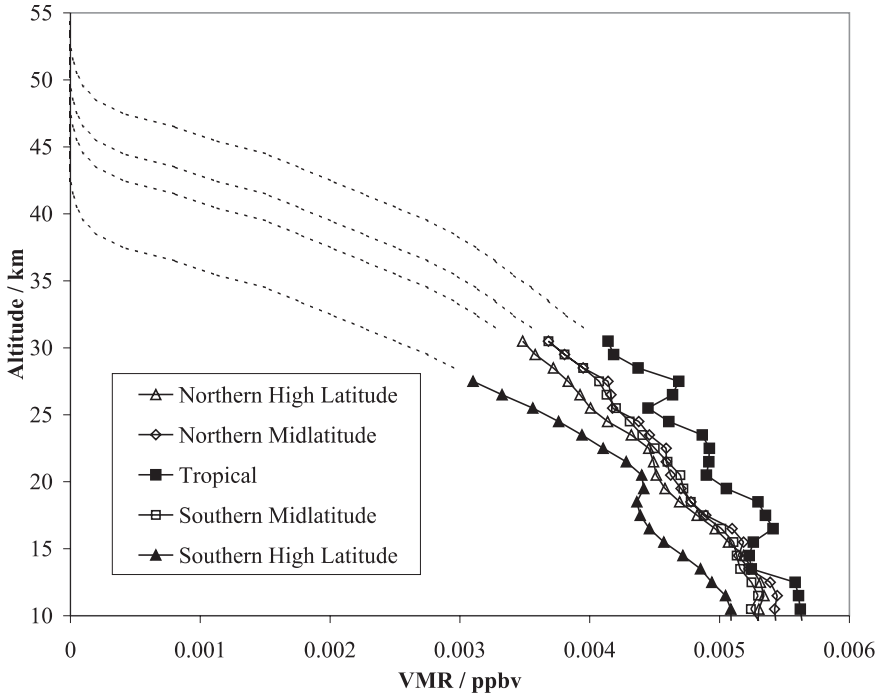

Figure 4-2: ACE-FTS retrieved profiles of SF_6 extended to the upper stratosphere based on a combination of SF_6 profiles found in *Patra et al.* [1997] and *Burgess et al.* [2004]. SF_6 makes a very small contribution to stratospheric F_{TOT}.

4.3 Results and Discussion

Figure 4-3 shows HF, COF_2, COClF, CF_y and F_{TOT} profiles in each latitude region, indicating that CF_y dominates in the lower stratosphere while HF dominates in the upper stratosphere. Using retrieved temperature profiles, the altitudes of the tropopause and stratopause were determined, and by extension an appropriate altitude range (17.5-50.5 km) for determination of mean stratospheric F_{TOT}. The temperature minimum was used to define the tropopause, rather than the lapse rate as recommended by the WMO, to avoid placing the tropopause at very low altitudes during the polar winters. F_{TOT} as a function of altitude in each region is given in Table 4-3. Mean values of F_{TOT} in each region ranging from 2.50 to 2.59 ppbv are given in Table 4-4. Aside from the highest value occurring in the tropics, there is no clear latitudinal dependence.

Table 4-3: F_{TOT} as a function of altitude from 17.5 to 50.5 km in five latitude zones.

Altitude / km	Total Fluorine / ppbv				
	North Polar	North Mid	Tropics	South Mid	South Polar
17.5	2.53	2.54	2.65	2.54	2.56
18.5	2.50	2.52	2.61	2.54	2.61
19.5	2.49	2.51	2.57	2.56	2.66
20.5	2.52	2.55	2.59	2.59	2.68
21.5	2.56	2.61	2.63	2.61	2.64
22.5	2.59	2.64	2.66	2.64	2.60
23.5	2.57	2.64	2.64	2.65	2.57
24.5	2.55	2.60	2.60	2.63	2.55
25.5	2.54	2.58	2.58	2.61	2.54
26.5	2.56	2.59	2.65	2.62	2.54
27.5	2.58	2.60	2.67	2.61	2.54
28.5	2.60	2.63	2.66	2.61	2.52
29.5	2.59	2.64	2.66	2.59	2.49
30.5	2.57	2.63	2.65	2.54	2.45
31.5	2.54	2.59	2.64	2.50	2.42
32.5	2.51	2.55	2.62	2.46	2.40
33.5	2.49	2.53	2.58	2.45	2.41
34.5	2.48	2.52	2.54	2.44	2.44
35.5	2.48	2.50	2.51	2.42	2.46
36.5	2.50	2.50	2.51	2.43	2.49
37.5	2.52	2.52	2.53	2.45	2.49
38.5	2.53	2.50	2.54	2.46	2.48
39.5	2.54	2.51	2.57	2.47	2.48
40.5	2.54	2.52	2.60	2.47	2.48
41.5	2.55	2.52	2.61	2.48	2.47
42.5	2.54	2.52	2.61	2.49	2.46
43.5	2.55	2.50	2.58	2.50	2.45
44.5	2.56	2.49	2.55	2.51	2.44
45.5	2.56	2.49	2.53	2.51	2.44
46.5	2.57	2.48	2.54	2.51	2.44
47.5	2.59	2.48	2.57	2.53	2.45
48.5	2.60	2.49	2.57	2.52	2.45
49.5	2.60	2.50	2.57	2.53	2.46
50.5	2.59	2.50	2.54	2.53	2.45

Table 4-4: Number of profiles for each latitude range (prior to removing outliers). Mean F_{TOT} and its slope (17.5-50.5 km range) with 1σ precision, and ACE-FTS HF and F_y at 55 km are also given.

Region	Profiles used	Mean F_{TOT} (ppbv)	Slope (ppbv/km)	HF at 55 km (ppbv)	Fy at 55 km (ppbv)
60-82°N	250	2.55±0.04	+0.0011±0.0006	2.08	2.11
30-60°N	287	2.54±0.05	-0.0036±0.0007	1.96	1.99
30°S-30°N	273	2.59±0.05	-0.0027±0.0007	1.87	1.95
30-60°S	238	2.53±0.07	-0.0037±0.0010	1.97	2.02
60-82°S	171	2.50±0.07	-0.0056±0.0008	1.94	1.97

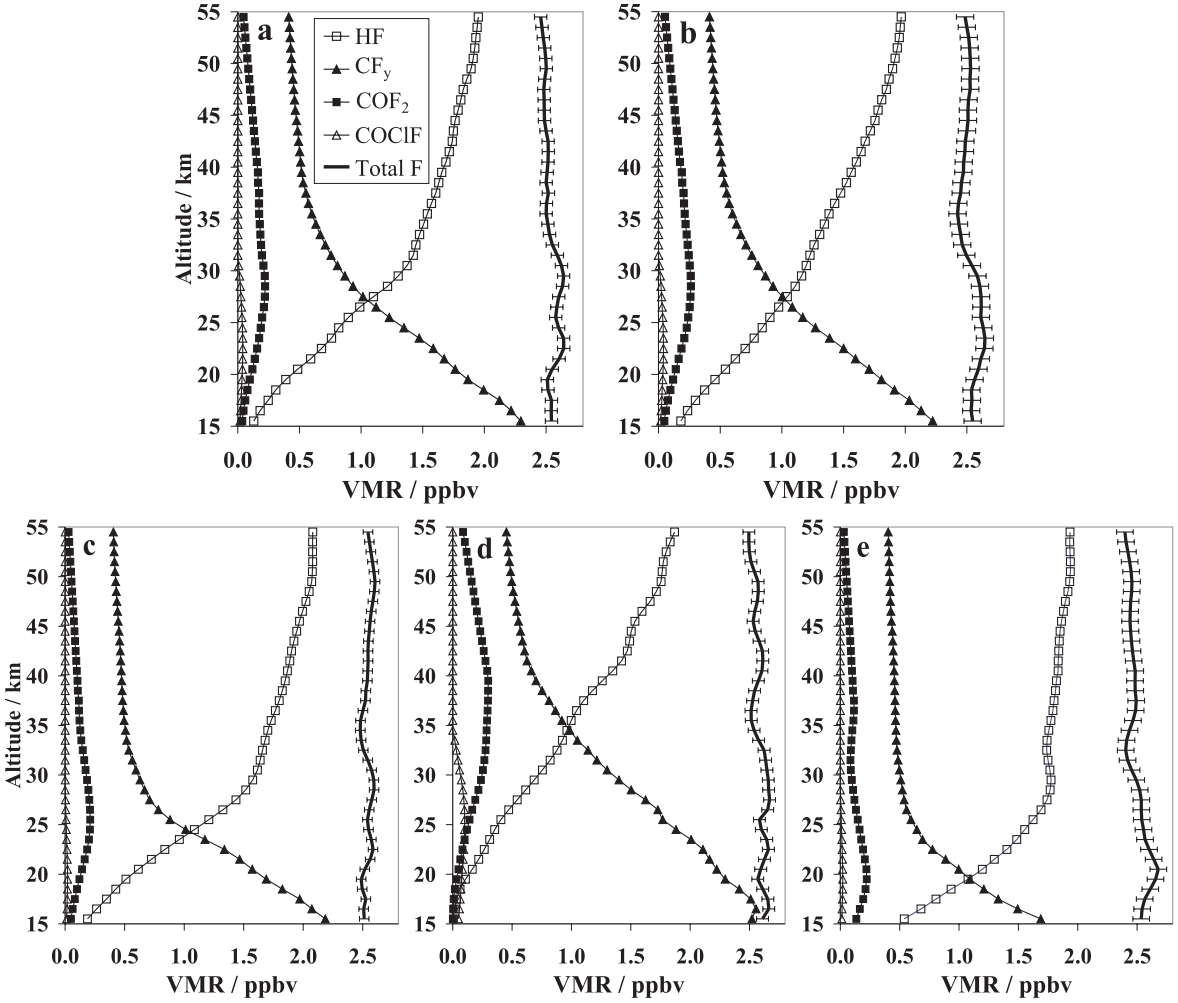

Figure 4-3: Stratospheric fluorine inventories for 2004: (a) northern midlatitudes (30-60ºN), (b) southern midlatitudes (30-60ºS), (c) northern high latitudes (60-82ºN), (d) tropics (30ºS-30ºN), (e) southern high latitudes (60-82ºS). SF_6 is not shown but its contribution is included in the F_{TOT} profiles. Error bars on the F_{TOT} profiles indicate the 1σ variability.

In all latitude zones, stratospheric F_{TOT} nearly forms a straight line, where slight deviations from a line may result from atmospheric variability, error in the data or possibly missing fluorine species that make a small contribution. The very short-lived species COHF and CF_3OH, which result from the dissociation of organic fluorine species [*Tuazon and Atkinson,* 1993], have not been included in this inventory and may account for some missing fluorine in the mid-stratosphere. If F_{TOT} is fit to a straight line, it is essentially vertical with a very slight negative slope in ppbv/km (Table 4-4), in four of five latitude zones, the exception being the northern high latitudes. Negative slopes would be qualitatively consistent with increasing fluorine over time since older air at high altitudes has a lower VMR than younger air at low altitudes; however, the slopes determined here are only marginally significant relative to their 1σ uncertainty. Additional evidence for the

continual increase in fluorine arises from the highest mean value of F_{TOT} occurring in the tropics which contains the youngest air if mean stratospheric circulation is considered. The lack of a clear pattern of latitudinal variation in the middle and high latitudes is consistent with the modeling work of *Neu and Plumb* [1999], which found greater mixing in the middle and high latitude stratosphere relative to the tropics. The reason for higher HF and F_{TOT} values in the northern hemisphere (especially at high latitudes) is not clear and could indicate a problem with the HF retrieval at high altitudes, or may be real atmospheric variability resulting from greater fluorine emissions in the northern hemisphere.

Due to the general decrease in signal-to-noise ratios with altitude in ACE-FTS spectra for most species, it was necessary for us to extrapolate certain profiles. This makes little difference for F_{TOT} when species occur at low levels like SF_6 or CFC-113, but the COF_2 extrapolation which began at about 40 km has a large impact on high altitude F_{TOT}. To ensure the validity of our mean stratospheric F_{TOT} values and slopes, the values were compared to equivalent values based on the 17.5-39.5 km range, which involved much less extrapolation. It indicated that the low altitude range F_{TOT} values were within ±0.02 ppbv from the values spanning the entire stratosphere.

The 1σ precision on mean F_{TOT} is 0.04-0.07 ppbv, obtained using the method of error determination from *Zander et al.* [1996] for total stratospheric chlorine. It is based on the standard deviation of points over a given altitude range and was adopted here as a reasonable estimate of the precision, but the absolute accuracy, which would include systematic errors from all sources for F_{TOT} is more difficult to determine. Propagating the uncertainty on each species to obtain the F_{TOT} uncertainty would largely overestimate the overall uncertainty because the variability in any given species is mostly a result of conversion to another species. Furthermore, it is difficult to accurately estimate the uncertainty for the modeled and extrapolated data.

Perhaps the best simple estimate of the absolute uncertainty on F_{TOT} can be made based on the uncertainty of HF, which is the dominant contributor to F_{TOT} at high altitudes. The retrieval of HF utilized spectroscopic parameters from the HITRAN 2004 database [*Rothman et al.*, 2005]. The HF line intensities in HITRAN that lie in the microwindows shown in Table 4-1, have uncertainties in the 2-5% range, which translates to a maximum of ~0.10 ppbv HF. The uncertainty contribution to the VMR of HF from the retrieval of pressure and temperature is estimated to be about 2% or about 0.04 ppbv. An additional source of uncertainty for the HF retrieval comes from the precision of the fit, which increases rapidly with altitude, but this random error can be reduced by averaging multiple profiles. The 1σ error contribution from the precision of the fit for the southern midlatitude mean profile, which had the highest number of profiles used to determine its mean, is only 0.001 ppbv at 18 km, and increases to 0.012 ppbv (or 0.6%) at 50 km, while for the northern high latitude mean profile, which used the fewest profiles, the precision is actually better at 0.010 ppbv at 50 km. Combining the upper limit estimates from these three sources of error gives an accuracy of 0.11 ppbv for HF at 50 km, which is dominated by the error in line intensities but includes both a systematic and random component. This value can be used to estimate the accuracy of the F_{TOT} values. On average, HF comprises 76% of F_{TOT} at 50 km (72-82% over the

five latitude zones), so scaling the error would give an accuracy of 0.15 ppbv for F_{TOT}, which is equivalent to 6% of mean F_{TOT}. Although the fluorine contribution to F_{TOT} from HF differs with latitude zone, it is reasonable to estimate that the accuracies should be comparable. This uncertainty is smaller than the estimated precision from random variability in the HF mean values at 50 km, but greater than the precision in F_{TOT} profiles over the 17.5-50.5 km range.

As mentioned earlier, HALOE on UARS measured HF from 1991-2005 which has been used to determine stratospheric inorganic fluorine (F_y) [*Russell et al.*, 1996; *Anderson et al.*, 2000]. F_y is calculated from HALOE HF measured at 55 km altitude by dividing HF by a latitude-dependent HF/F_y ratio. HF and F_y in the HALOE record continue to increase [*Anderson et al.*, 2004], with 2004 global mean HF and F_y values of 1.75 ppbv and 1.97 ppbv respectively (*J. Anderson,* private communication, 2006). By latitudinally weighting the HF values in Table 4-4, a global mean value of 1.95 ppbv for HF at 55 km was determined. This is 11% higher than the HALOE HF value, similar to earlier ACE and HALOE HF comparisons [*McHugh et al.*, 2005]. In contrast, the ACE-FTS global mean F_y of 2.00 ppbv is much closer to the HALOE value since our F_y at 55 km only consists of HF and COF_2 resulting in higher HF/F_y ratios. It is not clear which species in addition to HF and COF_2 contribute to F_y at 55 km, but organic species such as $CHClF_2$, CF_4, CF_3CF_3, C_3F_8 and *c*-C_4F_8 account for 0.38-0.46 ppbv of F_{TOT} at 55 km.

4.4 Conclusions

This chapter describes an inventory of global stratospheric fluorine including organic and inorganic species in five latitude zones during the period of February 2004 - January 2005 inclusive, based on measurements by the ACE-FTS, supplemented by altitude extensions based on modeling work, and some calculated profiles for minor species. This fluorine inventory includes several species that have not been included in past fluorine inventories, due to the changing composition of trace gases in the atmosphere as well as the unique ability of the ACE-FTS to retrieve some of these species. The sum of all significant fluorine-containing species at each altitude from 17.5-50.5 km, nearly makes a straight line, typically with a slight negative slope. Averaging these points gives mean stratospheric F_{TOT} values for each latitude region ranging from 2.50-2.59 ppbv, with a 1σ variability of 0.04-0.07 ppbv. The highest mean F_{TOT} is found in the tropics, and most F_{TOT} slopes are negative, both of which are qualitatively consistent with increasing levels of stratospheric fluorine and the mean global stratospheric circulation pattern.

References

Anderson, J., J.M. Russell III, Long Term Changes of HCl and HF as Observed by HALOE (2004), Abstract 363 in Ozone, vol. I, Proceedings of the XX Quadrennial Ozone Symposium, Kos, Greece, 1-8 June 2004, editor: C.S. Zerefos.

Anderson, J., J.M. Russell III, S. Solomon, L.E. Deaver (2000), Halogen Occultation Experiment confirmation of stratospheric chlorine decreases in accordance with the Montreal Protocol, *J. Geophys. Res.*, 105, 4483-4490.

Burgess, A.B., R.G. Grainger, A. Dudhia, V.H. Paynem V.L. Jay (2004), MIPAS measurement of sulfur hexafluoride (SF_6), *Geophys. Res. Lett.*, 31, L05112.

Burgess, A.B., R.G. Grainger, A. Dudhia (2006), Zonal mean atmospheric distribution of sulfur hexafluoride (SF_6), *Geophys. Res. Lett.*, 33, L07809.

Clerbaux, C., R. Colin, P.C. Simon, C. Granier (1993), Infrared cross sections and global warming potentials of 10 alternative hydrohalocarbons, *J. Geophys. Res.*, 98(D6), 10491-10497.

Coheur, P.F., C. Clerbaux, R. Colin (2003), Spectroscopic measurements of halocarbons and hydrohalocarbons by satellite-borne remote sensors, *J. Geophys. Res.*, 108, 4130.

Dufour, G., C.D. Boone, P.F. Bernath (2005), First measurements of CFC-113 and HCFC-142b from space using ACE-FTS infrared spectra, *Geophys. Res. Lett*. 32, L15S09.

Kaye, J.A., A.R. Douglass, C.H. Jackman, R.S. Stolarski (1991), Two-Dimensional Model Calculation of Fluorine-Containing Reservoir Species in the Stratosphere, *J. Geophys. Res.* 96, 12865-12881.

McHugh, M., B. Magill, K.A. Walker, C.D. Boone, P.F. Bernath J.M. Russell III (2005), Comparison of atmospheric retrievals from ACE and HALOE, *Geophys. Res. Lett.*, 32, L15S10.

Morris, R.A. T.M. Miller, A.A. Viggiano, J.F. Paulson (1995), Effects of electron and ion reactions on atmospheric lifetimes of fully fluorinated compounds, *J. Geophys. Res.*, 100(D1), 1287-1294.

Nassar, R., P.F. Bernath, C.D. Boone, G.L. Manney, S.D. McLeod, C.P. Rinsland, R. Skelton, K.A. Walker (2005), Stratospheric abundances of water and methane based on ACE-FTS measurements, *Geophys. Res. Lett.*, 32 L15S04.

Nassar, R., P.F. Bernath, C.D. Boone, S.D. McLeod, R. Skelton, K.A. Walker, C.P. Rinsland, P. Duchatelet (2006a), A global inventory of stratospheric fluorine in 2004 based on ACE-FTS measurements, *J. Geophys. Res.*, submitted.

Nassar, R., P.F. Bernath, C.D. Boone, C. Clerbaux, P.F. Coheur, G. Dufour, L. Froidevaux, E. Mahieu, J.C. McConnell, S.D. McLeod, D.P. Murtagh, C.P. Rinsland, K. Semeniuk, R. Skelton, K.A. Walker, R. Zander (2006b), A global inventory of stratospheric chlorine in 2004, *J. Geophys. Res.*, submitted.

Nemtchinov, V., P. Varanasi (2004), Absorption cross-sections of HFC-134a in the spectral region between 7 and 12 μm, *Journal of Quantitative Spectroscopy and Radiative Transfer*, 83, 285-294.

Neu, J.L., R.A. Plumb (1999), Age of air in a "leaky pipe" model of stratospheric transport, *J. Geophys. Res.*, 104, 19243-19255.

Patra, K.P., S. Lal, B.H. Subbaraya, C.H. Jackman, P. Rajaratnam (1997), Observed vertical profile of sulphur hexafluoride (SF_6) and its atmospheric applications, *J. Geophys. Res.*, 102, 8855-8859.

Ravishankara, A.R., S. Solomon, A.A. Turnipseed, R.F. Warren (1993), Atmospheric lifetimes of long-lived halogenated species, *Science*, 259, 194-199.

Rinsland, C.P., C. Boone, R. Nassar, K. Walker, P. Bernath, E. Mahieu, R. Zander, J.C. McConnell, L. Chiou (2005), Trends of HF, HCl, CCl_2F_2, CCl_3F, $CHClF_2$ (HCFC-22), and SF_6 in the lower stratosphere from Atmospheric Chemistry Experiment (ACE) and Atmospheric Trace Molecule Spectroscopy (ATMOS) measurements near 30ºN latitude, *Geophys. Res. Lett.*, 32, L16S03.

Rinsland C.P., E. Mahieu, R. Zander, R. Nassar, P. Bernath, C. Boone, L. S. Chiou (2006a), Long-term stratospheric carbon tetrafluoride (CF_4) increase inferred from 1985–2004 infrared space-based solar occultation measurements, *Geophys. Res. Lett.*, 33, L02808.

Rinsland, C.P., R. Nassar, C.D. Boone, P.F. Bernath, B. Jelley, L. Chiou, D.K. Weisenstein, G. Dufour, E. Mahieu, R. Zander (2006b), Spectroscopic Detection of COClF in the Tropical and Mid-Latitude Lower Stratosphere from Atmospheric Chemistry Experiment Infrared Spectra: Preliminary Retrievals and Comparison with Previous Measurements and Model Calculations, *Geophys. Res. Lett.*, submitted.

Rothman, L.S., D. Jacquemart, A. Barbe, D.C. Benner, M. Birk, L.R. Brown, M.R. Carleer, C. Chackerian Jr., K. Chance, L.H. Coudert, V. Dana, V.M. Devi, J.-M. Flaud, R.R. Gamache, A. Goldman, J.-M. Hartmann, K.W. Jucks, A.G. Maki, J.-Y. Mandin, S.T. Massie, J. Orphal, A. Perrin, C.P. Rinsland, M.A.H. Smith, J. Tennyson, R.N. Tolchenov, R.A. Toth, J. Vander Auwera, P. Varanasi, G. Wagner (2005), The HITRAN 2004 molecular spectroscopic database, *Journal of Quantitative Spectroscopy and Radiative Transfer*, 96, 139-204..

Rummukainen, M. (1996), Modeling stratospheric chemistry in a global three-dimensional chemical transport model, SCTM-1: Model development, *Finn. Meteorol. Inst. Contrib., 19*, 206 pages.

Russell, J.M. III, L.E. Deaver, M. Luo, R.J. Cicerone, J.H. Park, L.L. Gordley, G.C. Toon, M.R. Gunson, W.A. Traub, D.G. Johnson, K.W. Jucks, R. Zander, I.G. Nolt (1996), Validation of hydrogen fluoride measurements made by the Halogen Occultation Experiment from the UARS platform, *J. Geophys. Res.,* 101(D6), 10163-10174.

Sen, B., G.C. Toon, J.-F. Blavier, E.L. Fleming, C.H. Jackman (1996) Balloon-borne observations of midlatitude fluorine abundance, *J. Geophys. Res.*, 101, 9045-9054.

Stolarski, R.S., R.D. Rundel (1975), Fluorine photochemistry in the stratosphere, *Geophys. Res. Lett.*, 22, 385-388.

Tuazon, E.C., R. Atkinson (1993), Tropospheric Transformation Products of a Series of Hydroflurocarbons and Hydrochlorofluorocarbons, *J. Atmos. Chem.*, 17, 179-199.

Weisenstein, D.K., M.K.W. Ko, N.-D. Sze (1992), The Chlorine Budget of the Present-Day Atmosphere: A Modeling Study, *J. Geophys. Res.*, 97, 2547-2559.

World Meteorological Organization (2003), Scientific Assessment of Ozone Depletion: 2002. Global Ozone Research and Monitoring Project - Report No. 47, Geneva, Switzerland.

Zander, R., M.R. Gunson, C.B. Farmer, C.P. Rinsland, F.W. Irion, E. Mahieu (1992), The 1985 Chlorine and Fluorine Inventories in the Stratosphere Based on ATMOS Observations at 30º North Latitude, *J. Atmos. Chem*., 15, 171-186.

Zander, R., E. Mahieu, M.R. Gunson, M.C. Abrams, A.Y. Chang, M. Abbas, C. Aellig, A. Engel, A. Goldman, F.W. Irion, N. Kämpfer, H.A. Michelsen, M.J. Newchurch, C.P. Rinsland, R.J. Salawitch, G.P. Stiller, G.C. Toon (1996), The 1994 northern midlatitude budget of stratospheric chlorine derived from ATMOS/ATLAS-3 observations, *Geophys. Res. Lett.,* 23(17) 2357-2360.

Chapter 5

Stratospheric Water and Methane Abundances

5.1 Introduction

The general pattern of circulation governing the exchange of air between the stratosphere and troposphere is known as the Brewer-Dobson circulation [*Brewer*, 1949], as was briefly mentioned in Chapters 3 and 4. In the Brewer-Dobson circulation, air ascends in the tropical troposphere and crosses the tropical tropopause layer (TTL); then the tropical air moves poleward to stratospheric midlatitudes, and finally it descends at the poles (Figure 5-1). This wave-driven directional flow is responsible for most of the exchange between the stratosphere and troposphere, but a very small amount of additional exchange can occur in the midlatitudes.

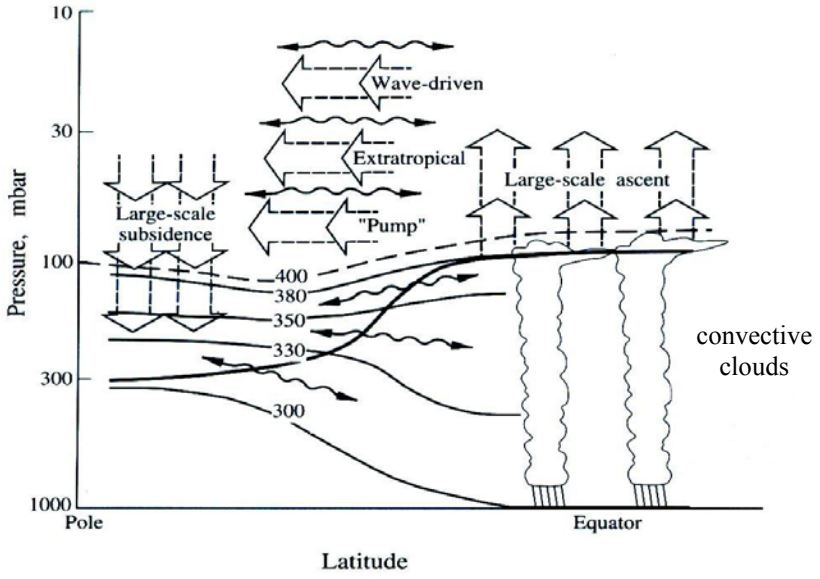

Figure 5-1: The pattern of large scale transport between the troposphere and stratosphere is shown by the broad arrows. The numbers and thin contour lines denote isentropic surfaces which will be described in the next chapter. A minor contribution to stratosphere-troposphere exchange occurs along the wavy arrows. Figure reproduced from *Holton et al.* [1995].

The amount of water that enters the stratosphere closely relates to this pattern of circulation, and water vapor in the stratosphere plays an important role in climate and the chemistry of Earth's atmosphere. Elevated levels of water, an important greenhouse gas, are known to enhance tropospheric warming and stratospheric cooling [*Rind and Lonergan*, 1995; *Shindell*, 2001]. Although numerous other greenhouse gases contribute to changes in the temperature profile of Earth's atmosphere, the presence of water in the stratosphere, accompanied by enhanced cooling, also increases the formation of polar stratospheric clouds (PSCs) during the polar winter. PSCs

then enable heterogeneous reactions to produce species that can catalytically destroy polar stratospheric ozone in the spring, as discussed in Chapter 3. The total volume of PSCs formed during a particular winter is perhaps the most important climate parameter driving the evolution of Arctic ozone loss [*Rex et al.*, 2004]. The removal of stratospheric water by sedimentation into PSCs which rapidly fall to lower altitudes, occurs frequently in the Antarctic vortex and sporadically in the Arctic vortex. The descent of water vapor in the vortex without sedimentation may also alter water vapor profiles significantly, particularly when the vortex is strong [*Nassar et al.*, 2005].

The major photochemical source of water in the stratosphere is oxidation of CH_4 by the net reaction:

$$CH_4 + 2O_2 \rightarrow 2H_2O + CO_2 \qquad (5.1)$$

in which one CH_4 molecule creates two H_2O molecules. The oxidation of all other hydrocarbons makes a negligible contribution to $[H_2O]$ (where the square brackets denote VMR). A high level of variability is often observed if one treats H_2O and CH_4 independently, but the quantity $[H_2O]+2[CH_4]$, referred to as potential water (PW), is essentially conserved with CH_4 oxidation. Total hydrogen, a truly conserved quantity, is often estimated by the sum of PW and $[H_2]$.

Numerous studies have detected an increase in stratospheric water vapor occurring over time periods as short as a few years and as long as the past half-century [*Oltmans et al.*, 2000; *Michelsen et al.*, 2000; *Rosenlof et al.*, 2001]. The increase can partially be attributed to an increase in CH_4 emissions, but the remainder is attributed to an increase in water vapor entering the stratosphere across the TTL. More recent evidence indicates that the increase in stratospheric $[H_2O]$ has ceased in the last few years, and has even shown a temporary decrease over a period of about 3-4 years [*Nedoluha et al.*, 2003; *Randel et al.*, 2004]. Understanding changes in stratospheric water vapor and water vapor entering the stratosphere, or $[H_2O]_e$, requires a better understanding of the relative importance of the numerous tropical dehydration processes and processes that control humidity near the TTL.

Determination of trends in water data is complicated by long-term variability, the quasi-biennial oscillation, as well as the seasonal variability of water vapor entering the stratosphere, with maximum water ascending through the TTL during the northern hemisphere (NH) summer and a minimum during the NH winter. This seasonal variability creates a pattern in the stratosphere that is a record of the amount of water that has passed the TTL, and is often referred to as the tape recorder effect [*Mote et al.*, 1996]. In addition to issues regarding the variability of water vapor, comparisons between the many water datasets are complicated by the different types of measurements (*in situ* or remote sounding), numerous different types of instruments (hygrometers, radiometers, spectrometers, etc.) and measurement platforms (ground, aircraft, balloon, or satellite). In spite of these factors, extensive attempts at comparison for the purpose of establishing water trends as well as measurement validation continue to be made [*SPARC,* 2000; *Michelsen et al.*, 2002].

This chapter examines ACE-FTS profiles of midlatitude [H_2O], [CH_4] and PW from the mid-troposphere to the mesopause, as described in *Nassar et al.* [2005b]. [H_2O] versus [CH_4] correlations are included to facilitate the direct comparison of potential water with past measurements made by the ATMOS instrument and furthermore compare the ACE-FTS calculated value of water entering the stratosphere to ATMOS values.

5.2 ACE-FTS H_2O and CH_4 Retrievals

The results in this chapter were obtained using ACE-FTS version 1.0 data. The v1.0 H_2O retrieval utilized 52 microwindows, in the 1362-2137 cm^{-1} range to retrieve profiles from 6.5 to 88.5 km altitude. 64 CH_4 microwindows in the 1245-2889 cm^{-1} range were used to retrieve profiles from 4.5 to 62.5 km altitude [*Boone et al.*, 2005]. The retrieved H_2O and CH_4 profiles each have statistical uncertainties (a measure of the random error in the fitting process that does not include systematic errors) of less than 2.0% for the stratosphere, but higher in the troposphere and mesosphere. A complete error analysis has not yet been carried out for all species measured by the ACE-FTS; however, *Clerbaux et al*. [2005] have done an error analysis for ACE-FTS CO measurements. Their analysis suggests that the total error is mainly due to measurement error with smaller contributions from other sources such as smoothing, instrument line shape and temperature retrievals. With the large number of microwindows used in the H_2O and CH_4 retrievals, measurement error is expected to be relatively small, thus exerting a negligible influence on the final results, but a more thorough error analysis is left for future work.

5.3 Results and Analysis

The specific data used in this work consist of NH measurements spanning February to April of 2004 scattered over a range of latitudes from 0 to 79.8ºN. The occultations were classified using a combination of potential vorticity data and [CH_4] versus [N_2O] correlations, as described in the following chapter and by *Nassar et al.* [2005a], where the classes and the correlation approach applied are similar to the method of *Michelsen et al.* [1998a, 1998b]. In this work, occultations that have been classified to be outside of the polar vortex region, but not in the tropics or subtropics, are referred to as midlatitude occultations.

Average profiles were created of midlatitude [H_2O] and [CH_4], and potential water (PW) was determined as [H_2O]+2[CH_4]. Figure 5-2 shows 83 individual midlatitude profiles of [H_2O] and [CH_4] as well as the mean profiles. The PW profile is also plotted and appears nearly vertical from ~20-50 km, as expected. It is shown without individual profiles, but rather error bars indicating one standard deviation variability for an individual profile from the mean PW. The statistical fitting uncertainties were ignored when calculating the error bars because they were typically small compared to the variability between profiles. Error bars could have been plotted for [H_2O] and [CH_4] independently and propagated to obtain an error on PW; however, this would ignore the anti-correlation between [H_2O] and [CH_4] which accounts for most of the observed variability in the middle to upper stratosphere (~30-48 km).

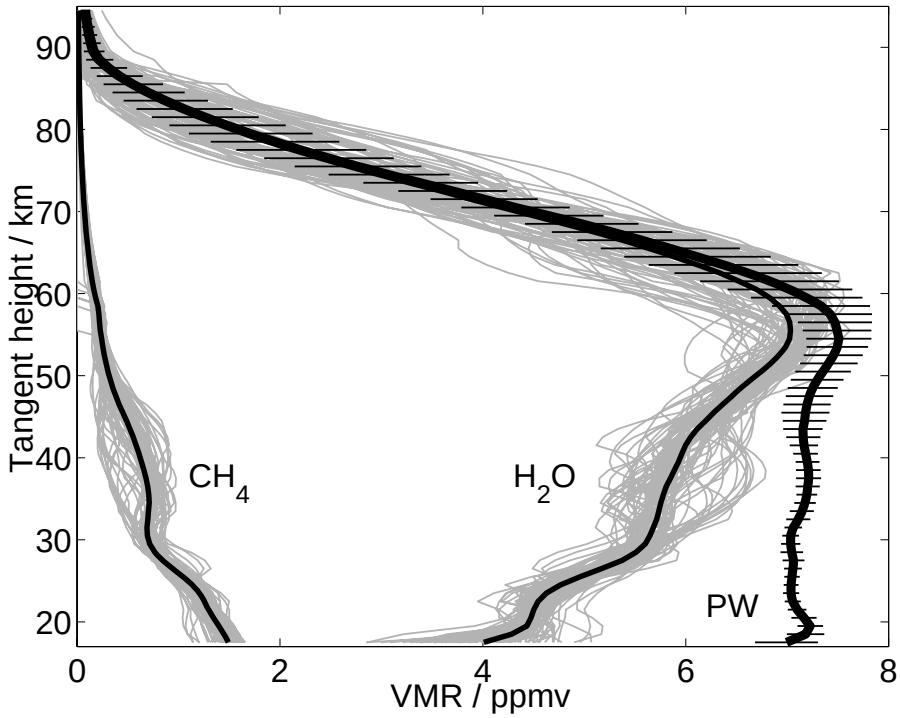

Figure 5-2: Midlatitude [H_2O], [CH_4] and PW profiles from 21 March to 2 April 2004 with latitude decreasing during this time period from 66ºN to 30ºN. The thick black lines are the averaged profiles taken from the 83 individual profiles shown as thin lines. The derivation of the error bars for PW is explained in Section 5.3.

In Figure 5-3, [H_2O] and [CH_4] correlations were plotted in the same manner as carried out with ATMOS data by *Michelsen et al.* [2000], which was based on earlier work by *Abbas et al.* [1996]. The 83 occultations used here and in the profiles were selected to minimize seasonal variation when comparing to ATMOS. To be consistent with the analysis by *Michelsen et al.* [2000], points from 18 to 40 km were plotted as open circles. The points in this range were fit to a line (and others ignored) for which the slope is approximately -2 (implying one CH_4 molecule oxidizes to two H_2O molecules), and the intercept represents the PW or the [H_2O] when CH_4 is fully oxidized. By this method, the slope is -2.02±0.06 and the intercept PW is 7.14±0.05 ppmv. From the profiles, PW is calculated to be 7.12±0.02 ppmv by taking the average PW at tangent heights from 18 to 40 km. The above uncertainty stated for the PW fit comes from the error in determining the intercept, and the uncertainty stated for PW from the profiles is the standard deviation from the mean. Both values agree within their calculated uncertainties, and one would expect to obtain the same value from both methods if the slope of the fit was fixed at exactly -2. Thus although the fit gives a larger uncertainty, it is most likely more realistic since it does not exclude the small contributions from side reactions for H_2O and CH_4 in addition to CH_4 oxidation, or other factors that may cause a deviation from an ideal slope of -2. If a systematic error of ±3% is applied and combined with the precision from the PW fit, then the best value for PW becomes 7.12±0.23 ppmv.

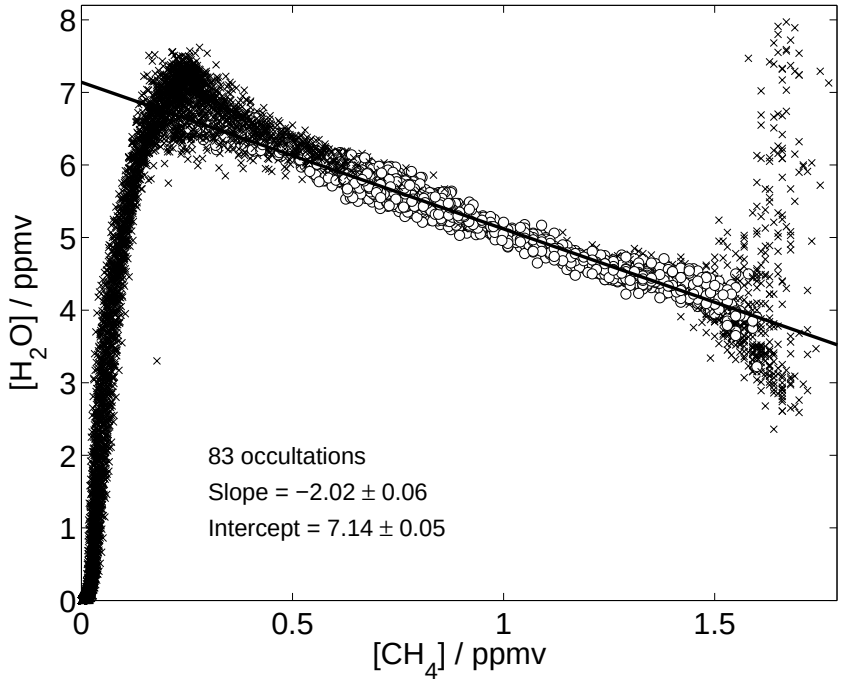

Figure 5-3: Correlation between midlatitude $[H_2O]$ and $[CH_4]$ to determine potential water, based on the same 83 occultations as in the previous figure. A linear fit was carried out for points between 18 and 40 km (open circles) to determine the slope and intercept.

The quantity of water entering the stratosphere across the TTL or $[H_2O]_e$ is difficult to determine directly from ACE-FTS measurements because of the high degree of variability of water vapor near the TTL. A full year of measurements would be required in order to properly average over both day-to-day variations and the large expected seasonal variation. However, $[H_2O]_e$ can be calculated using a variety of methods [*SPARC*, 2000]. Here the relationship:

$$[H_2O]_e = [H_2O] - \beta([CH_4]_e - [CH_4]) \qquad (5.2)$$

first proposed by *Hansen and Robinson* [1989] is used, where β is the magnitude of the slope of the correlation plot and $[CH_4]_e$ is the VMR of methane entering the stratosphere across the TTL. This rearranges to:

$$[H_2O]_e = [H_2O] + \beta[CH_4] - \beta[CH_4]_e \qquad (5.3)$$

$$\text{or } [H_2O]_e = PW - \beta[CH_4]_e \qquad (5.4)$$

The ACE-FTS measured $[CH_4]$ at 16 km (or ~100 hPa) from 38 tropical occultations (3-9 February and 3-8 April, 0-26°N) can be used to obtain the value of 1.726±0.069 ppmv for $[CH_4]_e$, which includes precision and a systematic error of ±3%. The *SPARC* [2000] assessment used a range of estimated values up to $[CH_4]_e$ = 1.72 ppmv (with zero uncertainty) in 1999. Table 5-1 shows $[H_2O]_e$ calculated using various combinations of $[CH_4]_e$ and β values. Despite having the highest

uncertainty, $[H_2O]_e$ = 3.65±0.29 ppmv from the fit and measured $[CH_4]_e$ is considered to be the best value.

Table 5-1: Calculated values of water entering the stratosphere, $[H_2O]_e$.

Parameters used [a]	**$[H_2O]_e$ ppmv** [b]
Measured $[CH_4]_e$ and β = 2.02±0.06	**3.65±0.29**
SPARC $[CH_4]_e$ and β = 2.02±0.06	3.67±0.24
Measured $[CH_4]_e$ and β = 2 (exact)	3.69±0.24
SPARC $[CH_4]_e$ and β = 2 (exact)	3.70±0.23

[a] The different parameters were used in the equation $[H_2O]_e$=PW-$\beta[CH_4]_e$, where PW=7.14±0.23 ppmv.
[b] The bold value is considered the most reasonable despite having the highest associated uncertainty.

5.4 Discussion and Conclusions

As mentioned in the introduction, many considerations must be taken into account when creating a time series between different instruments. However, the ATMOS and ACE-FTS instruments, measurement techniques, and retrievals are most likely similar enough to create a time series using ATMOS version 3 data and early ACE-FTS data. By analysis of the ACE-FTS data based on the method used for ATMOS data in *Michelsen et al.* [2000], PW is determined to be 7.14±0.23 ppmv and $[H_2O]_e$ is found to 3.65±0.29 ppmv from spring 2004 ACE-FTS measurements. In the ATMOS work, both the slope and intercept of the correlation plot were first determined from the fit, followed by redetermination of the intercept with the slope fixed at -2. PW was taken as the intercept with the slope constrained, and $[H_2O]_e$ was calculated based on this value. In this work, it was decided not to constrain the slope because it is reasonable for it to differ slightly from -2 as a result of side reactions involving H_2O and CH_4. Regardless, the slope of -2.02 obtained here was very close to -2, so it is directly compared to the ACE-FTS and ATMOS values (Table 5-2). This indicates a very small change in PW and no change in $[H_2O]_e$ between the last ATMOS measurements in 1994 and the ACE-FTS measurements in 2004. Thus one can conclude that the increase in PW of 0.065±0.008 ppmv/yr and the increase $[H_2O]_e$ of 0.041±0.007 ppmv/yr reported by *Michelsen et al.* [2000] for the period of 1985-1994 have not continued (Figure 5-3).

Table 5-2: ATMOS-ACE time series for PW and $[H_2O]_e$[a]

Mission	**Year** [b]	**PW ppmv**	**1σ PW ppmv** [c]	**$[H_2O]_e$ ppmv**	**1σ $[H_2O]_e$ ppmv** [d]
Spacelab-3	1985.42	6.47	±0.40, ±0.47	3.28	±0.47
ATLAS-1	1992.25	6.89	±0.14, ±0.31	3.53	±0.31
ATLAS-2	1993.33	7.05	±0.11, ±0.30	3.67	±0.31
ATLAS-3	1994.92	7.07	±0.08, ±0.29	3.65	±0.30
ACE	2004.33	7.14	±0.05, ±0.23	3.65	±0.29

[a] ATMOS values are taken from Table 3 of *Michelsen et al.* [2000].
[b] The fractional year has been determined from the year and month of the majority of observations.
[c] 1σ PW states the precision followed by the estimated accuracy on PW from each mission.
[d] 1σ $[H_2O]_e$ states the estimated accuracy on $[H_2O]_e$ from each mission.

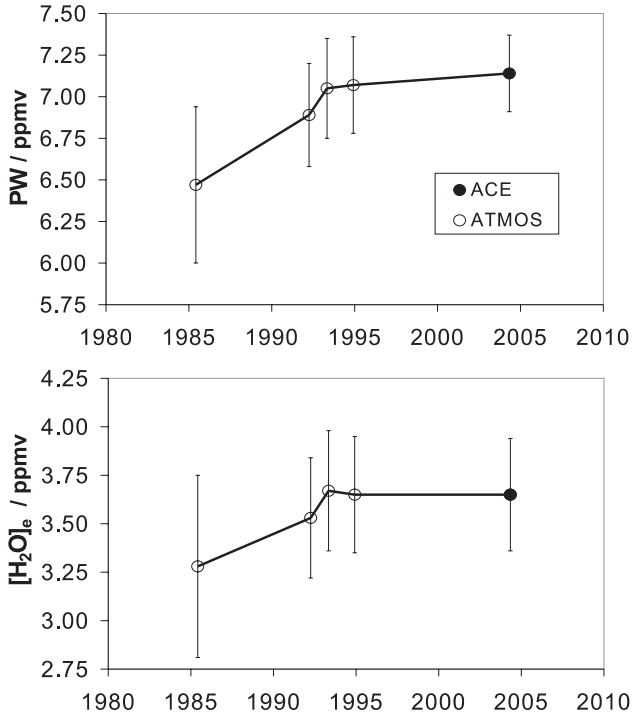

Figure 5-4: PW and $[H_2O]_e$ from 1985-2004 based on ATMOS and ACE-FTS measurements. The error bars represent the estimated one sigma accuracy on the ATMOS and ACE measurements. A more detailed error analysis for ACE H_2O and CH_4 will be done in the future.

The cessation of the ~50 year increase in stratospheric water observed here is consistent with other recent measurements of stratospheric water. For example, HALOE measurements at 40 km averaged between 50°S and 50°N [*Nedoluha et al.*, 2003] indicate an increase in PW from 1992-1995, a slight decrease from 1996-1999 and a slight increase from 1999-2002. They found that after the greater than 2%/year increase in $[H_2O]$ from 1991-1995, there was little change in $[H_2O]$ from 1996-2002, such that the total increase from 1991-2002 (40-50 km altitude) was slightly less than 1%/year and the increase in PW was only about 0.5%/year [*Nedoluha et al.*, 2003]. More recent HALOE work [*Randel et al.,* 2004] confirms this result. *Considine et al.* [2001] suggest that a fraction of the increase in $[H_2O]$ may relate to the eruption of Mt. Pinatubo in the Philippines in June 1991, but the eruption was probably not the sole cause of the observed changes. One can infer from the ACE-FTS results that the cessation of the rapid increase in PW is a result of the cessation of the increase in $[H_2O]_e$. However, at the present time no reliable prediction can be made regarding future stratospheric water vapor levels or trends, and it should be emphasized that further measurements and a better understanding of processes near the TTL are needed to determine whether or not stratospheric water will increase in the coming years.

References

Abbas, M.M., M.R. Gunson, M.J. Newchurch, H.A. Micehelsen, R.J. Salawitch, M. Allen, M.C. Abrams, A.Y. Chang, A. Goldman, F.W. Irion, E.J. Moyer, R. Nagaraju, C.P. Rinsland, G.P. Stiller, R. Zander (1996), The hydrogen budget of the stratosphere inferred from ATMOS measurements of H_2O and CH_4, *Geophys. Res. Lett.*, 23(17), 2405-2408.

Bernath, P.F., C.T. McElroy, M.C. Abrams, C.D. Boone, M. Butler, C. Camy-Peyret, M. Carleer, C. Clerbaux, P.-F. Coheur, R. Colin, P. DeCola, M. De Mazière, J.R. Drummond, D. Dufour, W.F.J. Evans, H. Fast, D. Fussen, K. Gilbert, D.E. Jennings, E.J. Llewellyn, R.P. Lowe, E. Mahieu, J.C. McConnell, M. McHugh, S.D. McLeod, D. Michelangeli, C. Midwinter, R. Nassar, F. Nichitiu, C. Nowlan, C.P. Rinsland, Y.J. Rochon, N. Rowlands, K. Semeniuk, P. Simon, R. Skelton, J.J. Sloan, M.-A. Soucy, K. Strong, P. Tremblay, D. Turnbull, K.A. Walker, I. Walkty, D.A. Wardle, V. Wehrle, R. Zander, J. Zou (2005), Atmospheric Chemistry Experiment (ACE): mission overview. *Geophys. Res. Lett.*, 32, L15S01.

Boone, C.D., R. Nassar, K.A. Walker, Y. Rochon, S.D. McLeod, C.P. Rinsland, P.F. Bernath (2005), Retrievals for the Atmospheric Chemistry Experiment Fourier Transform Spectrometer, *Applied Optics*, 44(33), 7218-7231.

Brewer, A.W. (1949), Evidence for a world circulation provided by the measurements of helium and water vapor distribution in the stratosphere, *Quarterly Journal of the Royal Meteorological Society*, 75, 351.

Clerbaux, C., P.F. Coheur, D. Hurtmans, B. Barret, M. Carleer, R. Colin, K. Semeniuk, J.C. McConnell, C.D. Boone, P. Bernath (2005), Carbon monoxide distribution from the ACE-FTS solar occultation measurements, *Geophys. Res. Lett.*, 32, L16S01.

Considine, D.B., J.E. Rosenfield, E.L. Fleming (2001), An interactive study of the influence of the Mount Pinatubo aerosol on stratospheric methane and water trends, *J. Geophys. Res.*, 106(D21), 27711–27727.

Hansen, A.R., G.D. Robinson (1989), Water vapor and methane in the upper stratosphere: An examination of some of the Nimbus 7 measurements, *J. Geophys. Res.*, 94(D6), 8474–8484.

Holton, J.R., P.H. Haynes, M.E. McIntyre, A.R. Douglass, R.B. Rood, L. Pfister (1995), Stratosphere-Troposphere Exchange, *Rev. Geophys.*, 33, 403-440.

Michelsen, H.A., F.W. Irion, G.L. Manney, G.C. Toon, M.R. Gunson (2000), Features and trends in Atmospheric Trace Molecule Spectroscopy (ATMOS) version 3 stratospheric water vapor and methane measurements, *J. Geophys. Res.*, 105(D18), 22713–22724.

Michelsen, H.A., G.L. Manney, F.W. Irion, G.C. Toon, M.R. Gunson, C.P. Rinsland, R. Zander, E. Mahieu, M.J. Newchurch, P.N. Purcell, E.E. Remsberg, J.M. Russell III, H.C. Pumphrey, J.W. Waters, R.M. Bevilacqua, K.K. Kelly, E.J. Hintsa, E.M. Weinstock, E.-W. Chiou, W.P. Chu, M.P. McCormick, C.R. Webster (2002), ATMOS version 3 water vapor measurements: Comparisons

with observations from two ER-2, Lyman-α hygrometers, MkIV, HALOE, SAGE II, MAS, and MLS, *J. Geophys. Res.*, 107(D3), 4027.

Mote, P.W., K.H. Rosenlof, M. E. McIntyre, E. S. Carr, J. C. Gille, J. R. Holton, J. S. Kinnersley, H. C. Pumphrey, J. M. Russell III, J. W. Waters (1996), An atmospheric tape recorder: The imprint of tropical tropopause temperatures on stratospheric water vapor, *J. Geophys. Res.*, 101(D2), 3989–4006.

Nassar, R., P.F. Bernath, C.D. Boone, G.L. Manney, S.D. McLeod, C.P. Rinsland, R.S. Skelton, K.A. Walker (2005a), ACE-FTS measurements across the edge of the winter 2004 Arctic vortex, *Geophys Res. Lett.*, 32, L15S05.

Nassar, R., P.F. Bernath, C.D. Boone, G.L. Manney, S.D. McLeod, C.P. Rinsland, R.S. Skelton, K.A. Walker (2005b), Stratospheric abundances of water and methane based on ACE-FTS measurements, *Geophys. Res. Lett.*, 32, L15S04.

Nedoluha, G.E., R.M. Bevilacqua, R.M. Gomez, B.C. Hicks, J.M. Russell III, B.J. Connor (2003), An evaluation of trends in middle atmospheric water vapor as measured by HALOE, WVMS, and POAM, *J. Geophys. Res.*, 108(D13), 4391.

Oltmans, S.J., H. Vömel, D.J. Hofmann, K.H. Rosenlof, D. Kley (2000), The increase in stratospheric water vapor from balloon-borne, frostpoint hygrometer measurements at Washington, D.C. and Boulder, Colorado, *Geophys. Res. Lett.*, 27(21), 3453–3456.

Randel, W.J., F. Wu, S.J. Oltmans, K. Rosenlof, G.E. Nedoluha (2004), Interannual changes of stratospheric water vapor and correlations with tropical tropopause temperatures, *J. Atmos. Sci.*, 61(17), 2133–2148.

Rex, M., R.J. Salawitch, P. von der Gathen, N.R.P. Harris, M.P. Chipperfield, B. Naujokat (2004), Arctic ozone loss and climate change, *Geophys. Res. Lett.*, 31, L04116.

Rind, D.E., P. Lonergan (1995), Modeled impacts of stratospheric ozone and water vapor perturbations with implications for high-speed civil transport aircraft, *J. Geophys. Res.*, 100(D4), 7381–7396.

Rosenlof, K.H., E.-W. Chiou, W.P. Chu, D. G. Johnson, K. K. Kelly, H. A. Michelsen, G. E. Nedoluha, E.E. Remsberg, G.C. Toon, M.P. McCormick (2001), Stratospheric water vapor increases over the past half-century, *Geophys. Res. Lett.*, 28(7), 1195-1198.

Shindell, D.T. (2001), Climate and ozone response to increased stratospheric water vapor, *Geophys. Res. Lett.*, 28, 1551-1554.

SPARC (2000), SPARC Assessment of Upper Tropospheric and Stratospheric Water Vapour, WMO/ICSU/IOC World Climate Research Programme, editors D. Kley, J.M. Russell III, C. Philips.

Chapter 6

Stratospheric Water Loss by Descent in the Polar Vortex

6.1 Introduction

The poleward transport of stratospheric air in the winter hemisphere is a regular consequence of the Brewer-Dobson circulation, described in the previous chapter. When a dynamical phenomenon known as a polar vortex is present, it can act as a barrier isolating air within it, and as a result, vortex air will cool and descend. This descent can be inferred by the effective removal of atmospheric tracer species from the stratosphere, transporting them to lower altitudes. When the vortex is weak, so is the barrier to transport, and mixing dilutes evidence of descent based on tracer species.

The Arctic vortex is generally warmer, more variable, and more difficult to predict than the Antarctic vortex. While the formation of PSCs occurs in both the Arctic and Antarctic vortices, temperatures in the Arctic vortex are rarely low enough for dehydration to occur. Dehydration is the process in which PSCs particles become large enough to sediment out, falling either to lower altitudes in the stratosphere or to the troposphere, and occurs regularly in the Antarctic vortex [*Hintsa et al.*, 1998], removing large quantities of water vapor from the Antarctic stratosphere. The loss of water vapor also occurs to a lesser degree via descent in the vortices. Improving our understanding of descent and other transport processes in the Arctic stratosphere is important for understanding Arctic ozone loss. There is currently no direct method for measuring vortex descent or descent rates, but the measurement of tracers is one method of investigating this phenomenon.

Meteorological analyses indicate that the 2003-2004 Arctic winter was remarkable in the ~50-year record [*Manney et al.*, 2005]. Overall, stratospheric temperatures were higher than normal, and a sudden stratospheric warming starting in late December caused disruptions in the middle and lower stratosphere lasting for weeks to months. However, after a brief disruption in late December/early January, the upper stratospheric vortex redeveloped and was the strongest and coldest on record since February and March 1979 [*Manney et al.*, 2005].

In this chapter, 450 ACE-FTS occultation measurements from mid-February to the end of March 2004 spanning 0-79.8ºN, are classified as vortex, vortex edge, midlatitude, subtropical or tropical, using meteorological data and $[CH_4]$ versus $[N_2O]$ correlations (where square brackets denote the volume mixing ratio). Profiles of $[N_2O]$, $[H_2O]$ and $[CH_4]$ are examined from the mid-troposphere to the mesopause, both inside and outside the Arctic polar vortex, and these are used to estimate descent rates in the vortex and the range of altitudes that are subject to descent [*Nassar et al.*, 2005b].

6.2 ACE-FTS H_2O, CH_4 and N_2O Retrievals

The results in this chapter were obtained using ACE-FTS version 1.0 data. The H_2O and CH_4 retrievals were briefly outlined in the previous chapter. 62 N_2O microwindows in the 1168-2816 cm^{-1} range were used to retrieve profiles from 4.5-59.5 km altitude. H_2O and CH_4 each have statistical uncertainties (a measure of the random error in the fitting process that does not include systematic errors) of less than 2% for the stratosphere, but higher values in the troposphere and mesosphere. N_2O has statistical uncertainties of less than 2% up to ~38 km, but VMRs above this point are very low so the relative uncertainty is larger. Above the highest measurement for each gas, VMRs were derived by assuming the shape of a climatological *a priori* profile and multiplying it by a constant determined from the fit [*Boone et al.*, 2005].

6.3 Occultation Classifications

The terms potential temperature (θ) and potential vorticity (PV) are frequently used in atmospheric dynamics. The potential temperature is the temperature that a parcel of air in a compressible atmosphere would have if brought adiabatically (i.e. with no gain or loss in heat or entropy) to the standard pressure at the surface of the Earth [*Brasseur et al.*, 1999]. It is often used as a quasi-altitude coordinate, where high θ values generally correspond to higher altitudes, although the correspondence is non-linear. Vorticity is a measure of the spin of a fluid parcel with respect to the coordinate system fixed to the Earth, and PV is a measure of the vertical component of the angular momentum of a fluid parcel in the same co-ordinate system [*Brasseur et al.*, 1999]. Unlike θ and vorticity, PV is a very abstract concept that is difficult to visualize. Due to the rotation of the Earth, PV bears some resemblance to latitude, since higher positive values of PV are typically found close to the north pole (in the northern hemisphere winter or spring when the Arctic vortex is present), the smallest values are found near the equator, and the most negative values are found near the south pole (during the southern hemisphere winter when the Antarctic vortex is present). Surfaces of constant θ are referred to as isentropic surfaces or isentropes, and surfaces of constant PV are PV contours, which can be shown on PV maps such as Figure 6-1.

PV maps can be used to determine the location and strength of the polar vortex, where a strong vortex is identified by a steep gradient in PV. In this work, PV maps based on data from the UK Met Office (MetO) are used which depict conditions in the upper stratosphere corresponding to an isentropic surface of θ = 1700 K (~50 km), the middle stratosphere at θ = 840 K (~30 km) and the lower stratosphere at θ = 465 K (~20 km) at 12:00 UT each day. February and March 2004 PV maps indicated that the NH vortex was strong in the upper stratosphere, highly variable in the middle stratosphere, and undefined in the lower stratosphere, so 30-50 km was chosen for determining the location of an occultation with respect to the vortex. The altitude selected for classification depends on the conditions of vortex during that particular year and tends to differ for the Arctic and Antarctic.

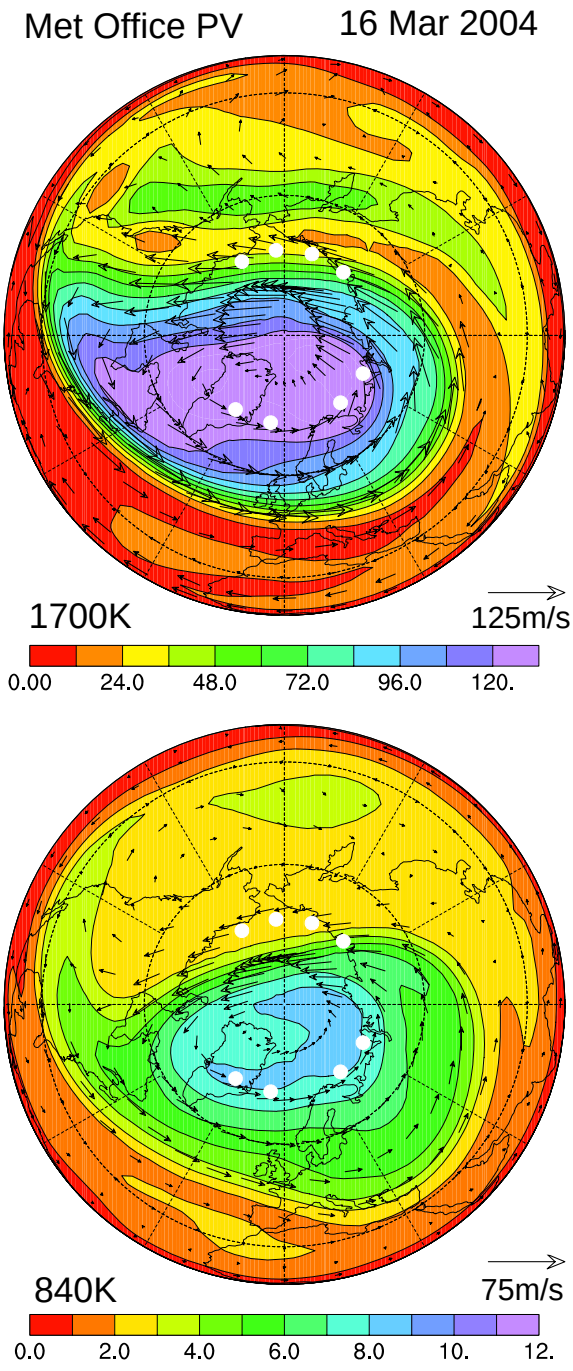

Figure 6-1: NH potential vorticity (PV) maps for 16 March 2004, 12:00 UT corresponding to θ = 1700 K (~50 km altitude) and θ = 840 K (~30 km). The north pole is at the center of each map with 90°W at the left and 90°E at the right. The color scale indicates PV (in 10^{-4} K m^2 kg^{-1} s^{-1}) and the arrows are wind vectors scaled to the arrow at the lower right of the map. The white spots are reference locations for eight occultations measured on 16 March 2004.

Stratospheric Water Loss by Descent in the Polar Vortex

To group profiles resulting from measurements of similar air masses, it was necessary to develop a system for classifying ACE-FTS occultations that began with determining the location of the vortex edge. For each occultation, θ, PV and equivalent latitude (EqL, the latitude that would enclose the same area between it and the pole as a given PV contour) were calculated from MetO data on a 1-km grid from 0.5 to 65.5 km altitude, to facilitate use with the ACE-FTS data. The vortex edge was found using a criterion very similar to that described by *Nash et al.* [1996], based on location of the maximum PV gradient as a function of EqL, constrained by approximate co-location of maximum wind speed. Since the vortex edge has a finite width, the distance in degrees EqL from the center of the vortex edge was determined for each tangent point with positive values inside the vortex, negative values outside, and null values when no vortex is present. This resulted in an array of EqL-distances which could include positives, negatives and nulls for a single occultation. With any vortex edge criterion, the best results are obtained when there is a single, strong, unambiguous vortex. The results of the above calculations are referred to as derived meteorological products (DMPs), and were provided to the ACE team (*G.L. Manney*, private communication, 2004-2005) for the investigation of vortex processes.

A second set of criteria was established to check the EqL-distance of each tangent point from 30-50 km, to see if it was inside the vortex, outside the vortex, or null. If the proportion of tangent points inside minus the proportion outside or null was greater than 0.5, the occultation was considered inside the vortex, and if less than -0.5, it was considered outside. If the difference was greater than or equal to -0.5 and less than or equal to 0.5 and the vortex was present for a significant portion of this range, an occultation was considered on the edge of the vortex. With these criteria, 450 NH ACE-FTS occultations from 2004 were classified as vortex, extravortex or vortex edge. If the vortex was not present, then occultations were classified as extravortex by default.

Tracer species such as CH_4 and N_2O are useful indicators of the recent dynamical and photochemical history of an air mass. The lifetime of CH_4 is controlled by its rate of oxidation by OH, $O(^1D)$, and Cl, whereas the lifetime of N_2O is determined by its rate of UV photolysis or reaction with $O(^1D)$ [*Michelsen et al.*, 1998a]. When horizontal mixing is rapid, correlations of these species should be compact, varying only with altitude. Correlations from dynamically isolated air masses may exhibit slight differences that can be used to classify them as tropical, midlatitude or vortex [*Michelsen et al.*, 1998a, b]. Figure 6-2 is a plot of $[CH_4]$ versus $[N_2O]$ with 150 tangent points for each of the 450 NH occultations.

Using definitions similar to those in *Michelsen et al.* [1998a], extravortex occultations were further classified as tropical, subtropical and midlatitude. Midlatitude here refers to occultations of any latitude that are both outside the vortex and have no tropical or subtropical characteristics. The dense main group of points is mainly due to midlatitude correlations, with correlations from tropical air above the main line and correlations from within the vortex or vortex edge slightly below and to the right. Subtropical correlations fall between distinct tropical and midlatitude correlations and typically arise from latitudes of ~16-30ºN. There are distinct

differences between subtropical, tropical, and midlatitude correlations, but the differences between vortex, vortex edge and midlatitude correlations are subtle. The five color-coded classes in Figure 6-2 loosely correspond to the color scheme on the PV maps. The correspondence is not exact because the vortex edge is defined by a strong PV gradient, rather than a single PV value.

These classifications are consistent with the upper and middle stratosphere PV maps, as expected, since both utilized the same MetO PV data. However, the accuracy of these classifications is limited by the introduction of derived meteorological products (θ, PV, EqL) from a data assimilation rather than a system based entirely on measurements and the use of the single reference location for each occultation, since each occultation is really a series of near-vertical measurements incurring a slight change in latitude, longitude, and time. Except for a few mid-February occultations, the remainder of the measurements used in this particular chapter occurred at a time of relatively low beta angle (β), so this should generally have a minor effect on these classifications. After the completion of this work, a process was begun to derive the DMP files based on the latitude and longitude as a function of altitude produced by the refraction model. The most recent set of DMP files (v2.2) uses the variable latitudes and longitudes, and classifications based on version 2.2 have been used to investigate the 2005 Arctic vortex [*Dufour et al.*, 2006].

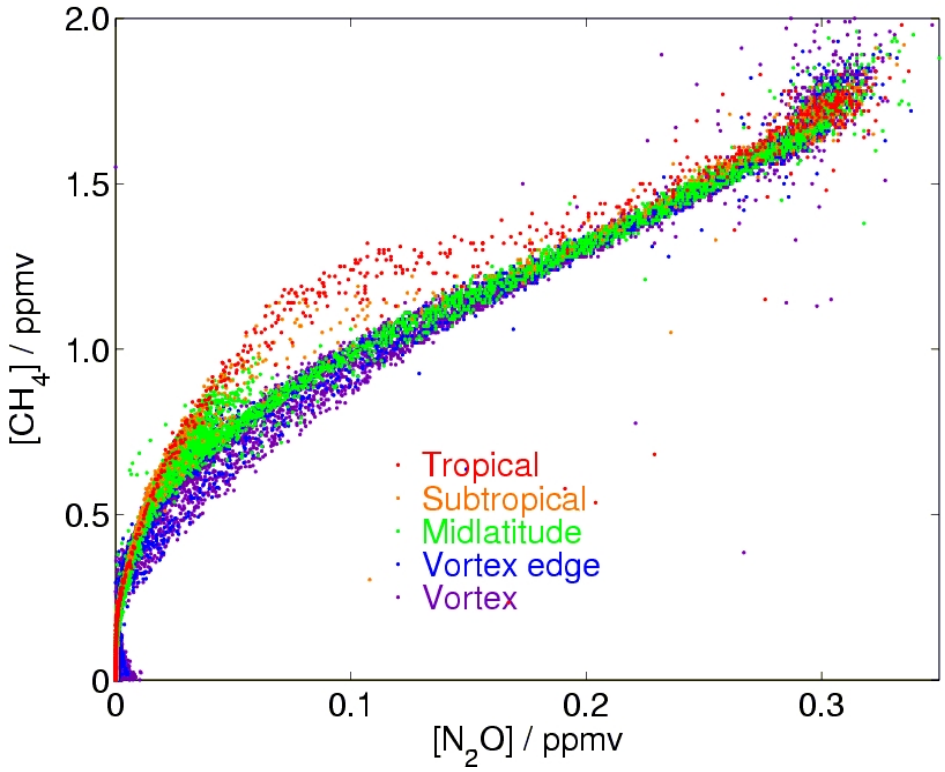

Figure 6-2: The $[N_2O]$ versus $[CH_4]$ correlation plot for 450 NH occultations during the period of 5 February to 31 March 2004. The five color-coded classes (Tropical, Subtropical, Midlatitude, Vortex Edge and Vortex) in the legend loosely correspond to the color scheme for the PV maps in Figure 6-1.

6.4 Vortex Measurements and Analysis

In February and March 2004, the upper stratospheric Arctic vortex was the strongest since regular observations began in 1979 [*Manney et al.*, 2005]. Figure 6-1 shows PV maps for 16 March, several days prior to break up, when the center of the vortex was located far off the pole. Figure 6-3 shows profiles of $[N_2O]$, $[H_2O]$, $[CH_4]$ and potential water (PW), where PW is approximated as $[H_2O]+2[CH_4]$. PW is a conserved quantity, unlike $[H_2O]$ and $[CH_4]$ which fluctuate with the extent of methane oxidation as discussed in the previous chapter and *Nassar et al.* [2005a]. The eight profiles in Figure 6-3 and represented by the white spots in Figure 6-1 were measured on 16 March between 3:48-20:07 UT, 71.5-72.3ºN and span a range of longitudes. The lower four spots (longitudes 64ºE, 40ºE, 33ºW, 58ºW) have been classified as in the vortex and the upper four (longitudes 150ºW, 174ºW, 161ºE, 137ºE) as midlatitude, although they are very close to the dispersed edge of the vortex. There is a clear differences between profiles from inside and outside the vortex, even though all were measured within 1º of latitude and a time span of less than 17 hours.

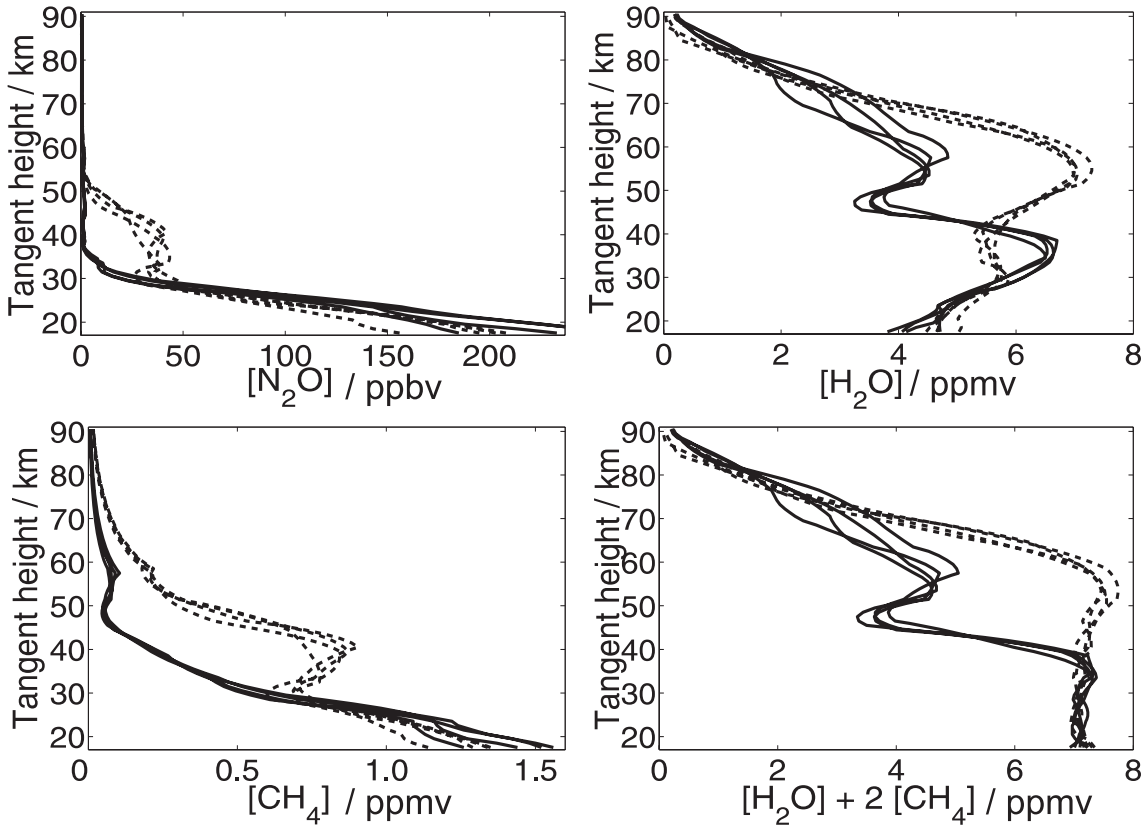

Figure 6-3: $[N_2O]$, $[H_2O]$, $[CH_4]$, and PW profiles at ~72ºN, inside the Arctic vortex at 64ºE, 40ºE, 33ºW, 58ºW (solid lines) and outside the Arctic vortex at 150ºW, 174ºW, 161ºE, 137ºE (dashed lines) on 16 March 2004. The measurement locations are shown in Figure 6-1.

Abrams et al. [1996a, 1996b] examined differences in ATMOS profiles of [CH_4], [N_2O] and [HF] at midlatitudes and high latitudes, both inside and outside the polar vortices. Although they found very little difference between midlatitude and high latitude profiles from outside the vortex, large differences were found between vortex and extravortex profiles. They determined descent rates in the Arctic and Antarctic vortices by dividing the vertical distance separating the profiles by the age of the vortex. The age of the vortex is difficult to define, since formation is a gradual process; however, using PV maps, the formation date of the upper stratospheric Arctic vortex was estimated as 15 October 2003. The vortex profiles of [N_2O], [CH_4] and [H_2O] near 34 km (Figure 6-3) have VMRs equivalent to extravortex values near 50 km, or a vertical separation of 16 km. Assuming unmixed descent (profiles are only altered by vertical motion) during the period of 15 October 2003 to 16 March 2004, the 16 km of descent observed over five months, gives an average descent rate of 3.2 km/month for upper stratospheric air originating in the 40-54 km range. Since the upper stratospheric vortex broke up and reformed, a value for average descent over the entire winter has little significance. However, by comparing averages of 12 vortex profiles from 18-21 February at 72.8-75.8ºN and 10 vortex profiles from 16-20 March at 65-71.8ºN (not shown), 4.5 km of upper stratospheric descent in one month are observed based on CH_4 and H_2O. This is a far better representation of descent during February and March when the vortex had reformed and strengthened after the late December breakup.

Figure 6-4 shows averages of 217 [N_2O], [CH_4], [H_2O] and PW profiles classified as inside the polar vortex compared to averages of 47 midlatitude profiles, all measured between 14 February and 22 March at 60-77ºN. The error bars indicate the 1σ variability in the profiles. While changes in the [N_2O] and [CH_4] profiles appear to be slightly dampened by averaging relative to the 16 March profiles (Figure 6-3), they are consistent with the results above. All four averaged profile comparisons in Figure 6-4 also indicate that below ~30 km in altitude, the vortex had a negligible influence.

Similarly, the [H_2O] and PW profiles show differences as high as ~77 km, indicating that the vortex may still reduce horizontal mixing at these altitudes. The [H_2O] and PW profiles in Figures 6-3 and 6-4 provide good evidence of mesospheric descent. However, the high variability indicated by the error bars in Figure 6-4, and examination of individual February and March profiles indicate that mixing in the mesosphere had resumed prior to the end of this period, so earlier data was desired to calculate mesospheric descent. [H_2O] and PW for the 12 vortex profiles from February described above, compared with one extravortex profile from 15 February at 63ºN (not shown), indicated 21.2 km of descent for air originating in the 60-74 km range. This is an average descent of 5.3 km/month in the lower mesosphere for the period of 15 October 2003 to 15 February 2004. Since mesospheric mixing resumed earlier than in the upper stratosphere, we do not estimate a late winter lower mesospheric descent rate.

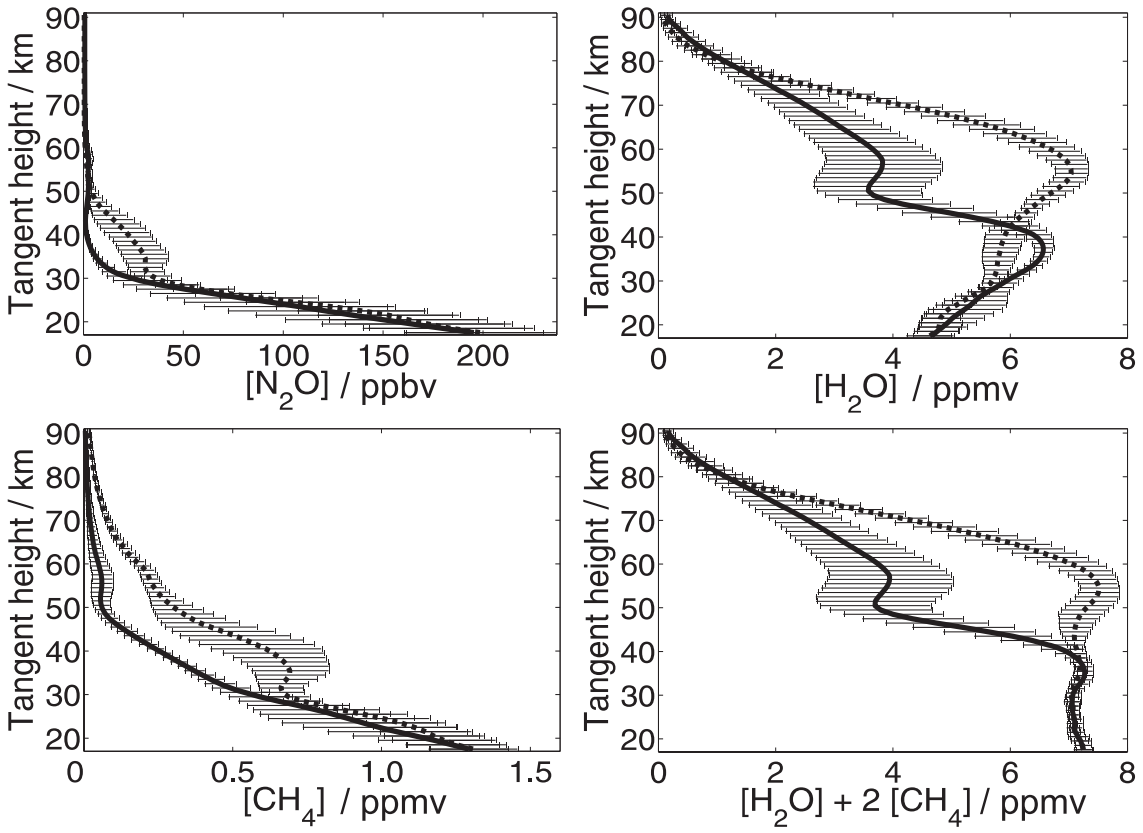

Figure 6-4: Average [H_2O], [CH_4], [N_2O] and PW profiles based on 217 profiles inside the Arctic vortex (solid line) and 47 profiles outside the vortex (dashed line), all measured between 14 February and 22 March 2004 at 60-77ºN. The error bars indicate the variability between profiles.

6.5 Discussion and Conclusions

The differences in vortex and extravortex profiles can be attributed to dissociation of H_2O, CH_4 and N_2O in the upper stratosphere and mesosphere, followed by unmixed descent in the stratospheric vortex to lower altitudes. The observation of unmixed descent confirms the general concept of the Brewer-Dobson circulation and demonstrates a mechanism for the removal of H_2O from the polar stratosphere, that does not involve dehydration. The inversions in the [H_2O] and PW profiles near 50 km altitude, which were very pronounced on 16 March but dampened in the average profiles, can be attributed to the vortex shifting non-uniformly with altitude in the days prior to the final spring break-up.

An average Arctic vortex descent rate of 3.2 km/month for the upper stratosphere has been determined based on N_2O, CH_4, and H_2O, and 5.3 km/month for the lower mesosphere based on H_2O and PW. An upper stratospheric descent rate of 4.5 km/month has been calculated based on CH_4 and H_2O for February and March 2004 when the vortex was strongest. In spite of the

temporary disruption to the upper stratospheric vortex, the average stratospheric descent rate is still close to the maximum value observed for the November 1994 Antarctic vortex (3.6 km/month) [*Abrams et al.*, 1996a] and much higher than the maximum for the April 1993 Arctic vortex (2.4 km/month) [*Abrams et al.*, 1996b]. It is also higher than descent rates quoted by *Greenblatt et al.* [2002a, 2002b], which include 11 other studies, although these are all for the middle to lower stratosphere where lower descent rates are expected. The February-March descent rate determined here is significantly higher than all of these previously measured descent rates. However, *Manney et al.* [1994] modeled descent at a range of altitudes for both hemispheres and obtained a value of 0.3 cm/s (equivalent to 7.8 km/month) for the 1992-1993 Arctic upper stratospheric vortex at a starting altitude of 47 km. *Rosenfield et al.* [1994] also modeled descent in both hemispheres at a range of altitudes and calculated 27 km of descent for air originating at 50 km. They used 1 November to 21 March as the period of descent, but assuming our descent period yields a rate of 5.4 km/month for the upper stratosphere. *Fisher et al.* [1993] determined a range of Antarctic vortex descent rates from 3 km/month in the middle stratosphere to 12 km/month in the mesosphere. To our knowledge, the only prior measurements of mesospheric descent were made by *Aellig et al.* [1996] using the Millimeter wave Atmospheric Sounder (MAS) to observe the spring 1992 Arctic vortex, but no estimate of a descent rate was given.

The methods for estimating descent rates presented here are admittedly somewhat crude, yet still give a useful estimate of a difficult-to-measure phenomenon. In the 2003-2004 winter, unmixed descent is a poor assumption, since the upper stratospheric vortex completely broke up in late December and recovered in early January [*Manney et al.*, 2005]. While this assumption should not effect our February-March descent rate of 4.5 km/month for the upper stratosphere, the upper stratospheric 2003-2004 winter average descent rate of 3.2 km/month and lower mesospheric average descent rate of 5.3 km/month represent minimum possible values. With limited measurements and no reliable meteorological data for the mesosphere, a more accurate estimate is difficult.

This work has shown that PV data and tracer species such as N_2O and CH_4 may be used to classify the type of air mass being measured. It also demonstrates the strength of the stratospheric vortex as a barrier to horizontal transport by the contrast between profiles of $[N_2O]$, $[CH_4]$ and $[H_2O]$ at similar latitudes inside and outside the vortex, as well as the effective containment of air up into the mesosphere. Furthermore, this work indicates that descent in the winter 2004 Arctic vortex was relatively rapid, and that evidence of unmixed descent extended to higher altitudes than observed in past years, likely due to a stronger than usual and more persistent upper stratospheric vortex in late winter.

References

Abrams, M.C., G.L. Manney, M.R. Gunson, M.M. Abbas, A.Y. Chang, A. Goldman, F.W. irion, H.A. Michelson, M.J. Newchurch, C.P. Rinsland, R.J. Salawitch, G.P. Stiller, R. Zander (1996), Trace gas transport in the Arctic Vortex inferred from ATMOS ATLAS-2 observations during April 1993, *Geophys. Res. Lett.*, 23(17), 2341-2344.

Abrams, M.C., G.L. Manney, M.R. Gunson, M.M. Abbas, A.Y. Chang, A. Goldman, F.W. irion, H.A. Michelson, M.J. Newchurch, C.P. Rinsland, R.J. Salawitch, G.P. Stiller, R. Zander (1996), ATMOS/ATLAS-3 observations of long-lived tracers and descent in the Antarctic vortex in November 1994, *Geophys. Res. Lett.*, 23(17), 2345-2348.

Aellig, C.P., J. Bacmeister, R.M. Bevilacqua, M. Daehler, D. Kriebel, T. Pauls, D. Siskind, N. Kämpfer, J. Langen, G. Hartmann, A. Berg, J.H. Park, J.M. Russell III (1996), Space-borne H_2O observations in the Arctic stratosphere and mesosphere in the spring of 1992, *Geophys. Res. Lett.*, 23(17), 2325-2328.

Bernath, P.F., C.T. McElroy, M.C. Abrams, C.D. Boone, M. Butler, C. Camy-Peyret, M. Carleer, C. Clerbaux, P.-F. Coheur, R. Colin, P. DeCola, M. De Mazière, J.R. Drummond, D. Dufour, W.F.J. Evans, H. Fast, D. Fussen, K. Gilbert, D.E. Jennings, E.J. Llewellyn, R.P. Lowe, E. Mahieu, J.C. McConnell, M. McHugh, S.D. McLeod, D. Michelangeli, C. Midwinter, R. Nassar, F. Nichitiu, C. Nowlan, C.P. Rinsland, Y.J. Rochon, N. Rowlands, K. Semeniuk, P. Simon, R. Skelton, J.J. Sloan, M.-A. Soucy, K. Strong, P. Tremblay, D. Turnbull, K.A. Walker, I. Walkty, D.A. Wardle, V. Wehrle, R. Zander, J. Zou (2005), Atmospheric Chemistry Experiment (ACE): mission overview, *Geophys. Res. Lett.*, 32, L15S01.

Boone, C.D., R. Nassar, K.A. Walker, Y. Rochon, S.D. McLeod, C.P. Rinsland, P.F. Bernath (2005), Retrievals for the Atmospheric Chemistry Experiment Fourier Transform Spectrometer, *Applied Optics*, 44(33), 7218-7231.

Brasseur, G.P, J.J. Orlando, G.S. Tyndall (1999), Atmospheric Chemistry and Global Change, Oxford University Press, New York.

Dufour, G., R. Nassar, C.D. Boone, R. Skelton, K.A. Walker, P.F. Bernath, C.P. Rinsland, K. Semeniuk, J.J. Jin, J.C. McConnell, G.L. Manney (2006), Partitioning between the inorganic chlorine reservoirs HCl and $ClONO_2$ during the Arctic winter 2005 from the ACE-FTS, *Atmospheric Chemistry and Physics Discussions*, 6, 1249-1273.

Fisher, M., A. O'Neil (1993), Rapid descent of mesospheric air into the stratospheric polar vortex, *Geophys. Res. Lett.*, 20(12), 1267-1270.

Greenblatt, J.B., H.-J. Jost, M. Loewenstein, J.R. Podolske, D.F. Hurst, J.W. Elkins, S.M. Schauffler, E.L. Atlas, R.L. Herman, C.R. Webster, T.P. Bui, F.L. Moore, E.A. Ray, S. Oltmans, H. Vömel, J.-F. Blavier, B. Sen, R.A. Stachnik, G.C. Toon, A. Engel, M. Müller, U. Schmidt, H. Bremer, R.B. Pierce, B.-M. Sinnhuber, M. Chipperfield, F. Lefèvre (2002), Tracer-based determination of vortex descent in the 1999/2000 Arctic winter, *J. Geophys. Res.*, 107, 8279.

Greenblatt, J.B., et al. (2002), Correction to "Tracer-based determination of vortex descent in the 1999/2000 Arctic winter" by Greenblatt et al., *J. Geophys. Res.*, 107, 8307.

Hintsa, E.J., P.A. Newman, H.H. Jonsson, C.R. Webster, R.D. May, R.L. Herman, L.R. Lait, M.R. Schoeberl, J.W. Elkins, P.R. Wamsley, G.S. Dutton, T.P. Bui, D.W. Kohn, J.G. Anderson (1998), Dehydration and denitrification in the Arctic polar vortex, *Geophys. Res. Lett.*, 25, 501-504.

Manney, G.L., R.W. Zurek, A. O'Neil, R. Swinbank (1994), On the Motion of Air through the Stratospheric Polar Vortex, *J. Atmos. Sci.*, 51, 2973-2994.

Manney, G.L., K. Krüger, J. L. Sabutis, S.A. Sena, S. Pawson (2005), The remarkable 2003-2004 winter and other recent warm winters in the Arctic stratosphere since the late 1990s, *J. Geophys. Res.*, 110, D04107.

Michelsen, H.A., G.L. Manney, M.R. Gunson, C.P. Rinsland, R. Zander (1998), Correlations of stratospheric abundances of CH_4 and N_2O derived from ATMOS measurements, *Geophys. Res. Lett.*, 25, 2777-2780.

Michelsen, H.A., G.L. Manney, M.R. Gunson, R. Zander (1998), Correlations of stratospheric abundances of NO_y, O_3, N_2O, and CH_4 derived from ATMOS measurements, *J. Geophys. Res.*, 103, 28347-28359.

Nash, E.R., P.A. Newman, J.E. Rosenfield, M.R. Schoeberl (1996), An objective determination of the polar vortex using Ertel's potential vorticity, *J. Geophys. Res.,* 101(D5), 9471-9478.

Nassar, R., P.F. Bernath, C.D. Boone, G.L. Manney, S.D. McLeod, C.P. Rinsland, R.S. Skelton, K.A. Walker (2005a), ACE-FTS measurements across the edge of the winter 2004 Arctic vortex, *Geophys Res. Lett.*, 32, L15S05.

Nassar, R., P.F. Bernath, C.D. Boone, G.L. Manney, S.D. McLeod, C.P. Rinsland, R.S. Skelton, K.A. Walker (2005b), Stratospheric abundances of water and methane based on ACE-FTS measurements, *Geophys. Res. Lett.*, 32, L15S04.

Rosenfield, J.E., P.A. Newman, M.R. Schoeberl (1994), Computations of diabatic descent in the stratospheric polar vortex, *J. Geophys. Res.*, 99(D8), 16677-16689.

Chapter 7

Variability in HDO/H_2O Abundance Ratios at the TTL

7.1 Introduction

The simple definitions of the tropopause given in Chapter 2 define it as a boundary based on a single point in a temperature profile, but the tropical tropopause is best understood as a transition layer between the troposphere and the stratosphere, rather than a simple boundary. This layer, referred to as the tropical tropopause layer (TTL) is the region of the tropics ranging from 14-19 km in altitude in which the chemical and dynamical properties of the atmosphere gradually change from properties characteristic of the troposphere to those characteristic of the stratosphere [*Holton and Gettelman*, 2001]. There are other more technical definitions for the boundaries of this layer based on dynamics, but this description is sufficient for the present work.

Water primarily enters the stratosphere by vertical transport across the TTL, then circulates to midlatitudes and descends at the poles, but the details regarding the entry process are still the subject of debate. The traditional understanding of the transport of water across the TTL was that condensation occurred as air parcels gradually ascended [*Brewer*, 1949]. This process, referred to as freeze-drying or dehydration, dictates that the humidity of the stratosphere is controlled by the coldest temperature region that the air encounters during ascent (illustrated in Figure 7-1), called the *cold trap*. The water vapor saturation VMR is the maximum VMR of water vapor that can occur in air of a given temperature and pressure, while the remainder condenses to form liquid or ice. If a simple cold trap was solely responsible for the abundance of water in the stratosphere, the stratospheric entry value $[H_2O]_e$ should be the same as the mean water vapor saturation VMR.

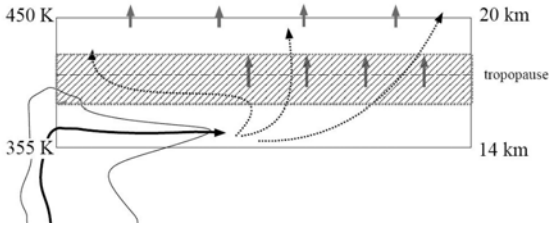

Figure 7-1: A schematic diagram illustrating dehydration by simple gradual ascent from *Sherwood and Dessler* [2000]. The horizontal axis represents the horizontal distance from the point where rising air enters the TTL region. Final dehydration of air occurs in the shaded area and is complete when it reaches the hygropause, which is the minimum in a water vapor profile.

It is now generally accepted that the abundance of water in the stratosphere is lower than predicted based solely on dehydration during simple gradual ascent, where air ascends uniformly for all longitudes throughout the tropics. Simple gradual dehydration at the mean temperature of the TTL should result in a water vapor saturation VMR and $[H_2O]_e$ of ~4.5 ppmv, whereas observed values of $[H_2O]_e$ are ~3-4 ppmv [*SPARC*, 2000]. In Chapter 5, a $[H_2O]_e$ value of 3.65±0.29 ppmv was determined for 2004 from ACE-FTS measurements [*Nassar et al.*, 2005].

Furthermore, long term records indicate a period of elevated levels of both stratospheric water vapor and $[H_2O]_e$ [*Oltmans et al.*, 2000; *Rosenlof et al.*, 2001] in spite of the fact that overall TTL temperatures decreased over the same time period [*Randel et al.*, 2000].

One proposed explanation for the dryness of the stratosphere focused on the fact that the temperature of the TTL is not uniform with longitude. The coldest temperatures typically occur over the Western Pacific in an area often referred to as the *Maritime Continent*, which includes Indonesia, Malaysia and neighboring countries. *Newell and Gould-Stewart* [1981] suggested that perhaps air (and therefore water vapor) primarily entered the stratosphere by ascending across the TTL above the Maritime Continent and they called this region of ascent the *Stratospheric Fountain*. If this were the prime entry point of water vapor, then the cold TTL temperatures found in this region would explain the low abundances of water vapor observed. Measurements of water vapor made since the fountain hypothesis, coupled with models, clearly indicate that this explanation is not correct, and the fountain region has even been identified as a localized region of net subsidence [*Sherwood,* 2000; *Gettelman,* 2000].

A much better explanation for the dryness of the stratosphere, that still retains the cold trap concept, was suggested by *Holton and Gettelman* [2001], who point out that while the net velocities of ascent in the tropics are typically ~0.5 mm/s, velocities of horizontal transport are typically ~5 m/s. Although horizontal motion occurs about 10^4 times more rapidly than vertical motion, it was generally not factored into simple dehydration models. *Holton and Gettelman* [2001] suggested that most air entering the stratosphere will at one time pass horizontally through the coldest part of the TTL, referred to as the Western Pacific cold trap, where it is becomes dehydrated. The dehydrated air then rises in a gradual and relatively uniform manner, entering the stratosphere at longitudes throughout the tropics.

The main alternative mechanisms to gradual ascent for regulating the abundance of water in the stratosphere are convective processes. These convective processes can either hydrate or dehydrate the stratosphere depending on whether the air injected carries more or less water than the mean stratospheric levels [*Danielsen,* 1982]. Convective dehydration suggests that air can cross the TTL by localized rapid vertical convection on the order of m/s. According to *Sherwood and Dessler* [2000], the air can encounter very cold stratospheric temperatures and become severely dehydrated, then later mix with moister air throughout the stratosphere, therefore lowering the mean stratospheric water vapor abundance, as illustrated in Figure 7-2.

Convective processes that hydrate the stratosphere have also been suggested [*Danielsen*, 1982]. One possible convective mechanism for increasing the humidity of the stratosphere by injecting water, is the rapid lofting of ice particles by convective updrafts. Convective updrafts are known to occur throughout the tropical troposphere but the degree to which they can penetrate the TTL to reach the stratosphere is not known. Although the formation of the lofted ice particles may have been controlled by the water vapor saturation VMR, if the updrafts carry these particles past the temperature minimum, they can vaporize in the stratosphere where the air is slightly warmer and not saturated with respect to water vapor.

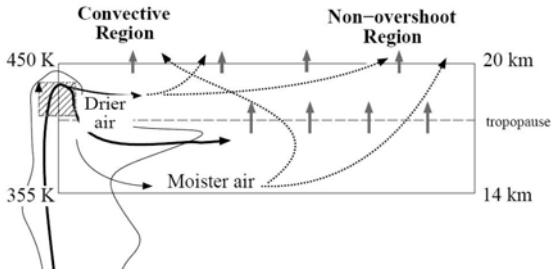

Figure 7-2: A schematic diagram illustrating convective dehydration, from *Sherwood and Dessler* [2000]. The horizontal axis represents the horizontal distance from a convective column. Localized convective overshoots that pass the tropopause are severely dehydrated (in the shaded area of the figure), but then mix with moister air that has entered in non-overshoot regions.

Measurements as well as models provide some evidence for the transport of water into the stratosphere by both convective and gradual processes. It is generally believed that gradual dehydration involving sufficient horizontal transport is the main process responsible for the low levels of water vapor entering the stratosphere, with convective dehydration playing a lesser role, but this is disputed. Clarification is required regarding the relative contributions of each mechanism, as well as the variability in these contributions, which may relate to the changes in $[H_2O]_e$ observed in recent years.

Mote et al. [1996] showed that the entry of water into the stratosphere exhibits a seasonal variation, with the maximum amount of water entering during the northern hemisphere (NH) summer and the minimum amount entering during the NH winter. The clear pattern left by the varying amounts of water vapor entering the stratosphere in the tropics is referred to as the *tropical tape recorder,* since it contains a record of water vapor maxima and minima over time.

This chapter is an investigation of water vapor in the TTL region in order to gain a better understanding of processes relating to water entering the stratosphere, such as the relative importance of the gradual and convective dehydration mechanisms, as well as convective ice lofting. Variability over a two year period is examined to determine if there is a pattern that may relate to the tropical tape recorder. The prime method for investigating these processes is by comparing HDO/H_2O vapor abundance ratios with temperature and water vapor VMR.

7.2 Water Isotopologues

According to the *International Union of Pure and Applied Chemistry* (IUPAC), isotopes are atoms with the same number of protons but a different number of neutrons. For example hydrogen has the isotopes: ^1H, ^2H and ^3H, which are named hydrogen, deuterium and tritium, and are abbreviated as H, D and T. IUPAC defines isotopologues as molecules which differ only by their isotopic composition [*Brenninkmeijer et al.*, 2003]. The main water isotopologues and their abundances are shown in Table 7-1. Species such as those in Table 7-1 are often called isotopes, although this is not consistent with IUPAC nomenclature since the term isotopes should be used in reference to atoms, not molecules. The term isotopomer is sometimes used as well, but it is also incorrect in

this case. Isotopomer is short for isotopic-isomer, which refers to a molecule with the same isotopic atoms as another molecule, but in a different arrangement. Water does not actually have any isotopomers, whereas ozone for example, has the isotopomers $^{16}O^{18}O^{16}O$ and $^{18}O^{16}O^{16}O$, which are also isotopologues. Mass numbers for each atom in a species can be shown as left superscripts (as above), which is the most precise approach when discussing isotopologues, but can get very cumbersome. Since no isotopologues with more than one isotopically differing atom (i.e., D_2O or $HD^{17}O$) are dealt with in this chapter, discretion has been used to only include mass numbers when it would otherwise not be clear from the context if referring to a specific isotopologue or the total of all isotopologues in a species.

Table 7-1: The four most abundant isotopologues of water [*IUPAC*, 1994; *Coplen*, 1994].

Isotopologue	Standard abundance
$H_2{}^{16}O$	0.997317
$HD^{16}O$	0.00031069
$H_2{}^{18}O$	0.00199983
$H_2{}^{17}O$	0.000372
Total of above species	0.99999952

Since HDO and the other heavy isotopologues of water have a lower vapor pressure than H_2O, fractionation will occur during certain processes such as condensation or sublimation. These processes result in the condensed phase (liquid or ice) becoming enriched in the heavier isotopologue and the vapor becoming depleted. For this reason, the isotopic composition of water vapor in the TTL region can act as a useful tracer for determining the type of hydration or dehydration processes which have occurred. The standard convention is to express the VMR ratio of a less abundant isotopologue to the primary isotopologue, relative to the standard abundance in the reference *VSMOW* (*Vienna Standard Mean Ocean Water*) using the following relationship:

$$\delta D = 1000 \times \left[\frac{\left([HDO]/[H_2O]\right)_{measurement}}{\left([HDO]/[H_2O]\right)_{VSMOW}} - 1 \right] \qquad (7.1)$$

Water vapor with 67% of its HDO removed would be described as δD = -670‰ or -670 per mil. Some early atmospheric δD ratios were measured in samples of upper tropospheric air collected during an aircraft campaign [*Ehalt*, 1974]. A large dataset of more recent *in situ* measurements has been obtained with the ALIAS (Aircraft Laser Infrared Absorption Spectrometer) instrument [*Webster and Heymsfield*, 2003], while the main set of remote measurements analyzed in the literature come from ATMOS [*Rinsland et al.,* 1991; *Moyer et al.* 1996; *Ridal*, 2002; *Ridal and Siskind*, 2002; *Kuang et al.,* 2003], and are mostly stratospheric measurements. *Moyer et al.* [1996] were the first to suggest that δD could be used to investigate dehydration and stratospheric water entry mechanisms, but the ATMOS dataset only included 16 tropical occultations, with only four extending below the stratosphere to span the TTL region. An examination of some of the ATMOS results is given in the discussion section.

7.3 ACE-FTS H_2O and HDO Retrievals and the Tropical Dataset

The ACE-FTS measures the four water isotopologues listed in Table 7-1, as well as multiple isotopologues of other species including CH_4 and N_2O. HDO is now included as an update to version 2.2; however, data for the other non-primary isotopologues have not yet been released. The v2.2 H_2O retrieval used in this work utilizes 67 microwindows to retrieve H_2O from 5.5 to 88.5 km in altitude. Four of these microwindows are in the 953-975 cm^{-1} range, and one is near 2137 cm^{-1}, but the majority are in the 1362-2004 cm^{-1} range. The HDO retrieval utilizes 26 microwindows in the 1402-1498 cm^{-1} and 2612-2724 cm^{-1} ranges to retrieve HDO from 6.5 to 37.5 km in altitude. About 30 of the approximately 500 occultations used in this work were processed with a slightly modified v2.2 update for HDO. The modified retrieval was necessary when the initial retrieval did not process to completion in v2.2, and in a few cases HDO was retrieved for a second time when the initial retrieved result had unphysical oscillations or spikes due to clouds in the FOV. Of the retrievals attempted a second time, any that still had problems were omitted from the averages. Although the large number of species studied by the ACE-FTS is an obvious strength of infrared FTS remote sensing, the retrieval difficulties that result from clouds in the FOV are a limitation, which result in a *clear sky bias,* since retrievals of measurements near appreciable cloud thickness frequently fail.

For all ACE-FTS species, including both primary and minor isotopologues, VMR values represent the total VMR for all isotopologues of the species based on a retrieval using that specific isotopologue. The ACE-FTS data are provided in this way as a direct result of the manner in which line intensities are given in the HTRAN database [*Rothman et al.*, 2005], which is the primary source of spectroscopic parameters for ACE-FTS retrievals. HITRAN line intensities have been divided by their standard abundance so that spectral lines of any isotopologue can be used to directly retrieve the total VMR of a species by assuming it was measured at standard abundance conditions. Stating the combined VMR of all isotopologues is the most straightforward method for the majority of ACE-FTS data users who most likely want profiles of total water and not just the $H_2{}^{16}O$ isotopologue, or total methane and not just $^{12}CH_4$; therefore, to obtain the actual HDO or ^1H_2O VMR, the given VMR value must be multiplied by its standard abundance as given in the HITRAN database.

Since the ACE orbit (described in Chapter 1) has been optimized for measurements over the poles and midlatitudes, tropical measurements (defined here as 25ºS-25ºN) are sparse. As a general rule, ACE only has the opportunity for tropical measurements during even numbered months (February, April, August, June, October, December), and these measurements occur only at times in the ACE orbit when the beta angle (β) is high. High β occultations have a greater number of individual tangent point measurements than lower β occultations, and this causes problems for two reasons. Firstly (as mentioned in Chapter 1), this makes the measurement time longer, resulting in a profile that is not really vertical since the occultation is smeared over a large horizontal distance, mostly in the north-south direction. For an occultation with β=60º, the horizontal change between the surface and 17 km is ~6370 km if the effects of refraction are

included. The second problem results from the fact that more individual FTS spectra in an occultation results in a larger volume of data for downlink. With a limited amount of downlink capacity available to ACE, very high β occultations are frequently not downlinked because a single one of these can have the same data volume as three low β occultations, and tropical measurements are generally of a lower priority than middle and high latitude measurements for the ACE mission.

Figure 7-3 shows an example of temperature, [H_2O] vapor and δD profiles for the southern hemisphere (SH) tropics during the months of April 2004 and 2005 averaged together. Much of the stratospheric variability in the [H_2O] profiles is a result of methane oxidation (Chapter 5 and *Nassar et al.*, [2005]). The temperature profiles and [H_2O] profiles have a comparable amount of variability, although the temperature profiles have a smoother shape. The δD profiles exhibit the most random variability, much of which can be attributed to spectral noise because of the lower SNR for HDO and the fact that δD is derived from two quantities ([H_2O] and [HDO]), each contributing to the error. The position of the hygropause (or water vapor minimum) is located at a slightly higher altitude than the temperature minimum, and both are above the altitude of maximum HDO depletion indicated by the minimum in the δD profile.

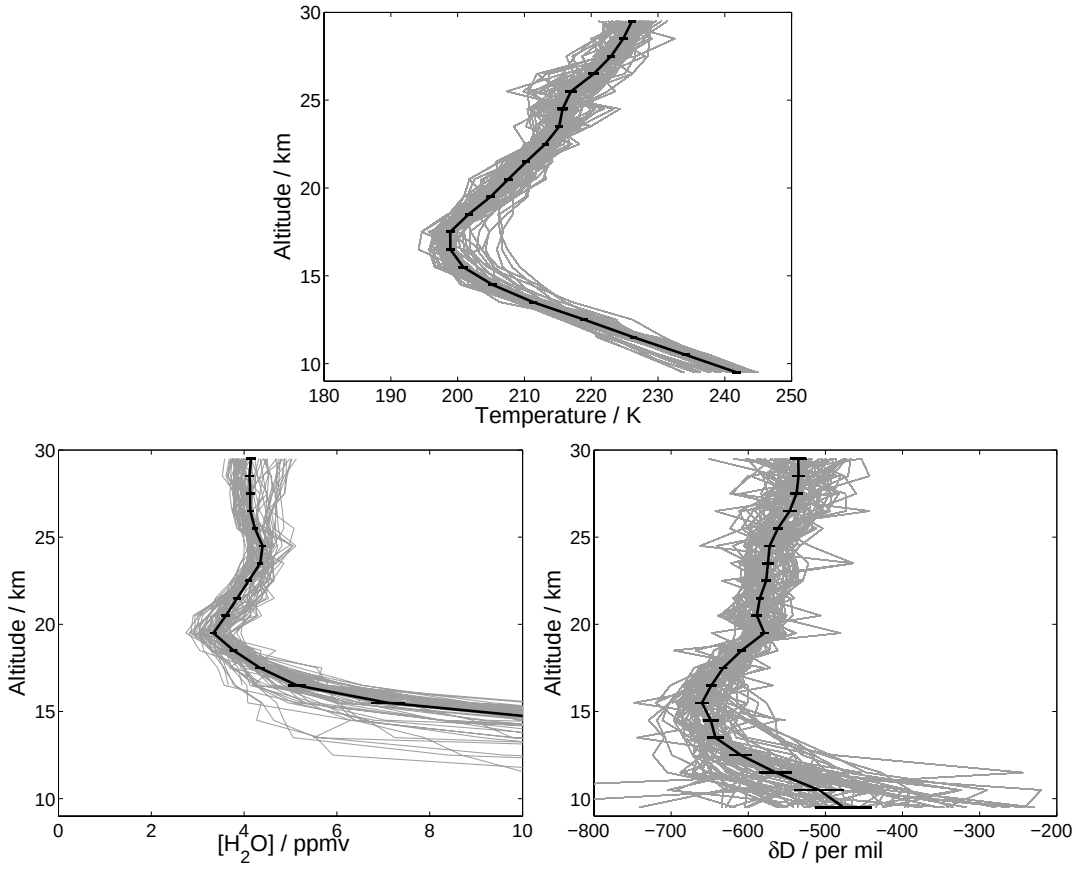

Figure 7-3: 68 temperature, [H_2O] vapor and δD profiles for the SH tropics (0-25ºS) during August 2004 and 2005 (gray lines). The thicker black lines are the combined August 2004-2005 mean profiles, with error bars indicating the 2σ variability of the mean profiles.

Moyer et al. [1996] corrected their δD profiles for the stratospheric production of H_2O by CH_4 (discussed in Chapter 5) and the production of HDO by the reaction:

$$CH_3D + 2O_2 \rightarrow CO_2 + H_2O + HDO \qquad (7.2)$$

The corrected profile was nearly vertical between ~20-35 km, but showed less depletion below that altitude range. Experimentation with applying a correction for the oxidation of methane was carried out with ACE-FTS data. The correction to δD for the oxidation of methane involves subtracting the resulting contributions to each water isotopologue in the ratio, which are designated as $\Delta[^1H_2O]$ and Δ[HDO]. (Isotopologues are labeled here with at least one mass number (or D for ^2H) to distinguish them from the total of all isotopologues for a species. The other unlabelled atoms in the isotopologue can be assumed to be of the primary isotope.) Δ[HDO] can be determined as $[CH_3D]_e$-$[CH_3D]$, where $[CH_3D]_e$ is the mean value entering the stratosphere and $[CH_3D]$ is the value at a given altitude. $\Delta[^1H_2O]$ is found in a similar manner but includes the oxidation products of $^{12}CH_4$, $^{13}CH_4$ and CH_3D. Both $[CH_3D]$ and $[^{13}CH_4]$ can be retrieved from ACE-FTS measurements, but these retrievals have not been checked internally or compared to other measurements. Initial inspection indicates that they are noisy (which is the case for most weakly absorbing species), and have a higher rate of failure than the primary isotopologue. Therefore, assumed values for these species and their entry values were utilized based on their standard abundances with respect to CH_4 [*De Bievre*, 1984], and the entry value of methane in Chapter 5. The steps in the calculation of the methane correction are given below, first for HDO (equations 7.3 to 7.6), then for ^1H_2O (equations 7.7 to 7.11), where the sum of all isotopologues for water or methane have no mass numbers and CH_3D_{std} is the standard abundance of CH_3D.

$$[HDO]_{corrected} = [HDO] - \Delta[HDO] \qquad (7.3)$$

$$[HDO]_{corrected} = [HDO] - ([CH_3D]_e - [CH_3D]) \qquad (7.4)$$

$$[HDO]_{corrected} = [HDO] - CH_3D_{std}\,([CH_4]_e - [CH_4]) \qquad (7.5)$$

$$[HDO]_{corrected} = [HDO] - 0.00061575(1.726\ \text{ppmv} - [CH_4]) \qquad (7.6)$$

$$[^1H_2O]_{corrected} = [^1H_2O] - \Delta[^1H_2O] \qquad (7.7)$$

$$[^1H_2O]_{corrected} = [^1H_2O] - 2([^{12}CH_4]_e - [^{12}CH_4]) - 2([^{13}CH_4]_e - [^{13}CH_4]) - ([CH_3D]_e - [CH_3D]) \qquad (7.8)$$

$$[^1H_2O]_{corrected} = [^1H_2O] - 2 \times {}^{12}CH_{4\,std}\,([CH_4]_e - [CH_4]) - 2 \times {}^{13}CH_{4\,std}\,([CH_4]_e - [CH_4]) - CH_3D_{std}\,([CH_4]_e - [CH_4]) \qquad (7.9)$$

$$[^1H_2O]_{corrected} = [^1H_2O] - (2 \times 0.98827 + 2 \times 0.01110 + 0.00061575)(1.726\ \text{ppmv} - [CH_4]) \qquad (7.10)$$

$$[^1H_2O]_{corrected} = [^1H_2O] - 1.9935575\,(1.726\ \text{ppmv} - [CH_4]) \qquad (7.11)$$

An uncorrected mean δD profile and the corrected δD profile are compared in Figure 7-4, which indicates that the methane correction causes the profile to become more vertical. Ultimately, it was decided that it is preferable not to apply the correction to the ACE-FTS δD profiles in order to avoid potentially introducing a bias from assumed profiles, since it has been shown that the stratospheric chemistry of CH_3D may differ from that of $^{12}CH_4$ [*Irion*, 1996], which would contribute error with this method of correction. Future investigation may utilize the ACE-FTS retrievals of the minor methane isotopologues to carry out the correction for methane oxidation in the stratosphere, but Figure 7-4 indicates that the correction is insignificant below ~18.5 km, which is the most important altitude range for the current work, as will be explained later in this chapter.

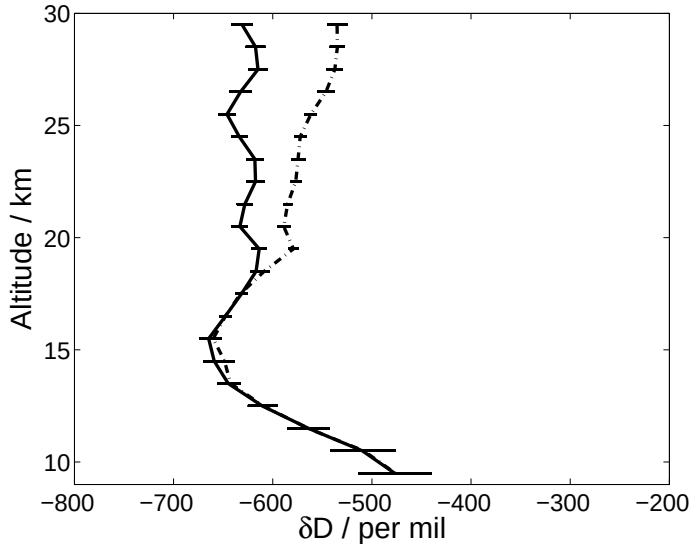

***Figure 7-4*:** SH August mean δD profiles with no correction for methane oxidation (dash-dot line), and with a correction based on assumed abundances of $^{12}CH_4$, $^{13}CH_4$, and CH_3D (solid line). The error bars indicate the 2σ variability of the mean profiles.

7.4 Month-to-Month Comparisons

Tropical monthly averages in each hemisphere for ACE-FTS measurements in 2004 and 2005 will now be examined. For some of the reasons mentioned in the previous section, there were not enough June or December occultations available to obtain monthly averages, so only February, April, August and October are compared. These months approximately correspond to the NH seasons (February - winter, April - spring, August - summer, October - autumn). The number of occultations averaged in each hemisphere for each month are shown in Table 7-2, along with the mean latitude of the measurements. Figure 7-5 shows the separate hemisphere comparisons of the monthly-averaged temperature, [H_2O] vapor and δD profiles. In an initial analysis, profiles were separated by month and year; however, close examination indicated significant hemispheric asymmetry, so in a second trial, profiles were separated by month, year and hemisphere.

Unfortunately, if fewer than ~15 profiles are averaged, δD profiles often have a jagged shape. To prevent basing averages on very low numbers of profiles, while still adequately examining seasonal and hemispheric variability, equivalent months in 2004 and 2005 were combined in the current comparison and for the majority of this work. When a sufficient number of profiles were available for a given month in both 2004 and 2005, large differences between the years were not observed, as will be shown later.

The latitude and longitude values from the refraction model for the 17.5 km point (the approximate position of the cold point tropopause or temperature minimum) were used to determine whether or not an occultation was considered tropical, and to which hemisphere it belonged. The 17.5 km point differed from the 30 km reference point by up to 1.5º latitude, but longitudes typically differed by less than 0.25º. If a latitude and longitude array was not available from the model (which occurred less than 5% of the time), then the latitude and longitude were determined by interpolating between latitude and longitude shifts in neighboring occultations, since they have a very similar β effect.

Table 7-2: The number of tropical occultations in each hemisphere sorted by month, along with the mean latitude of the 17.5 km tangent point in the measurements.

		2004		2005		2004 and 2005	
		n	**Mean Latitude**	***n***	**Mean Latitude**	***N***	**Mean Latitude**
NH	**Feb**	24	13.7º	8	17.5º	32	14.7º
	Apr	31	12.3º	67	13.6º	98	13.2º
	Aug	51	13.3º	44	11.2º	95	12.3º
	Oct	6[a]	3.4º	20	4.3º	26	4.1º
SH	**Feb**	7	-5.5º	27[b]	-15.2º	34	-13.2º
	Apr	10	-6.1º	38	-12.4º	48	-11.1º
	Aug	30	-11.1º	38	-11.1º	68	-11.1º
	Oct	39	-14.1º	56	-16.6º	95	-15.6º

[a] Includes one equatorial profile with the 17.5 km point in the SH, but the troposphere is mostly in the NH
[b] Includes one profile with a reference date and time of 2005-01-31, 23:01 UT

Figure 7-5 indicates that for both hemispheres, the coldest temperatures occurred in February, followed by April, then October and finally August. This is consistent with the model results of *Holton and Gettelman* [2001] (shown in Figure 7-6), although in the ACE-FTS results some variation in the altitude of the temperature minimum was also found to occur between seasons for the NH, which is qualitatively consistent with the conclusions of *Seidel et al.* [2001] based on radiosonde measurements. In the NH, the ACE profiles were more evenly spread than in the SH, where February and April profiles were nearly coincident, as were October and August.

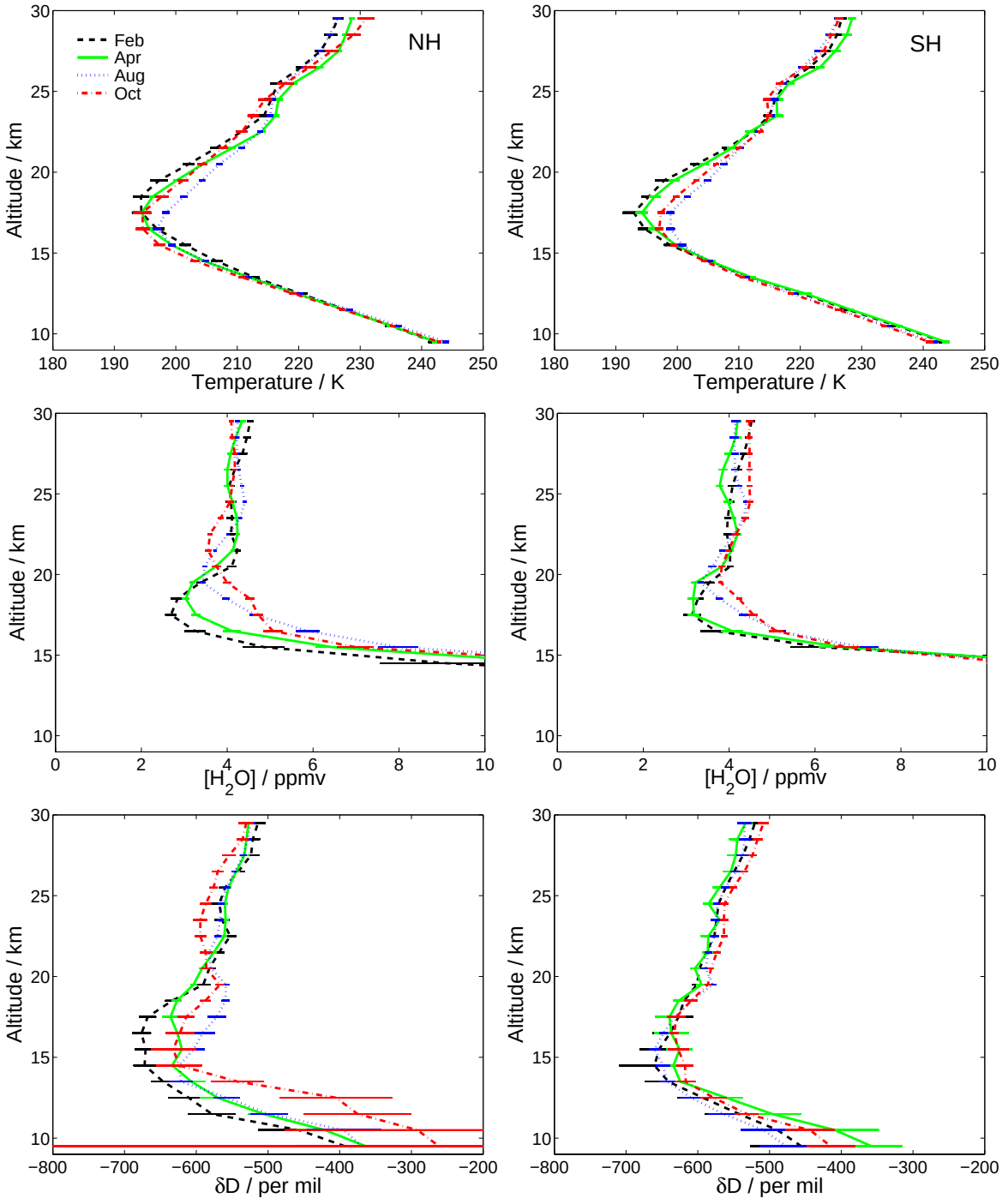

Figure 7-5: Combined 2004-2005 monthly averaged NH (left) and SH (right) profiles of temperature, water vapor and δD. The error bars indicate the 2σ variability of the mean profiles.

For water vapor profiles in both hemispheres, the lowest VMR values occurred in February, followed by April, then August and finally October; however, the shape of the profiles changed significantly from one month to the next. The ACE-FTS water vapor results had some similarities to the modeled profiles of *Holton and Gettelman* [2001], but significant differences as well. The ordering of profiles by season was approximately the same, but minima in the ACE-FTS profiles were not as sharp as in the modeled work. The lack of sharp minima is believed to be real, but may be a result of the vertical resolution of the measurements. Additionally, a reduction in the sharpness of the minima is expected due to the fact that the ACE profiles have been averaged over variability, some of which may result from changes in latitude, but this effect would likely be too small to explain the entire difference.

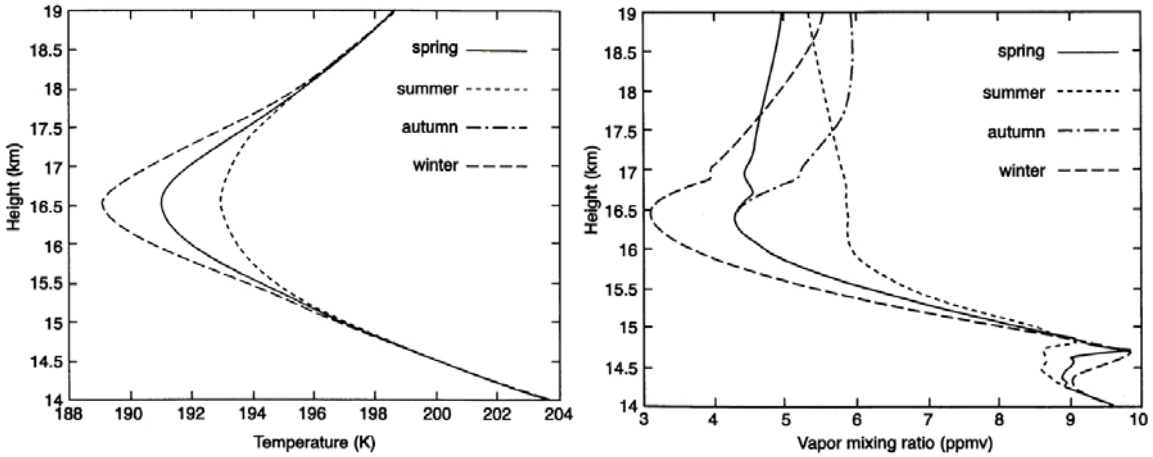

Figure 7-6: Modeled temperature and water vapor VMR profiles for the four NH seasons at the Western Pacific cold trap, directly reproduced from *Holton and Gettelman* [2001]. The temperature profiles are the same for the spring and autumn. Line styles for the four seasons shown here essentially coincide with the line styles for the months in Figure 7-5, but note that the *x*- and *y*-axis ranges are narrower than for the plots showing ACE-FTS profiles in Figure 7-5.

In the ACE-FTS water vapor profiles, it appears that the minimum in the profile, corresponding to the most dehydrated air, is propagating upward in time, while the air is simultaneously undergoing mixing and chemical production of water from methane. This upward propagation demonstrates the tropical tape recorder effect. In both hemispheres, the April profiles even show a weak secondary minimum in the lower stratosphere which may be from the previous winter. The minima appear to be separated by ~9 km, which implies a mean upward propagation rate of 9 km/year or ~0.285 mm/s, whereas the separation between tape recorder minima modeled in *Mote et al.* [1996] is about 10-11 km. The slightly lower rate of upward propagation in the ACE data may just be a result of a relaxed definition of the tropics, including measurements up to 25º latitude, which is very close to the subtropical jets where net downward motion in the troposphere dominates. It may also result from peaks being dampened by averaging, where there was variability in the individual profile peak heights. It is not clear why the secondary peak is more prominent in April than during other months (although for October it would be partially above this altitude range); however, in the stratosphere the extent of methane oxidation will have a large

impact on the profiles as discussed in Chapter 5. It should be noted that there is a larger than expected vertical offset for the NH October [H_2O] vapor minimum, which may be the result of a latitudinal bias, since it is more tropical (i.e. has a lower mean latitude) than the other averages.

The δD profiles in the NH exhibit a large amount of seasonal variability, while those in the SH show much less. In both hemispheres, February profiles are the most depleted, with the NH February average reaching -676‰ at 16.5 km and the SH February average reaching -660‰ at 14.5 km. In the NH, the ordering of the amount of depletion in the δD profiles is the same ordering as for the minimum temperature values. In the SH the correspondence is not as clear, since the SH August profiles are depleted nearly as much as the February profiles, and the SH April and October δD profiles were very similar although their temperature and water vapor profiles were different.

The monthly-averaged profiles indicate that the coldest tropopause temperatures generally correspond to the most depletion for each hemisphere. This might suggest that temperature is the most important factor controlling $[H_2O]_e$, which would be consistent with gradual dehydration as the dominant dehydration mechanism. However, two factors prevent one from concluding this immediately. The first is the fact that the altitudes of maximum depletion are often below the temperature minima, and the net upward propagation of tropical air implies that the depletion would have occurred before the air encountered the temperature minima. Only the shapes of the NH February and April profiles and the SH April and October profiles may indicate some depletion occurring directly at the altitude of the temperature minima. This depletion may still be associated with the Western Pacific cold trap, because the Maritime Continent is actually known to be a region with a slight net subsidence (as mentioned earlier), and furthermore, the cold trap is known to have a thin layer of cirrus clouds directly below it [*Holton and Gettelman*, 2001]. Cirrus clouds are filament-like clouds that are primarily composed of ice crystals, so they appear white when they form a thick layer; however, subvisible thin cirrus clouds are even more common in the tropics. Cirrus tend to occur in the TTL at ~16-17 km, and are frequently found above convective anvils [*Hartmann et al.*, 2001], which are tower-like (cumulonimbus) clouds associated with upward convective motion. These clouds can span a large vertical distance, with their tops reaching ~13-14 km altitude. Modeling work by *Hartmann et al.* [2001] has shown that when cirrus are located above convective anvils, they can produce a localized cooling directly above the cirrus, and it has been suggested that this may be the origin of the Western Pacific cold trap. While the details of the model are beyond the scope of this work, the important points are that the Western Pacific has been shown to be a localized region of net subsidence, and the formation of cirrus directly below indicates the possibility that water vapor has been frozen above and transported to a slightly lower altitude. The slight changes in altitude are small enough that transport could still occur quasi-horizontally, i.e., without crossing isentropes (defined in Chapter 6).

Further verification for the importance of low temperatures can be seen by Figure 7-7, which shows correlations between δD and temperature for each individual tangent point in the 9-30 km range. The correlations are not very compact because a range of δD are expected for any given

set of meteorological conditions [*Gettelman and Webster*, 2005]; however, they do indicate that the largest amounts of depletion (very negative δD values) only occur with low temperatures.

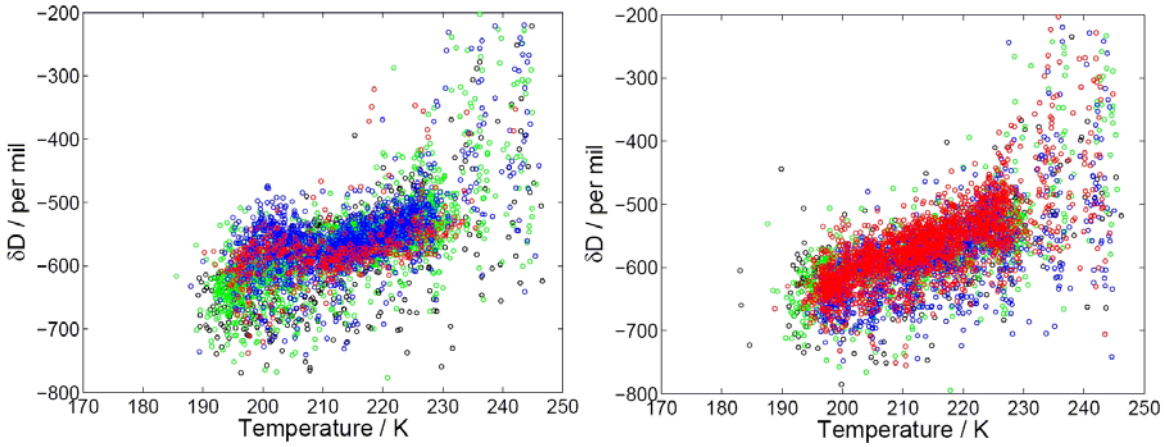

Figure 7-7: δD versus temperature correlations for the NH (left) and the SH (right). The data have been plotted in 'layers' in the following order: February (black), April (green), August (blue), and October (red) and include all individual tangent points between 9 and 30 km. The plots indicate a good correlation for the majority of points, especially those at lower temperatures.

The second complicating factor is the unexplained amount of depletion in the SH during August, that is not consistent with the pattern of higher depletion coinciding with lower mean temperatures. Although the variability in the SH August δD profiles, shown in Figure 7-3, was acknowledged earlier, the mean δD profile is still a very reasonable representation. If August 2004 and 2005 are displayed separately, as in Figure 7-8, they show very little difference, so this δD value does not appear to be an anomaly, but rather a true seasonal effect. The Western Pacific cold trap itself is a seasonal phenomenon, with the largest temperature deviation (~4 K) during the time of NH winter, a lesser deviation in spring and autumn, and essentially no deviation during the summer [*Holton and Gettelman*, 2001; *Seidel et al.*, 2001], so it should not be expected to play a major role in the August HDO depletion. The SH August profiles likely indicate the influence of convective processes, since the cold trap is absent.

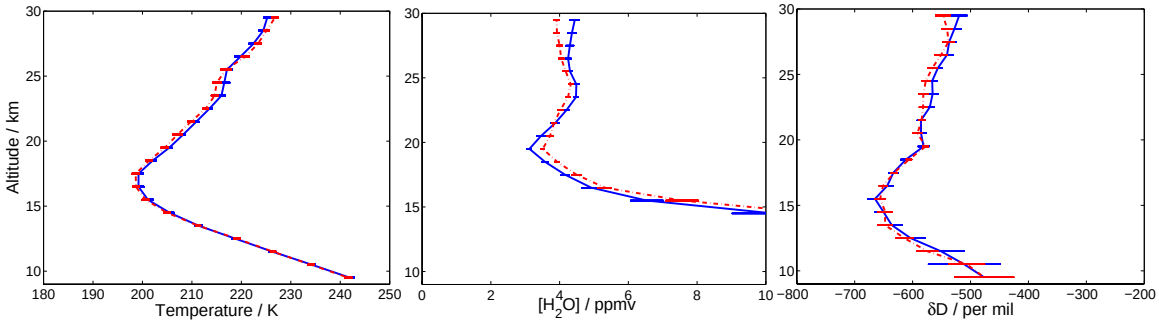

Figure 7-8: A comparison of SH August 2004 (blue solid line) and 2005 (red dash-dot line) mean temperature, [H_2O] and δD profiles, showing that all pairs of profiles, especially the temperature and δD profiles are very similar. The error bars indicate the 2σ variability of the mean profiles.

Variability in HDO/H_2O Abundance Ratios at the TTL

The most common method for determining whether or not convective processes have played a role in regulating $[H_2O]_e$ is by comparing the observed δD values to those predicted for the equilibrium fractionation for a given temperature profile, referred to as Rayleigh distillation. The method for calculation of Rayleigh distillation profiles is described in detail in *Johnson et al.* [2001]. The Rayleigh profiles typically begin at ~ -86‰ above the ocean and should decrease monotonically to ~950‰ at the coldest tropopause [*Webster and Heymsfield*, 2003]. The individual points from each ACE-FTS δD profile up to 18.5 km (shown in Figures 7-9 and 7-10), differ from a Rayleigh distribution, with very few points exceeding -800‰. Deviation from the Rayleigh distribution is usually cited as evidence for convective processes enriching air in HDO. However, recently *Gettelman and Webster* [2005] have shown that the deviation from the Rayleigh curve does not require convective dehydration, and can be explained by the lofting of ice particles during convective episodes.

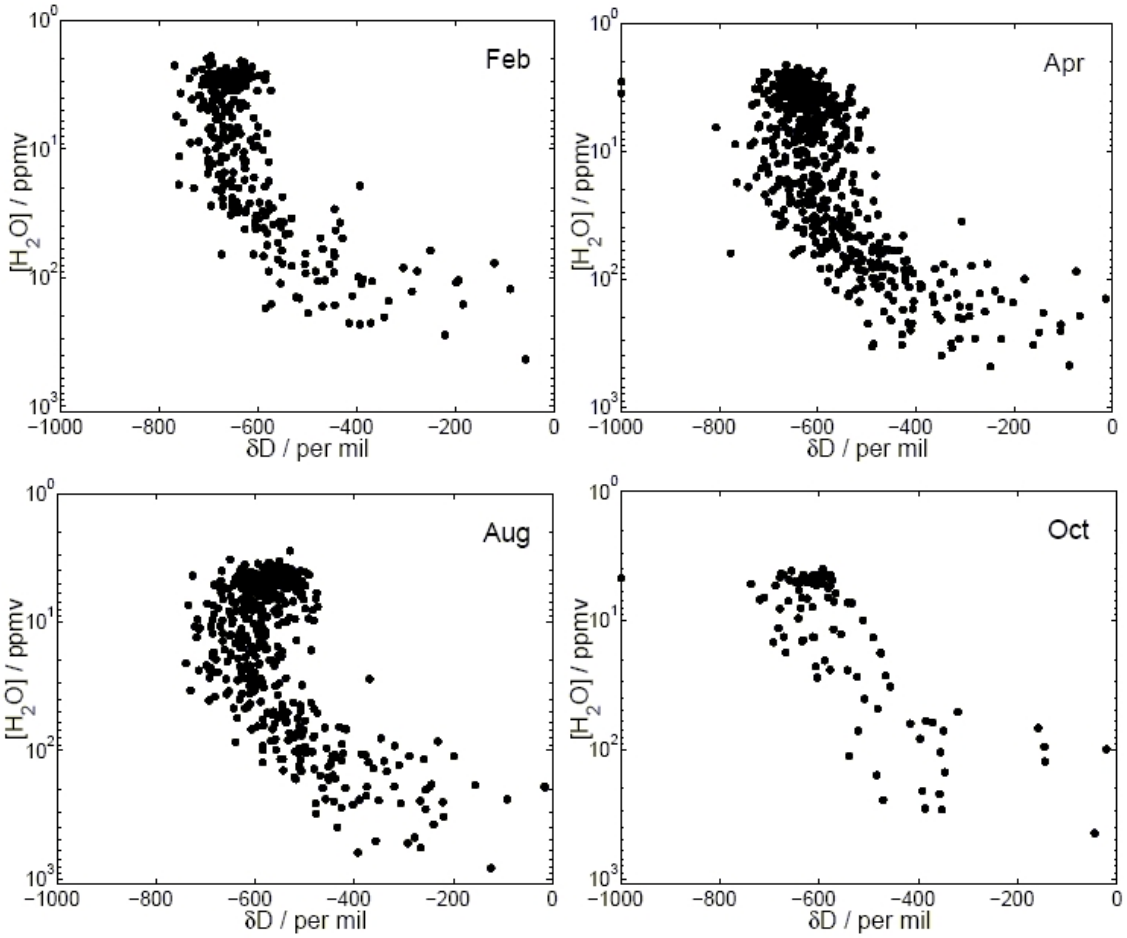

Figure 7-9: $[H_2O]$ versus δD correlations for all individual points in the tropical SH from 9.5-18.5 km. No part of the distribution approaches -950‰, as would be expected near the tropopause under Rayleigh distillation.

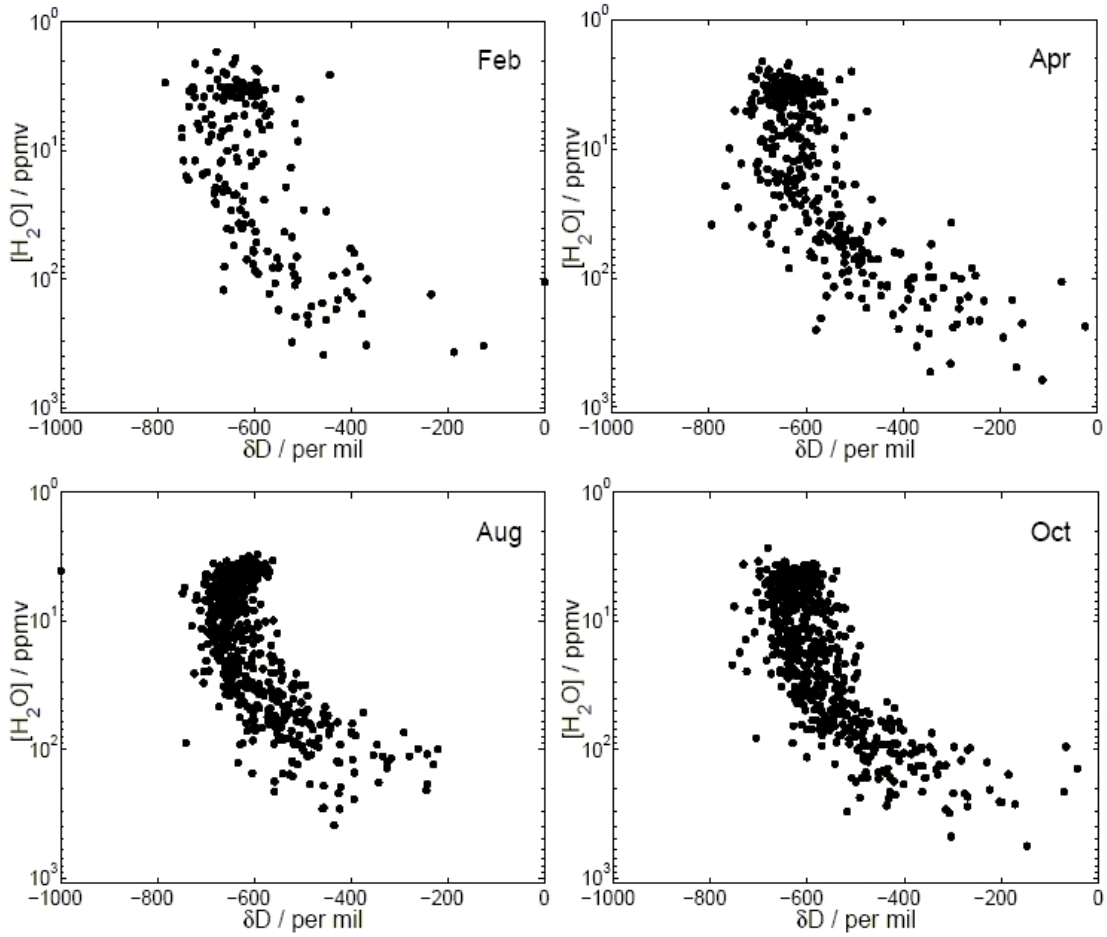

Figure 7-10: Same as the previous figure, but for the NH.

Unfortunately, deviation of δD from the Rayleigh distribution alone can not definitively be used to determine whether the HDO enrichment relative to the Rayleigh curve has occurred via convective dehydration or the lofting of ice particles [*Keith*, 2000]. While it is common to describe the tropics as a region of net ascent, clear sky regions of the tropics may have a net subsidence (*I. Folkins*, private communication, 2006), while localized convection in clouds is common up to ~14-15 km [*Folkins et al.*, 1999] and could be responsible for most of the ascent. The frequency of this convection penetrating the TTL is much less certain and likely less common. However, ice lofting does not need to penetrate the TTL in order to influence δD profiles in the TTL, since the lofting of ice to altitudes just below the TTL will enrich that altitude in HDO, some of which would subsequently be transported upward by gradual ascent, as suggested by *Moyer et al.* [1996].

7.5 Discussion

Moyer et al. [1996] state in their conclusions that: "Isotopic data from the stratosphere alone may be sufficient to demonstrate whether the final dehydration of stratospheric air occurs in slow ascent

rather than in convective penetration with a mixture of evaporated ice, if a clear seasonal cycle in stratospheric δD is detectable." *Ridal* [2002] and *Ridal and Siskind* [2002] modeled δD ratios throughout the stratosphere including seasonal effects, and suggested that their results were consistent with ATMOS. However, in these three papers, it is not definitively stated what the authors believe the seasonal variation means in the context of mechanisms for entry of water into the stratosphere. *Sherwood and Dessler* [2003] state that one might interpret a seasonal variation in δD at the TTL as an indication that convective processes do not often go beyond ~16-17 km to penetrate the tropopause, because these processes would cause mixing and thus remove any seasonal signature. However, they refute this by stating that their model shows that it really depends on the details of the convective processes, and that processes that simply dilute water vapor, such as injecting dry air into the stratosphere, do not alter δD values, although injecting ice particles which introduces water, would cause a change. This means that convective dehydration should produce a near vertical altitude versus δD profile, but convective ice lofting should not.

Kuang et al. [2003] utilized ATMOS slant column retrievals, which used better spectroscopic constants than were available in the past. They determined a near-vertical δD profile with a value of about -670‰ (after correcting for methane oxidation) based on 11 tropical occultations (Figure 7-11). The ACE-FTS δD profiles show much less depletion in the stratosphere as a result of opting not to apply a methane correction, but they also show less depletion in the troposphere which is not related to methane oxidation. Some of the mean δD profiles shown in Figure 7-5 (NH February, NH April, SH April and SH October) have a nearly vertical range between ~14-19 km corresponding to the TTL, but none are vertical over as wide of a range as in *Kuang et al.* [2003].

One potential deficiency in the work of *Kuang et al.* [2003] may be the use of slant columns rather than VMR profiles retrieved by inversion. They argued that the use of slant columns reduces error in the [HDO]/[H_2O] ratio because error is added by the multiple steps of the inversion process. While that may be true, showing profiles based directly on slant columns has the effect of greatly decreasing the vertical resolution of the measurements and dampening any horizontal structure in the profile. This occurs because a point at any given altitude in their plots does not represent the VMR at that altitude, but represents the integrated VMR for a slant column with a tangent height equal to that altitude. Each slant column of course contains contributions from higher altitudes (as shown in Figure 1-3) which effectively contaminate the measurement if they are not properly accounted for by inversion. This probably explains why *Kuang et al.* [2003] have δD values of about -650‰ as low as 11 km and a nearly vertical distribution of δD, while the δD profiles in *Moyer et al.* [1996], which were also based on ATMOS data (but did not reach as low in altitude), showed less depletion and a deviation from vertical below ~20 km. Although *Kuang et al.*, [2003] state that they have a vertical resolution of ~2 km, the use of slant columns rather than profiles obtained by inversion, would make the effective vertical resolution much worse. Vertical resolution really cannot be defined in a direct way when using slant columns because the shape of a profile will determine how much of an impact the effective contamination from upper levels will make. The exponential decrease in pressure somewhat reduces the effect

just mentioned, but it can still be significant. *Dessler and Sherwood* [2003] cite the nearly vertical result obtained by *Kuang et al.* [2003] as evidence for the dominance of convective dehydration, but based on the use of slant columns rather than retrieved profiles, this should be questioned.

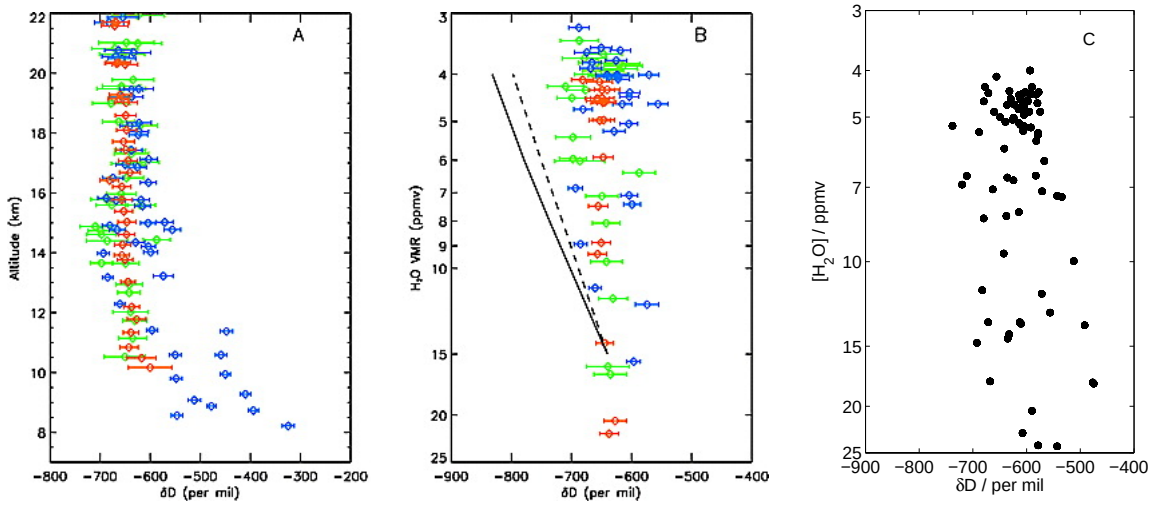

Figure 7-11: Altitude versus δD (left) and [H_2O] versus δD (middle) based on ATMOS slant column data, measured between November 10-12, 1994 in the tropical NH, directly reproduced from *Kuang et al.* [2003]. The different colored points indicate measurements in different filters or wavenumber bands for the ATMOS instrument. The solid line is the calculated Rayleigh distillation curve and the dotted line is the calculated curve if some supersaturation is allowed in their model, as described in that paper. The ACE-FTS [H_2O] versus δD relationship based on 26 profiles from October 2004 and 2005, is shown on the right for comparison. The corresponding altitude versus δD profile was shown in Figure 7-5 and did not have a vertical portion for a significant range anywhere near the TTL.

Keith [2000] suggested that in order to determine if ice was lofted through the tropopause by convection or of it evaporated in the upper troposphere then ascended to the stratosphere, observations of isotopic fractionation at the top of the TTL are much more helpful than those in the stratosphere. In the ACE-FTS [H_2O] versus δD correlation plots, rather than correct for methane oxidation, only points up to 18.5 km were included, below which point methane oxidation should not have much effect. These correlations emphasize the variability observed here, which has also been observed by *in situ* techniques [*Webster and Heymsfield*, 2003; *Gettelman and Webster*, 2005], but in the ATMOS data, the [H_2O] versus δD relationship was nearly vertical. Over a narrow range of [H_2O], (for example 3-25 ppmv as shown in Figure 7-11 above), one might interpret the ACE-FTS [H_2O] versus δD relationship as vertical, despite the fact that Figure 7-5 indicates that the δD profiles are not vertical for a significant range in the TTL region. This illustrates that a vertical distribution in [H_2O] versus δD does not necessarily correspond to a

vertical distribution in altitude versus δD, because the former depends on the shape of the [H_2O] profile.

Given all of these considerations, the seasonal variation in δD and the correlation between that variation with temperature seem consistent with gradual dehydration, rather than with convective dehydration. The altitude of maximum HDO depletion may relate to net subsidence in the *clear sky* region carrying depleted air to a slightly lower altitude or more localized periodic upward convective episodes lofting ice particles. It is not clear whether or not the convective ice lofting actually penetrates the TTL or just provides a source of HDO enriched air directly below the TTL, but convective episodes in the troposphere, which are known to be common, can contribute to the maximum HDO depletion beginning below the TTL, as well as the deviation from a Rayleigh distribution. There also appears to be seasonal variability in the extent of convective ice lofting as well, but this variability is not directly correlated with temperature. Since known processes such as gradual dehydration and convective ice lofting can (qualitatively) account for the observations described, and there is no obvious evidence of upward convection frequently overshooting the tropopause, convective dehydration does not likely play a major role in contributing to the dryness of the stratosphere.

7.6 Potential Improvements and Future Work

The separation of occultations into NH and SH using the equator was the simplest, although a somewhat arbitrary separation point for understanding differences between the hemispheres. In a meteorological sense, a major factor that dictates the difference between the NH and SH in the troposphere is the direction of circulation. While the Brewer-Dobson circulation (described in previous chapters) controls the pattern of atmospheric circulation in the stratosphere, tropospheric circulation is much more complicated. Tropical tropospheric circulation relates to the Brewer-Dobson circulation because air rises in convective clouds in a narrow latitude band called the inter-tropical convergence zone (ITCZ) [*Salby*, 1991] and moves away from the ITCZ in opposite directions just below the tropopause, before descending at the subtropical jets near 30º latitude. The ITCZ, which effectively divides the two hemispheres, does not lie exactly on the equator, but varies somewhat with longitude and season, and is most often found between 5-10ºN, but occasionally appears in the Western Pacific as far as 5-10ºS [*Holton*, 2004]. A more sophisticated analysis of the data would involve separating the hemispheres by the center of the variable ITCZ based on meteorological data, rather than by the equator, in order to avoid averaging together measurements of air which may be physically isolated by the ITCZ. Furthermore, an analysis of tracers such as described in Chapter 6 could be used to discern tropical air from subtropical air rather than the arbitrary 25ºN/S boundaries.

This work was only intended as a first look at ACE-FTS HDO measurements, and was not intended to answer all remaining questions about atmospheric transport and dehydration. Although only ~500 occultations considered tropical were available in this work, the ACE-FTS is continuing to accumulate tropical measurements which can be used for future investigation of transport at the

TTL. For example, with more measurements a study of longitudinal variability may be possible. Investigations are also possible involving HDO at middle and high latitudes, for which many more measurements are currently available. In future work, $H_2{}^{17}O$ and $H_2{}^{18}O$ can also be used [*Kaye et al.*, 1990] to try to confirm the present findings or in conjunction with HDO, for example examining δD vs. $\delta^{18}O$ correlations. Lastly, interpretation of the current findings, or future studies, could be strengthened if they were shown to agree with a model.

7.7 Summary and Conclusions

This work examined the seasonal variation in tropical temperature, water vapor and δD profiles in 2004 and 2005, using ACE-FTS measurements. The minimum temperature and altitude of the cold point tropopause were found to exhibit a significant seasonal variation in the NH, while only the minimum temperature varied in the SH. δD also showed a seasonal variation which was stronger in the NH than in the SH, with the lowest δD values occurring during February in the NH, corresponding to the coldest temperature. In both hemispheres, there was a strong correlation between temperature and δD which can be interpreted as evidence that gradual ascent is most likely the main method for the entry of water into the stratosphere. This would be consistent with gradual dehydration, including horizontal transport through a cold trap, as the main mechanism responsible for the dryness of the stratosphere. However, the results also indicated a role for convective processes, evidenced by the relatively high HDO depletion in the SH during August and the general deviation from the Rayleigh distillation curves which begins in the troposphere. These upward convective processes may or may not penetrate the TTL, and do not necessarily contain a role for the convective dehydration mechanism. Convective episodes which readily reach the tropical upper troposphere but do not penetrate the TTL can loft ice crystals enriching air just below the TTL with HDO. The ice enriched in HDO could later vaporize and can subsequently gradually ascend across the TTL, fractionating but resulting in less depletion than if it were not previously enriched. This seems consistent with the small deviation from the Rayleigh distribution that is observed at the bottom of the TTL and the altitude of maximum HDO depletion. Convective dehydration should produce a vertical distribution in altitude versus δD profiles which has generally not been observed in the ACE-FTS data over large altitude ranges, and although some prior work [*Kuang et al.*, 2003] does indicate a vertical relationship, the result is questionable. Consideration of the ACE-FTS results along with previous work, does not rule out the possibility of convective dehydration, but its inclusion does not appear necessary to explain these observations.

References

Brenninkmeijer, C.A.M, C. Janssen, J. Kaiser, T. Röckmann, T.S. Rhee, S.S. Assonov (2003), Isotope Effects in the Chemistry of Atmospheric Trace Compounds, *Chem. Rev.*, 103, 5125-5161.

Brewer, A.W. (1949), Evidence for a world circulation provided by the measurements of helium and water vapor distribution in the stratosphere, *Quarterly Journal of the Royal Meteorological Society*, 75, 351.

Coplen, T.B. (1995), Reporting of stable hydrogen, carbon, and oxygen isotopic abundances, *Pure Appl. Chem.,* 66, 273-276.

Danielsen, E.F. (1982), A dehydration mechanism for the stratosphere, *Geophys. Res. Lett.*, 9, 605-608.

De Bievre, P., N.E. Holden, I.L. Barnes (1984), Isotopic Abundances and Atomic Weights of the Elements, *J. Phys. Chem. Ref. Data,* 13, 809-891.

Dessler, A.E., S.C. Sherwood (2003), A model of HDO in the tropical tropopause layer, *Atmospheric Chemistry and Physics*, 3, 2173-2181.

Ehalt, D.H. (1974), Vertical Profiles of HTO, HDO, and H_2O in the troposphere, *NCAR Tech. Note NCAR-TN/STR-100*, 131 pages, National Center for Atmospheric Research, Boulder, Colorado.

Folkins, I., M. Loewenstein, J. Podolske, S.J. Oltmans, M. Proffitt (1999), A barrier to vertical mixing at 14 km in the tropics: Evidence from ozonesondes and aircraft measurements, *J. Geophys. Res.*, 104(D18), 22095-22102.

Gettelman, A., J.R. Holton, A. Douglass (2000), Simulations of water vapor in the lower troposphere and upper stratosphere, *J. Geophys. Res.*, 105(D7), 9003-9023.

Gettelman, A., C.R. Webster (2005), Simulations of water isotope abundances in the upper troposphere and lower stratosphere and implications for stratosphere troposphere exchange, *J. Geophys. Res.*, 110, D17301.

Hartmann, D.L. J.R. Holton, Q. Fu (2001), The heat balance of the tropical tropopause, cirrus, and stratospheric dehydration, *Geophys. Res. Lett.*, 28(10), 1969-1972.

Holton, J.R. (2004), *An introduction to dynamic meteorology*, Elsevier Academic Press, New York.

Holton, J.R., A. Gettelman (2001), Horizontal transport and the dehydration of the stratosphere, *Geophys. Res. Lett.*, 28(14), 2799-2802.

Irion, F.W., E.J. Moyer, M.R. Gunson, C.P. Rinsland, Y.L. Yung, H.A. Michelsen, R.J. Salawitch, A.Y. Chang, M.J. Newchurch, M.M. Abbas, M.C. Abrams, R. Zander (1996), Stratospheric observations of CH_3D and HDO from ATMOS infrared solar spectra: Enrichments of deuterium in methane and implications for HD, *Geophys. Res. Lett.*, 23(17), 2381-2384.

IUPAC (1994), Atomic Weights of the Elements 1993, *Pure Appl. Chem.*, 66, 2423-2444.

Johnson, D.G., K.W. Jucks, W.A. Traub, K.V. Chance (2001), Isotopic composition of stratospheric water vapor: Implications for transport, *J. Geophys. Res.*, 106(D11), 12219-12226.

Kaye, J.A. (1990), Analysis of the Origins and Implications of the ^{18}O Content of Stratospheric Water Vapor, *J. Atmos. Chem.,* 10, 39-57.

Keith, D.W. (2000), Stratosphere-troposphere exchange: Inferences from the isotopic compostion of water vapor, *J. Geophys. Res.*, 105(D12), 15167-15173.

Kuang, Z., G.C. Toon, P.O. Wennberg, Y.L. Yung (2003), Measured HDO/H_2O ratios across the tropical tropopause, *Geophys. Res. Lett.*, 30(7), 1372.

Mote, P.W., K.H. Rosenlof, M.E. McIntyre, E.S. Carr, J.C. Gille, J.R. Holton, J.S. Kinnersley, H.C. Pumphrey, J.M. Russell III, J. Waters (1996), An atmospheric tape recorder: The imprint of tropical tropopause temperatures on stratospheric water vapor, *J. Geophys. Res.*, 101, 3989–4006.

Moyer, J.M., F.W. Irion, Y.L. Yung, M.R. Gunson (1996), ATMOS stratospheric deuterated water and implications for troposphere-stratosphere transport, *Geophys. Res. Lett.,* 23(17), 2385-2388.

Nassar, R., P.F. Bernath, C.D. Boone, G.L. Manney, S.D. McLeod, C.P. Rinsland, R.S. Skelton, K.A. Walker (2005), Stratospheric abundances of water and methane based on ACE-FTS measurements, *Geophys. Res. Lett.*, 32, L15S04.

Newell, R.E., S. Gould-Stewart (1981), A Stratospheric Fountain?, *J. Atmos. Sci.*, 38, 2789-2796.

Oltmans, S.J., H. Vömel, D.J. Hofmann, K.H. Rosenlof, D. Kley (2000), The increase in stratospheric water vapor from balloon-borne, frostpoint hygrometer measurements at Washington, D.C. and Boulder, Colorado, *Geophys. Res. Lett.*, 27(21), 3453–3456.

Randel, W.J., A. Gettelman, F. Wu, J.M. Russell, J. Zawodny, S. Oltmans (2000), Seasonal variation of water vapor in the lower stratosphere observed in Halogen Occultation Experiment data, *J. Geophys. Res.*, 106, 14313-14325.

Ridal, M. (2002), Isotopic ratios of water vapor and methane in the stratosphere: Comparisons between ATMOS measurements and a one-dimensional model, *J. Geophys. Res.*, 107(D16), 4285.

Ridal, M., D.E. Siskind (2002), A two-dimensional simulation of the isotopic composition of water vapor and methane in the upper atmosphere, *J. Geophys. Res.*, 107(D24), 4807.

Rinsland, C.P., M.R. Gunson, J.C. Foster, R.A. Toth, C.B. Farmer, R. Zander (1991), Stratospheric profiles of heavy water isotopes and CH_3D from analysis of the ATMOS Spacelab 3 infrared solar spectra. *J. Geophys. Res.*, 96(D1), 1057-1068.

Rosenlof, K.H., E.-W. Chiou, W.P. Chu, D. G. Johnson, K. K. Kelly, H. A. Michelsen, G. E. Nedoluha, E.E. Remsberg, G.C. Toon, M.P. McCormick (2001), Stratospheric water vapor increases over the past half-century, *Geophys. Res. Lett.*, 28(7), 1195-1198.

Rothman, L.S., D. Jacquemart, A. Barbe, D.C. Benner, M. Birk, L.R. Brown, M.R. Carleer, C. Chackerian Jr., K. Chance, L.H. Coudert, V. Dana, V.M. Devi, J.-M. Flaud, R.R. Gamache, A. Goldman, J.-M. Hartmann, K.W. Jucks, A.G. Maki, J.-Y. Mandin, S.T. Massie, J. Orphal, A. Perrin, C.P. Rinsland, M.A.H. Smith, J. Tennyson, R.N. Tolchenov, R.A. Toth, J. Vander Auwera,

P. Varanasi, G. Wagner (2005), The HITRAN 2004 molecular spectroscopic database, *Journal of Quantitative Spectroscopy and Radiative Transfer*, 96, 139-204.

Salby, M.L., H.H. Hendon, K. Woodberry, K. Tanaka (1991), Analysis of global cloud imagery from multiple satellites, *Bulletin of the American Meteorological Society*, 72, 467-480.

Seidel, D.J. R.J. Ross, J.K. Angell (2001), Climatological characteristics of the tropical tropopause revealed by radiosondes, *J. Geophys. Res.*, 106, 7857-7878.

Sherwood, S. (2000), A "stratospheric drain" over the Maritime continent, *Geophys. Res. Lett.*, 27, 677-680.

Sherwood, S.C, A.E. Dessler (2000), On the control of stratospheric humidity, *Geophys. Res. Lett.*, 27(16), 2513-2516.

Sherwood, S.C, A.E. Dessler (2003), Convective Mixing near the Tropical Tropopause: Insights from Seasonal Variations, *Journal of the Atmospheric Sciences*, 60(21), 2674-2685.

SPARC (2000), SPARC Assessment of Upper Tropospheric and Stratospheric Water Vapour, WMO/ICSU/IOC World Climate Research Programme, editors D. Kley, J.M. Russell III, C. Philips.

Webster, C.R., A.J. Heymsfield (2003), Water Isotope Ratios D/H, $^{18}O/^{16}O$, $^{17}O/^{16}O$ in and out of Clouds Map Dehydration Pathways, *Science*, 302, 1742-1745.

Chapter 8

Conclusions

A general overview of the ACE mission and ACE-FTS instrument were given in Chapter 1, including some description of ACE-FTS pre-launch testing and science commissioning. Chapter 2 discussed the retrieval process, with a focus on the creation of *a priori* temperature and pressure profiles, which are based on meteorological data in the troposphere and lower stratosphere, combined with a climatological model for higher altitudes. As the primary goal of the ACE mission is the study of processes that relate to ozone depletion, the present work has investigated several topics that relate to this goal, either directly or indirectly. These studies demonstrate the tremendous scientific value of ACE-FTS measurements of temperature, pressure and VMRs of many atmospheric species.

Chapter 3 discussed the key role of stratospheric chlorine in ozone depletion, with an examination of the main chemical processes involved. The first global inventory of stratospheric chlorine was created based primarily on ACE-FTS measurements. This chlorine inventory is valuable for the purpose of building on past chlorine inventories and illustrating the changing levels of total stratospheric chlorine. Chapter 3 has shown that midlatitude total stratospheric chlorine was 3.65 ppmv in 2004 (with a 1σ estimated accuracy of ± 0.13 ppbv and precision of ± 0.09 ppbv). This confirmed that global total stratospheric chlorine is now declining as a result of the international restrictions required under the *Montreal Protocol on Substances that Deplete the Ozone Layer*. This work is significant because it resulted in a slightly higher value for total stratospheric chlorine than one can infer based on measurements by the UARS-HALOE instrument, which is now retired, but had been the main source of global stratospheric chlorine values for many years through its measurements of HCl near the stratopause. A higher value of total stratospheric chlorine could mean a potential delay in the full recovery of stratospheric ozone, which is expected to occur sometime around 2060 [*Prather et al.*, 1990, 1996; *WMO*, 1999].

Chapter 4 presents the first global inventory of stratospheric fluorine. This fluorine inventory was also based primarily on ACE-FTS measurements, utilizing a very similar approach to the chlorine inventory. Although fluorine does not actually participate in the destruction of stratospheric ozone, the fluorine inventory included many chlorine-containing species and confirms the approach used in the chlorine inventory, as well as emphasized the fact that there now exists a very good understanding of the partitioning of these species in the atmosphere.

The importance of this work can be highlighted by the interest that it has received from the lead authors of a report entitled *A Scientific Assessment of Ozone Depletion: 2006*. This report is a joint effort headed by the World Meteorological Organization (WMO), with the cooperation of the United Nations Environment Programme (UNEP), the European Commission (EC), the US National Aeronautics and Space Administration (NASA) and the US National Oceanic and

Atmospheric Administration (NOAA). This comprehensive report, commonly referred to as *The WMO Report* is jointly produced by these organizations every four years, and serves as the main scientific document for international policy decisions with regard to protection of the ozone layer. Lead authors of *Chapter 1: Long-Lived Compounds* and *Chapter 2: Halogenated Very Short-Lived Substances*, have expressed their interest in including a summary of the ACE-FTS chlorine and fluorine results in the report, which will be released in early 2007.

Chapter 5 was an analysis of water vapor in the stratosphere, beginning with the pattern of global circulation and the chemical balance between water and methane. The midlatitude stratospheric VMR of potential water, which is approximately $[H_2O]+2[CH_4]$, was found to be 7.14±0.23 ppmv and the VMR of water entering the stratosphere $[H_2O]_e$ in the tropics was found to be 3.65±0.29 ppmv, both in April 2004. The results were directly compared with measurements by ATMOS, confirming that the increases in two these quantities observed by other instruments over many years has ceased for the time being. Chapter 6 was a more detailed look at the dynamics of the stratosphere, with a particular emphasis on the Arctic vortex. Water is removed from the stratosphere in the polar vortices either by dehydration and sedimentation or by descent. Mean descent rates in the Arctic vortex in the late winter and spring of 2004 were investigated using tracer species measured by the ACE-FTS in conjunction with derived meteorological data products. The analysis showed that descent was relatively rapid in the upper stratospheric Arctic vortex, which was exceptionally strong during that winter.

The goal of Chapter 7 was to investigate transport of water in the tropics in order to understand the dryness of the stratosphere and investigate dehydration and entry mechanisms for water at the TTL. The work involved a first look at ACE-FTS measurements of HDO, which undergoes fractionation with respect to H_2O, making $[HDO]/[H_2O]$ ratios a useful tracer for understanding the recent history of an air parcel containing water vapor. A comparison of temperature, $[H_2O]$ and δD profiles revealed clear signs of seasonal variability in these three quantities. Understanding the variability in δD profiles was difficult, but can be interpreted as evidence supporting dehydration by gradual ascent if some tropical subsidence or convective ice lofting in the troposphere are included. Ice lofting, which is known to occur in the troposphere, can influence δD producing a deviation from Rayleigh distillation, without necessarily penetrating the TTL. The interpretation of the temperature, $[H_2O]$ and δD profiles could not rule out the possibility of convective dehydration, but it does not appear necessary to explain the ACE-FTS results, thus does not likely have a large role in the dryness of stratosphere.

The recovery of the stratospheric ozone layer depends on both the reduction of chlorine species and other ozone depleting substances in the atmosphere, as well as a reduction in the effects of stratospheric water. Water in the stratosphere enables the formation of PSCs in the polar vortices, and the total volume of PSCs has been identified as perhaps the single most important factor determining the amount of Arctic ozone loss in a particular year [*Rex et al.*, 2004]. Furthermore, water as well as nearly all molecular chlorine and fluorine species, behave as greenhouse gases affecting the radiative balance of Earth's atmosphere. Since increased levels of

atmospheric greenhouse gases warm the troposphere and cool the stratosphere, they can potentially increase the amount of ozone depletion by enhancing PSC formation, and also contribute to the serious problem of global climate change. Therefore, continually improving our understanding of chlorine, fluorine and water in the stratosphere is important in the context of both stratospheric ozone depletion and global climate change.

This work has investigated several important topics in atmospheric science, which have been reported or will soon appear in the scientific literature [*Nassar et al.*, 2005a, 2005b, 2006a, 2006b], and it is reasonable to believe that measurements acquired from the ACE mission, will continue to be used to further the scientific understanding in this field for many years to come.

References

Nassar, R., P.F. Bernath, C.D. Boone, G.L. Manney, S.D. McLeod, C.P. Rinsland, R.S. Skelton, K.A. Walker (2005a), ACE-FTS measurements across the edge of the winter 2004 Arctic vortex, *Geophys Res. Lett.*, 32, L15S05.

Nassar, R., P.F. Bernath, C.D. Boone, G.L. Manney, S.D. McLeod, C.P. Rinsland, R.S. Skelton, K.A. Walker (2005b), Stratospheric abundances of water and methane based on ACE-FTS measurements, *Geophys. Res. Lett.*, 32, L15S04.

Nassar, R., P.F. Bernath, C.D. Boone, C. Clerbaux, P.F. Coheur, G. Dufour, L. Froidevaux, E. Mahieu, J.C. McConnell, S.D. McLeod, D.P. Murtagh, C.P. Rinsland, K. Semeniuk, R. Skelton, K.A. Walker, R. Zander (2006a), A global inventory of stratospheric chlorine in 2004, *J. Geophys. Res.*, submitted.

Nassar, R., P.F. Bernath, C.D. Boone, S.D. McLeod, R. Skelton, K.A. Walker, C.P. Rinsland, P. Duchatelet (2006b), A global inventory of stratospheric fluorine in 2004 based on ACE-FTS measurements, *J. Geophys. Res.*, submitted.

Prather, M.J., R.T. Watson (1990), Stratospheric ozone depletion and future levels of atmospheric chlorine and bromine, *Nature*, 344, 729-734.

Prather, M., P. Midgely, F.S. Rowland, R. Stolarski (1996), The ozone layer: the road not taken, *Nature*, 381, 551-554.

Rex, M., R.J. Salawitch, P. von der Gathen, N.R.P. Harris, M.P. Chipperfield, B. Naujokat (2004), Arctic ozone loss and climate change, *Geophys. Res. Lett.*, 31, L04116.

World Meteorological Organization (1999), Scientific Assessment of Ozone Depletion: 1998. Global Ozone Research and Monitoring Project - Report No. 44, Geneva, Switzerland.

Appendix 1: Sample *A Priori* Output File and Program Code

A) Sample *a priori* output file
B) ACE_ap.F
C) recipes.F
D) climatology.c
E) drao.c
F) geoupgfz.c

Appendix 1

A) Sample *A Priori* Output File

ace.ss3109 CMC_high 29.5000
start_YYYYMMDD= 2004 3 10 DOY= 70

TANGENT_HEIGHT (km)	TEMPERATURE (deg_C)	PRESSURE (hPa)	DENSITY (molecules/cm^3)	AVERAGE_MM (g/mol)	DOY (day)	UTS (s)	LATITUDE (deg)	LONGITUDE (deg)
0.5	239.00	0.932E+03	0.283E+20	28.960	71	25.7	77.17477	-103.96925
1.5	243.50	0.809E+03	0.241E+20	28.960	71	25.4	77.17140	-103.95009
2.5	240.47	0.703E+03	0.212E+20	28.960	71	25.2	77.16802	-103.93377
3.5	234.57	0.608E+03	0.188E+20	28.960	71	24.9	77.16462	-103.92002
4.5	231.07	0.525E+03	0.165E+20	28.960	71	24.6	77.16120	-103.90854
5.5	226.76	0.452E+03	0.145E+20	28.960	71	24.3	77.15776	-103.89906
6.5	222.88	0.389E+03	0.126E+20	28.960	71	24.0	77.15431	-103.89132
7.5	222.52	0.333E+03	0.108E+20	28.960	71	23.8	77.15083	-103.88505
8.5	225.42	0.286E+03	0.919E+19	28.960	71	23.5	77.14734	-103.88003
9.5	227.01	0.246E+03	0.785E+19	28.960	71	23.2	77.14382	-103.87601
10.5	227.81	0.212E+03	0.674E+19	28.960	71	22.9	77.14028	-103.87279
11.5	227.99	0.182E+03	0.579E+19	28.960	71	22.6	77.13672	-103.87016
12.5	225.59	0.157E+03	0.504E+19	28.960	71	22.3	77.13313	-103.86794
13.5	223.60	0.135E+03	0.437E+19	28.960	71	22.0	77.12952	-103.86596
14.5	222.70	0.116E+03	0.376E+19	28.960	71	21.7	77.12589	-103.86408
15.5	221.80	0.992E+02	0.324E+19	28.960	71	21.4	77.12223	-103.86214
16.5	220.70	0.851E+02	0.279E+19	28.960	71	21.1	77.11855	-103.86005
17.5	219.71	0.729E+02	0.240E+19	28.960	71	20.8	77.11484	-103.85768
18.5	218.41	0.624E+02	0.207E+19	28.960	71	20.5	77.11110	-103.85496
19.5	217.12	0.533E+02	0.178E+19	28.960	71	20.2	77.10735	-103.85182
20.5	215.82	0.456E+02	0.153E+19	28.960	71	19.9	77.10357	-103.84819
21.5	214.43	0.389E+02	0.131E+19	28.960	71	19.6	77.09976	-103.84404
22.5	213.13	0.332E+02	0.113E+19	28.960	71	19.3	77.09593	-103.83934
23.5	212.31	0.283E+02	0.966E+18	28.960	71	18.9	77.09207	-103.83408
24.5	212.38	0.241E+02	0.822E+18	28.960	71	18.6	77.08820	-103.82824
25.5	212.65	0.205E+02	0.699E+18	28.960	71	18.3	77.08429	-103.82184
26.5	209.97	0.174E+02	0.601E+18	28.960	71	18.0	77.08037	-103.81490
27.5	206.58	0.148E+02	0.519E+18	28.960	71	17.6	77.07643	-103.80745
28.5	203.30	0.123E+02	0.437E+18	28.960	71	17.3	77.07246	-103.79951
29.5	200.02	0.107E+02	0.387E+18	28.960	71	17.0	77.06847	-103.79113
30.5	203.04	0.929E+01	0.331E+18	28.960	71	16.7	77.06447	-103.78237
31.5	206.05	0.808E+01	0.284E+18	28.960	71	16.3	77.06044	-103.77326
32.5	209.07	0.703E+01	0.243E+18	28.960	71	16.0	77.05640	-103.76387
33.5	212.08	0.611E+01	0.209E+18	28.960	71	15.7	77.05234	-103.75425
34.5	215.10	0.532E+01	0.179E+18	28.960	71	15.3	77.04826	-103.74447
35.5	218.11	0.463E+01	0.154E+18	28.960	71	15.0	77.04417	-103.73458
36.5	221.13	0.402E+01	0.132E+18	28.960	71	14.7	77.04007	-103.72465
37.5	224.14	0.350E+01	0.113E+18	28.960	71	14.3	77.03595	-103.71474
38.5	227.16	0.304E+01	0.971E+17	28.960	71	14.0	77.03182	-103.70490
39.5	230.17	0.265E+01	0.833E+17	28.960	71	13.6	77.02768	-103.69518
40.5	233.18	0.230E+01	0.716E+17	28.960	71	13.3	77.02353	-103.68563
41.5	236.20	0.200E+01	0.615E+17	28.960	71	13.0	77.01937	-103.67631
42.5	239.21	0.174E+01	0.528E+17	28.960	71	12.6	77.01520	-103.66725
43.5	242.23	0.152E+01	0.454E+17	28.960	71	12.3	77.01103	-103.65849
44.5	245.24	0.132E+01	0.390E+17	28.960	71	11.9	77.00684	-103.65006
45.5	247.17	0.115E+01	0.336E+17	28.960	71	11.6	77.00266	-103.64198
46.5	249.10	0.998E+00	0.290E+17	28.960	71	11.2	76.99847	-103.63428
47.5	251.03	0.868E+00	0.251E+17	28.960	71	10.9	76.99427	-103.62696
48.5	252.95	0.764E+00	0.219E+17	28.960	71	10.6	76.99008	-103.62003
49.5	253.38	0.669E+00	0.191E+17	28.960	71	10.2	76.98588	-103.61349
50.5	253.53	0.586E+00	0.167E+17	28.960	71	9.9	76.98168	-103.60734
51.5	253.42	0.513E+00	0.147E+17	28.960	71	9.5	76.97748	-103.60156
52.5	253.07	0.449E+00	0.128E+17	28.960	71	9.2	76.97328	-103.59613
53.5	252.47	0.393E+00	0.113E+17	28.960	71	8.8	76.96908	-103.59104
54.5	251.66	0.344E+00	0.990E+16	28.960	71	8.5	76.96489	-103.58626
55.5	250.63	0.301E+00	0.869E+16	28.960	71	8.1	76.96069	-103.58174
56.5	249.42	0.263E+00	0.763E+16	28.960	71	7.8	76.95650	-103.57747
57.5	248.03	0.230E+00	0.671E+16	28.960	71	7.4	76.95232	-103.57340
58.5	246.50	0.200E+00	0.589E+16	28.960	71	7.1	76.94814	-103.56948
59.5	244.84	0.175E+00	0.517E+16	28.960	71	6.7	76.94396	-103.56568
60.5	243.08	0.152E+00	0.454E+16	28.960	71	6.4	76.93979	-103.56195
61.5	241.23	0.133E+00	0.398E+16	28.960	71	6.0	76.93562	-103.55823
62.5	239.32	0.115E+00	0.349E+16	28.960	71	5.7	76.93146	-103.55449
63.5	237.36	0.100E+00	0.305E+16	28.957	71	5.3	76.92731	-103.55068
64.5	235.37	0.868E-01	0.267E+16	28.955	71	5.0	76.92316	-103.54675
65.5	233.37	0.752E-01	0.233E+16	28.952	71	4.6	76.91902	-103.54266
66.5	231.37	0.650E-01	0.203E+16	28.950	71	4.3	76.91489	-103.53836
67.5	229.39	0.562E-01	0.177E+16	28.947	71	3.9	76.91077	-103.53381
68.5	227.44	0.485E-01	0.154E+16	28.944	71	3.6	76.90665	-103.52898
69.5	225.53	0.418E-01	0.134E+16	28.942	71	3.3	76.90254	-103.52383
70.5	223.67	0.359E-01	0.116E+16	28.939	71	2.9	76.89844	-103.51833
71.5	221.88	0.309E-01	0.101E+16	28.936	71	2.6	76.89435	-103.51246

72.5	220.17	0.265E-01	0.873E+15	28.934	71	2.2	76.89027	-103.50620
73.5	218.72	0.228E-01	0.754E+15	28.933	71	1.9	76.88619	-103.49952
74.5	217.66	0.195E-01	0.649E+15	28.932	71	1.5	76.88213	-103.49241
75.5	216.92	0.167E-01	0.559E+15	28.930	71	1.2	76.87808	-103.48487
76.5	216.40	0.143E-01	0.480E+15	28.929	71	0.9	76.87404	-103.47690
77.5	216.04	0.123E-01	0.412E+15	28.928	71	0.5	76.87000	-103.46848
78.5	215.76	0.105E-01	0.353E+15	28.927	71	0.2	76.86598	-103.45964
79.5	215.66	0.894E-02	0.300E+15	28.925	70	86399.9	76.86197	-103.45037
80.5	215.13	0.774E-02	0.261E+15	28.959	70	86399.5	76.85797	-103.44070
81.5	214.67	0.663E-02	0.224E+15	28.958	70	86399.2	76.85399	-103.43063
82.5	214.02	0.567E-02	0.192E+15	28.957	70	86398.8	76.85001	-103.42020
83.5	213.10	0.485E-02	0.165E+15	28.956	70	86398.5	76.84605	-103.40941
84.5	211.87	0.415E-02	0.142E+15	28.955	70	86398.2	76.84211	-103.39830
85.5	210.27	0.354E-02	0.122E+15	28.953	70	86397.9	76.83817	-103.38689
86.5	208.24	0.302E-02	0.105E+15	28.950	70	86397.5	76.83425	-103.37520
87.5	205.76	0.257E-02	0.906E+14	28.946	70	86397.2	76.83035	-103.36327
88.5	202.80	0.219E-02	0.781E+14	28.940	70	86396.9	76.82646	-103.35111
89.5	199.33	0.185E-02	0.674E+14	28.933	70	86396.6	76.82259	-103.33876
90.5	195.38	0.157E-02	0.581E+14	28.923	70	86396.2	76.81874	-103.32622
91.5	191.09	0.132E-02	0.501E+14	28.911	70	86395.9	76.81490	-103.31353
92.5	186.78	0.111E-02	0.430E+14	28.896	70	86395.6	76.81108	-103.30068
93.5	182.67	0.927E-03	0.368E+14	28.878	70	86395.3	76.80728	-103.28770
94.5	178.98	0.773E-03	0.313E+14	28.856	70	86395.0	76.80350	-103.27457
95.5	175.89	0.642E-03	0.264E+14	28.832	70	86394.7	76.79975	-103.26131
96.5	173.55	0.532E-03	0.222E+14	28.804	70	86394.4	76.79601	-103.24790
97.5	172.11	0.440E-03	0.185E+14	28.773	70	86394.1	76.79230	-103.23432
98.5	171.73	0.363E-03	0.153E+14	28.739	70	86393.7	76.78860	-103.22054
99.5	172.60	0.300E-03	0.126E+14	28.702	70	86393.4	76.78494	-103.20653
100.5	174.96	0.249E-03	0.103E+14	28.662	70	86393.1	76.78130	-103.19224
101.5	178.91	0.207E-03	0.838E+13	28.619	70	86392.8	76.77768	-103.17762
102.5	184.42	0.173E-03	0.679E+13	28.574	70	86392.5	76.77409	-103.16260
103.5	191.47	0.145E-03	0.550E+13	28.526	70	86392.3	76.77053	-103.14711
104.5	200.07	0.123E-03	0.446E+13	28.477	70	86392.0	76.76700	-103.13105
105.5	210.21	0.105E-03	0.363E+13	28.426	70	86391.7	76.76350	-103.11434
106.5	221.89	0.906E-04	0.296E+13	28.374	70	86391.4	76.76002	-103.09685
107.5	235.00	0.787E-04	0.242E+13	28.322	70	86391.1	76.75658	-103.07848
108.5	249.34	0.689E-04	0.200E+13	28.269	70	86390.8	76.75317	-103.05910
109.5	264.53	0.608E-04	0.166E+13	28.217	70	86390.5	76.74980	-103.03856
110.5	279.94	0.540E-04	0.140E+13	28.165	70	86390.3	76.74646	-103.01672
111.5	295.09	0.484E-04	0.119E+13	28.113	70	86390.0	76.74315	-102.99343
112.5	309.79	0.435E-04	0.102E+13	28.063	70	86389.7	76.73988	-102.96852
113.5	323.89	0.393E-04	0.880E+12	28.013	70	86389.5	76.73665	-102.94181
114.5	337.31	0.357E-04	0.767E+12	27.964	70	86389.2	76.73345	-102.91314
115.5	349.98	0.326E-04	0.674E+12	27.916	70	86388.9	76.73030	-102.88233
116.5	361.94	0.298E-04	0.597E+12	27.869	70	86388.7	76.72718	-102.84918
117.5	373.25	0.274E-04	0.531E+12	27.822	70	86388.4	76.72410	-102.81352
118.5	384.07	0.252E-04	0.474E+12	27.776	70	86388.2	76.72106	-102.77516
119.5	394.62	0.232E-04	0.426E+12	27.731	70	86387.9	76.71807	-102.73391
120.5	405.19	0.214E-04	0.383E+12	27.686	70	86387.7	76.71511	-102.68959
121.5	416.13	0.199E-04	0.346E+12	27.642	70	86387.4	76.71220	-102.64202
122.5	427.90	0.184E-04	0.312E+12	27.598	70	86387.2	76.70933	-102.59104
123.5	441.43	0.172E-04	0.281E+12	27.555	70	86387.0	76.70651	-102.53648
124.5	455.39	0.160E-04	0.254E+12	27.513	70	86386.7	76.70373	-102.47818
125.5	469.09	0.149E-04	0.231E+12	27.471	70	86386.5	76.70100	-102.41600
126.5	482.52	0.140E-04	0.210E+12	27.430	70	86386.3	76.69831	-102.34982
127.5	495.68	0.131E-04	0.192E+12	27.390	70	86386.1	76.69567	-102.27952
128.5	508.59	0.123E-04	0.176E+12	27.350	70	86385.8	76.69308	-102.20500
129.5	521.25	0.116E-04	0.161E+12	27.310	70	86385.6	76.69053	-102.12619
130.5	533.67	0.110E-04	0.149E+12	27.271	70	86385.4	76.68803	-102.04303
131.5	545.84	0.103E-04	0.137E+12	27.233	70	86385.2	76.68558	-101.95549
132.5	557.78	0.978E-05	0.127E+12	27.195	70	86385.0	76.68318	-101.86356
133.5	569.48	0.926E-05	0.118E+12	27.157	70	86384.8	76.68083	-101.76725
134.5	580.96	0.877E-05	0.109E+12	27.120	70	86384.6	76.67853	-101.66660
135.5	592.21	0.833E-05	0.102E+12	27.084	70	86384.4	76.67628	-101.56168
136.5	603.24	0.791E-05	0.949E+11	27.047	70	86384.3	76.67408	-101.45259
137.5	614.06	0.752E-05	0.887E+11	27.011	70	86384.1	76.67193	-101.33946
138.5	624.67	0.716E-05	0.830E+11	26.975	70	86383.9	76.66983	-101.22245
139.5	635.08	0.682E-05	0.777E+11	26.939	70	86383.7	76.66779	-101.10173
140.5	645.28	0.650E-05	0.729E+11	26.903	70	86383.6	76.66579	-100.97754
141.5	655.29	0.620E-05	0.685E+11	26.868	70	86383.4	76.66385	-100.85013
142.5	665.10	0.592E-05	0.645E+11	26.833	70	86383.2	76.66197	-100.71976
143.5	674.72	0.566E-05	0.607E+11	26.797	70	86383.1	76.66014	-100.58677
144.5	684.16	0.541E-05	0.573E+11	26.762	70	86382.9	76.65836	-100.45148
145.5	693.41	0.518E-05	0.541E+11	26.728	70	86382.8	76.65663	-100.31427
146.5	702.48	0.496E-05	0.511E+11	26.693	70	86382.6	76.65497	-100.17553
147.5	711.38	0.475E-05	0.484E+11	26.658	70	86382.5	76.65335	-100.03570
148.5	720.11	0.455E-05	0.458E+11	26.624	70	86382.4	76.65180	-99.89523
149.5	728.67	0.437E-05	0.434E+11	26.589	70	86382.2	76.65030	-99.75457

B) ACE_ap.F

```
      PROGRAM MAIN

************************************************************************
*                                    Ray Nassar (last updated 2005-09-08)
*
* PURPOSE:  To create tangent height vs. temperature and tangent height
*     vs. pressure a priori profiles primarily for the ACE-FTS forward
*     model but with many other potential uses.
*
*     The profiles will combine an upper atmospheric model with
*     meteorological data for enhanced accuracy in the troposphere
*     and lower stratosphere.
*
*-----------------------------------------------------------------------
* MAIN INPUTS: occultation, daily and average solar flux,
*     3-hourly aps, meteorological temperature and pressure
*
* MAIN OUTPUTS: altitude, temperature, pressure, density,
*     average molecular mass, tangent point dates, times, latitudes
*     and longitudes, retval error code.
*
* (The above is simply instructive and not meant to be a complete I/O
* list since numerous subroutines make up this a priori "program")
*
*-----------------------------------------------------------------------
* METHOD:
*
* "ORBITPTS" reads values for latitude, longitude, date,
* universal time, and tangent point altitude from the ACE database.
* for a given occultation.
*
* "DOFIT" fits "t vs. alt", "lat vs. t" and "long vs. t" to cubic
* functions using a subroutine from the book "Numerical Recipes in
* Fortran" by W.H. Press et al. These are then put on a 1 km grid
* with 150 grid points at 0.5,1.5,....149.5 km in altitude.
* Data points that are flagged as bad or do not meet a minimum
* requirement for accuracy will be rejected in the subroutine
* REMOVE_COUNT based on a threshold set
* with the parameter acctest in the subroutine TIMETESTER.
*
* "APF107" reads raw values of ap and Solar Flux at 10.7 cm from the
* Solar and Geomagnetic portion of the ACE Database.
* It calculates an array of the necessary ap values.  This array is
* described in the subroutine.
*
* "DATETODOY" makes conversions between standard dates and DOY
*
* "DOMSIS" calls the model NRL-MSISE-2000 (Official Beta Release v2.0)
* to calculate number densities, temperature and pressure.
*
* "IODBASE" reads the temperature and pressure versus altitude input
* based on CMC from the database.  These are on a 1-km altitude grid
* ending around 30 km depending on the altitude equivalent to 10 hPa.
*
* "SPLICE" determines the position of the stratopause and combines the
* MSIS temperature and log pressure profiles with meteorological data for
* the lower atmosphere from the Canadian Meteorological Centre (CMC)
```

```
* of the Meteorological Service of Canada (MSC).
* Smoothing is applied to the combined temperature profiles, however,
* due to the very near linear relationship between altitude and log
* pressure, smoothing is not used.  Density is calculated from P and T
* using the ideal gas law.
*
* "GEOMETRIC" changes the geopotential heights given by the CMC
* to geometric heights.  It uses a cubic spline subroutine and the
* splint subroutine (but called splineint here) from "Numerical Recipes".
* These are used to represent the curves, interpolate and replot on the
* 0.5...149.5 km grid.
*
* Finally, the data is written to database/file and the
* temperature profile can be plotted or used as an a priori profile
* for the ACE-FTS forward model, possibly the MAESTRO forward model
* or a variety of other uses.
*
*-----------------------------------------------------------------------
* FURTHER COMMENTS:
*
* This file must be complied with:
* MSIS2000.F, recipes.F and -lace (lace refers to the ACE library).
*
* Call as "ACE_ap ace.ss1234"
*      where ace.ss1234 means ACE sunset-1234
*
* The input CMC data, output data filename and the splice range are
* derived from the occultation.
*
* The value for "acctest" may be changed in the subroutine "REMOVE_COUNT"
*
* Note: many WRITE statements have been commented out but retained
* because they are useful to aid with troubleshooting.
*
*-----------------------------------------------------------------------
* Current RETVAL Error Codes:
*
* Retval(1) Occultation format
*            = -1 -> occultation format incorrect
* Retval(2) Date
*            = -1 -> invalid date
* Retval(3) Solar Flux
*            = 0 -> Full 81-day F107 average (only possible if post-processing)
*            = 1 -> Realtime processing (incomplete future F107 data for 81-day
*                   average)
*            = 2 -> Have F107 (missing some, but enough for ave)
*            = 3 -> Missing F107 (but enough for average)
*            = 4 -> Have F107 (but not enough for average, used default)
*            = 5 -> Missing F107 (not enough for average, used default)
* Retval(4) Ap
*            = 0 -> Complete ap data taken from archives
*            = 1 -> ap data for one or more days from email not archive
*                          (necessary for near realtime processing)
*            = 5 -> no ap data available for one or more of the desired days,
*                   used default
* Retval(5) MSC profile version
*            = 0 -> appropriate CMC profile used
*            = 1 -> analysis 1 (6-12 hr) used instead of 2 (12-18 hr)
*            = 2 -> forecast profile used instead of anlaysis2
*            = 3 ->
*            = 4 -> global profile used rather than regional
```

```
*            = -1-> No CMC profile available, MSIS used for full range
*                        or zeroes written out
* Retval(6) MSC profile properties
*            = 0 -> Meteorological profile extends above "cold-point"
*            = 1 -> Meteorological data does not reach "cold-point"
* Retval(7) Fitting probelms (?)
*            =
* Retval(10)= 1 -> Erroneously used current day F107 rather than previous day
*-----------------------------------------------------------------------

      integer tp, gp, bp, nspectra, s, RETVAL(10), loop
      parameter (tp = 150) !Maximum number of tangent points
      parameter (gp = 150) !Number of 1 km grid points, on half integers

      integer yrs(tp), mons(tp), days(tp), hrs(tp), DOY(tp), flags(tp)
      integer leftover(tp), IYD(gp)

      real*4 x, SW(25), F107(gp), F107A(gp), AP(7,gp), CMChifloat
      real*8 zpdgmts(tp), tplats(tp), tplons(tp), tanhts(tp)
      real*8 UTS(gp), XSTL(gp), ALT(gp), XLAT(gp), XLONG(gp)
      real*8 UTSR, XLATR, XLONGR
      real*8 D(9,gp), T(2,gp), bottom
      real*8 TND(gp), TMSIS(gp), PRESSURE(gp), PMSIS(gp), AVEMM(gp)
      real*4 Aap(gp), Tap(gp), Pap(gp), Dap(gp)

      character datetime(tp)*30
      character occultation*16
      character logfile*24
      character time*10

      integer lyear, lmonth, lday, lhour, lminute, lsecond, lDOY

* SW are switches in MSIS that may be turned on or off.
* nspectra is the number of spectra in the database for the occultation
* pyear, pmonth etc are needed for past days in AP averages
* Note: pDOY(1) is the desired date, pDOY(2) is the previous day, etc.
* zpdgmts is the UT for zero path difference (the start of a scan) in seconds
* tplats and tplons are the tangent point lat/lon
* 'bottom' is the integer value in km above the lowest usable ATMOS data
* for a given occultation, it is not necessarily the same as ALLMET used
* later, RETVAL is an error code explained later
* TND is the Total Number Density and PRESSURE is pressure
* See comments in MSIS for an explanation of some other parameters

      x = GETARG(1, occultation)

      CALL GMDATETIME(lyear,lmon,lday,lhour,lmin,lsec,lDOY,time)

      write (logfile,'(A)') "a_priori_logfile"
      open (75, file = logfile, access = 'APPEND')
      write (75,*) occultation," start ",lyear,lmon,lday,' ',time

      if (occultation (1:3).eq.'ace') then
            CALL orbitpts(tp,gp,bp,occultation,yrs,mons,days,hrs,
     & flags,zpdgmts,tanhts,tplats,tplons,datetime,nspectra,bottom)
      else
            RETVAL(1) = -1
            write (*,*) "Occultation format not recognized"
      endif

      do i = 1,tp,1
```

```
              if (yrs(i).ge.00.and.yrs(i).le.99) yrs(i) = 2000 + yrs(i)
       enddo

       CALL DATETODOY (tp,yrs,mons,days,DOY,leftover,RETVAL(2))
       if (RETVAL(2).lt.0) goto 900
       if (DOY(1).le.DOY(tp)) s = 1
       if (DOY(1).gt.DOY(tp)) s = tp

* Subroutine DATETODOY is called to convert the standard date to DOY format
* The logic above will skip computation if a date error has been detected.

*---------------------------------------------------------------------

       CALL APF107 (gp,bp,yrs(s),mons(s),days(s),hrs(s),leftover(s),
     & DOY(s),F107,F107A,ap,RETVAL(3),RETVAL(4))
*
* The subroutine APF107 reads solar (F10.7) and geomagnetic data (ap)
* from a database.  Sample values can be used when testing the software.
*
*      Sample values for 1994-11-11 22:00:44:
*      do j=1,gp,1
*             F107(j) = 79.
*             F107A(j) = 85.037
*             ap(1,j) = 8.
*             ap(2,j) = 7.
*             ap(3,j) = 5.
*             ap(4,j) = 4.
*             ap(5,j) = 6.
*             ap(6,j) = 10.
*             ap(7,j) = 25.875
*      enddo
*---------------------------------------------------------------------

       CALL DOFIT (tp,gp,bp,nspectra,occultation,flags,DOY(s),IYD,
     & zpdgmts,tanhts,tplats,tplons,alt,uts,xlat,xlong,xstl,
     &       utsr, xlatr, xlongr)

       CALL DOMSIS (bp,gp,IYD,UTS,ALT,XLAT,XLONG,XSTL,
     & F107,F107A,AP,D,T,TND,PRESSURE,AVEMM)

       do I=1,gp,1
              TMSIS(I) = T(2,I)
              PMSIS(I) = PRESSURE(I)
       enddo

       CALL IODBASE (gp, occultation, CMChifloat, TMSIS, PMSIS,
     & XLAT, XLONG, UTS, XLATR, XLONGR, UTSR, datetime,
     &       Aap, Tap, Pap, Dap, AVEMM, RETVAL)

* Subroutine IO reads the CMC input file, calls SPLICE and writes the output
* Subroutine SPLICE (called by IO) combines the MSIS upper profile
* and the CMC lower profiles

       CALL writeout (occultation,yrs(s),mons(s),days(s),IYD,UTS,xlat,
     & xlong,Aap,XSTL,gp,Tap,Pap,Dap,CMChifloat,AVEMM,RETVAL,bp)

* Writeout can be used to write out certain parameters to monitor
* and can be modified to write to a file.  The profile itself however,
* is already written out in the subroutine "SPLICE"

       CALL GMDATETIME(lyear,lmon,lday,lhour,lmin,lsec,lDOY,time)
```

```
       write(75,*)occultation," end   ",lyear,lmon,lday,' ',time,retval
       close(75)

       STOP
 900   END


*---- SUBROUTINES FOLLOW -----------------------------------------------*

*****************************************************************************

       SUBROUTINE orbitpts (tp,gp,bp,occultation,yr,mon,day,hr,
     & flag,zpdgmt,tpalt,tplat,tplon,datetime,nspectra,bottom)

*****************************************************************************

       integer tp, gp, bp, nspectra, flag(tp)
       integer yr(tp), mon(tp), day(tp), hr(tp), min(tp)
       real*4 sec(tp), tpalt4(tp), tplat4(tp), tplon4(tp)
       real*8 zpdgmt(tp), tpalt(tp), tplat(tp), tplon(tp), bottom
       character datetime(tp)*30, occultation*16

       CALL check_pgenv
       CALL check_dbgenv
       CALL ORBITCALL (occultation,tp,tpalt4,tplat4,tplon4,datetime)

       do i=1, tp, 1
              read(datetime(i),'(1X,I4,1X,I2,1X,I2,1X,I2,1X,I2,1X,E5)')
     & yr(i),mon(i),day(i),hr(i),min(i),sec(i)
              zpdgmt(i) = 3600*hr(i)+60*min(i)+sec(i)
              nspectra = i
              tpalt(i) = DBLE(tpalt4(i))
              tplat(i) = DBLE(tplat4(i))
              tplon(i) = DBLE(tplon4(i))
*      write(*,*) i, yr(i),mon(i),day(i),hr(i),min(i),sec(i), zpdgmt(i)
*      write (*,*) i, zpdgmt(i), tpalt4(i), tplat4(i), tplon4(i)
       enddo

* The loop above reads the datetime into integers or reals
* It also has a counter called nspectra
* The loop below finds the lowest useable ATMOS tangent height and
* designates the tangent grid point immediately above it as 'bottom'
* It begins with an initial value of 150 that is immediately rewritten.

       bottom = dfloat(gp)
       do i=1, 150, 1
              if (flag(i).eq.0) then
                     if (tpalt(i).lt.bottom) then
                            bottom = dint(tpalt(i)-0.5) + 1.5
                            !dint() truncates a real to an integer
                     endif
              endif
       enddo
       bp = dint(bottom)

       return
       END

*****************************************************************************
```

```
      SUBROUTINE orbitcall(occultation,tp,alt4,lat4,lon4,date)

*****************************************************************

      integer npts, getorbit_occvec
      external getorbit_occvec
      character occultation*12, dir*24, infile*32, outfile*92
      character*30 date(tp)
      real*4 alt4(tp), lat4(tp), lon4(tp)

      call check_pgenv
      call check_dbgenv

      npts = getorbit_occvec(occultation,alt4,date,lat4,lon4,tp)

      dir = 'ACEsplice/'

*     write (outfile,'(A,A,A)') dir(1:lnblnk(dir)),
*    & occultation(1:lnblnk(occultation)),'.STK'
*     open (75, file = outfile)
*     do i=1, npts
*        write (75,'(3F12.6,2x,30A)') alt4(i),lat4(i),lon4(i),date(i)
*     enddo
*     close (75)
*     write (*,*) npts, "  ", occultation

      return
      END

*****************************************************************

      SUBROUTINE DATETODOY (tp,year,month,day,DOY,leftover,retval2)

*****************************************************************
* This subroutine will:
*
* convert a standard date to day-of-year (DOY) format required by MSIS
* DOY ranges from 1-365 or 1-366 for leap years
*
* Note that the built in Fortran function GMDATETIME uses the range
* 0-365. To distinguish between the two variables, the later is renamed
* DOY0.
*
* It also determines if the date is valid and if we have solar data
* available  for the given date.
*
*----------------------------------------------------------------

      integer nday(12), nleap(12), daysum(12), leapsum(12)
      integer gp, tp, RETVAL2
      integer year(tp), month(tp), day(tp), DOY(tp), Leftover(tp)

* lefttover is used for determining which years are leap year

* RETVAL2 Error Codes
*  0 -> everything is OK
*  1 -> no solar data is available from 'databace' or invalid date

      data nday   /31,28,31,30, 31, 30, 31, 31, 30, 31, 30, 31/
      data daysum / 0,31,59,90,120,151,181,212,243,273,304,334/
      data nleap  /31,29,31,30, 31, 30, 31, 31, 30, 31, 30, 31/
```

Appendix 1

```
      data leapsum/ 0,31,60,91,121,152,182,213,244,274,305,335/

      do i = 1, tp, 1

      if (year(i).lt.1947.or.year(i).ge.2100)then
            RETVAL2 = -1
            write (*,*) 'DATE   ', year(i), month(i), day(i)
            write (*,*)  'Year not in our data range'
      elseif (month(i).lt.1.or.month(i).gt.12) then
            RETVAL2 = -1
            write (*,*) 'DATE   ', year(i), month(i), day(i)
            write (*,*)  'Invalid month'
      else
      leftover(i) = mod(year(i),4)
         if(leftover(i).ne.0)then
            continue
            if (day(i).le.0.or.day(i).gt.nday(month(i))) then
                  RETVAL2 = -1
                  write (*,*) 'DATE   ', year(i), month(i), day(i)
                  write (*,*)  'Invalid month or day'
            else
                  DOY(i) = daysum(month(i))+ day(i)
            endif
         else
         continue
            if (day(i).le.0.or.day(i).gt.nleap(month(i))) then
                  RETVAL2 = -1
                  write (*,*) 'DATE   ', year(i), month(i), day(i)
                  write (*,*)  'Invalid month or day'
            else
                  DOY(i) = leapsum(month(i)) + day(i)
            endif
         endif
      endif

      enddo

      return
      END

*****************************************************************************

      SUBROUTINE DOYTODATE (DOY, year, month, day)

*****************************************************************************

      integer year, month, day, DOY, leftover
      integer daysum(13), ldaysum(13)

      data daysum / 0,31,59,90,120,151,181,212,243,273,304,334,365/
      data ldaysum/ 0,31,60,91,121,152,182,213,244,274,305,335,366/

      leftover = mod(year,4)

      if(leftover.ne.0)then
            do i=1,12,1
                  if (DOY.gt.daysum(i).and.DOY.le.daysum(i+1)) then
                        month = i
                        day = DOY - daysum(i)
                  endif
            enddo
```

```
      elseif(leftover.eq.0)then
            do i=1,12,1
                  if (DOY.gt.ldaysum(i).and.DOY.le.ldaysum(i+1)) then
                        month = i
                        day = DOY - ldaysum(i)
                  endif
            enddo
      endif

*     write(*,*)"DOY=",DOY," year =",year," month =",month," day =",day

      return
      END

*****************************************************************************

      SUBROUTINE GMDATETIME (year,mon,day,hr,min,sec,DOY,timeout)

*****************************************************************************

      integer stime, tarray(9), time
      integer year, mon, day, hr, min, sec, DOY0, DOY
      character hour*2, minute*2, second*2, timeout*10

      stime = time()                    !Built in Fortran function
      call gmtime(stime, tarray)        !Built in Fortran subroutine

*     (1) seconds (0-61)  >59 bug due to ctime(3C)function
*     (2) minutes (0-59)
*     (3) hours (0-23)
*     (4) day of month (1-31)
*     (5) months since January (0-11)
*     (6) Year minus 1900
*     (7) Day of week (Sunday = 0)
*     (8) Day of year (0-365)
*     (9) Daylight savings time (1 if DST in effect)

      year = 1900 + tarray(6)
      mon = tarray(5) + 1
      day = tarray(4)
      hr = tarray(3)
      min = tarray(2)
      sec = tarray(1)
      DOY0 = tarray(8)
      DOY = tarray(8) + 1

      if (hr.lt.10) then
            write (hour,'(A,I1)'),'0', hr
      else
            write (hour,'(I2)'), hr
      endif

      if (min.lt.10) then
            write (minute,'(A,I1)'),'0',min
      else
            write (minute,'(I2)'), min
      endif

      if (sec.lt.10) then
            write (second,'(A,I1)'),'0',sec
```

```
       else
              write (second,'(I2)'), sec
       endif

       write (timeout, '(A2,A1,A2,A1,A2)'),hour,':',minute,':',second

      return
       end

*****************************************************************************

       SUBROUTINE APF107(gp,bp,year,month,day,hr,leftover,curDOY,
     & F107,F107A,ap,RETVAL3,RETVAL4)

*****************************************************************************

       integer gp, bp
       integer year, month, day, hr, curDOY, div, leftover, k
       integer pyear(5), pmonth(5), pday(5), pDOY(5), ap32(32), ap8(8)
       integer gyear, gmonth, gday, gDOY, RETVAL3, RETVAL4, RETVALap
       real*4 F107(gp), F107A(gp), ap(7,gp)
       real*4 gF107, gF107A

       pyear(1) = year
       pDOY(1) = curDOY
       RETVAL4 = 0

*-----------------------------------------------------------------------
       do i=1,4,1
              gDOY   = pDOY(i)
              gyear = pyear(i)

              call apcaller (gyear, gDOY, ap8, RETVALap)

              if (RETVALap.ge.RETVAL4) then
                     RETVAL4 = RETVALap
              else
                     continue
              endif

*             write (*,*) "RETVALap RETVAL4",RETVALap, RETVAL4

              do j=1,8,1
                     k = (8*(4-i)+1)+(j-1)
                     ap32(k) = ap8(j)
*                    write (*,*) pDOY(i), k, "  ap = ", ap32(k)
              enddo

              if (pDOY(i).ne.1)then
                     pDOY(i+1) = pDOY(i)-1
                     pyear(i+1) = pyear(i)
              elseif (pDOY(i).eq.1.and.leftover.ne.1)then
                     pDOY(i+1) = 365
                     pyear(i+1) = pyear(i)-1
              elseif (pDOY(i).eq.1.and.leftover.eq.1)then
                     pDOY(i+1) = 366
                     pyear(i+1) = pyear(i)-1
              endif
       enddo
*-----------------------------------------------------------------------
```

```
      div = (hr-(mod(hr,3)))/3
*     write (*,*) "hour and div", hr, div

* "div" determines which of the 8 3-hour blocks of the day to use

      do j=bp,gp,1
            AP(1,j)=dfloat((ap32(25)+ap32(26)+ap32(27)+ap32(28)
     &   +ap32(29)+ap32(30)+ap32(31)+ap32(32)))/8.0
            AP(2,j)=ap32(25+div)
            AP(3,j)=ap32(24+div)
            AP(4,j)=ap32(23+div)
            AP(5,j)=ap32(22+div)
            AP(6,j)=(ap32(21+div)+ap32(20+div)+ap32(19+div)+ap32(18+div)
     &   +ap32(17+div)+ap32(16+div)+ap32(15+div)+ap32(14+div))/8.0
            AP(7,j)=(ap32(13+div)+ap32(12+div)+ap32(11+div)+ap32(10+div)
     &   +ap32(9+div)+ap32(8+div)+ap32(7+div)+ap32(6+div))/8.0
      enddo

* MSIS comments state that:
* "F107, F107A, and AP effects are neither large nor well established
* below 80 km and should be set to 150, 150 and 4 respectively."
* However, when SW(9) is turned on, to use the ap array, setting all ap
* values in the array at 4 tends to produce a very minor discontinuity
* at 80 km for some occulutations, therefore actual ap values are used
* for the whole MSIS calculation.

* The ap loop uses ap values from the database to calculate
* the ap array with the following values:
* (1,j) DAILY Ap
* (2,j) 3 HR ap INDEX FOR CURRENT TIME
* (3,j) 3 HR ap INDEX FOR 3 HRS BEFORE CURRENT TIME
* (4,j) 3 HR ap INDEX FOR 6 HRS BEFORE CURRENT TIME
* (5,j) 3 HR ap INDEX FOR 9 HRS BEFORE CURRENT TIME
* (6,j) AVERAGE OF eight 3 HR aps FROM 12 - 33 HRS PRIOR TO CURRENT TIME
* (7,j) AVERAGE OF eight 3 HR aps FROM 36 - 57 HRS PRIOR TO CURRENT TIME

*     Sample values for 1994-11-11 22:00:44
*     do j=bp,gp,1
*           F107(j) = 79.
*           F107A(j) = 85.037
*           ap(1,j) = 8.
*           ap(2,j) = 7.
*           ap(3,j) = 5.
*           ap(4,j) = 4.
*           ap(5,j) = 6.
*           ap(6,j) = 10.
*           ap(7,j) = 25.875
*     enddo
*     write (*,*) "F107 ", F107(99)
*     write (*,*) "F107A ", F107A(99)
*     write (*,*) "ap1 ", ap(1,99)
*     write (*,*) "ap2 ", ap(2,99)
*     write (*,*) "ap3 ", ap(3,99)
*     write (*,*) "ap4 ", ap(4,99)
*     write (*,*) "ap5 ", ap(5,99)
*     write (*,*) "ap6 ", ap(6,99)
*     write (*,*) "ap7 ", ap(7,99)

*-----------------------------------------------------------------------

      call F107CALLER(year,curDOY,pyear(2),pDOY(2),gF107,gF107A,RETVAL3)
```

```
       do j=bp,80,1
              F107(j) = 150.
              F107A(j) = 150.
       enddo
       do j=81,gp,1
              F107(j) = gF107
              F107A(j) = gF107A
       enddo

*      write (*,*) "pDOY =",pDOY(2)," F107 =",F107(81)

* The fixed F107(A) values are chosen because MSIS comments state that:
* "F107, F107A, and AP effects are neither large nor well established
* below 80 km and should be set to 150, 150 and 4 respectively."
* Please note that F107A is an 81-day average centred on the current day.
* i.e. 40 'past' days and 40 'future' days are average.
* If processing data where there is available solar data for
* fewer than 40 future days then "delta2" is determined to include as
* many days as possible and Retval(3) = 1.

       return
       end

*****************************************************************************

      SUBROUTINE APCALLER (year,DOY,ap,RETVAL)

*****************************************************************************

       integer year, month, day, DOY, AP(8), RETVAL
       real*4 apavg
      INTEGER getap
      EXTERNAL getap

       CALL DOYTODATE (DOY, year, month, day)
       CALL check_pgenv
      CALL check_dbgenv

      RETVAL = getap (year, month, day, ap)

       apavg=(float(ap(1)+ap(2)+ap(3)+ap(4)+ap(5)+ap(6)+ap(7)+ap(8)))/8

       if (apavg.le.0) then             !Default values
              RETVAL = 5
              ap(1)= 15
              ap(2)= 15
              ap(3)= 14
              ap(4)= 13
              ap(5)= 14
              ap(6)= 14
              ap(7)= 15
              ap(8)= 15
              write(*,*)"ap data missing from dbase, DEFAULT values used"
*      These are based on rounded average values from 1932-01 to 2002-01.
       else
              continue
       endif

*      write (*,*) "*************", year, month, day
*      write (*,*) 'ap=',ap(1),ap(2),ap(3),ap(4),ap(5),ap(6),ap(7),ap(8)
```

```
       return
       END

*****************************************************************************

      SUBROUTINE F107CALLER (year,DOY,pyear,pDOY,pflux,Fluxave,RETVAL3)

*****************************************************************************
*
*      The MSIS parameter F107A is an 81-day average of F107 values
*      This average is taken centred on the profile's date
*      with 40 days before and 40 days after.
*      For the near-real time running of MSIS, F107 data 40 days into
*      the future will not be available, so the value of DELTA2 will be
*      set to 0.
*
*****************************************************************************
#DEFINE MAXFLUXES 81

      integer year,  month,  day,  DOY
       integer pyear, pmonth, pday, pDOY
       integer retval3, DELTA1, DELTA2
       integer VALs, getfluxes, Nfluxes, Rfluxes
      integer cyr, cmon, cday, chr, cmin, csec, cDOY !(c for current)

       real*4 FLUX(MAXFLUXES), Fluxsum(MAXFLUXES+1), pflux, Fluxave, zzzz
       character DATES*24(MAXFLUXES), time*10
       external getfluxes

       CALL GMDATETIME (cyr,cmon,cday,chr,cmin,csec,cDOY,time)

*      Note: GMDATETIME uses a DOY from 0-365 rather than 1-366 so
*      the variable DOY0 is introduced.
*      Therefore, DOY-1 (for MSIS) = DOY0 (GMDATETIME).

       Nfluxes = 0
       Rfluxes = 0
       DELTA1 = -40
       DELTA2 = 0                                        !For real time processing!
       DELTA2 = (cyr-year)*365 + (cDOY-DOY)!For accuracy beyond a priori use

*      The above equation does not fuly account for leap years but is
*      sufficient for this purpose since DELTA2 cannot be greater than 40.

*      write (*,*) "cYear ",cyr," cDOY ",cdoy," year ",year," DOY ",doy
*      write (*,*) 'pre-DELTA2 =',  DELTA2

       if (DELTA2.gt.40) DELTA2 = +40
       if (DELTA2.le.0)    DELTA2 = 0
*      if (DELTA2.lt.40) RETVAL3 = 1 !Realtime, missing future F107 data

      CALL check_pgenv
      CALL check_dbgenv
       CALL DOYTODATE(DOY,year,month,day)
       CALL DOYTODATE(pDOY,pyear,pmonth,pday)

*      write (*,*) "date ", year, month, day, DOY
*      write (*,*) "pdate ", pyear, pmonth, pday, pDOY

       VALs = getfluxes(YEAR, MONTH, DAY, pyear, pmonth, pday,
```

```
     & pflux, DELTA1, DELTA2, FLUX, NFLUXES, DATES)

       FLUXSUM(0) = 0
       rfluxes = 0

       do i=1, Nfluxes
              if (flux(i).gt.1..and.flux(i).lt.500.) then
                     rfluxes = rfluxes + 1
                     Fluxsum(rfluxes)=Fluxsum(rfluxes-1)+FLUX(i)
              endif
       enddo

       if(pflux.gt.0.and.rfluxes.eq.81.and.rfluxes.eq.Nfluxes) then
              RETVAL3 = 0 !Perfect
              Fluxave = FLUXSUM(Rfluxes)/Rfluxes
       elseif
     &(pflux.gt.0.and.rfluxes.ge.1.and.rfluxes.gt.(nfluxes-9))then
              RETVAL3 = 2 !Have pflux (missing some but enough for ave)
              Fluxave = FLUXSUM(Rfluxes)/Rfluxes
       elseif(pflux.gt.0.and.rfluxes.ge.1.and.rfluxes.eq.Nfluxes.
     & and.delta2.lt.40) then
              RETVAL3 = 1 !For real-time processing
              Fluxave = FLUXSUM(Rfluxes)/Rfluxes
       elseif
     &(pflux.le.0.and.rfluxes.ge.1.and.rfluxes.gt.(nfluxes-9))then
              RETVAL3 = 3  !Missing pflux (but enough for average)
              call defaultF107(year, month, pflux, zzzz)
              Fluxave = FLUXSUM(Rfluxes)/Rfluxes
       elseif
     &(pflux.gt.0.and.rfluxes.ge.1.and.rfluxes.le.(nfluxes-9))then
              RETVAL3 = 4 !Have pflux (but not enough for average)
              call defaultF107(year, month, zzzz, Fluxave)
       else
              RETVAL3 = 5 !Missing pflux (not enough for average)
              call defaultF107(year, month, pflux, Fluxave)
       endif

* The requirement rfluxes.gt.(nfluxes-9) is somewhat arbitrary

       write (*,*) "DATE", year, month, day
*      write (*,*) "N fluxes = ", Nfluxes
*      write (*,*) "R fluxes = ", Rfluxes
*      write (*,*) "DELTA1 =", delta1
*      write (*,*) "DELTA2 =", delta2
*      write (*,*) "F107 Average = ", Fluxave
*      write (*,*) "Current Flux = ", pflux
*      write (*,*) "RETVAL3 =", retval3

*      do i = 1,81,3
*             write (*,*) i, flux(i), i+1, flux(i+1), i+2,  flux(i+2)
*      enddo

      return
       END

**********************************************************************

       SUBROUTINE defaultF107 (year, month, F107, F107ave)

**********************************************************************
```

```
      integer year, month, n
      real*4 F107dat(133), F107ave

      n = (year-2002)*12 + (month - 9)  !Based on the F107 data below

   10 if (n.gt.133) then
            n = n - 133
            goto 10
      endif

      data F107dat /176.0,188.1,187.6,209.9,207.0,189.9,
     &              193.1,203.4,178.7,175.6,167.0,170.4,
     &              176.7,173.1,186.7,172.4,164.0,164.8,
     &              173.9,166.7,139.3,129.4,137.1,129.4,
     &              133.6,135.9,134.1,136.0,142.7,128.8,
     &              116.5,115.4,108.4,108.0,113.4,109.0,
     &              108.8,109.7,103.3,100.9, 93.6, 98.7,
     &              105.7, 98.3,101.7,102.3, 91.9, 88.1,
     &               82.8, 79.9, 82.7, 81.5, 79.9, 78.8,
     &               77.4, 75.8, 76.0, 78.4, 79.4, 81.3,
     &               79.2, 74.4, 80.5, 83.7, 81.1, 77.5,
     &               78.3, 75.3, 74.7, 72.7, 70.4, 72.1,
     &               77.7, 77.8, 82.9, 80.5, 80.1, 78.6,
     &               83.5, 82.9, 85.9, 86.7, 83.6, 92.3,
     &               93.2, 88.1, 96.6,101.0, 97.5,101.1,
     &               96.6,100.6,108.0,113.2,120.5,128.4,
     &              116.8,127.1,142.0,133.5,140.1,156.0,
     &              166.2,170.6,165.7,170.0,180.2,157.6,
     &              162.6,162.0,174.8,174.8,166.8,169.4,
     &              180.5,190.0,173.1,170.0,149.2,169.8,
     &              191.2,173.9,184.3,194.7,204.1,194.1,
     &              194.5,193.1,175.2,181.6,191.7,183.7, 183.6/

      F107 = F107dat(n)
      F107ave = (F107dat(n-1)+F107dat(n)+F107dat(n+1))/3

* Roughly 90 day average centered on the current month
* instead of 81 day average centred on the current day.

* The above default values were calculated using the monthly average
* F107 values from the period of 1958-06 to 2002-09 covering 4
* 11.09 year sunspot cycles.
* Monthly average F107 values for the period of 2002-10 to 2013-11
* were determined using the values from 133, 266, 399, 532 months prior.
* (i.e. averaging corresponding months over past 4 periods of the 11.1
* year sunspot cycle.) For subsequent sunspot cycles the process repeats.

      write (*,*) "***** No F10.7 data in database, DEFAULT F10.7 used"
*     write (*,*) "F107(i+-)",F107dat(n-1),F107dat(n),F107dat(n+1)
*     write (*,*) "F107ave", F107ave

      return
      END

*****************************************************************************

      SUBROUTINE DOFIT(tp,gp,bp,nspectra,occultation,flags,DOYs,IYD,
     &       times,tanhts,tplats,tplons,alt,uts,xlat,xlong,xstl,
     & utsr,xlatr,xlongr)

*****************************************************************************
```

Appendix 1

```
* This subroutine receives the input read from the ATMOS runlog
* and sends the proper data to "LFIT" a subroutine from "Numerical
* Recipes in Fortran" by W.H. Press et al.
* The parameter acctest must be set to determine the largest permissible
* time difference (in seconds) for points on a tangent height vs. time
* plot.
*---------------------------------------------------------------------

      integer tp, gp, bp, nspectra, nct, ncl, count1, count2, nloop

      parameter (nct = 4) !number of coefficients for time fit
      parameter (ncl = 8) !number of coefficients for lat/long fits

      integer iat(nct), ial(ncl), flags(tp), flag(tp), DOYs, IYD(gp)
      real*8 tco(nct), ltco(ncl), lnco(ncl), shift
      real*8 zzt(nct,nct), zzl(ncl,ncl), zzz
      real*8 times(tp), tanhts(tp), tplats(tp), tplons(tp)
      real*8 time(tp), tanht(tp), tplat(tp), tplon(tp), error(tp)
      real*8 uts(gp), alt(gp), xlat(gp), xlong(gp), xstl(gp)
      real*8 UTSR, ALTR, XLATR, XLONGR, XSTLR

      character occultation*16
      external funcs

      nloop = nspectra

*---------------------------------------------------------------------
  100 count1 = 0

      CALL remove_count (tp, nloop, tanhts, times, tplats, tplons,
     &  flags,count1,error,tanht,time,tplat,tplon,flag)

      do i = 1,count1,1                        !Tests for sunrise over midnight
            if((time(i-1)-time(i)).gt.86340) time(i) = time(i)+86400
      enddo
      do i = count1,1,-1               !Tests for sunset over midnight
            if((time(i+1)-time(i)).gt.86340) time(i) = time(i)+86400.
      enddo
      do i = 1,count1,1
*     write(*,*)i,tanht(i),time(i),time(i-1)-time(i),time(i+1)-time(i)
      enddo

      do i = 1,nct,1
            iat(i) = 1
      enddo

      CALL lfit(tanht,time,error,count1,tco,iat,nct,zzt,nct,zzz,funcs)

      CALL timetester(nct,tp, count1,count2, flags, tco, time, tanht)

      do i = 1, count1, 1
            tanhts(i) = tanht(i)
            if (time(i).lt.86400) times(i) = time(i)
            if (time(i).ge.86400) times(i) = time(i)-86400.
            tplats(i) = tplat(i)
            tplons(i) = tplon(i)
      enddo

*     write (*,*) "***count1",count1,"  count2",count2
      nloop = count1
      if (count1.ne.count2) goto 100
```

```
*-----------------------------------------------------------------------
      do i = 1,count1,1
            if (tplon(i).lt.0) tplon(i) = 360 + tplon(i)
            if (tplon(i).gt.360) tplon(i) = tplon(i) - 360
            if (tplat(i).gt.90) tplat(i) = 180 - tplat(i)
            if (tplat(i).lt.-90) tplat(i) = -180 - tplat(i)
      enddo
*-----------------------------------------------------------------------

      shift = time(1)
      do i=1, count1, 1
            if (time(i).lt.time(1)) shift = time(i)
      enddo
      do i=1, count1, 1
            time(i) = time(i) - shift
      enddo

* The above two loops find the smallest time then shift the times by this
* amount to give lfit smaller numbers to work with, which results in a much
* better fit.

      do i = 1,ncl,1
            ial(i) = 1
      enddo
      CALL lfit(time,tplat,error,count1,ltco,ial,ncl,zzl,ncl,zzz,funcs)
      CALL lfit(time,tplon,error,count1,lnco,ial,ncl,zzl,ncl,zzz,funcs)

      do i=1, count1, 1
            time(i) = time(i) + shift
      enddo
*-----------------------------------------------------------------------
      do i = 1,gp,1
            ALT(i) = dfloat(i)-0.5
            UTS(i) = 0
            do j = 1,nct,1
                  UTS(i) = UTS(i)+((tco(j))*((ALT(i))**(j-1)))
            enddo
            XLAT(i) = 0
            do j = 1,ncl,1
                  XLAT(i) = XLAT(i)+((ltco(j))*((UTS(i)-shift)**(j-1)))

            enddo
            XLONG(i) = 0
            do j = 1,ncl,1
                  XLONG(i)=XLONG(i)+((lnco(j))*((UTS(i)-shift)**(j-1)))
            enddo
            IYD(i) = DOYs
      enddo

*     open (63, file = 'ACEsplice/lfit_out')
      do i = 1,gp,1
            if (UTS(i).ge.86400.0) IYD(i) = IYD(i)+1
            if (UTS(i).ge.86400.0)     UTS(i) = UTS(i)-86400.0
            XSTL(i) = UTS(i)/3600 + XLONG(i)/15
            if (xlat(i).gt. 90) xlat(i) =  180 - xlat(i)
            if (xlat(i).lt.-90) xlat(i) = -180 - xlat(i)
            if (xlong(i).gt. 180) xlong(i) = xlong(i) - 360
            if (xlong(i).lt.-180) xlong(i) = xlong(i) + 360
            if (xstl(i).gt.24) xstl(i) = xstl(i) - 24
            if (xstl(i).lt.24) xstl(i) = 24 - xstl(i)
*           write (63,*)alt(i),iyd(i),time(i),uts(i),
```

```
*     &                          tplat(i),xlat(i),tplon(i),xlong(i)
      enddo
*     close(63)

* Tangent heights (altitudes) are created for layers (0.5 to gp-0.5 km)
* i.e. 0.5, 1.5, 2.5, ... 149.5 km.  The program determines the
* latitude, longitude and UT based on time relative to the time for a
* hypothetical 0 km measurement, and set the Local Standard Time in
* accordance with the UT. The equations for TIME, XLAT, and XLONG
* were determined using a cubic fit from numerical recipes based on
* ATMOS occultation pts from the runlog.

* "NOTES ON INPUT VARIABLES" in MSIS states:
* UT, Local Time and Longitude are used independently in the
* model and are not of equal importance for every situation.
* For the most physically realistic calculation, these three
* variables should be consistent (STL=UT/3600+LONG/15).
* The equation of time departures from the above formula
* for apparent local time can be included if available but
* are of minor importance.

* Note the calculation: STL=UT/3600+LONG/15 can produce local times
* outside of the usual 0-24 hour range, corresponding to a date change.
*-----------------------------------------------------------------------

* The following is used to determine the time, lat and long for
* a tangent height of ALTR which is used as the reference altitude for
* calling the CMC data.  This is typically chosen to be 30.0 km

      ALTR = 30.0
      UTSR = 0.0
      do j = 1,nct,1
            UTSR = UTSR+((tco(j))*(ALTR**(j-1)))
      enddo

      XLATR = 0.0
      do j = 1,ncl,1
            XLATR = XLATR+((ltco(j))*((UTSR-shift)**(j-1)))
      enddo

      XLONGR = 0.0
      do j = 1,ncl,1
            XLONGR = XLONGR+((lnco(j))*((UTSR-shift)**(j-1)))
      enddo
      if (UTSR.ge.86400.0) UTSR = UTSR-86400.0
      XSTLR = UTSR/3600 + XLONGR/15

      return
      END

*****************************************************************************

      SUBROUTINE REMOVE_COUNT (tp, nloop, tanhts, times, tplats, tplons,
     &  flags,count1,error,tanht,time,tplat,tplon, flag)

*****************************************************************************

      integer tp, nloop, count1
      integer flags(tp), flag(tp)

      real*8 times(tp),tanhts(tp),tplats(tp),tplons(tp)
```

```
      real*8 time(tp), tanht(tp), tplat(tp), tplon(tp), error(tp)

      do i=1, nloop, 1
            if(flags(i).eq.0)then
            ! This skips the points that are flagged as bad
                  count1 = count1 + 1
                  error(count1) = 1
                  tanht(count1) = tanhts(i)
                  time(count1) = times(i)
                  tplat(count1) = tplats(i)
                  tplon(count1) = tplons(i)
                  flag(count1) = flags(i)
*                 write(*,*)count1,tanht(count1),time(count1)
*     &            ,tplat(count1),tplon(count1)
            endif
      enddo

      return
      end

*****************************************************************************

      SUBROUTINE TIMETESTER (nct,tp,count1,count2,flags,tco,time,tanht)

*****************************************************************************

      integer count1, count2, nct, tp
      integer flags(tp)
      real*8 time(tp), timetest(tp), tanht(tp), tco(nct), acctest

      acctest = 2.75

      count2 = 0
      do i = 1, count1, 1
            timetest(i) = 0
            do j = 1,nct,1
            timetest(i) = timetest(i)+((tco(j))*((tanht(i))**(j-1)))
            enddo
            if ((dabs(timetest(i)-time(i))).gt.acctest) then
                  flags(i) = 99
            else
                  count2 = count2 + 1
                  flags(i) = 0
            endif
      enddo

      return
      end

*****************************************************************************

      SUBROUTINE DOMSIS (bp,gp,DOY,UT,ALT,XLAT,XLONG,XSTL,
     & F107A,F107,AP,D,T,TND,PRESSURE,AVEMM)

*****************************************************************************
*
* This subroutine calls MSIS2000 to calculate temperature and densities
* It calculates total number density, then pressure using ideal gas law
*
*---------------------------------------------------------------------------
```

Appendix 1

```
      integer bp, gp, DOY(gp)
      real*4 SW(25), F107A(gp), F107(gp), AP(7,gp) !AP(gp)

      real*4 UT4(gp), ALT4(gp), XLAT4(gp), XLONG4(gp), XSTL4(gp)
      real*8 UT(gp),  ALT(gp),  XLAT(gp),  XLONG(gp),  XSTL(gp)

      real*4 D4(9,gp), T4(2,gp)
      real*8 D(9,gp),  T(2,gp),  TND(gp),  PRESSURE(gp), AVEMM(gp)

* TND is the Total Number Density and PRESSURE is obviously pressure
* See comments in MSIS for an explanation of other parameters

      DATA SW/8*1.,-1.,16*1./
      CALL TSELEC(SW)

* The data are 25 switches, which are explained in MSIS2000
* comments and are activated by calling TSELEC in MSIS2000.
* The common block in TSELEC gives GTD7 access to the switches.
*
* SW(9) relates to AP
* WHEN SW(9)=-1     AP - MAGNETIC INDEX ARRAY
* WHEN SW(9)= 0     AP - MAGENTIC INDEX PARTIAL ARRAY
* WHEN SW(9)= 1     AP - MAGNETIC INDEX DAILY
*
* The array is defined in the subroutine APF107
*     write (*,*) "SW8=",SW(8),"  SW9=",SW(9),"  SW10=",SW(10)

*     open (77, file = 'MSISoutput')

      do i = bp, gp, 1

      UT4(i) = SNGL(UT(i))
      ALT4(i) = SNGL(ALT(i))
      XLAT4(i) = SNGL(XLAT(i))
      XLONG4(i) = SNGL(XLONG(i))
      XSTL4(i) = SNGL(XSTL(i))

      call GTD7(DOY(i),UT4(i),ALT4(i),XLAT4(i),XLONG4(i),XSTL4(i),
     & F107A(i),F107(i),AP(1,i),48,D4(1,i),T4(1,i))

      do j=1,9
            D(J,i) = DBLE(D4(J,i))
      enddo
            T(1,i) = DBLE(T4(1,i))
            T(2,i) = DBLE(T4(2,i))

      TND(I)= D(1,I)+D(2,I)+D(3,I)+D(4,I)+D(5,I)+D(7,I)+D(8,I)+D(9,I)
      PRESSURE(I)= (1000000./100.)*TND(I)*1.380658E-23*T(2,I)

      AVEMM(i)= (4.002602*D(1,i) + 15.9994*D(2,i) + (2*14.00674)*D(3,i)
     & + (2*15.9994)*D(4,i) + 39.948*D(5,i)
     & + 1.00794*D(7,i) + 14.00674*D(8,i)) / TND(i)

*     write (77,*) i, AVEMM(i)

      enddo

*     do i=1,7
*           write (*,*) "ap",i,"",ap(i,99)
*     enddo
```

```
*      close (77)

* The loop calculates total number density (TND) of molecules and
* pressure in mbar based on total number density and ideal gas law
* 1000000 cm^3 per m^3 and 100 Pa/hPa (1mbar = 1hPa)
* AVEMM is the Average Molecular Mass of air at a given altitude
* Up to about 65 km the average molecular mass is 28.96 g/mol which is
* slightly greater than the molecular mass of the main component N2.
* Above this height N2 and O2 break up to for N and O so ave_mm decreases

       return
       END

*****************************************************************************

       SUBROUTINE IODBASE (gp, occultation, CMChifloat, TMSIS, PMSIS,
     & XLAT, XLONG, UTS, XLATR, XLONGR, UTSR, datetime,
     & Aap, Tap, Pap, Dap, AVEMM, RETVAL)

*****************************************************************************
* This subroutine will read the CMC input from the database and then
* write the spliced output to a new file.
*----------------------------------------------------------------------------

#define in_tablename "mscdata"
#define out_tablename "a_priori_tp"

       integer gp, n, nn, retval(10), retvalA, retvalB
       parameter (maxa = 40)

       real*8 ALT(gp), TMSIS(gp), PMSIS(gp)
       real*8 XLAT(gp), XLONG(gp), UTS(gp), AVEMM(gp)
       real*4 XLAT4(gp), XLONG4(gp), UTS4(gp), AVEMM4(gp)
       real*8 XLATR, XLONGR, UTSR
       real*4 Aap(gp), Tap(gp), Pap(gp), Dap(gp), CMChifloat

       external getMSC, write_apriori
       integer getMSC, write_apriori

       integer numalt, dataid, timestampseconds
       real*4 longitude, latitude
       real*4 altitude(MAXA), temperature(MAXA), pressure(MAXA)

       character*30 datetime(gp)

       character dir*128
       character occultation*16
       character occulttypenum*12
       character injectiondate*36
       character fullfilename*256
       character datatype*24
       character timestamptext*36
       character date*24
       character time*24
       character outfile*128
       character CMC_data*32

       CALL check_pgenv
       CALL check_dbgenv

       n = lnblnk(occultation)
```

```
      dot = 0
      do i=1,n,1
            if (occultation(i:i).eq.'.') then
                  if (dot.eq.0) then
                        nn = i
                        dot = 1
                  else
                        n = i
                        goto 100
                  endif
            endif
  100 enddo

      occulttypenum = occultation(nn+1:n)

*     This works for any occultations with names such as:
*     ace.0112, ace.sr123, ace.ss123456789
*     where the occultation number (and type) are enclosed by dots.

      write (*,*) in_tablename

      retvalA = getMSC (occulttypenum, in_tablename, dataid,
     & injectiondate, fullfilename, datatype,
     & timestamptext, timestampseconds, numalt,
     & longitude, latitude, altitude, temperature, pressure, MAXA)

      if (retvalA.eq.0) then
            if (datatype.eq.'anal (reg2)') RETVAL(5) = 0
            if (datatype.eq.'anal (glb2)') RETVAL(5) = 0
            if (datatype.eq.'anal (reg1)') RETVAL(5) = 1
            if (datatype.eq.'anal (glb1)') RETVAL(5) = 1
            if (datatype.eq.'prog (reg)')  RETVAL(5) = 2
            if (datatype.eq.'prog (glb)')  RETVAL(5) = 2

            CALL DOCMC (gp, maxa, datatype, occulttypenum, numalt,
     & timestamptext, altitude, temperature, pressure, latitude,
     &       TMSIS, PMSIS, date, time, Aap, Tap, Pap, Dap,
     & CMChifloat, retval(6))
      else
            RETVAL(5) = retvalA
            datatype = 'no_CMC'

            CALL NOCMC (gp, occultation, ALT, TMSIS, PMSIS,
     & XLATR, XLONGR, UTSR, datetime, date, time,
     &       latitude,longitude, Aap,Tap,Pap,Dap, CMChifloat, RETVAL(6))
      endif

      do i = 1,gp
            XLAT4(i) = SNGL(XLAT(i))
            XLONG4(i) = SNGL(XLONG(i))
            UTS4(i) = SNGL(UTS(i))
            avemm4(i) = SNGL(AVEMM(i))
*           write (*,*) date, time, Aap(i), timestamptext
      enddo

      write (CMC_data,'(A,A,A)') occulttypenum(1:lnblnk(occulttypenum)),
     & '_', datatype(1:lnblnk(datatype))
      write (*,*) "CMC  ", CMC_data

      retvalB = write_apriori (out_tablename, occultation, CMC_data,
     & date, time, latitude, longitude, gp, numalt, CMChifloat,
```

```
     & Aap, Tap, Pap, Dap, aveMM4, xlat4, xlong4, uts4, RETVAL)

       write (*,*) RETVAL

  999  return
       END

*************************************************************************

       SUBROUTINE DOCMC (gp, maxa, datatype, occulttypenum, numalt,
     & timestamptext, altitude, temperature, pressure, latitude,
     &       TMSIS, PMSIS, date, time, Aap, Tap, Pap, Dap,
     & CMChifloat, retval6)

*************************************************************************

       integer CMCLOW, CMCHIGH, MSISLOW, gp, maxa, retval6, Q

       real*8 ALT(gp), GEOLAT(maxa)
       real*8 XLAT(gp), XLONG(gp), UTS(gp), AVEMM(gp)
       real*4 XLAT4(gp), XLONG4(gp), UTS4(gp), AVEMM4(gp)
       real*8 TCMC(MAXA), TCMCZ(MAXA), TMSIS(gp), TS(55)
       real*8 PCMC(MAXA), PCMCZ(MAXA), PMSIS(gp), PS(55)
       real*4 Aap(gp), Tap(gp), Pap(gp), Dap(gp)

       integer numalt, dataid, timestampseconds
       real*4 longitude, latitude, CMChifloat
       real*4 altitude(MAXA), temperature(MAXA), pressure(MAXA)

       character dir*128
       character occultation*16
       character occulttypenum*12
       character injectiondate*36
       character fullfilename*256
       character datatype*24
       character timestamptext*36
       character date*24
       character time*24
       character outfile*128

       do i = 1, lnblnk(datatype)
              if (datatype(i:i).eq.'(') then
                     do j = i, lnblnk(datatype)
                            datatype(j:j) = datatype(j+1:j+1)
                     enddo
              endif
              if (datatype(i:i).eq.')') datatype(i:i) = ''
       enddo
       do i = 1, lnblnk(datatype)
              if (datatype(i:i).eq.' ') datatype(i:i) = '_'
       enddo

       do i = 1, lnblnk(timestamptext)
              if (timestamptext(i:i).eq.' ') then
                     date = timestamptext(1:i-1)
                     time = timestamptext(i+1:lnblnk(timestamptext))
              endif
       enddo

*      write (*,*) timestamptext, date, time
*      write (*,*) "occult typenum = ", occulttypenum
```

Appendix 1

```
*      write (*,*) "forecast (prog) or analysis (anal): ", modelstage
*      write (*,*) dataid
*      write (*,*) injectiondate
*      write (*,*) fullfilename
*      write (*,*) datatype
*      write (*,*) "F77 timestamptext ", timestamptext
*      write (*,*) timestampseconds
*      write (*,*) numalt
*      write (*,*) longitude, latitude

       CMCHIGH = numalt
       do  i=1,CMCHIGH
              ALT(i) = DBLE(altitude(i))
              TCMC(i) = DBLE(temperature(i))
              PCMC(i) = DBLE(pressure(i))
              GEOLAT(i) = DBLE(latitude)
*             write (*,'(3F12.3)') ALT(i), TCMC(i), PCMC(i)
       enddo

       CMCLOW = 1
       do i=1, CMCHIGH, 1
              if (TCMC(i).le.0) CMCLOW = CMCLOW + 1
       enddo
       Q = CMCHIGH-CMCLOW+1                    !Number of points to spline

* Finds the lowest useable CMC datapoint
*-----------------------------------------------------------------------
       CALL GEOMETRIC(Q,CMCLOW,CMCHIGH,GEOLAT,ALT,TCMC,PCMC,TCMCZ,PCMCZ)
*
* Converts geopotential altitudes to geometric altitudes and uses a
* spline to interpolate and put back on the same altitude grid spacings.
* New pressures and temperature are calculated for each grid point.
*
       CALL SPLICE (gp, maxa, ALT, CMCHIGH, TCMCZ, PCMCZ,
     & TMSIS, PMSIS, CMCLOW, Aap, Tap, Pap, Dap, retval6)
*-----------------------------------------------------------------------

       CMChifloat = float(CMCHIGH)-0.5

       return
       END

**************************************************************************

       SUBROUTINE NOCMC (gp, occultation, ALT, TMSIS, PMSIS,
     & XLATR, XLONGR, UTSR, datetime, date, time,
     &       latitude, longitude, Aap, Tap, Pap, Dap, CMChifloat, RETVAL)

**************************************************************************

       integer gp, RETVAL

       real*4 Aap(gp), Tap(gp), Pap(gp), Dap(gp), CMChifloat
       real*8 ALT(gp), TMSIS(gp), PMSIS(gp)
       real*8 XLATR, XLONGR, UTSR
       real*4 latitude, longitude

       character occultation*16
       character*30 datetime(gp)
       character date*24
       character time*24
```

```
      integer hr, min, sec
      character*2 hour, minute, second

      if (occultation(5:6).eq.'ss') n = 30
      if (occultation(5:6).eq.'sr') n = 150-30

      do i = 1, lnblnk(datetime(n))
            if (datetime(n)(i:i).eq.' ') then
                  date = datetime(n)(2:i-1)
                  !time = datetime(n)(i+1:lnblnk(datetime(n)))
                  !Above is a shortcut, but it is less accurate
            endif
      enddo

      hr  = AINT((SNGL(UTSR))/3600)
      min = AINT((SNGL(UTSR)-(hr*3600))/60)
      sec = AINT(SNGL(UTSR)-(hr*3600)-(min*60))

      if (hr.lt.10) then
            write (hour,'(A,I1)'),'0', hr
      else
            write (hour,'(I2)'), hr
      endif

      if (min.lt.10) then
            write (minute,'(A,I1)'),'0',min
      else
            write (minute,'(I2)'), min
      endif

      if (sec.lt.10) then
            write (second,'(A,I1)'),'0',sec
      else
            write (second,'(I2)'), sec
      endif

      write (time, '(A2,A1,A2,A1,A2)'),hour,':',minute,':',second
*     write (*, '(A10,A1,A8)') date, ' ', time

      do i = 1, gp
*           Aap(i)= dfloat(i)-0.5
*           Tap(i)= SNGL(TMSIS(I))
*           Pap(i)= SNGL(PMSIS(I))
*           Dap(i)= 100.*Pap(i)/(1000000.*1.380658E-23*Tap(i))

********************** MSIS default above, zeroes below **************

            Aap(i)= 0
            Tap(i)= 0
            Pap(i)= 0
            Dap(i)= 0
*           write (*,*) Aap(i), Tap(i), Pap(i), Dap(i), date, time
      enddo

      latitude = SNGL(XLATR)
      if (latitude.gt.90) latitude =  180 - latitude
      if (latitude.lt.-90) latitude = -180 - latitude

      longitude = SNGL(XLONGR)
      if (longitude.gt.180) longitude = longitude - 360
      if (longitude.lt.-180) longitude = longitude + 360
```

```
       CMChifloat = 0.0

       return
       END

*************************************************************************
*
       SUBROUTINE GEOMETRIC (N, LO, HI, deg, ALT, TCMC, PCMC, TZ, PZ)
*
*************************************************************************
*
*      Change Geopotential height (H) to Geometric height (Z)
*      Interpolates P and T back onto the proper grid.
*      Uses the numerical recipes:
*      SUBROUTINE OSPLINE ( X, Y, N, YP1, YPN, Y2 )
*      SUBROUTINE SPLINEINT( XA, YA, Y2A, N, X, Y)
*
*      CALL GEOMETRIC      (Q, LO, HI, lat, ALT, TCMC, PCMC, TCMCZ, PCMCZ)
*      SUBROUTINE GEOMETRIC(N, LO, HI, deg, ALT, TCMC, PCMC,  TZ,    PZ)
*-----------------------------------------------------------------------

       integer N, LO, HI
       real*8 ALT(HI), PCMC(HI), TCMC(HI), deg(HI)
       real*8 Z(HI), PZ(HI), TZ(HI)
       real*8 Zn(N), PZn(N), TZn(N)
       real*8 H(N), PH(N), TH(N)
       real*8 rad(N), x(N), y(N), y2(N), val, pi
       parameter (pi=3.14159265358979)

       do i = 1,N                        !N = HI-LO+1
              H(i) = ALT(i+LO-1)
              PH(i) = PCMC(i+LO-1)
              TH(i) = TCMC(i+LO-1)
              rad(i) = pi*deg(i+LO-1)/180
              x(i) = (1.+0.002644*dcos(2*rad(i)))*H(i)
     &      + (1.+0.0089*dcos(2*rad(i)))*H(i)*H(i)/6245
              y(i) = dlog(PH(i))
       enddo

      CALL ospline(x,y,N,1.d30,1.d30,y2)
       Zn(1) = H(1)
       PZn(1) = PH(1)
       do i = 2,N
              Zn(i) = H(i)
              CALL splineint(x,y,y2,N,zn(i),val)
       PZn(i) = dexp(val)
       enddo

      CALL ospline(x,TH,N,1.d30,1.d30,y2)
       TZn(1) = TH(1)
       do i = 2,N
              CALL splineint(x,TH,y2,N,zn(i),val)
       TZn(i) = val
       enddo

       do i = 1,HI
       if (i.lt.LO) then
              Z(i) = dfloat(i)-0.5
              PZ(i) = -1000
              TZ(i) = -1000
```

```
       elseif (i.ge.LO) then
              Z(i)= ZN(i-LO+1)
              PZ(i)=PZN(i-LO+1)
              TZ(i)=TZN(i-LO+1)
       endif
*             write (*,*) i, Z(I), TZ(I), PZ(I)
       enddo
       return
      end

*********************************************************************

       SUBROUTINE SPLICE (gp, maxa, ALT, CMCHIGH, TCMC, PCMC,
     & TMSIS, PMSIS, CMCLOW, Aap, Tap, Pap, Dap, Flag7)

*********************************************************************
* This subroutine will:
*
* Splice meteorological data (CMC/NCEP) with modeled data from MSIS2000.
* It will use a 'linear' splice over the desired range and smooth the
* upper and lower ends of the splice.
*
*--------------------------------------------------------------------

       integer CMCLOW, CMCHIGH, MSISLOW, stratpi, gp, maxa, flag7
       real*8 tropt, stratpt, stratph, ALT(gp), ALTS(55)
       real*8 TCMC(maxa), TMSIS(gp), TS(55), m,  b
       real*8 PCMC(maxa), PMSIS(gp), PS(55), pm, pb
       real*4 Aap(gp), Tap(gp), Pap(gp), Dap(gp)

       tropt = 500.0
       do i = CMCLOW, CMCHIGH
              if (TCMC(i).lt.tropt) tropt = TCMC(i)
       enddo
       if (abs(tropt-TCMC(CMCHIGH)).lt.0.001) flag7 = 1

       stratpt = 200.0
       do i = 40,60,1
              if(TMSIS(i).ge.stratpt) then
                     stratpt = TMSIS(i)
                     stratpi = i
                     stratph = dfloat(stratpi) - 0.5
*                    write (*,*) i, stratph, stratpt
              endif
       enddo
       MSISLOW = stratpi-4 ! lowest MSIS point to be used

*      write (*,*) stratpi, stratph, stratpt
*      write (*,*) CMCHIGH, MSISLOW

* "stratpt" is the temperature at the gridpoint closest to the stratopause
* which is taken to be the temperature minimum from 40-60 km,
* but it is initialized at 200 K
* "stratpi" is the index on the stratopause temperature
* "stratph" is the tangent height of the stratopause on the nearest half-
* integer km

       m=(dfloat(MSISLOW)-dfloat(CMCHIGH))/(TMSIS(MSISLOW)-TCMC(CMCHIGH))
       b = ((dfloat(CMCHIGH))-0.5) - (m*TCMC(CMCHIGH))

       pm =(dfloat(MSISLOW)-dfloat(CMCHIGH))/
```

Appendix 1

```
     & (DLOG(PMSIS(MSISLOW))-DLOG(PCMC(CMCHIGH)))
       pb = ((dfloat(CMCHIGH))-0.5) - (pm*DLOG(PCMC(CMCHIGH)))

*      write (*,*) " "
*      write (*,*) "TMSIS(msislow)", tmsis(msislow)
*      write (*,*) "PMSIS(msislow)", pmsis(msislow)
*      write (*,*) "DLOG(PMSIS(msislow)) ", DLOG(PMSIS(MSISLOW))
*      write (*,*) "DLOG(PCMC(CMChigh)) ", DLOG(PCMC(CMChigh))
*      write (*,*) "m, b, pm, pb", m, b, pm, pb

       do i = CMCHIGH-1, MSISLOW+1, 1
              ALTS(i) = dfloat(i) - 0.5
              TS(i) = (ALTS(i) - b)/m
              PS(i) = dexp((ALTS(i) - pb)/pm)
       enddo

*-------------------------------------------------------------------------------
*      TS(CMCHIGH)   = (TCMC(CMCHIGH-2)+TS(CMCHIGH+2))/2
*      TS(CMCHIGH-1) = (TCMC(CMCHIGH-2)+TS(CMCHIGH))/2
*      TS(CMCHIGH+1) = (TS(CMCHIGH)+TS(CMCHIGH+2))/2
*
*      The above option can be used to smooth the transition from CMC data
*      to the interpolated area for a more visually appealing profile,
*      however the overall accuracy is worse than without the smoothing
*      (below).

       TS(CMCHIGH) = TCMC(CMCHIGH)
       TS(CMCHIGH-1) = TCMC(CMCHIGH-1)
       TS(CMCHIGH+1) = (TS(CMCHIGH)+TS(CMCHIGH+2))/2

*-------------------------------------------------------------------------------
       TS(MSISLOW)   = (TS(MSISLOW-2)+TMSIS(MSISLOW+2))/2
       TS(MSISLOW-1) = (TS(MSISLOW-2)+TS(MSISLOW))/2
       TS(MSISLOW+1) = (TS(MSISLOW)+TMSIS(MSISLOW+2))/2

* The above is used to smooth the ends of the temperature splice
* Note the smoothing rewrites TS and ALTS values at the ends of the splice

       do i = MSISLOW+2,gp, 1
              ALT(i) = dfloat(i) - 0.5
       enddo

*      ap below refers to "a priori" and not the planetary geomagnetism.
*-----------------------------------------------------------------------
       do I = CMCLOW,CMCHIGH-2,1
              Tap(i)=SNGL(TCMC(I))
              Pap(i)=SNGL(PCMC(I))
              Aap(i)=SNGL(ALT(I))
       enddo
*-----------------------------------------------------------------------
              Tap(CMCHIGH-1)=SNGL(TS(CMCHIGH-1))
              Pap(CMCHIGH-1)=SNGL(PS(CMCHIGH-1))
              Aap(CMCHIGH-1)=SNGL(ALTS(CMCHIGH-1))

              Tap(CMCHIGH)=SNGL(TS(CMCHIGH))
              Pap(CMCHIGH)=SNGL(PS(CMCHIGH))
              Aap(CMCHIGH)=SNGL(ALTS(CMCHIGH))
*-----------------------------------------------------------------------
       do I = CMCHIGH+1, MSISLOW-1, 1
              Tap(i)=SNGL(TS(I))
              Pap(i)=SNGL(PS(I))
```

```
              Aap(i)=SNGL(ALTS(I))
       enddo
*-----------------------------------------------------------------------
              Tap(MSISLOW)=SNGL(TS(MSISLOW))
              Pap(MSISLOW)=SNGL(PS(MSISLOW))
              Aap(MSISLOW)=SNGL(ALTS(MSISLOW))

              Tap(MSISLOW+1)=SNGL(TS(MSISLOW+1))
              Pap(MSISLOW+1)=SNGL(PS(MSISLOW+1))
              Aap(MSISLOW+1)=SNGL(ALTS(MSISLOW+1))
*-----------------------------------------------------------------------
       do I = MSISLOW+2, gp, 1
              Tap(I)=SNGL(TMSIS(I))
              Pap(i)=SNGL(PMSIS(I))
              Aap(i)=SNGL(ALT(I))
       enddo
*-----------------------------------------------------------------------
       do I = CMCLOW,gp,1
              Dap(i)=100.*Pap(i)/(1000000.*1.380658E-23*Tap(i))
*             write (*,*) Tap(i), Pap(i), Dap(i)
       enddo

       return
       END

*************************************************************************

       SUBROUTINE WRITEOUT(occultation,year,month,day,DOY,UTS,xlat,
     & xlong,Aap,XSTL,gp,Tap,Pap,Dap,CMChifloat,AVEMM,retval,bp)

*************************************************************************
*
* This subroutine can be used to write certain parameters to the monitor
* during program development and troubleshooting.  It can also be easily
* modified to write to a file/database for archiving.
*
*************************************************************************

       integer year, month, day,RETVAL, gp, bp, s, DOY(gp)
       real*8 UTS(gp), xlat(gp), xlong(gp), XSTL(gp), AVEMM(gp)
       real*4 Aap(gp), Tap(gp), Dap(gp), Pap(gp), CMChifloat
       character occultation*16, dir*24, writefile*48

       if (DOY(1).le.DOY(gp)) s = 1
       if (DOY(1).gt.DOY(gp)) s = gp

       dir = ''

       write (writefile,'(A,A,A)') dir(1:lnblnk(dir)),
     & occultation(1:lnblnk(occultation)),'.ap'!'.aptest'

       open (8, file = writefile, ERR = 99)

       write(8,*) occultation, "CMC_high", CMChifloat
       write(8,*) "start_YYYYMMDD=",year,month,day," DOY=",DOY(s)
       write(8,*) ""
       write(8,*) "TANGENT_HEIGHT  TEMPERATURE  PRESSURE     DENSITY
     &    AVERAGE_MM   DOY      UTS        LATITUDE    LONGITUDE"
       write(8,*) "     (km)        (deg_C)      (hPa)  (molecules/cm^3)
     &  (g/mol)     (day)        (s)          (deg)        (deg)"
       write(8,*) ""
```

Appendix 1

```
      do I=1,gp,1
             write(8,100) Aap(i), Tap(i), Pap(i), Dap(i), aveMM(i)
     & ,DOY(i), UTS(i), xlat(i), xlong(i)
       enddo
       close(8)

  100  format(F9.1,F16.2,E13.3,E13.3,F11.3,I8,F13.1,F13.5,F13.5)
   99  return
       END
```

C) recipes.F

```
**********************************************************************

      SUBROUTINE lfit(x,y,sig,ndat,a,ia,ma,covar,npc,chisq,funcs)

**********************************************************************

      INTEGER ma, ia(ma), npc, ndat, MMAX
      real*8 chisq, a(ma), covar(npc,npc), sig(ndat), x(ndat), y(ndat)
      EXTERNAL funcs
      PARAMETER (MMAX = 10)

* Uses: gaussj
* Given a set of dat points x(1:ndat), Y(1:ndat) with individual standard
* deviations sig(1:ndat), use chi-squared minimization to fit for some or all
* of the coefficients...

      INTEGER i,j,k,l,m,mfit
      real*8 sig2i, sum, wt, ym, afunc(MMAX), beta(MMAX)
      mfit=0
      do j=1,ma
            if(ia(j).ne.0) mfit = mfit + 1
      enddo

      if(mfit.eq.0) pause 'lfit: no parameters to be fitted'

      do j=1, mfit

* Initializes the symmetric matrix

            do k=1,mfit
                  covar(j,k)=0.
            enddo
            beta(j)=0
      enddo

* Loop over data to accumulate coefficients of the normal equations.

      do i=1, ndat
            call funcs(x(i), afunc, ma)
            ym=y(i)
            if(mfit.lt.ma) then

* Subtract off dependences on known pieces of the fitting function.

                  do j=1, ma
                        if(ia(j).eq.0) ym=ym-a(j)*afunc(j)
                  enddo
            endif
            sig2i=1./sig(i)**2
            j=0
            do l=1,ma
                  if(ia(l).ne.0)then
                        j=j+1
                        wt=afunc(l)*sig2i
                        k=0
                        do m=1,l
                              if(ia(m).ne.0)then
```

```
                                        k=k+1
                                        covar(j,k)=covar(j,k)+wt*afunc(m)
                                  endif
                            enddo
                            beta(j)=beta(j)+ym*wt
                      endif
                enddo
          enddo

* Fill in the above diagonal from symmetry

          do j=2, mfit
                do k=1, j-1
                      covar(k,j)=covar(j,k)
                enddo
          enddo

          call gaussj(covar,mfit,npc,beta,1,1)

* Matrix solution

          j=0
          do l=1, ma
                if (ia(l).ne.0) then
                      j=j+1
                      a(l)=beta(j)
                endif
          enddo
          chisq=0
          do i=1, ndat
                call funcs(x(i), afunc, ma)
                sum=0
                do j=1, ma
                      sum = sum + a(j)*afunc(j)
                enddo
                chisq=chisq+((y(i)-sum)/sig(i))**2
          enddo

          call covsrt(covar,npc,ma,ia,mfit)

* Sort covariance matrix to true order of fitting coefficients

          return
          END

*************************************************************************

          SUBROUTINE gaussj(a,n,np,b,m,mp)

*************************************************************************

*     a(,)     = covar(,)
*     n        = mfit
*     np       = npc
*     b(,)     = beta(,)
*     m = 1
*     mp       = 1

* using mainpolytest.f to test before using mainpolyfit.f

*************************************************************************
```

```
INTEGER m,mp,n,np,NMAX
real*8 a(np,np),b(np,mp)
PARAMETER (NMAX = 50)

INTEGER i,icol,irow,j,k,l,ll,indxc(NMAX),indxr(NMAX), ipiv(NMAX)
real*8 big, dum, pivinv

do j=1,n
       ipiv(j)=0
enddo
do i=1,n
       big = 0.
       do j=1,n
              if(ipiv(j).ne.1) then
                     do k=1,n
                            if(ipiv(k).eq.0) then
                                   if(abs(a(j,k)).ge.big)then
                                          big = abs(a(j,k))
                                          irow = j
                                          icol = k
                                   endif
                            elseif (ipiv(k).gt.1)then
                                   pause 'singular matrix in gaussj (A)'
                            endif
                     enddo
              endif
       enddo
       ipiv(icol) = ipiv(icol) + 1

       if (irow.ne.icol) then
              do l = 1,n
                     dum = a(irow,l)
                     a(irow,l) = a(icol,l)
                     a(icol,l) = dum
              enddo

              do l = 1,m
                     dum = b(irow,l)
                     b(irow,l) = b(icol,l)
                     b(icol,l) = dum
              enddo
       endif

       indxr(i) = irow
       indxc(i) = icol

       if(a(icol,icol).eq.0.) pause 'singular matrix in gaussj (B)'
       pivinv = 1./a(icol,icol)
       a(icol,icol)=1
       do l=1,n
              a(icol,l) = a(icol,l)*pivinv
       enddo

       do l=1,m
              b(icol,l) = b(icol,l)*pivinv
       enddo

       do ll=1,n
              if(ll.ne.icol) then
                     dum = a(ll,icol)
```

```
                        a(ll,icol)=0
                        do l=1,n
                               a(ll,l)=a(ll,l)-a(icol,l)*dum
                        enddo
                        do l=1,m
                               b(ll,l)=b(ll,l)-b(icol,l)*dum
                        enddo
                endif
        enddo
enddo

do l=n,1,-1
        if(indxr(l).ne.indxc(l))then
                do k=1,n
                        dum = a(k,indxr(l))
                        a(k,indxr(l))=a(k,indxc(l))
                        a(k,indxc(l))=dum
                enddo
        endif
enddo

return
END

*******************************************************************

      SUBROUTINE covsrt(covar,npc,ma,ia,mfit)

*******************************************************************

      INTEGER ma, mfit, npc, ia(ma)
      real*8 covar(npc,npc)

      INTEGER i,j,k
      real*8 swap

      do i = mfit+1, ma
        do j=1,i
          covar(i,j)=0
          covar(j,i)=0
        enddo
      enddo

      k=mfit

      do j=ma, 1, -1
        if(ia(j).ne.0)then
          do i=1,ma
            swap = covar(i,k)
            covar(i,k) = covar(i,j)
            covar(i,j) = swap
          enddo
          do i=1,ma
            swap = covar(k,i)
            covar(k,i) = covar(j,i)
            covar(j,i) = swap
          enddo
          k=k-1
        endif
      enddo
```

```
       return
       END

*************************************************************************

       SUBROUTINE funcs(x,afunc,ma)

*************************************************************************

       real*8 x, afunc(ma)
       integer ma

       do i = 1, ma, 1
              afunc(i) = x**(i-1)
       enddo

       return
       END

*************************************************************************

C        OSPLINE,     RHN,      3 JUNE 1986
C=============================================================
C
C     S U B R O U T I N E        O - S - P - L - I - N - E
C
C    PURPOSE:
C     TO PERFORM CUBIC SPLINE INTERPOLATION.
C     This subroutine is based on the "SPLINE" routine from
C     "Numerical Recipes", W.H. Press, B.P. Flannery, S.A. Teukolsky,
C     W.T. Vetterling, Cambridge Univ. Press, 1986, p.88.
C     It has been modified to contain comments and to have the
C     number of layers in a physical model as its maximum number
C     of points.
C
C    CALLING SEQUENCE:
C       CALL OSPLINE ( X, Y, N, YP1, YPN, Y2 )
C
C    ARGUMENTS:
C      X........INDENDENT VARIABLE ARRAY, IN ASCENDING ORDER
C      Y........DEPENDENT VARIABLE ARRAY
C      N........NUMBER OF points IN X AND Y
C      YP1......FIRST DERIVATIVE OF Y AT FIRST POINT
C      YPN......FIRST DERIVATIVE OF Y AT NTH POINT
C      Y2.......ARRAY OF VALUES FROM WHICH "splineint" DOES ACTUAL
C                    INTERPOLATION
C
C    ARGUMENT TYPES:
C      X, Y, YP1, YPN, Y2:      real*8
C      N:                       INTEGER*4
C
C    RETURNED VALUE(S):    Y2(N)
C
C=============================================================
c
      SUBROUTINE OSPLINE ( X, Y, N, YP1, YPN, Y2 )

      INTEGER*4 N, I, K
      REAL*8 X(N), Y(N), Y2(N), U(200),YP1,SIG, P, YPN, QN, UN
C
      IF (YP1.GT.0.99D30) THEN
```

```
         Y2(1)=0.
         U(1)=0.
      ELSE
         Y2(1)=-0.5
         U(1)=(3./(X(2)-X(1)))*((Y(2)-Y(1))/(X(2)-X(1))-YP1)
      ENDIF
      DO 11 I=2,N-1
         SIG=(X(I)-X(I-1))/(X(I+1)-X(I-1))
         P=SIG*Y2(I-1)+2.
         Y2(I)=(SIG-1.)/P
         U(I)=(6.*((Y(I+1)-Y(I))/(X(I+1)-X(I))-(Y(I)-Y(I-1))
     *       /(X(I)-X(I-1)))/(X(I+1)-X(I-1))-SIG*U(I-1))/P
11       CONTINUE
      IF (YPN.GT.0.99E30) THEN
         QN=0.
         UN=0.
      ELSE
         QN=0.5
         UN=(3./(X(N)-X(N-1)))*(YPN-(Y(N)-Y(N-1))/(X(N)-X(N-1)))
      ENDIF
      Y2(N)=(UN-QN*U(N-1))/(QN*Y2(N-1)+1.)
      DO 12 K=N-1,1,-1
         Y2(K)=Y2(K)*Y2(K+1)+U(K)
12       CONTINUE
      RETURN
      END
c
*****************************************************************************

      SUBROUTINE SPLINEINT(XA,YA,Y2A,N,X,Y)

*****************************************************************************
*      called splint for spline interpolation in numerical recipes,
*      changed splint to splineint since MSIS had a version of splint too
*---------------------------------------------------------------------------

       integer*4 N, KHI, KLO, K
      REAL*8 XA, YA, Y2A, X, Y, H, A, B

      DIMENSION XA(N),YA(N),Y2A(N)
      KLO=1
      KHI=N
1     IF (KHI-KLO.GT.1) THEN
        K=(KHI+KLO)/2
        IF(XA(K).GT.X)THEN
          KHI=K
        ELSE
          KLO=K
        ENDIF
      GOTO 1
      ENDIF
      H=XA(KHI)-XA(KLO)
      IF (H.EQ.0.) PAUSE 'Bad XA input.'
      A=(XA(KHI)-X)/H
      B=(X-XA(KLO))/H
      Y=A*YA(KLO)+B*YA(KHI)+
     *      ((A**3-A)*Y2A(KLO)+(B**3-B)*Y2A(KHI))*(H**2)/6.
      RETURN
      END
*****************************************************************************
```

D) climatology.c

```
#include "aceql.h"
#include "debug.h"
#include "config.h"
#include <stdlib.h>
#include <string.h>

#define sddbg(x,y) \
    if (getenv("DEBUG")) { \
    fprintf( stderr, "DEBUG:%s:%d: ", __FILE__, __LINE__ ); \
    fprintf( stderr, x,y ); \
    fprintf( stderr, "\n" ); \
    }

/*-------------------------------------------------------------------------*/

#define CAL "getap_"

int getap_ (year, month, day, ap)
int *year, *month, *day, ap[8];
{
    PGconn *conn;
    PGresult *res;

    int i, j;
    char sql_query[8192];
    static int numtables = 2;
    static char *aptable[] = {"solar_activity_archive","solar_activity_email"};

    /* Connect to climatology database */
    conn = PQconnectdb(connstr("climatology"));
    sql_checkconn(conn);

    j=0;
    while (j < numtables) {

    /* Assemble query */
           sprintf( sql_query,
             "SELECT ap[1], ap[2], ap[3], ap[4], ap[5], ap[6], ap[7], ap[8] "
             "FROM %s WHERE date = '%4d-%02d-%02d 00:00:00+0';",
             aptable[j], *year, *month, *day );

//           printf ("j = %d  %s \n", j, aptable[j]);
           res = sql_exec(conn,sql_query);

    /* Check for results */
           if ( PQntuples(res) == 0 ) {
      message( CAL, "No results returned from the database.  Bailing out." );
             if (j == 1) return(1);
             if (j == 0) j++;
           }

    /* assign database values to the output variables */
           else{
             for (i=0;i<8;i++) { ap[i] = (int)getval(res, 0, i); }
//           printf ("j = %d  %s ap#1 = %d\n", j, aptable[j], ap[0]);
             if (ap[0]=='\0' && ap[1]=='\0' && ap[2]=='\0' && ap[3]=='\0' &&
             ap[4]=='\0' && ap[5]=='\0' && ap[5]=='\0' && ap[7]=='\0' && j==0)
             j++;
```

```
            else break;
          }
    }

    PQclear(res);             /* Clear the query             */
    sql_closeconn(conn);

       return(j);
}
#undef CAL
/*-------------------------------------------------------------------------*/

#define CAL "getfluxes_"

int getfluxes_ (year, month, day, pyear, pmonth, pday,
                           pflux, dd1, dd2, flux, n_fluxes, dates,len_dates)
int *year, *month, *day;
int *pyear, *pmonth, *pday;
int *dd1, *dd2, *n_fluxes;
float *flux;
float *pflux;
char *dates;
long len_dates;

{
    PGconn *conn;
    PGresult *res1, *res2;

    int i,j;
    char datestring[24];
    char pdatestring[24];
    char sql_query1[8192];
    char sql_query2[8192];
    static int numtables = 2;
//  static char *soltable[] ={"solar_activity_archive","solar_activity_email"};
    static char *soltable[] = {"solar_drao_email","solar_activity_archive"};

    /* Connect to climatology database */
    conn = PQconnectdb(connstr("climatology"));
    sql_checkconn(conn);

    sprintf (datestring, "%4d-%02d-%02d 00:00:00+0", *year, *month, *day);
    sprintf (pdatestring, "%4d-%02d-%02d 00:00:00+0", *pyear, *pmonth, *pday);

    j=0;
    while (j < numtables) {
       /*Assemble query for previous day F107*/

       sprintf (sql_query1,"SELECT flux FROM %s WHERE date = '%s';",soltable[j],
pdatestring);
       res1 = sql_exec(conn,sql_query1);

       if ( PQntuples(res1) == 0 ) {
         message( CAL, "No results returned from the database.  Bailing out." );
//           printf ("j = %d\n", j);
             if (j == 1) return(-1);
       if (j == 0) j++;
       }

       else   {
             *pflux = (float)getval(res1, 0, 0);
```

```
//            PQclear(res1);
//            printf ("j = %d  %s pflux = %f\n", j, soltable[j], *pflux);

              if (*pflux == '\0') j++;
              else break;
       }
        PQclear(res1);
    }

    /* Second query */
    /* Assemble query for 81-day F107 average centred on the present day*/
    sprintf(sql_query2, "SELECT flux, date FROM %s "
             "WHERE date >= ( timestamp '%s' + interval '%d days' ) "
              "AND date <= ( timestamp '%s' + interval '%d days' );",
             soltable[j], datestring, *dd1, datestring, *dd2 );

    res2 = sql_exec(conn,sql_query2);

    /* Check for results */
    if ( PQntuples(res2) == 0 ) {
        message( CAL, "No results returned from the database.  Bailing out." );
        return(-1);
    }

    /* assign database values to the output variables */

//     printf ("n_fluxes = %d %s\n", *n_fluxes, soltable[j]);
    *n_fluxes = (int)PQntuples(res2);
//     printf ("n_fluxes = %d\n", *n_fluxes);

    for (i=0; i<PQntuples(res2); i++) {
        flux[i] = (float)getval(res2, i, 0);
        sprintf( dates, "%s", PQgetvalue(res2, i, 1) );
        dates = dates + len_dates;
    }

    PQclear(res2);             /* Clear the query             */
    sql_closeconn(conn);

    return(0);
}
#undef CAL

/*-------------------------------------------------------------------------*/
#define CAL "getmsc_"
#define _SINGLEMODE

int getmsc_ ( occultation, tablename,
                      dataid, injectiondate, fullfilename, datatype,
                      timestamptext, timestampseconds, numalt,
                      longitude, latitude,
                      altitude, temperature, pressure, MAXARRAYSIZE,
                      len_occultation, len_tablename,
                      len_injectiondate, len_fullfilename, len_datatype,
                      len_timestamptext )
char *occultation;
char *tablename;
int  *dataid;
char *injectiondate;
char *fullfilename;
char *datatype;
```

Appendix 1

```
char *timestamptext;
int  *timestampseconds;
int  *numalt;
#ifdef _SINGLEMODE
float *longitude, *latitude;
float *altitude, *temperature, *pressure;
#else
double *longitude, *latitude;
double *altitude, *temperature, *pressure;
#endif
long   *MAXARRAYSIZE;
long len_occultation, len_tablename;
long len_injectiondate, len_fullfilename, len_datatype;
long len_timestamptext;

{
static int number_of_datatypes = 6;
static char *datatype_order[] = {
       "anal (reg2)",
       "anal (reg1)",
       "anal (glb2)",
       "anal (glb1)",
       "prog (glb)",
       "prog (reg)"  };

    PGconn *conn;
    PGresult *res;

    int i;
    char sql_query[8192];
    char *c_occultation;
    char *c_tablename;
    char *arval, *endptr;
    char dtypemsg[40];

    c_occultation = f77word( occultation, len_occultation );
    c_tablename   = f77word( tablename,   len_tablename );

    sddbg( "c_occultation: %s", c_occultation );
    sddbg( "c_tablename:   %s", c_tablename );

    /* Connect to climatology database */
    conn = PQconnectdb(connstr("climatology"));
    sql_checkconn(conn);

    i=0;
    while ( i < number_of_datatypes ) {

        /* Assemble query */
        sprintf( sql_query,"SELECT dataid, date_trunc('second',injectiondate),"
            "fullfilename, datatype, timestamptext, timestampseconds, numalt, "
            "longitude, latitude, altitude, temperature, pressure "
            "FROM %s WHERE occultation = '%s' and datatype = '%s' "
            "ORDER BY injectiondate DESC LIMIT 1;",
            c_tablename, c_occultation, datatype_order[i] );

        res = sql_exec(conn,sql_query);

        /* Check for results */
       if ( PQntuples(res) == 1 ) {
             printf("*** Found datatype %s\n",datatype_order[i]);
```

```
                    break;
                }
                else {
                    sprintf( dtypemsg, "%s not found for this occultation",
                    datatype_order[i]);
                message( CAL, dtypemsg );
                    i++;
                }
            sddbg( "Results from database = %d\n", PQntuples(res) );
    }

    if (PQntuples(res) == 0) return(-1);

    *dataid = (int)getval(res, 0, 0);
    i = cstring2f77( PQgetvalue(res, 0, 1), injectiondate, len_injectiondate);
    i = cstring2f77( PQgetvalue(res, 0, 2), fullfilename, len_fullfilename);
    i = cstring2f77( PQgetvalue(res, 0, 3), datatype, len_datatype);
    i = cstring2f77( PQgetvalue(res, 0, 4), timestamptext, len_timestamptext);
    *timestampseconds = (int)getval(res, 0, 5);
    *numalt = (int)getval(res, 0, 6);

    if (*numalt > *MAXARRAYSIZE ) die( "numalt > MAXARRAYSIZE", conn );

#ifdef _SINGLEMODE
    *longitude = (float)getval(res, 0, 7);
    *latitude = (float)getval(res, 0, 8);
    i = sqlarray2float( PQgetvalue(res,0,9), altitude, *MAXARRAYSIZE);
    i = sqlarray2float( PQgetvalue(res,0,10), temperature, *MAXARRAYSIZE);
    i = sqlarray2float( PQgetvalue(res,0,11), pressure, *MAXARRAYSIZE);
#else
    *longitude = (double)getval(res, 0, 7);
    *latitude = (double)getval(res, 0, 8);
    i = sqlarray2double( PQgetvalue(res,0,9), altitude, *MAXARRAYSIZE);
    i = sqlarray2double( PQgetvalue(res,0,10), temperature, *MAXARRAYSIZE);
    i = sqlarray2double( PQgetvalue(res,0,11), pressure, *MAXARRAYSIZE);
#endif

    PQclear(res);             /* Clear the query            */
    sql_closeconn(conn);

    return(0);
}
#undef CAL
#undef _SINGLEMODE

/*--------------------------------------------------------------------------*/

int write_apriori_ (tablename2, occultation, cmc_data,
                    date, time, lat_ref, long_ref, gp, numalt, cmchigh,
                    z, t, p, d, avemm, lat, lon, uts, flags,
                    len_tablename2, len_occultation, len_cmc_data,
                    len_date, len_time)

char *tablename2;
char *occultation;
char *cmc_data;
char *date, *time;

long len_tablename2;
long len_occultation;
long len_cmc_data;
```

Appendix 1

```
long len_date, len_time;

int *gp, *numalt, *flags;

float *cmchigh;
float *lat_ref, *long_ref;
float *z, *t, *p, *d, *avemm, *lon, *lat, *uts;

{
       PGconn *conn;
       PGresult *res;

       char sql_write[20000];
       char *c_occultation;
       char *c_tablename2;
       char *c_cmc_data;
       char *c_date, *c_time;
       int x;
       char zarray[4096];
       char tarray[4096];
       char parray[4096];
       char darray[4096];
       char mmarray[4096];
       char latarray[4096];
       char lonarray[4096];
       char utsarray[4096];
       char flagarray[1024];

       c_tablename2  = f77word (tablename2, len_tablename2);
       c_occultation= f77word (occultation, len_occultation);
       c_cmc_data          = f77word (cmc_data, len_cmc_data);
       c_date       = f77word (date, len_date);
       c_time       = f77word (time, len_time);

       conn = PQconnectdb(connstr("climatology"));
       sql_checkconn(conn);

       sprintf(zarray,     "%4.1 f",z[0]);
       sprintf(tarray,     "%5.2 f",t[0]);
       sprintf(parray,     "% .3 e",p[0]);
       sprintf(darray,     "% .3 e",d[0]);
       sprintf(mmarray,  "%5.3 f",avemm[0]);
       sprintf(latarray,   "%6.3 f",lat[0]);
       sprintf(lonarray,   "%6.3 f",lon[0]);
       sprintf(utsarray,   "%6.2 f",uts[0]);
       sprintf(flagarray,"%    d",flags[0]);

       for (x=1; x < 150; x++){
              sprintf(zarray,     "%s,%4.1 f",zarray,z[x]);
              sprintf(tarray,     "%s,%5.2 f",tarray,t[x]);
              sprintf(parray,     "%s,% .3 e",parray,p[x]);
              sprintf(darray,     "%s,% .3 e",darray,d[x]);
              sprintf(mmarray,    "%s,%5.2 f",mmarray,avemm[x]);
              sprintf(latarray,   "%s,%6.3 f",latarray,lat[x]);
              sprintf(lonarray,   "%s,%6.3 f",lonarray,lon[x]);
              sprintf(utsarray,   "%s,%6.2 f",utsarray,uts[x]);
       }
       for (x=1; x < 10; x++){
              sprintf(flagarray,"%s,%    d",flagarray,flags[x]);
       }
```

```
//     printf ("%s %s\n", c_date, c_time);

       sprintf(sql_write,
        "INSERT INTO %s "
        "(occultation, cmc_data, injectionstamp, datetimestamp,"
        "lat_ref, long_ref, cmc_high, z,t,p,d, ave_mm, lat, long, uts, flags)"
        "VALUES "
        "('%s','%s','now','%s %s',%6.3f,%6.3f,"
        "%f,'{%s}','{%s}','{%s}','{%s}','{%s}','{%s}','{%s}','{%s}','{%s}')",
        c_tablename2,
        c_occultation, c_cmc_data, c_date, c_time,
        *lat_ref, *long_ref, *cmchigh,
        zarray,tarray,parray,darray,mmarray,
        latarray,lonarray,utsarray,flagarray);

      res = sql_insert(conn,sql_write);

       PQclear(res);           /* Clear the query  */
       sql_closeconn(conn);
       return(0);
}

/*--------------------------------------------------------------------------*/

int getapriori_tp_ (occultation, tablename, injectionstamp, datetimestamp,
cmc_data,  lat_ref, lon_ref, cmc_high, gp,  z,t,p,d,ave_mm, lat,lon,uts, flags,
len_occultation, len_tablename, len_injectionstamp, len_datetimestamp,
len_cmc_data)

char *occultation, *injectionstamp, *datetimestamp, *tablename, *cmc_data;

long len_occultation, len_tablename, len_injectionstamp, len_datetimestamp,
len_cmc_data;
long *gp;

int *flags;

float *lat_ref, *lon_ref, *cmc_high;
float *z, *t, *p, *d, *ave_mm;
float *lat, *lon, *uts;

{
    char sql_query[8192];
    char *c_occultation;
    char *c_tablename;
    char *c_injectionstamp;
    char *c_datetimestamp;
    int i, id, retval;

    PGconn *conn;
    PGresult *res;

    c_occultation = f77word( occultation, len_occultation );
    c_tablename   = f77word( tablename,   len_tablename );

    sddbg( "c_occultation: %s", c_occultation );
    sddbg( "c_tablename:   %s", c_tablename );

    /* Connect to climatology database */
    conn = PQconnectdb(connstr("climatology"));
    sql_checkconn(conn);
```

Appendix 1

```
//     printf ("%s\n%s\n\n", c_tablename, c_occultation);

    sprintf( sql_query,
    "SELECT injectionstamp,datetimestamp,cmc_data,lat_ref,long_ref,cmc_high, "
    "z,t,p,d,ave_mm,lat,long,uts,flags FROM %s WHERE occultation = '%s' "
    "ORDER BY id DESC LIMIT 1;",
     c_tablename, c_occultation);

      res = sql_exec(conn,sql_query);

       i = cstring2f77(PQgetvalue(res,0,0), injectionstamp,len_injectionstamp);
       i = cstring2f77(PQgetvalue(res,0,1), datetimestamp, len_datetimestamp);
       i = cstring2f77(PQgetvalue(res,0,2), cmc_data, len_cmc_data);

       *lon_ref  = (float)getval(res,0,3);
       *lat_ref  = (float)getval(res,0,4);
       *cmc_high = (float)getval(res,0,5);

       i = sqlarray2float(PQgetvalue(res,0,6), z, *gp);
       i = sqlarray2float(PQgetvalue(res,0,7), t, *gp);
       i = sqlarray2float(PQgetvalue(res,0,8), p, *gp);
       i = sqlarray2float(PQgetvalue(res,0,9), d, *gp);
       i = sqlarray2float(PQgetvalue(res,0,10), ave_mm, *gp);
       i = sqlarray2float(PQgetvalue(res,0,11), lat, *gp);
       i = sqlarray2float(PQgetvalue(res,0,12), lon, *gp);
       i = sqlarray2float(PQgetvalue(res,0,13), uts, *gp);
       i = sqlarray2int (PQgetvalue(res,0,14), flags, 10);

    PQclear(res);             /* Clear the query            */
    sql_closeconn(conn);

    return(0);
}
```

E) drao.c

```
#include "aceql.h"
#include "debug.h"
#include "config.h"
#include <stdio.h>
#include <string.h>
#include <stdlib.h>

// Program writes solar flux emails from DRAO to the database 3 times per day
// and finds the average

// To compile:
// cc -I../acelib/include -I/usr/local/pgsql/include -c filename.c
// f77 -L../acelib -R../acelib -o executable filename.o -lace -lpq

// To run:
// cat inputfilename | executable

int main(void)
{
	PGconn *conn;
	PGresult *res;
	FILE *infile;

	int i, j, k, max, hr, mtype, m[3];

	char input[1000][80], d[12], date[32], hr_ch[4];
	char sql_check[96], sql_query[1096], sql_write[1096];
	char fstr[8], tstr[8], daily_ave[8];

	float flux, fluxq[3], fluxes[3], fluxsum, flux_ave;

	//Must read date, hour, flux, measurement type from the email

	i = 0;
	max = 500;
	while (i < max){
		fscanf(stdin,"%s",input[i]);
		if(input[i][0]=='U' &&input[i][1]=='R'
		&&input[i][2]=='A' &&input[i][3]=='N' &&input[i][4]=='J'){
			i = 0;
		}
		else if(input[i][0]=='d' &&input[i][1]=='d'
			&&input[i][2]=='2'&&input[i][3]=='.' &&input[i][4]=='d'){
			i = 319;
		}
		else if(input[i][0]=='F' &&input[i][1]=='M'){
			i = 321;
			max = 323;
		}
//		printf("%d %s\n",i, input[i]);
		i++;
	}

	sprintf (hr_ch, "%c%c\0",input[15][0],input[15][1]);
	hr = atoi(hr_ch);

	sprintf (d, "%s",input[17]);
	sprintf (date, "%c%c%c%c-%c%c-%c%c 00:00:00+00\0",
```

Appendix 1

```
              d[0],d[1],d[2],d[3],d[5],d[6],d[8],d[9]);

       flux = (float) atof(input[32]);
       sprintf (fstr, "%3.1f", flux);

       printf ("date = %s  hr = %d  flux = %f \n", date, hr, flux);

       if (atoi(input[322]) == 2) {mtype = 1; sprintf (tstr, "1");}
       if (atoi(input[322]) == 1) {mtype = 2, sprintf (tstr, "2");}
       printf ("mtype = %d, tstr = %s\n", mtype, tstr);
//     FM - 2 means primary flux measurement used
//     FM - 1 means secondary flux measurement used (but it seems backwards)

//     printf ("max %d\n", max);
//     for (i=0; i < max; i++ ){
//           printf("II %d %s\n",i, input[i]);
//     }

       check_pgenv_();
       check_dbgenv_();
       conn = PQconnectdb(connstr("climatology"));
       res = sql_insert(conn, "SET timezone TO UTC;");

       fluxq[0] = 0;
       fluxq[1] = 0;
       fluxq[2] = 0;

       sprintf(sql_check,"SELECT flux1,flux,flux3 FROM solar_drao_email "
       "WHERE date ='%s';",date);
       res = sql_exec(conn, sql_check);
       if ( PQntuples(res) > 0 ) {
             fluxq[0] = getval(res,0,0);
             fluxq[1] = getval(res,0,1);
             fluxq[2] = getval(res,0,2);
       }
//     printf ("RESULT = %f %f %f\n", fluxq[0], fluxq[1], fluxq[2]);

if (hr==17) {m[0]=mtype; fluxes[0]=flux; fluxes[1]=fluxq[1]; fluxes[2]=fluxq[2];}
if (hr==18) {m[0]=mtype; fluxes[0]=flux; fluxes[1]=fluxq[1]; fluxes[2]=fluxq[2];}
if (hr==20) {m[1]=mtype; fluxes[1]=flux; fluxes[0]=fluxq[0]; fluxes[2]=fluxq[2];}
if (hr==22) {m[2]=mtype; fluxes[2]=flux; fluxes[0]=fluxq[0]; fluxes[1]=fluxq[1];}
if (hr==23) {m[2]=mtype; fluxes[2]=flux; fluxes[0]=fluxq[0]; fluxes[1]=fluxq[1];}

       k = 0;
       if (fluxes[0] > 0.001) {k++;}
       if (fluxes[1] > 0.001) {k++;}
       if (fluxes[2] > 0.001) {k++;}

       fluxsum = fluxes[0] + fluxes[1] + fluxes[2];
       flux_ave = fluxsum/((float)k);

//     printf ("flux_ave = %f\n", flux_ave);
       sprintf (daily_ave, "%3.1f",flux_ave);

       // Write data to climatology database

       if((hr==17 || hr==18) && fluxq[0]<=0.001 && fluxq[1]<=0.001 && fluxq[2]<=0.001)
       {
             sprintf (sql_write, "INSERT into solar_drao_email "
             "(date, flux1, hr1, mt1, daily_ave)"
             " VALUES ('%s','%s',%d,'%s','%s');", date, fstr, hr, tstr, fstr);
```

```
	}
	else if (hr==17 || hr==18) {
		sprintf (sql_write, "UPDATE solar_drao_email SET flux1 = '%s', "
		"hr1 = %d, mt1 = '%s', daily_ave = '%s'"
		" WHERE date = '%s';", fstr, hr, tstr, daily_ave, date);
	}

	if (hr==20 && fluxq[0]<=0.001 && fluxq[1]<=0.001 && fluxq[2]<=0.001) {
		sprintf (sql_write, "INSERT into solar_drao_email "
		"(date, flux, hr, mt, daily_ave) "
		"VALUES('%s', '%s', %d, '%s', '%s');", date, fstr, hr, tstr, fstr);
	}
	else if (hr==20) {
		sprintf (sql_write, "UPDATE solar_drao_email SET flux = '%s', "
		"hr = %d, mt = '%s', daily_ave = '%s'"
		" WHERE date = '%s';", fstr, hr, tstr, daily_ave, date);
	}

	if((hr==22 || hr==23) && fluxq[0]<=0.001 && fluxq[1]<=0.001 && fluxq[2]<=0.001)
	{
		sprintf (sql_write, "INSERT into solar_drao_email "
		"(date, flux3, hr3, mt3, daily_ave) "
		"VALUES('%s', '%s', %d, '%s', '%s');", date, fstr, hr, tstr, fstr);
	}
	else if (hr==22 || hr==23) {
		sprintf (sql_write, "UPDATE solar_drao_email SET flux3 = '%s', "
		"hr3 = %d, mt3 = '%s', daily_ave = '%s'"
		" WHERE date = '%s';", fstr, hr, tstr, daily_ave, date);
	}
	printf ("%s\n", sql_write);

	sql_checkconn(conn);
	res = sql_insert(conn,sql_write);

	PQclear(res);		//Clear the query
	sql_closeconn(conn);

return(0);
}
```

Appendix 1

F) geoupgfz.c

```
#include "aceql.h"
#include "debug.h"
#include "config.h"
#include <stdio.h>
#include <string.h>
#include <stdlib.h>

//     open and read file
//     separate into yyyy mm dd kp ap etc.
//     write to database

// To compile:
// cc -Iacelib/include -I/usr/local/pgsql/include -c geoupgfz.c
// f77 -L.. -o geoupgfz geoupgfz.o -lace -lpq

void main(int argc, char *argv[])
{
       PGconn *conn;
       PGresult *res;
       FILE *infile;

       int g, h, i, j, k;
       int year, days, line;
       int ap[9], kp[8], kpnum;

       char archive_file[1096];
       char ch[72];
       char year_ch[2];
       char ap_ch[3], aparray[24];
       char kp_ch[2], kparray[16];
       char fullkp[2], fullkparray[24];
       char kpnum_ch[4], kpsum[4], kp2D[8][2];

       static char date[10];
       char sql_write[1096], sql_check[1096];

       if (argc < 2) {
              printf("Call the program as geoupgfz filename\n");
              exit(1);
       }

       if (argc == 2){
              sprintf(archive_file,"../Solar_Geomagnetic/KP_AP/%s",argv[1]);
              //printf("%s\n",archive_file);
       }

       if ((infile = fopen(archive_file, "r"))==NULL){
              printf("Cannot open source file\n");
              exit(1);
       }

       check_pgenv_();
       check_dbgenv_();
       conn = PQconnectdb(connstr("climatology"));

       days = 366;
       line = 1;
       while (line <= days){
```

```
        i=0;
        while (i <= 72){
                ch[i] = getc(infile);
                if (ch[i] == ' ' && i < 6) ch[i] = '0';
                if (ch[i] == '\n') break;
                if (ch[i] == EOF) line = days;
                i++;
        }
        sprintf(year_ch, "%c%c",ch[0],ch[1]);
        year = 2000 + atoi(year_ch);
        sprintf (date, "%d-%c%c-%c%c +00", year,ch[2],ch[3],ch[4],ch[5]);

// KP and FULL KP
        h=0;
        for (h=0; h < 8; h++) {
                sprintf(kp_ch, "%c%c", ch[2*h+12],'\0');
                kp[h] = atoi(kp_ch);

                if (ch[2*h+13] == '3')sprintf (fullkp, "%d+",kp[h]);
                else if (ch[2*h+13] == '0') sprintf (fullkp, "%d",kp[h]);
                else if (ch[2*h+13] == '7') sprintf (fullkp, "%d-", kp[h]+1);

                kp2D[h][0] = fullkp[0];
                kp2D[h][1] = fullkp[1];
                if (h == 0) {
                  sprintf (fullkparray,"%c%c%c",kp2D[h][0],kp2D[h][1],'\0');
                  //sprintf (kparray, "%c%c", kp2D[h][0],'\0');
                }
                else {

  sprintf(fullkparray,"%s,%c%c%c",fullkparray,kp2D[h][0],kp2D[h][1],'\0');

                        //sprintf (kparray,"%s,%c%c",kparray,kp2D[h][0],'\0');
                }
        }

// FULL KP SUM
        sprintf (kpnum_ch, "%c%c%c", ch[28],ch[29],'\0');
        kpnum = atoi(kpnum_ch);

        if (ch[30] == '3')sprintf (kpsum, "%d+",kpnum);
        else if (ch[30] == '0') sprintf (kpsum, "%d",kpnum);
        else if (ch[30] == '7') sprintf (kpsum, "%d-", kpnum+1);

// AP ARRAY and AP AVERAGE
        j=0;
        for (j=0; j <=8; j++) {
                sprintf (ap_ch,"%c%c%c", ch[3*j+31],ch[3*j+32],ch[3*j+33]);
                ap[j] = atoi(ap_ch);
        }
        k=0;
        sprintf (aparray, "%d",ap[0]);
        for (k=1; k<8; k++){
                sprintf (aparray,"%s,%d",aparray,ap[k]);
        }
        line++;
        if (line > days) break;

// Write data to climatology database

        sprintf(sql_check,"SELECT ap_avg FROM solar_activity_archive "
```

Appendix 1

```
            "WHERE date = '%s';",date);
            res = sql_exec(conn, sql_check);

            if (PQntuples(res) == 0) {
                  sprintf(sql_write, "INSERT INTO solar_activity_archive "
                  "(date, kp_full, kp_sum, ap, ap_avg) "
                  "VALUES ('%s','{%s}','%s','{%s}','%d')\n", date, fullkparray,
                  kpsum, aparray, ap[8]);

                  printf("(date, kp_full, kp_sum, ap, ap_avg) "
                  "VALUES ('%s','{%s}','%s','{%s}','%d') INSERTED\n", date,
                  fullkparray, kpsum, aparray, ap[8]);
            }
            else   {
                  sprintf(sql_write, "UPDATE solar_activity_archive SET "
                  "kp_full = '{%s}', kp_sum = '%s', ap = '{%s}', ap_avg = '%d' "
                  "WHERE date = '%s'\n", fullkparray,kpsum,aparray,ap[8],date);
                  printf("(date, kp_full, kp_sum, ap, ap_avg) "
                  "VALUES ('%s','{%s}','%s','{%s}','%d') UPDATED\n", date,
                  fullkparray, kpsum, aparray, ap[8]);
            }
      sql_checkconn(conn);
      res = sql_insert(conn,sql_write);
      }
      printf ("\n");
      fclose(infile);
      PQclear(res);           //Clear the query
      sql_closeconn(conn);
}
```

Appendix 2: Chlorine Tables

Appendix 2

Table A2-1: Northern high latitude VMR profiles of chlorine-containing species, CCl_y, Cl_y and Cl_{TOT} in ppbv. Trailing zeros are not necessarily significant.

z/km	CH_3Cl	CCl_4	CFC11	CFC12	CFC113	HCFC22	HCFC142b	CH_3CCl_3	CFC114	CFC114a	CFC115
10.5	0.64031	0.10027	0.23390	0.49961	0.06622	0.16230	0.01169	0.02522	0.01333	0.00151	0.00636
11.5	0.58251	0.08838	0.22698	0.49245	0.06261	0.16865	0.01306	0.02469	0.01326	0.00149	0.00633
12.5	0.54440	0.07638	0.21781	0.48111	0.05738	0.16261	0.01350	0.02429	0.01321	0.00147	0.00630
13.5	0.51579	0.07632	0.20460	0.46139	0.05729	0.15994	0.01149	0.02301	0.01305	0.00142	0.00623
14.5	0.46653	0.06644	0.18911	0.44761	0.05345	0.15663	0.01446	0.02115	0.01282	0.00136	0.00612
15.5	0.42865	0.05898	0.17088	0.42858	0.03791	0.15591	0.01366	0.01922	0.01257	0.00129	0.00602
16.5	0.39662	0.04848	0.15171	0.40604	0.02867	0.15016	0.01329	0.01730	0.01233	0.00122	0.00591
17.5	0.34492	0.03483	0.12827	0.37776	0.02500	0.14955	0.01361	0.01460	0.01197	0.00112	0.00577
18.5	0.29217	0.02599	0.09931	0.34288	0.01600	0.13916	0.01334	0.01164	0.01154	0.00101	0.00561
19.5	0.26037	0.01766	0.07538	0.31331	0.00800	0.13803	0.01252	0.00938	0.01117	0.00091	0.00547
20.5	0.23128	0.01584	0.05249	0.28946	0.00200	0.13879	0.01228	0.00771	0.01085	0.00083	0.00537
21.5	0.20270	0.00938	0.03385	0.25862	0.00000	0.13253	0.01194	0.00602	0.01047	0.00074	0.00524
22.5	0.18322	0.00350	0.02599	0.21843	0.00000	0.12827	0.01157	0.00441	0.00997	0.00062	0.00510
23.5	0.14393	0.00000	0.01812	0.17609	0.00000	0.11412	0.01117	0.00333	0.00943	0.00051	0.00496
24.5	0.09815	0.00000	0.01199	0.13847	0.00000	0.10513	0.01075	0.00250	0.00890	0.00039	0.00484
25.5	0.06643	0.00000	0.00666	0.10428	0.00000	0.09436	0.01034	0.00200	0.00839	0.00029	0.00473
26.5	0.03527	0.00000	0.00437	0.07410	0.00000	0.08642	0.00978	0.00160	0.00798	0.00021	0.00466
27.5	0.01764	0.00000	0.00250	0.05507	0.00000	0.07944	0.00904	0.00127	0.00731	0.00000	0.00461
28.5	0.00588	0.00000	0.00128	0.04405	0.00000	0.07394	0.00830	0.00100	0.00691	0.00000	0.00457
29.5	0.00353	0.00000	0.00040	0.03305	0.00000	0.06954	0.00760	0.00073	0.00636	0.00000	0.00455
30.5	0.00176	0.00000	0.00017	0.02341	0.00000	0.06551	0.00699	0.00050	0.00592	0.00000	0.00453
31.5	0.00088	0.00000	0.00007	0.01515	0.00000	0.06175	0.00651	0.00033	0.00556	0.00000	0.00452
32.5	0.00044	0.00000	0.00002	0.00682	0.00000	0.05810	0.00612	0.00023	0.00524	0.00000	0.00451
33.5	0.00024	0.00000	0.00001	0.00434	0.00000	0.05452	0.00576	0.00017	0.00494	0.00000	0.00450
34.5	0.00012	0.00000	0.00001	0.00434	0.00000	0.05150	0.00543	0.00013	0.00465	0.00000	0.00449
35.5	0.00006	0.00000	0.00000	0.00248	0.00000	0.04915	0.00511	0.00010	0.00436	0.00000	0.00449
36.5	0.00003	0.00000	0.00000	0.00248	0.00000	0.04702	0.00480	0.00007	0.00412	0.00000	0.00448
37.5	0.00000	0.00000	0.00000	0.00155	0.00000	0.04499	0.00453	0.00005	0.00393	0.00000	0.00448
38.5	0.00000	0.00000	0.00000	0.00155	0.00000	0.04308	0.00432	0.00003	0.00376	0.00000	0.00448
39.5	0.00000	0.00000	0.00000	0.00093	0.00000	0.04134	0.00414	0.00000	0.00360	0.00000	0.00448
40.5	0.00000	0.00000	0.00000	0.00093	0.00000	0.03986	0.00396	0.00000	0.00345	0.00000	0.00448
41.5	0.00000	0.00000	0.00000	0.00058	0.00000	0.03856	0.00379	0.00000	0.00331	0.00000	0.00448
42.5	0.00000	0.00000	0.00000	0.00058	0.00000	0.03729	0.00364	0.00000	0.00319	0.00000	0.00448
43.5	0.00000	0.00000	0.00000	0.00035	0.00000	0.03607	0.00351	0.00000	0.00308	0.00000	0.00447
44.5	0.00000	0.00000	0.00000	0.00035	0.00000	0.03488	0.00339	0.00000	0.00298	0.00000	0.00447
45.5	0.00000	0.00000	0.00000	0.00023	0.00000	0.03376	0.00328	0.00000	0.00289	0.00000	0.00447
46.5	0.00000	0.00000	0.00000	0.00023	0.00000	0.03275	0.00317	0.00000	0.00279	0.00000	0.00447
47.5	0.00000	0.00000	0.00000	0.00015	0.00000	0.03181	0.00307	0.00000	0.00270	0.00000	0.00447
48.5	0.00000	0.00000	0.00000	0.00015	0.00000	0.03090	0.00297	0.00000	0.00262	0.00000	0.00447
49.5	0.00000	0.00000	0.00000	0.00010	0.00000	0.03002	0.00288	0.00000	0.00254	0.00000	0.00447
50.5	0.00000	0.00000	0.00000	0.00010	0.00000	0.02914	0.00280	0.00000	0.00247	0.00000	0.00447
51.5	0.00000	0.00000	0.00000	0.00007	0.00000	0.02838	0.00272	0.00000	0.00240	0.00000	0.00447
52.5	0.00000	0.00000	0.00000	0.00007	0.00000	0.02801	0.00264	0.00000	0.00233	0.00000	0.00447
53.5	0.00000	0.00000	0.00000	0.00005	0.00000	0.02789	0.00256	0.00000	0.00227	0.00000	0.00447
54.5	0.00000	0.00000	0.00000	0.00005	0.00000	0.02777	0.00250	0.00000	0.00224	0.00000	0.00447

HCFC141b	Halon1211	HCl	$ClONO_2$	ClO	HOCl	$COCl_2$	COClF	ClOOCl	CCl_y	Cl_y	Cl_{TOT}
0.01987	0.00321	0.19709	0.00000	0.00000	0.00000	0.02200	0.00000	0.00000	3.26959	0.24109	3.51068
0.01941	0.00307	0.26099	0.00000	0.00000	0.00000	0.02300	0.00250	0.00000	3.12319	0.30949	3.43268
0.01907	0.00298	0.34688	0.10047	0.00000	0.00000	0.02400	0.00500	0.00000	2.96347	0.50035	3.46382
0.01805	0.00269	0.44241	0.07453	0.16931	0.00000	0.02500	0.00750	0.09937	2.84392	0.94248	3.78640
0.01665	0.00230	0.55605	0.11977	0.17493	0.00000	0.02600	0.01000	0.08821	2.65980	1.08916	3.74896
0.01531	0.00194	0.68722	0.17949	0.19721	0.00000	0.02700	0.01250	0.09395	2.44162	1.31831	3.75993
0.01406	0.00162	0.85926	0.22750	0.18806	0.00000	0.02850	0.01500	0.06870	2.22186	1.48422	3.70608
0.01239	0.00122	1.05250	0.30005	0.16341	0.00000	0.03000	0.01750	0.04185	1.96450	1.67715	3.64165
0.01066	0.00085	1.23810	0.37955	0.12506	0.00000	0.03100	0.01920	0.01926	1.66812	1.86242	3.53055
0.00935	0.00059	1.43260	0.46791	0.09620	0.00000	0.03200	0.02000	0.00874	1.43539	2.09818	3.53357
0.00837	0.00042	1.64930	0.55681	0.09134	0.00000	0.03200	0.01920	0.00589	1.25713	2.39243	3.64957
0.00732	0.00027	1.84660	0.61185	0.08704	0.00051	0.02800	0.01750	0.00399	1.06412	2.62749	3.69161
0.00618	0.00014	1.99880	0.65116	0.08993	0.00306	0.02300	0.01500	0.00324	0.90390	2.81043	3.71433
0.00516	0.00007	2.12980	0.68652	0.09146	0.00465	0.01800	0.01250	0.00260	0.72098	2.96614	3.68712
0.00430	0.00003	2.23120	0.71643	0.07815	0.00791	0.01400	0.01000	0.00146	0.56648	3.07461	3.64109
0.00359	0.00001	2.31520	0.74478	0.06380	0.01469	0.01000	0.00750	0.00072	0.43497	3.16742	3.60239
0.00306	0.00000	2.42690	0.78109	0.05995	0.02157	0.00500	0.00500	0.00047	0.32473	3.30545	3.63018
0.00263	0.00000	2.53170	0.80009	0.06591	0.02805	0.00001	0.00250	0.00000	0.25204	3.42827	3.68031
0.00231	0.00000	2.61050	0.79012	0.08250	0.03335	0.00000	0.00000	0.00000	0.20609	3.51647	3.72256
0.00208	0.00000	2.65670	0.74403	0.11327	0.03835	0.00000	0.00000	0.00000	0.17158	3.55235	3.72393
0.00189	0.00000	2.69620	0.68722	0.16135	0.04269	0.00000	0.00000	0.00000	0.14321	3.58746	3.73067
0.00173	0.00000	2.72780	0.62588	0.21783	0.04804	0.00000	0.00000	0.00000	0.11974	3.61955	3.73929
0.00160	0.00000	2.75340	0.57000	0.27834	0.05636	0.00000	0.00000	0.00000	0.09727	3.65809	3.75536
0.00149	0.00000	2.76140	0.48160	0.34902	0.06773	0.00000	0.00000	0.00000	0.08710	3.65975	3.74685
0.00141	0.00000	2.75500	0.39939	0.42781	0.07925	0.00000	0.00000	0.00000	0.08278	3.66145	3.74423
0.00135	0.00000	2.75190	0.27421	0.50191	0.08976	0.00000	0.00000	0.00000	0.07549	3.61778	3.69328
0.00131	0.00000	2.76240	0.13769	0.56764	0.09654	0.00000	0.00000	0.00000	0.07235	3.56427	3.63662
0.00128	0.00000	2.78810	0.05782	0.62303	0.09812	0.00000	0.00000	0.00000	0.06767	3.56708	3.63476
0.00125	0.00000	2.82530	0.02868	0.66070	0.09721	0.00000	0.00000	0.00000	0.06510	3.61189	3.67699
0.00122	0.00000	2.86100	0.01147	0.67777	0.09389	0.00000	0.00000	0.00000	0.06146	3.64413	3.70559
0.00120	0.00000	2.89660	0.00574	0.68301	0.08762	0.00000	0.00000	0.00000	0.05946	3.67296	3.73242
0.00119	0.00000	2.94740	0.00115	0.68022	0.08068	0.00000	0.00000	0.00000	0.05697	3.70945	3.76642
0.00117	0.00000	3.01450	0.00057	0.66158	0.07589	0.00000	0.00000	0.00000	0.05528	3.75254	3.80782
0.00115	0.00000	3.09090	0.00011	0.62354	0.06997	0.00000	0.00000	0.00000	0.05322	3.78453	3.83775
0.00113	0.00000	3.17600	0.00001	0.56746	0.06538	0.00000	0.00000	0.00000	0.05169	3.80885	3.86054
0.00112	0.00000	3.25830	0.00001	0.50455	0.05957	0.00000	0.00000	0.00000	0.04998	3.82243	3.87241
0.00111	0.00000	3.36410	0.00001	0.43081	0.05345	0.00000	0.00000	0.00000	0.04865	3.84837	3.89702
0.00110	0.00000	3.46910	0.00001	0.37444	0.04733	0.00000	0.00000	0.00000	0.04725	3.89088	3.93813
0.00110	0.00000	3.56550	0.00001	0.31979	0.04090	0.00000	0.00000	0.00000	0.04608	3.92620	3.97228
0.00109	0.00000	3.62550	0.00001	0.26787	0.03448	0.00000	0.00000	0.00000	0.04485	3.92785	3.97270
0.00109	0.00000	3.67710	0.00001	0.22476	0.02981	0.00000	0.00000	0.00000	0.04374	3.93168	3.97542
0.00109	0.00000	3.73170	0.00001	0.17000	0.02514	0.00000	0.00000	0.00000	0.04269	3.92685	3.96955
0.00109	0.00000	3.78860	0.00001	0.14000	0.01905	0.00000	0.00000	0.00000	0.04210	3.94766	3.98976
0.00108	0.00000	3.83100	0.00001	0.12000	0.01295	0.00000	0.00000	0.00000	0.04173	3.96397	4.00570
0.00108	0.00000	3.86760	0.00001	0.09000	0.00673	0.00000	0.00000	0.00000	0.04148	3.96434	4.00582

Appendix 2

Table A2-2: Northern midlatitude VMR profiles of chlorine-containing species, CCl_y, Cl_y and Cl_{TOT} in ppbv. Trailing zeros are not necessarily significant.

z/km	CH_3Cl	CCl_4	CFC11	CFC12	CFC113	HCFC22	HCFC142b	CH_3CCl_3	CFC114	CFC114a	CFC115
10.5	0.78966	0.10824	0.23399	0.50085	0.06324	0.16560	0.01179	0.02590	0.01341	0.00153	0.00640
11.5	0.65775	0.11092	0.23371	0.50208	0.06348	0.17054	0.01204	0.02608	0.01344	0.00154	0.00641
12.5	0.60602	0.10040	0.22478	0.48443	0.05962	0.16651	0.01197	0.02431	0.01321	0.00147	0.00630
13.5	0.55255	0.08280	0.21234	0.46819	0.05940	0.16169	0.01359	0.02327	0.01308	0.00143	0.00624
14.5	0.51833	0.07391	0.20252	0.45639	0.05548	0.16170	0.01318	0.02203	0.01292	0.00139	0.00617
15.5	0.48792	0.07342	0.19331	0.45484	0.04516	0.16364	0.01587	0.02121	0.01282	0.00136	0.00613
16.5	0.45460	0.06189	0.17905	0.43974	0.03550	0.16131	0.01354	0.01959	0.01262	0.00130	0.00604
17.5	0.40847	0.04930	0.15742	0.41597	0.03100	0.15519	0.01368	0.01724	0.01232	0.00122	0.00591
18.5	0.35632	0.04024	0.13606	0.38878	0.02500	0.14895	0.01268	0.01437	0.01194	0.00111	0.00576
19.5	0.31970	0.03401	0.10714	0.35771	0.01700	0.14480	0.01243	0.01175	0.01156	0.00101	0.00561
20.5	0.28203	0.02254	0.08897	0.33326	0.00900	0.13310	0.01225	0.00999	0.01128	0.00094	0.00551
21.5	0.25989	0.01308	0.06409	0.29958	0.00000	0.13568	0.01210	0.00787	0.01089	0.00084	0.00538
22.5	0.22091	0.00958	0.04919	0.27344	0.00000	0.14229	0.01186	0.00640	0.01056	0.00076	0.00527
23.5	0.19497	0.00500	0.03431	0.24282	0.00000	0.13948	0.01153	0.00495	0.01016	0.00067	0.00515
24.5	0.17559	0.00227	0.02271	0.20077	0.00000	0.13744	0.01118	0.00369	0.00965	0.00055	0.00501
25.5	0.11886	0.00068	0.01262	0.16214	0.00000	0.12697	0.01079	0.00299	0.00914	0.00044	0.00489
26.5	0.06310	0.00023	0.00827	0.12169	0.00000	0.12215	0.01038	0.00250	0.00876	0.00036	0.00481
27.5	0.03155	0.00009	0.00473	0.08717	0.00000	0.11752	0.00999	0.00200	0.00836	0.00028	0.00473
28.5	0.01052	0.00000	0.00243	0.06975	0.00000	0.11109	0.00944	0.00160	0.00799	0.00021	0.00466
29.5	0.00631	0.00000	0.00076	0.05230	0.00000	0.10273	0.00873	0.00127	0.00769	0.00016	0.00462
30.5	0.00316	0.00000	0.00032	0.03705	0.00000	0.09436	0.00802	0.00100	0.00731	0.00000	0.00458
31.5	0.00158	0.00000	0.00013	0.02397	0.00000	0.08642	0.00735	0.00073	0.00670	0.00000	0.00456
32.5	0.00079	0.00000	0.00005	0.01079	0.00000	0.07944	0.00675	0.00050	0.00616	0.00000	0.00455
33.5	0.00042	0.00000	0.00002	0.00687	0.00000	0.07394	0.00629	0.00033	0.00573	0.00000	0.00454
34.5	0.00021	0.00000	0.00002	0.00687	0.00000	0.06954	0.00591	0.00023	0.00539	0.00000	0.00454
35.5	0.00011	0.00000	0.00000	0.00392	0.00000	0.06551	0.00557	0.00017	0.00508	0.00000	0.00453
36.5	0.00005	0.00000	0.00000	0.00392	0.00000	0.06175	0.00525	0.00013	0.00479	0.00000	0.00452
37.5	0.00001	0.00000	0.00000	0.00245	0.00000	0.05810	0.00494	0.00010	0.00450	0.00000	0.00452
38.5	0.00001	0.00000	0.00000	0.00245	0.00000	0.05452	0.00463	0.00007	0.00423	0.00000	0.00451
39.5	0.00001	0.00000	0.00000	0.00147	0.00000	0.05150	0.00438	0.00005	0.00399	0.00000	0.00451
40.5	0.00001	0.00000	0.00000	0.00147	0.00000	0.04915	0.00418	0.00003	0.00381	0.00000	0.00450
41.5	0.00001	0.00000	0.00000	0.00092	0.00000	0.04702	0.00400	0.00000	0.00364	0.00000	0.00450
42.5	0.00001	0.00000	0.00000	0.00092	0.00000	0.04499	0.00382	0.00000	0.00349	0.00000	0.00450
43.5	0.00001	0.00000	0.00000	0.00056	0.00000	0.04308	0.00366	0.00000	0.00334	0.00000	0.00449
44.5	0.00001	0.00000	0.00000	0.00056	0.00000	0.04134	0.00351	0.00000	0.00320	0.00000	0.00449
45.5	0.00001	0.00000	0.00000	0.00036	0.00000	0.03986	0.00339	0.00000	0.00309	0.00000	0.00449
46.5	0.00001	0.00000	0.00000	0.00036	0.00000	0.03856	0.00328	0.00000	0.00299	0.00000	0.00448
47.5	0.00001	0.00000	0.00000	0.00024	0.00000	0.03729	0.00317	0.00000	0.00289	0.00000	0.00448
48.5	0.00001	0.00000	0.00000	0.00024	0.00000	0.03607	0.00307	0.00000	0.00280	0.00000	0.00448
49.5	0.00001	0.00000	0.00000	0.00016	0.00000	0.03488	0.00297	0.00000	0.00270	0.00000	0.00448
50.5	0.00001	0.00000	0.00000	0.00016	0.00000	0.03376	0.00287	0.00000	0.00262	0.00000	0.00447
51.5	0.00001	0.00000	0.00000	0.00011	0.00000	0.03275	0.00278	0.00000	0.00254	0.00000	0.00447
52.5	0.00001	0.00000	0.00000	0.00011	0.00000	0.03181	0.00270	0.00000	0.00247	0.00000	0.00447
53.5	0.00001	0.00000	0.00000	0.00008	0.00000	0.03090	0.00263	0.00000	0.00240	0.00000	0.00447
54.5	0.00001	0.00000	0.00000	0.00008	0.00000	0.03002	0.00255	0.00000	0.00233	0.00000	0.00447

HCFC141b	Halon1211	HCl	$ClONO_2$	ClO	HOCl	$COCl_2$	COClF	ClOOCl	CCl_y	Cl_y	Cl_{TOT}
0.02047	0.00339	0.16506	0.00000	0.00000	0.00000	0.02200	0.00000	0.00000	3.45172	0.20906	3.66078
0.02064	0.00343	0.19917	0.00000	0.00000	0.00000	0.02300	0.00000	0.00000	3.33906	0.24517	3.58423
0.01909	0.00298	0.25848	0.04181	0.00000	0.00000	0.02400	0.00050	0.00000	3.15793	0.34879	3.50672
0.01825	0.00274	0.33849	0.06917	0.00000	0.00000	0.02500	0.00200	0.00000	2.95496	0.45966	3.41461
0.01729	0.00248	0.41953	0.08206	0.09632	0.00000	0.02600	0.00400	0.00000	2.81357	0.65390	3.46747
0.01670	0.00231	0.51776	0.10010	0.15460	0.00000	0.02700	0.00650	0.00000	2.72004	0.83296	3.55301
0.01556	0.00201	0.65389	0.13566	0.18633	0.00000	0.02850	0.00900	0.00000	2.52592	1.04188	3.56780
0.01402	0.00162	0.80957	0.19365	0.19887	0.00000	0.03000	0.01207	0.00000	2.28612	1.27415	3.56028
0.01226	0.00119	0.98613	0.27263	0.12980	0.00000	0.03100	0.01690	0.00000	2.04031	1.46745	3.50777
0.01072	0.00086	1.16500	0.36599	0.09439	0.00000	0.03200	0.02259	0.00000	1.78912	1.71197	3.50110
0.00971	0.00066	1.34920	0.50428	0.07813	0.00087	0.03200	0.02856	0.00000	1.55794	2.02504	3.58298
0.00847	0.00044	1.48210	0.60688	0.06844	0.00522	0.02800	0.03457	0.00000	1.32125	2.25321	3.57446
0.00757	0.00030	1.59520	0.71645	0.06032	0.00794	0.02300	0.04068	0.00000	1.17042	2.46659	3.63701
0.00660	0.00018	1.68350	0.78919	0.05686	0.01349	0.01800	0.04599	0.00000	1.00959	2.62503	3.63462
0.00556	0.00009	1.75290	0.84126	0.05877	0.02506	0.01400	0.04915	0.00000	0.85065	2.75513	3.60578
0.00468	0.00004	1.84750	0.89017	0.06144	0.03680	0.01000	0.05066	0.00000	0.66394	2.90656	3.57050
0.00409	0.00002	1.97620	0.94783	0.06600	0.04785	0.00500	0.05146	0.00000	0.50349	3.09934	3.60283
0.00354	0.00001	2.09580	0.97362	0.07916	0.05690	0.00001	0.04972	0.00000	0.38306	3.25522	3.63828
0.00306	0.00000	2.20180	0.94721	0.10134	0.06542	0.00000	0.04356	0.00000	0.30981	3.35932	3.66913
0.00270	0.00000	2.29360	0.89533	0.13302	0.07282	0.00000	0.03401	0.00000	0.25416	3.42878	3.68293
0.00242	0.00000	2.36150	0.81578	0.17728	0.08195	0.00000	0.02483	0.00000	0.20763	3.46135	3.66898
0.00221	0.00000	2.43080	0.70532	0.22489	0.09614	0.00000	0.01761	0.00000	0.16824	3.47476	3.64300
0.00208	0.00000	2.50370	0.59476	0.26827	0.11554	0.00000	0.01167	0.00000	0.13123	3.49394	3.62517
0.00200	0.00000	2.56800	0.45742	0.31313	0.13520	0.00000	0.00745	0.00000	0.11545	3.48120	3.59666
0.00196	0.00000	2.62930	0.33204	0.35830	0.15312	0.00000	0.00464	0.00000	0.10938	3.47740	3.58678
0.00188	0.00000	2.68240	0.22804	0.40098	0.16469	0.00000	0.00277	0.00000	0.09798	3.47888	3.57686
0.00181	0.00000	2.73190	0.11457	0.43795	0.16739	0.00000	0.00100	0.00000	0.09302	3.45281	3.54583
0.00174	0.00000	2.78650	0.04809	0.47106	0.16582	0.00000	0.00000	0.00000	0.08526	3.47147	3.55672
0.00167	0.00000	2.84470	0.02385	0.50126	0.16017	0.00000	0.00000	0.00000	0.08057	3.52997	3.61054
0.00160	0.00000	2.90160	0.00954	0.51932	0.14947	0.00000	0.00000	0.00000	0.07466	3.57993	3.65459
0.00155	0.00000	2.96160	0.00477	0.51898	0.13763	0.00000	0.00000	0.00000	0.07160	3.62299	3.69459
0.00151	0.00000	3.01730	0.00095	0.50048	0.12946	0.00000	0.00000	0.00000	0.06766	3.64819	3.71585
0.00146	0.00000	3.05990	0.00048	0.46783	0.11936	0.00000	0.00000	0.00000	0.06506	3.64757	3.71263
0.00142	0.00000	3.10530	0.00010	0.42938	0.11153	0.00000	0.00000	0.00000	0.06187	3.64631	3.70818
0.00137	0.00000	3.17020	0.00001	0.38682	0.10162	0.00000	0.00000	0.00000	0.05961	3.65864	3.71825
0.00132	0.00000	3.25850	0.00001	0.33871	0.09118	0.00000	0.00000	0.00000	0.05728	3.68840	3.74568
0.00127	0.00000	3.33990	0.00001	0.28601	0.08074	0.00000	0.00000	0.00000	0.05556	3.70666	3.76222
0.00123	0.00000	3.40820	0.00001	0.23647	0.06977	0.00000	0.00000	0.00000	0.05366	3.71445	3.76811
0.00120	0.00000	3.49780	0.00001	0.19064	0.05881	0.00000	0.00000	0.00000	0.05207	3.74726	3.79933
0.00117	0.00000	3.57890	0.00001	0.15396	0.05085	0.00000	0.00000	0.00000	0.05039	3.78372	3.83411
0.00115	0.00000	3.62640	0.00001	0.12660	0.04289	0.00000	0.00000	0.00000	0.04896	3.79590	3.84486
0.00113	0.00000	3.66240	0.00001	0.09941	0.03249	0.00000	0.00000	0.00000	0.04757	3.79431	3.84189
0.00112	0.00000	3.70300	0.00001	0.07796	0.02210	0.00000	0.00000	0.00000	0.04639	3.80306	3.84945
0.00111	0.00000	3.72570	0.00001	0.07052	0.01148	0.00000	0.00000	0.00000	0.04518	3.80771	3.85289
0.00110	0.00000	3.72920	0.00001	0.04898	0.00087	0.00000	0.00000	0.00000	0.04407	3.77906	3.82313

Table A2-3: Tropical VMR profiles of chlorine-containing species, CCl_y, Cl_y and Cl_{TOT} in ppbv.
Trailing zeros are not necessarily significant.

z/km	CH_3Cl	CCl_4	CFC11	CFC12	CFC113	HCFC22	HCFC142b	CH_3CCl_3	CFC114	CFC114a	CFC115
10.5	0.94455	0.11761	0.24345	0.52541	0.05167	0.17857	0.00925	0.02827	0.01373	0.00163	0.00656
11.5	0.82252	0.10795	0.25213	0.53163	0.05829	0.17923	0.01009	0.02803	0.01370	0.00162	0.00654
12.5	0.77776	0.11035	0.25194	0.52693	0.06536	0.17620	0.01205	0.02772	0.01366	0.00161	0.00652
13.5	0.72541	0.10468	0.24831	0.51287	0.06486	0.17951	0.01404	0.02740	0.01361	0.00159	0.00650
14.5	0.67117	0.10985	0.24574	0.50523	0.06326	0.18095	0.01657	0.02715	0.01358	0.00158	0.00648
15.5	0.65888	0.10943	0.24975	0.51210	0.05990	0.17854	0.01838	0.02691	0.01355	0.00157	0.00647
16.5	0.62610	0.10608	0.25105	0.52080	0.05514	0.18510	0.01851	0.02661	0.01351	0.00156	0.00645
17.5	0.60853	0.10414	0.24812	0.51550	0.04400	0.18762	0.01839	0.02609	0.01344	0.00154	0.00641
18.5	0.57264	0.09546	0.23046	0.49886	0.03300	0.18057	0.01479	0.02451	0.01323	0.00148	0.00632
19.5	0.51494	0.08018	0.21007	0.47224	0.02200	0.17490	0.01427	0.02230	0.01296	0.00140	0.00619
20.5	0.45114	0.06660	0.19931	0.45328	0.01400	0.16196	0.01423	0.02033	0.01271	0.00133	0.00608
21.5	0.41087	0.05683	0.17737	0.43812	0.00600	0.16227	0.01419	0.01932	0.01259	0.00129	0.00602
22.5	0.42094	0.04600	0.13614	0.43017	0.00000	0.17422	0.01414	0.01841	0.01247	0.00126	0.00597
23.5	0.43638	0.03200	0.12000	0.41061	0.00000	0.17090	0.01407	0.01669	0.01225	0.00120	0.00588
24.5	0.39122	0.02000	0.10000	0.37578	0.00000	0.16359	0.01398	0.01367	0.01184	0.00109	0.00572
25.5	0.37000	0.01000	0.08000	0.35160	0.00000	0.15731	0.01384	0.01080	0.01141	0.00097	0.00556
26.5	0.33000	0.00500	0.06000	0.33300	0.00000	0.15511	0.01365	0.00915	0.01113	0.00090	0.00546
27.5	0.31000	0.00300	0.04000	0.29114	0.00000	0.15227	0.01340	0.00766	0.01084	0.00083	0.00536
28.5	0.28000	0.00150	0.02000	0.23286	0.00000	0.14918	0.01313	0.00597	0.01045	0.00074	0.00524
29.5	0.25000	0.00000	0.00800	0.17466	0.00000	0.14625	0.01287	0.00467	0.01007	0.00065	0.00513
30.5	0.22000	0.00000	0.00200	0.12377	0.00000	0.14407	0.01268	0.00382	0.00972	0.00057	0.00503
31.5	0.18000	0.00000	0.00000	0.08008	0.00000	0.14229	0.01252	0.00328	0.00940	0.00050	0.00495
32.5	0.14000	0.00000	0.00000	0.03603	0.00000	0.13951	0.01228	0.00300	0.00916	0.00045	0.00489
33.5	0.10000	0.00000	0.00000	0.02292	0.00000	0.13569	0.01194	0.00250	0.00896	0.00041	0.00485
34.5	0.07000	0.00000	0.00000	0.02292	0.00000	0.13152	0.01157	0.00200	0.00877	0.00037	0.00481
35.5	0.05000	0.00000	0.00000	0.01310	0.00000	0.12697	0.01117	0.00160	0.00854	0.00032	0.00476
36.5	0.03000	0.00000	0.00000	0.01310	0.00000	0.12215	0.01075	0.00127	0.00829	0.00027	0.00472
37.5	0.02000	0.00000	0.00000	0.00819	0.00000	0.11752	0.01034	0.00100	0.00803	0.00022	0.00467
38.5	0.01000	0.00000	0.00000	0.00819	0.00000	0.11109	0.00978	0.00073	0.00778	0.00017	0.00463
39.5	0.00000	0.00000	0.00000	0.00491	0.00000	0.10273	0.00904	0.00050	0.00731	0.00000	0.00460
40.5	0.00000	0.00000	0.00000	0.00491	0.00000	0.09436	0.00830	0.00033	0.00670	0.00000	0.00457
41.5	0.00000	0.00000	0.00000	0.00306	0.00000	0.08642	0.00760	0.00023	0.00616	0.00000	0.00455
42.5	0.00000	0.00000	0.00000	0.00306	0.00000	0.07944	0.00699	0.00017	0.00573	0.00000	0.00454
43.5	0.00000	0.00000	0.00000	0.00186	0.00000	0.07394	0.00651	0.00013	0.00539	0.00000	0.00453
44.5	0.00000	0.00000	0.00000	0.00186	0.00000	0.06954	0.00612	0.00010	0.00508	0.00000	0.00452
45.5	0.00000	0.00000	0.00000	0.00120	0.00000	0.06551	0.00576	0.00007	0.00479	0.00000	0.00451
46.5	0.00000	0.00000	0.00000	0.00120	0.00000	0.06175	0.00543	0.00005	0.00450	0.00000	0.00450
47.5	0.00000	0.00000	0.00000	0.00079	0.00000	0.05810	0.00511	0.00003	0.00423	0.00000	0.00449
48.5	0.00000	0.00000	0.00000	0.00079	0.00000	0.05452	0.00480	0.00000	0.00399	0.00000	0.00449
49.5	0.00000	0.00000	0.00000	0.00052	0.00000	0.05150	0.00453	0.00000	0.00381	0.00000	0.00448
50.5	0.00000	0.00000	0.00000	0.00052	0.00000	0.04915	0.00432	0.00000	0.00364	0.00000	0.00448
51.5	0.00000	0.00000	0.00000	0.00037	0.00000	0.04702	0.00414	0.00000	0.00349	0.00000	0.00448
52.5	0.00000	0.00000	0.00000	0.00037	0.00000	0.04499	0.00396	0.00000	0.00334	0.00000	0.00448
53.5	0.00000	0.00000	0.00000	0.00026	0.00000	0.04308	0.00379	0.00000	0.00320	0.00000	0.00448
54.5	0.00000	0.00000	0.00000	0.00026	0.00000	0.04134	0.00364	0.00000	0.00309	0.00000	0.00447

HCFC141b	Halon1211	HCl	$ClONO_2$	ClO	HOCl	$COCl_2$	COClF	ClOOCl	CCl_y	Cl_y	Cl_{TOT}
0.02283	0.00410	0.03185	0.00000	0.00000	0.00000	0.02200	0.00000	0.00000	3.71084	0.07585	3.78670
0.02258	0.00402	0.00000	0.00000	0.00000	0.00000	0.02300	0.00000	0.00000	3.60862	0.04600	3.65462
0.02224	0.00392	0.01177	0.01102	0.00000	0.00000	0.02400	0.00000	0.00000	3.58176	0.07079	3.65256
0.02191	0.00382	0.01372	0.00000	0.00000	0.00000	0.02500	0.00000	0.00000	3.46968	0.06372	3.53340
0.02167	0.00374	0.03009	0.00073	0.00000	0.00000	0.02600	0.00000	0.00000	3.41087	0.08281	3.49369
0.02142	0.00367	0.03308	0.00805	0.00000	0.00000	0.02700	0.00150	0.00000	3.41062	0.09663	3.50725
0.02114	0.00358	0.06494	0.00219	0.00000	0.00000	0.02850	0.00300	0.00000	3.37648	0.12713	3.50361
0.02065	0.00344	0.12668	0.00000	0.00000	0.00000	0.03000	0.00500	0.00000	3.29783	0.19168	3.48951
0.01926	0.00303	0.24661	0.00504	0.00000	0.00000	0.03100	0.00750	0.00000	3.08877	0.32115	3.40992
0.01750	0.00253	0.40901	0.06328	0.13460	0.00100	0.03200	0.01000	0.00000	2.80484	0.68189	3.48673
0.01607	0.00215	0.57524	0.14144	0.09791	0.00600	0.03200	0.01447	0.00000	2.56965	0.89907	3.46871
0.01538	0.00196	0.72228	0.23833	0.10850	0.00913	0.02800	0.03005	0.00000	2.36547	1.16429	3.52975
0.01477	0.00181	0.85411	0.34638	0.06207	0.01550	0.02300	0.04581	0.00000	2.18206	1.36987	3.55193
0.01367	0.00153	0.96569	0.45791	0.04254	0.02880	0.01800	0.06243	0.00000	2.04231	1.59337	3.63568
0.01184	0.00110	1.05240	0.54265	0.04211	0.04230	0.01400	0.07783	0.00000	1.79771	1.78529	3.58301
0.01017	0.00075	1.13310	0.62047	0.04822	0.05500	0.01000	0.08875	0.00000	1.60817	1.96554	3.57370
0.00922	0.00057	1.25350	0.71211	0.05866	0.06540	0.00500	0.09463	0.00000	1.44074	2.19430	3.63504
0.00834	0.00042	1.40240	0.78341	0.07180	0.07520	0.00001	0.09819	0.00000	1.25876	2.43102	3.68977
0.00729	0.00027	1.55580	0.80423	0.09135	0.08370	0.00000	0.09671	0.00000	1.03442	2.63179	3.66621
0.00639	0.00016	1.71680	0.77999	0.11566	0.09420	0.00000	0.08302	0.00000	0.83597	2.78967	3.62563
0.00568	0.00010	1.87360	0.71591	0.14131	0.11050	0.00000	0.06188	0.00000	0.67880	2.90320	3.58200
0.00511	0.00006	2.02560	0.64865	0.16696	0.13280	0.00000	0.04344	0.00000	0.53986	3.01744	3.55730
0.00470	0.00004	2.17060	0.57191	0.19510	0.15540	0.00000	0.02911	0.00000	0.40639	3.12212	3.52851
0.00440	0.00003	2.30350	0.45868	0.22763	0.17600	0.00000	0.01856	0.00000	0.33339	3.18437	3.51776
0.00411	0.00002	2.43060	0.34497	0.26414	0.18930	0.00000	0.01147	0.00000	0.29627	3.24048	3.53675
0.00379	0.00002	2.53720	0.23694	0.30254	0.19240	0.00000	0.00686	0.00000	0.24925	3.27594	3.52519
0.00346	0.00001	2.64110	0.11891	0.33657	0.19060	0.00000	0.00200	0.00000	0.22167	3.28918	3.51085
0.00312	0.00000	2.73300	0.04997	0.36402	0.18410	0.00000	0.00000	0.00000	0.19466	3.33108	3.52574
0.00280	0.00000	2.81820	0.02478	0.38311	0.17180	0.00000	0.00000	0.00000	0.17558	3.39790	3.57348
0.00254	0.00000	2.89840	0.00991	0.38957	0.15820	0.00000	0.00000	0.00000	0.14739	3.45609	3.60348
0.00231	0.00000	2.97920	0.00496	0.38404	0.14880	0.00000	0.00000	0.00000	0.13608	3.51699	3.65308
0.00213	0.00000	3.04930	0.00099	0.37552	0.13720	0.00000	0.00000	0.00000	0.12197	3.56301	3.68498
0.00199	0.00000	3.11490	0.00050	0.36005	0.12820	0.00000	0.00000	0.00000	0.11303	3.60364	3.71668
0.00187	0.00000	3.16350	0.00010	0.33882	0.11680	0.00000	0.00000	0.00000	0.10362	3.61922	3.72284
0.00175	0.00000	3.21100	0.00001	0.30837	0.10480	0.00000	0.00000	0.00000	0.09784	3.62418	3.72202
0.00163	0.00000	3.26470	0.00001	0.27436	0.09280	0.00000	0.00000	0.00000	0.09122	3.63187	3.72309
0.00153	0.00000	3.34290	0.00001	0.24041	0.08020	0.00000	0.00000	0.00000	0.08631	3.66352	3.74983
0.00144	0.00000	3.42680	0.00001	0.20588	0.06760	0.00000	0.00000	0.00000	0.08071	3.70029	3.78101
0.00136	0.00000	3.50640	0.00001	0.18051	0.05845	0.00000	0.00000	0.00000	0.07609	3.74537	3.82146
0.00130	0.00000	3.55280	0.00001	0.15046	0.04930	0.00000	0.00000	0.00000	0.07178	3.75257	3.82435
0.00125	0.00000	3.57770	0.00001	0.12871	0.03735	0.00000	0.00000	0.00000	0.06880	3.74377	3.81257
0.00122	0.00000	3.59360	0.00001	0.11000	0.02540	0.00000	0.00000	0.00000	0.06579	3.72901	3.79480
0.00119	0.00000	3.62750	0.00001	0.08000	0.01320	0.00000	0.00000	0.00000	0.06323	3.72071	3.78394
0.00117	0.00000	3.67160	0.00001	0.06000	0.00100	0.00000	0.00000	0.00000	0.06061	3.73261	3.79322
0.00115	0.00000	3.71050	0.00001	0.04000	0.00000	0.00000	0.00000	0.00000	0.05845	3.75051	3.80896

Appendix 2

Table A2-4: Southern midlatitude VMR profiles of chlorine-containing species, CCl_y, Cl_y and Cl_{TOT} in ppbv. Trailing zeros are not necessarily significant.

z/km	CH_3Cl	CCl_4	CFC11	CFC12	CFC113	HCFC22	HCFC142b	CH_3CCl_3	CFC114	CFC114a	CFC115
10.5	0.67312	0.09992	0.23112	0.49598	0.06256	0.15949	0.00882	0.02590	0.01341	0.00153	0.00640
11.5	0.60577	0.09995	0.23037	0.49238	0.06130	0.16353	0.01216	0.02558	0.01337	0.00152	0.00638
12.5	0.57277	0.09353	0.22504	0.48352	0.06059	0.16158	0.01282	0.02464	0.01325	0.00149	0.00632
13.5	0.54759	0.08725	0.21806	0.47086	0.05979	0.16040	0.01369	0.02360	0.01312	0.00145	0.00626
14.5	0.50445	0.07799	0.20833	0.45679	0.05344	0.15752	0.01427	0.02220	0.01294	0.00139	0.00618
15.5	0.47877	0.07163	0.19681	0.44802	0.04463	0.15906	0.01366	0.02091	0.01279	0.00135	0.00611
16.5	0.42871	0.06314	0.17936	0.42633	0.03674	0.16015	0.01410	0.01899	0.01255	0.00128	0.00601
17.5	0.37329	0.05463	0.15411	0.39913	0.03000	0.15531	0.01341	0.01634	0.01221	0.00119	0.00586
18.5	0.33957	0.04280	0.12594	0.37058	0.02400	0.14954	0.01268	0.01374	0.01185	0.00109	0.00572
19.5	0.29423	0.02816	0.09701	0.34323	0.01700	0.14765	0.01243	0.01150	0.01152	0.00100	0.00560
20.5	0.25750	0.01735	0.07222	0.31678	0.00900	0.14510	0.01225	0.00961	0.01121	0.00092	0.00549
21.5	0.22867	0.01000	0.04954	0.28910	0.00000	0.14229	0.01210	0.00772	0.01086	0.00083	0.00537
22.5	0.19618	0.00399	0.03804	0.25680	0.00000	0.14214	0.01186	0.00613	0.01049	0.00075	0.00525
23.5	0.17211	0.00208	0.02653	0.22403	0.00000	0.13839	0.01153	0.00472	0.01008	0.00065	0.00513
24.5	0.16071	0.00094	0.01756	0.19223	0.00000	0.13231	0.01118	0.00376	0.00969	0.00056	0.00502
25.5	0.10871	0.00028	0.00975	0.16532	0.00000	0.12697	0.01079	0.00319	0.00933	0.00048	0.00493
26.5	0.05773	0.00009	0.00640	0.13797	0.00000	0.12215	0.01038	0.00250	0.00903	0.00042	0.00487
27.5	0.02886	0.00004	0.00366	0.11135	0.00000	0.11752	0.00999	0.00200	0.00876	0.00037	0.00481
28.5	0.00962	0.00000	0.00188	0.08907	0.00000	0.11109	0.00944	0.00160	0.00836	0.00032	0.00477
29.5	0.00577	0.00000	0.00059	0.06681	0.00000	0.10273	0.00873	0.00127	0.00799	0.00028	0.00473
30.5	0.00289	0.00000	0.00024	0.04733	0.00000	0.09436	0.00802	0.00100	0.00769	0.00024	0.00469
31.5	0.00144	0.00000	0.00010	0.03062	0.00000	0.08642	0.00735	0.00073	0.00747	0.00020	0.00466
32.5	0.00072	0.00000	0.00004	0.01378	0.00000	0.07944	0.00675	0.00050	0.00705	0.00017	0.00463
33.5	0.00038	0.00000	0.00002	0.00877	0.00000	0.07394	0.00629	0.00033	0.00670	0.00000	0.00460
34.5	0.00019	0.00000	0.00002	0.00877	0.00000	0.06954	0.00591	0.00023	0.00616	0.00000	0.00458
35.5	0.00010	0.00000	0.00000	0.00501	0.00000	0.06551	0.00557	0.00017	0.00573	0.00000	0.00456
36.5	0.00005	0.00000	0.00000	0.00501	0.00000	0.06175	0.00525	0.00013	0.00539	0.00000	0.00454
37.5	0.00001	0.00000	0.00000	0.00313	0.00000	0.05810	0.00494	0.00010	0.00508	0.00000	0.00453
38.5	0.00001	0.00000	0.00000	0.00313	0.00000	0.05452	0.00463	0.00007	0.00479	0.00000	0.00452
39.5	0.00001	0.00000	0.00000	0.00188	0.00000	0.05150	0.00438	0.00005	0.00450	0.00000	0.00451
40.5	0.00001	0.00000	0.00000	0.00188	0.00000	0.04915	0.00418	0.00003	0.00423	0.00000	0.00450
41.5	0.00001	0.00000	0.00000	0.00117	0.00000	0.04702	0.00400	0.00000	0.00399	0.00000	0.00449
42.5	0.00001	0.00000	0.00000	0.00117	0.00000	0.04499	0.00382	0.00000	0.00381	0.00000	0.00449
43.5	0.00001	0.00000	0.00000	0.00071	0.00000	0.04308	0.00366	0.00000	0.00364	0.00000	0.00448
44.5	0.00001	0.00000	0.00000	0.00071	0.00000	0.04134	0.00351	0.00000	0.00349	0.00000	0.00448
45.5	0.00001	0.00000	0.00000	0.00046	0.00000	0.03986	0.00339	0.00000	0.00334	0.00000	0.00448
46.5	0.00001	0.00000	0.00000	0.00046	0.00000	0.03856	0.00328	0.00000	0.00320	0.00000	0.00447
47.5	0.00001	0.00000	0.00000	0.00030	0.00000	0.03729	0.00317	0.00000	0.00309	0.00000	0.00447
48.5	0.00001	0.00000	0.00000	0.00030	0.00000	0.03607	0.00307	0.00000	0.00299	0.00000	0.00447
49.5	0.00001	0.00000	0.00000	0.00020	0.00000	0.03488	0.00297	0.00000	0.00289	0.00000	0.00447
50.5	0.00001	0.00000	0.00000	0.00020	0.00000	0.03376	0.00287	0.00000	0.00280	0.00000	0.00447
51.5	0.00001	0.00000	0.00000	0.00014	0.00000	0.03275	0.00278	0.00000	0.00270	0.00000	0.00447
52.5	0.00001	0.00000	0.00000	0.00014	0.00000	0.03181	0.00270	0.00000	0.00262	0.00000	0.00447
53.5	0.00001	0.00000	0.00000	0.00010	0.00000	0.03090	0.00263	0.00000	0.00254	0.00000	0.00447
54.5	0.00001	0.00000	0.00000	0.00010	0.00000	0.03002	0.00255	0.00000	0.00247	0.00000	0.00447

HCFC141b	Halon1211	HCl	$ClONO_2$	ClO	HOCl	$COCl_2$	COClF	ClOOCl	CCl_y	Cl_y	Cl_{TOT}
0.02047	0.00338	0.20190	0.00000	0.00000	0.00000	0.02200	0.00000	0.00000	3.27241	0.24590	3.51831
0.02018	0.00330	0.23008	0.00000	0.00000	0.00000	0.02300	0.00050	0.00000	3.19758	0.27658	3.47416
0.01937	0.00306	0.28545	0.01132	0.00000	0.00000	0.02400	0.00200	0.00000	3.09674	0.34677	3.44351
0.01851	0.00282	0.34373	0.03319	0.00000	0.00000	0.02500	0.00400	0.00000	2.99199	0.43092	3.42291
0.01742	0.00251	0.42581	0.03678	0.10212	0.00000	0.02600	0.00650	0.00000	2.82585	0.62321	3.44906
0.01648	0.00226	0.53877	0.06139	0.15547	0.00000	0.02700	0.00900	0.00000	2.69068	0.81863	3.50931
0.01516	0.00190	0.69940	0.10771	0.16754	0.00000	0.02850	0.01207	0.00000	2.47934	1.04372	3.52306
0.01345	0.00148	0.89487	0.15514	0.15054	0.00000	0.03000	0.01690	0.00000	2.22116	1.27745	3.49861
0.01188	0.00111	1.10300	0.24918	0.09668	0.00000	0.03100	0.02259	0.00000	1.96164	1.53346	3.49510
0.01058	0.00083	1.29820	0.37134	0.08794	0.00000	0.03200	0.02856	0.00000	1.68259	1.85004	3.53262
0.00949	0.00062	1.46180	0.50635	0.06505	0.00087	0.03200	0.03457	0.00000	1.43964	2.13264	3.57228
0.00838	0.00043	1.59070	0.62879	0.05676	0.00522	0.02800	0.04068	0.00000	1.21898	2.37814	3.59712
0.00740	0.00028	1.70210	0.72919	0.05497	0.00794	0.02300	0.04599	0.00000	1.05504	2.58619	3.64123
0.00643	0.00017	1.78530	0.80787	0.05124	0.01349	0.01800	0.04915	0.00000	0.91179	2.74305	3.65483
0.00562	0.00010	1.86680	0.85925	0.04874	0.02506	0.01400	0.05066	0.00000	0.79326	2.87850	3.67176
0.00499	0.00006	1.94120	0.88868	0.05093	0.03680	0.01000	0.05146	0.00000	0.65168	2.98907	3.64074
0.00450	0.00004	2.04130	0.90922	0.06177	0.04785	0.00500	0.04972	0.00000	0.52610	3.11986	3.64597
0.00409	0.00002	2.13880	0.90918	0.07467	0.05690	0.00001	0.04356	0.00000	0.42746	3.22312	3.65058
0.00354	0.00002	2.23850	0.87961	0.09418	0.06542	0.00000	0.03401	0.00000	0.34796	3.31172	3.65968
0.00306	0.00001	2.32910	0.82836	0.11720	0.07282	0.00000	0.02483	0.00000	0.28380	3.37231	3.65611
0.00270	0.00000	2.41220	0.75946	0.13976	0.08195	0.00000	0.01761	0.00000	0.22961	3.41098	3.64059
0.00242	0.00000	2.48810	0.68105	0.16281	0.09614	0.00000	0.01167	0.00000	0.18379	3.43977	3.62356
0.00221	0.00000	2.56010	0.57667	0.19330	0.11554	0.00000	0.00745	0.00000	0.13958	3.45306	3.59263
0.00208	0.00000	2.61680	0.44227	0.23675	0.13520	0.00000	0.00464	0.00000	0.12136	3.43565	3.55701
0.00200	0.00000	2.67130	0.32609	0.29293	0.15312	0.00000	0.00277	0.00000	0.11482	3.44620	3.56103
0.00196	0.00000	2.71770	0.22394	0.35765	0.16469	0.00000	0.00100	0.00000	0.10164	3.46498	3.56662
0.00188	0.00000	2.76420	0.11247	0.42361	0.16739	0.00000	0.00000	0.00000	0.09656	3.46767	3.56423
0.00181	0.00000	2.80880	0.04723	0.47944	0.16582	0.00000	0.00000	0.00000	0.08791	3.50129	3.58920
0.00174	0.00000	2.85720	0.02343	0.51506	0.16017	0.00000	0.00000	0.00000	0.08319	3.55586	3.63905
0.00167	0.00000	2.90620	0.00937	0.52563	0.14947	0.00000	0.00000	0.00000	0.07665	3.59066	3.66731
0.00160	0.00000	2.95540	0.00469	0.51865	0.13763	0.00000	0.00000	0.00000	0.07334	3.61637	3.68971
0.00155	0.00000	3.01190	0.00094	0.50432	0.12946	0.00000	0.00000	0.00000	0.06894	3.64661	3.71555
0.00151	0.00000	3.06400	0.00047	0.48494	0.11936	0.00000	0.00000	0.00000	0.06629	3.66877	3.73506
0.00146	0.00000	3.12070	0.00009	0.45742	0.11153	0.00000	0.00000	0.00000	0.06287	3.68975	3.75262
0.00142	0.00000	3.18780	0.00001	0.42434	0.10162	0.00000	0.00000	0.00000	0.06057	3.71376	3.77434
0.00137	0.00000	3.25210	0.00001	0.38345	0.09118	0.00000	0.00000	0.00000	0.05807	3.72674	3.78481
0.00132	0.00000	3.31250	0.00001	0.32955	0.08074	0.00000	0.00000	0.00000	0.05628	3.72279	3.77907
0.00127	0.00000	3.37920	0.00001	0.26627	0.06977	0.00000	0.00000	0.00000	0.05426	3.71526	3.76952
0.00123	0.00000	3.45990	0.00001	0.20175	0.05881	0.00000	0.00000	0.00000	0.05265	3.72047	3.77312
0.00120	0.00000	3.53080	0.00001	0.14488	0.05085	0.00000	0.00000	0.00000	0.05090	3.72654	3.77744
0.00117	0.00000	3.59720	0.00001	0.09898	0.04289	0.00000	0.00000	0.00000	0.04944	3.73908	3.78852
0.00115	0.00000	3.65720	0.00001	0.06747	0.03249	0.00000	0.00000	0.00000	0.04800	3.75718	3.80517
0.00113	0.00000	3.70630	0.00001	0.05344	0.02210	0.00000	0.00000	0.00000	0.04678	3.78184	3.82862
0.00112	0.00000	3.74010	0.00001	0.04227	0.01148	0.00000	0.00000	0.00000	0.04552	3.79386	3.83939
0.00111	0.00000	3.77470	0.00001	0.04774	0.00087	0.00000	0.00000	0.00000	0.04440	3.82332	3.86772

Appendix 2

Table A2-5: Southern high latitude VMR profiles of chlorine-containing species, CCl_y, Cl_y and Cl_{TOT} in ppbv. Trailing zeros are not necessarily significant.

z/km	CH_3Cl	CCl_4	CFC11	CFC12	CFC113	HCFC22	HCFC142b	CH_3CCl_3	CFC114	CFC114a	CFC115
10.5	0.60731	0.10424	0.23073	0.48588	0.05679	0.15868	0.01534	0.02505	0.01330	0.00150	0.00635
11.5	0.54114	0.09190	0.21841	0.46685	0.05843	0.15815	0.01712	0.02290	0.01303	0.00142	0.00622
12.5	0.45878	0.07652	0.19894	0.43743	0.05175	0.15627	0.01628	0.01993	0.01266	0.00131	0.00606
13.5	0.38199	0.06325	0.16760	0.39733	0.04719	0.14844	0.01481	0.01607	0.01217	0.00118	0.00585
14.5	0.31676	0.04445	0.13009	0.35495	0.03766	0.13674	0.01452	0.01230	0.01164	0.00104	0.00564
15.5	0.25149	0.02631	0.09062	0.31020	0.02483	0.12371	0.01252	0.00893	0.01109	0.00089	0.00544
16.5	0.20317	0.01822	0.05948	0.26127	0.01681	0.11693	0.01195	0.00643	0.01057	0.00076	0.00527
17.5	0.15914	0.01305	0.03378	0.21281	0.01500	0.11795	0.01203	0.00452	0.01001	0.00063	0.00511
18.5	0.13032	0.00303	0.01917	0.17206	0.00800	0.11569	0.01228	0.00342	0.00950	0.00052	0.00498
19.5	0.10348	0.00080	0.00463	0.13719	0.00200	0.10964	0.00904	0.00250	0.00901	0.00042	0.00486
20.5	0.08194	0.00000	0.00000	0.10823	0.00000	0.10385	0.00830	0.00200	0.00853	0.00032	0.00476
21.5	0.07578	0.00000	0.00000	0.08489	0.00000	0.09070	0.00760	0.00160	0.00810	0.00023	0.00468
22.5	0.06271	0.00000	0.00000	0.06541	0.00000	0.07695	0.00699	0.00127	0.00777	0.00017	0.00463
23.5	0.05216	0.00000	0.00000	0.04945	0.00000	0.06821	0.00651	0.00100	0.00748	0.00000	0.00459
24.5	0.04397	0.00000	0.00000	0.03554	0.00000	0.06678	0.00612	0.00073	0.00704	0.00000	0.00456
25.5	0.02975	0.00000	0.00000	0.02170	0.00000	0.06551	0.00576	0.00050	0.00664	0.00000	0.00454
26.5	0.01579	0.00000	0.00000	0.01211	0.00000	0.06175	0.00543	0.00033	0.00625	0.00000	0.00452
27.5	0.00790	0.00000	0.00000	0.00760	0.00000	0.05810	0.00511	0.00023	0.00586	0.00000	0.00451
28.5	0.00263	0.00000	0.00000	0.00608	0.00000	0.05452	0.00480	0.00017	0.00554	0.00000	0.00450
29.5	0.00158	0.00000	0.00000	0.00456	0.00000	0.05150	0.00453	0.00013	0.00528	0.00000	0.00450
30.5	0.00079	0.00000	0.00000	0.00323	0.00000	0.04915	0.00432	0.00010	0.00505	0.00000	0.00449
31.5	0.00039	0.00000	0.00000	0.00209	0.00000	0.04702	0.00414	0.00007	0.00484	0.00000	0.00449
32.5	0.00020	0.00000	0.00000	0.00094	0.00000	0.04499	0.00396	0.00005	0.00463	0.00000	0.00449
33.5	0.00011	0.00000	0.00000	0.00060	0.00000	0.04308	0.00379	0.00003	0.00444	0.00000	0.00449
34.5	0.00005	0.00000	0.00000	0.00060	0.00000	0.04134	0.00364	0.00000	0.00429	0.00000	0.00449
35.5	0.00003	0.00000	0.00000	0.00034	0.00000	0.03986	0.00351	0.00000	0.00414	0.00000	0.00449
36.5	0.00001	0.00000	0.00000	0.00034	0.00000	0.03856	0.00339	0.00000	0.00401	0.00000	0.00448
37.5	0.00000	0.00000	0.00000	0.00021	0.00000	0.03729	0.00328	0.00000	0.00388	0.00000	0.00448
38.5	0.00000	0.00000	0.00000	0.00021	0.00000	0.03607	0.00317	0.00000	0.00375	0.00000	0.00448
39.5	0.00000	0.00000	0.00000	0.00013	0.00000	0.03488	0.00307	0.00000	0.00363	0.00000	0.00448
40.5	0.00000	0.00000	0.00000	0.00013	0.00000	0.03376	0.00297	0.00000	0.00352	0.00000	0.00448
41.5	0.00000	0.00000	0.00000	0.00008	0.00000	0.03275	0.00288	0.00000	0.00342	0.00000	0.00448
42.5	0.00000	0.00000	0.00000	0.00008	0.00000	0.03181	0.00280	0.00000	0.00332	0.00000	0.00448
43.5	0.00000	0.00000	0.00000	0.00005	0.00000	0.03090	0.00272	0.00000	0.00323	0.00000	0.00447
44.5	0.00000	0.00000	0.00000	0.00005	0.00000	0.03002	0.00264	0.00000	0.00313	0.00000	0.00447
45.5	0.00000	0.00000	0.00000	0.00003	0.00000	0.02914	0.00256	0.00000	0.00305	0.00000	0.00447
46.5	0.00000	0.00000	0.00000	0.00003	0.00000	0.02838	0.00250	0.00000	0.00301	0.00000	0.00447
47.5	0.00000	0.00000	0.00000	0.00002	0.00000	0.02801	0.00246	0.00000	0.00300	0.00000	0.00447
48.5	0.00000	0.00000	0.00000	0.00002	0.00000	0.02789	0.00245	0.00000	0.00299	0.00000	0.00447
49.5	0.00000	0.00000	0.00000	0.00001	0.00000	0.02777	0.00244	0.00000	0.00297	0.00000	0.00447
50.5	0.00000	0.00000	0.00000	0.00001	0.00000	0.02765	0.00243	0.00000	0.00296	0.00000	0.00447
51.5	0.00000	0.00000	0.00000	0.00001	0.00000	0.02753	0.00242	0.00000	0.00295	0.00000	0.00447
52.5	0.00000	0.00000	0.00000	0.00001	0.00000	0.02740	0.00241	0.00000	0.00293	0.00000	0.00447
53.5	0.00000	0.00000	0.00000	0.00001	0.00000	0.02724	0.00240	0.00000	0.00291	0.00000	0.00447
54.5	0.00000	0.00000	0.00000	0.00001	0.00000	0.02709	0.00238	0.00000	0.00289	0.00000	0.00447

HCFC141b	Halon1211	HCl	$ClONO_2$	ClO	HOCl	$COCl_2$	COClF	ClOOCl	CCl_y	Cl_y	Cl_{TOT}
0.01971	0.00316	0.09390	0.00000	0.00000	0.00000	0.02200	0.00000	0.00000	3.18630	0.13790	3.32420
0.01796	0.00266	0.11889	0.00000	0.00000	0.00000	0.02300	0.00250	0.00000	2.99061	0.16739	3.15800
0.01579	0.00207	0.15777	0.16409	0.14881	0.00000	0.02400	0.00500	0.00000	2.69178	0.52367	3.21545
0.01329	0.00144	0.19532	0.22871	0.11240	0.00000	0.02500	0.00750	0.05988	2.34605	0.71369	3.05974
0.01104	0.00093	0.23087	0.24419	0.20263	0.00000	0.02600	0.01000	0.13711	1.94989	1.01391	2.96380
0.00909	0.00055	0.25948	0.25199	0.23973	0.00000	0.02700	0.01250	0.13672	1.53468	1.09114	2.62582
0.00759	0.00031	0.29588	0.28513	0.41817	0.00000	0.02850	0.01500	0.30050	1.21907	1.67218	2.89125
0.00628	0.00015	0.32130	0.31210	0.63560	0.00000	0.03000	0.01750	0.50748	0.96597	2.36146	3.32743
0.00528	0.00007	0.36239	0.38193	0.75287	0.00000	0.03100	0.01920	0.50907	0.74195	2.59653	3.33848
0.00447	0.00004	0.43340	0.50484	0.88332	0.00000	0.03200	0.02000	0.49836	0.55981	2.90228	3.46209
0.00377	0.00002	0.57522	0.70633	0.90189	0.00000	0.03200	0.01920	0.36148	0.44657	2.98960	3.43617
0.00321	0.00000	0.79649	1.01080	0.83584	0.00051	0.02800	0.01750	0.20985	0.37644	3.13684	3.51328
0.00279	0.00000	1.13500	1.27180	0.67386	0.00306	0.02300	0.01500	0.09725	0.30739	3.33921	3.64660
0.00245	0.00000	1.52650	1.38640	0.36662	0.00465	0.01800	0.01250	0.02249	0.25323	3.37764	3.63087
0.00218	0.00000	1.88690	1.34930	0.19290	0.00791	0.01400	0.01000	0.00495	0.21315	3.48491	3.69806
0.00196	0.00000	2.15450	1.22440	0.10087	0.01469	0.01000	0.00750	0.00043	0.16766	3.52282	3.69047
0.00178	0.00000	2.31090	1.07800	0.15672	0.02157	0.00500	0.00500	0.00000	0.12876	3.58219	3.71095
0.00165	0.00000	2.41070	0.94300	0.21655	0.02805	0.00001	0.00250	0.00000	0.10654	3.60082	3.70736
0.00155	0.00000	2.47930	0.82346	0.26363	0.03335	0.00000	0.00000	0.00000	0.09328	3.59974	3.69303
0.00149	0.00000	2.53210	0.69721	0.31805	0.03835	0.00000	0.00000	0.00000	0.08517	3.58572	3.67088
0.00145	0.00000	2.57650	0.56282	0.38985	0.04269	0.00000	0.00000	0.00000	0.07853	3.57186	3.65039
0.00143	0.00000	2.61640	0.44242	0.46007	0.04804	0.00000	0.00000	0.00000	0.07296	3.56694	3.63990
0.00141	0.00000	2.67250	0.33707	0.51595	0.05636	0.00000	0.00000	0.00000	0.06775	3.58187	3.64962
0.00138	0.00000	2.73170	0.23760	0.54728	0.06773	0.00000	0.00000	0.00000	0.06441	3.58431	3.64872
0.00135	0.00000	2.79440	0.16587	0.55191	0.07925	0.00000	0.00000	0.00000	0.06200	3.59143	3.65343
0.00133	0.00000	2.86200	0.11391	0.55438	0.08976	0.00000	0.00000	0.00000	0.05951	3.62005	3.67956
0.00129	0.00000	2.93280	0.05720	0.56067	0.09654	0.00000	0.00000	0.00000	0.05773	3.64721	3.70494
0.00126	0.00000	2.99750	0.02402	0.56328	0.09812	0.00000	0.00000	0.00000	0.05576	3.68292	3.73869
0.00124	0.00000	3.06210	0.01191	0.55358	0.09721	0.00000	0.00000	0.00000	0.05413	3.72479	3.77892
0.00122	0.00000	3.12540	0.00477	0.52842	0.09389	0.00000	0.00000	0.00000	0.05238	3.75248	3.80486
0.00120	0.00000	3.18960	0.00238	0.49393	0.08762	0.00000	0.00000	0.00000	0.05090	3.77353	3.82444
0.00118	0.00000	3.25070	0.00048	0.45513	0.08068	0.00000	0.00000	0.00000	0.04946	3.78698	3.83645
0.00117	0.00000	3.31300	0.00024	0.41505	0.07589	0.00000	0.00000	0.00000	0.04822	3.80417	3.85239
0.00115	0.00000	3.37760	0.00005	0.37438	0.06997	0.00000	0.00000	0.00000	0.04696	3.82199	3.86895
0.00114	0.00000	3.43830	0.00000	0.33903	0.06538	0.00000	0.00000	0.00000	0.04579	3.84271	3.88850
0.00113	0.00000	3.49010	0.00000	0.30454	0.05957	0.00000	0.00000	0.00000	0.04461	3.85422	3.89883
0.00113	0.00000	3.53500	0.00000	0.26603	0.05345	0.00000	0.00000	0.00000	0.04369	3.85448	3.89817
0.00112	0.00000	3.57900	0.00000	0.22488	0.04733	0.00000	0.00000	0.00000	0.04323	3.85122	3.89444
0.00112	0.00000	3.62550	0.00000	0.18500	0.04090	0.00000	0.00000	0.00000	0.04306	3.85141	3.89447
0.00111	0.00000	3.67220	0.00000	0.14859	0.03448	0.00000	0.00000	0.00000	0.04289	3.85527	3.89816
0.00111	0.00000	3.69980	0.00000	0.11734	0.02981	0.00000	0.00000	0.00000	0.04272	3.84696	3.88968
0.00110	0.00000	3.71450	0.00000	0.08851	0.02514	0.00000	0.00000	0.00000	0.04254	3.82816	3.87070
0.00110	0.00000	3.72930	0.00000	0.07688	0.01905	0.00000	0.00000	0.00000	0.04236	3.82524	3.86759
0.00110	0.00000	3.75290	0.00000	0.07912	0.01295	0.00000	0.00000	0.00000	0.04215	3.84498	3.88713
0.00110	0.00000	3.76660	0.00000	0.08221	0.00673	0.00000	0.00000	0.00000	0.04194	3.85554	3.89748

Appendix 3: Fluorine Tables

Table A3-1: Northern high latitude VMR profiles of fluorine-containing species, CF_y, F_y and F_{TOT} in ppbv. Trailing zeros are not necessarily significant.

z/km	CF_4	CFC11	CFC12	CFC113	HCFC22	HCFC142b	HFC134a	mPFC	mCFC	mHCFC	HF	COF_2	COClF	SF_6	CF_y	F_y	F_{TOT}
10.5	0.06563	0.23950	0.50974	0.06322	0.16954	0.01040	0.02964	0.02691	0.14273	0.09833	0.03757	0.00000	0.00000	0.00530	2.45758	0.06938	2.52696
11.5	0.06563	0.23534	0.50424	0.06346	0.17039	0.01266	0.03220	0.02691	0.14119	0.09883	0.04115	0.00000	0.00250	0.00534	2.45851	0.07570	2.53421
12.5	0.06563	0.22995	0.49659	0.06341	0.17070	0.01378	0.03103	0.02691	0.13905	0.09901	0.06208	0.01610	0.00500	0.00531	2.43389	0.13117	2.56506
13.5	0.06563	0.21976	0.48306	0.05940	0.17034	0.01335	0.03046	0.02691	0.13526	0.09880	0.08464	0.02485	0.00750	0.00525	2.37676	0.17334	2.55010
14.5	0.06563	0.20566	0.46879	0.05448	0.16349	0.01387	0.02834	0.02691	0.13126	0.09482	0.12797	0.03524	0.01000	0.00519	2.29026	0.23956	2.52983
15.5	0.06563	0.18834	0.45092	0.04415	0.16082	0.01323	0.02658	0.02691	0.12626	0.09328	0.18776	0.04815	0.01250	0.00507	2.18600	0.32697	2.51297
16.5	0.06563	0.16715	0.42691	0.03530	0.15948	0.01293	0.02491	0.02691	0.11953	0.09250	0.26406	0.06336	0.01500	0.00497	2.07275	0.43557	2.50832
17.5	0.06563	0.14030	0.39726	0.03933	0.15360	0.01306	0.02381	0.02691	0.11123	0.08909	0.34721	0.08078	0.01750	0.00483	1.97110	0.55523	2.52633
18.5	0.06563	0.10855	0.36410	0.03605	0.14447	0.01301	0.02239	0.02691	0.10195	0.08379	0.42511	0.09945	0.01920	0.00469	1.82458	0.67137	2.49594
19.5	0.06563	0.07842	0.33240	0.03291	0.13671	0.01408	0.02119	0.02691	0.09307	0.07929	0.51037	0.11986	0.02000	0.00458	1.69006	0.79757	2.48763
20.5	0.06563	0.05780	0.30087	0.02979	0.13195	0.01359	0.02045	0.02691	0.08424	0.07653	0.61500	0.14219	0.01920	0.00451	1.57198	0.94566	2.51764
21.5	0.06733	0.04064	0.26406	0.02614	0.13160	0.01355	0.02040	0.02761	0.07394	0.07633	0.72411	0.16399	0.01750	0.00449	1.46629	1.09654	2.56283
22.5	0.06816	0.03120	0.22031	0.02181	0.12874	0.01326	0.01995	0.02795	0.06169	0.07467	0.83732	0.18475	0.01500	0.00445	1.33802	1.24855	2.58657
23.5	0.06850	0.02176	0.17333	0.01716	0.11861	0.01222	0.01838	0.02809	0.04853	0.06879	0.95948	0.20018	0.01250	0.00432	1.17452	1.39826	2.57278
24.5	0.06861	0.01440	0.12992	0.01286	0.10579	0.01090	0.01640	0.02813	0.03638	0.06136	1.08540	0.20829	0.01000	0.00414	1.01208	1.53680	2.54888
25.5	0.06883	0.00800	0.09631	0.00953	0.09436	0.00972	0.01463	0.02822	0.02697	0.05473	1.20700	0.21024	0.00750	0.00401	0.88113	1.65902	2.54015
26.5	0.06943	0.00525	0.06878	0.00681	0.08642	0.00890	0.01339	0.02847	0.01926	0.05012	1.32550	0.20899	0.00500	0.00393	0.78303	1.77203	2.55506
27.5	0.07013	0.00300	0.04923	0.00487	0.07944	0.00818	0.01231	0.02875	0.01378	0.04608	1.43510	0.20294	0.00250	0.00383	0.70971	1.86648	2.57619
28.5	0.07082	0.00154	0.03939	0.00390	0.07394	0.00762	0.01146	0.02904	0.01103	0.04289	1.51680	0.19485	0.00000	0.00372	0.66724	1.92882	2.59606
29.5	0.07146	0.00048	0.02954	0.00292	0.06954	0.00716	0.01078	0.02930	0.00827	0.04033	1.57570	0.18397	0.00000	0.00358	0.62860	1.96512	2.59372
30.5	0.07199	0.00020	0.02093	0.00207	0.06551	0.00675	0.01015	0.02952	0.00586	0.03799	1.61530	0.17199	0.00000	0.00348	0.59473	1.98018	2.57491
31.5	0.07237	0.00008	0.01354	0.00134	0.06175	0.00636	0.00957	0.02967	0.00379	0.03582	1.63850	0.16010	0.00000	0.00327	0.56444	1.97832	2.54276
32.5	0.07268	0.00003	0.00610	0.00060	0.05810	0.00598	0.00901	0.02980	0.00171	0.03370	1.65770	0.14735	0.00000	0.00312	0.53413	1.97112	2.50525
33.5	0.07284	0.00001	0.00388	0.00038	0.05452	0.00562	0.00845	0.02987	0.00109	0.03162	1.67990	0.13593	0.00000	0.00295	0.51693	1.96946	2.48639
34.5	0.07290	0.00001	0.00388	0.00038	0.05150	0.00530	0.00798	0.02989	0.00109	0.02987	1.70230	0.12709	0.00000	0.00275	0.50691	1.97298	2.47989
35.5	0.07303	0.00000	0.00222	0.00022	0.04915	0.00506	0.00762	0.02994	0.00062	0.02850	1.73060	0.12039	0.00000	0.00250	0.49515	1.98638	2.48153
36.5	0.07336	0.00000	0.00222	0.00022	0.04702	0.00484	0.00729	0.03008	0.00062	0.02727	1.76570	0.11673	0.00000	0.00225	0.48939	2.01266	2.50205
37.5	0.07391	0.00000	0.00138	0.00014	0.04499	0.00463	0.00697	0.03030	0.00039	0.02610	1.79880	0.11488	0.00000	0.00200	0.48277	2.04056	2.52333
38.5	0.07457	0.00000	0.00138	0.00014	0.04308	0.00444	0.00668	0.03057	0.00039	0.02499	1.82460	0.10614	0.00000	0.00175	0.47916	2.04738	2.52654
39.5	0.07525	0.00000	0.00083	0.00008	0.04134	0.00426	0.00641	0.03085	0.00023	0.02398	1.84890	0.10326	0.00000	0.00150	0.47479	2.06442	2.53921
40.5	0.07568	0.00000	0.00083	0.00008	0.03986	0.00411	0.00618	0.03103	0.00023	0.02312	1.86780	0.09800	0.00000	0.00110	0.47166	2.07040	2.54206
41.5	0.07589	0.00000	0.00052	0.00005	0.03856	0.00397	0.00598	0.03111	0.00014	0.02236	1.88720	0.09310	0.00000	0.00080	0.46731	2.07820	2.54551
42.5	0.07596	0.00000	0.00052	0.00005	0.03729	0.00384	0.00578	0.03114	0.00014	0.02163	1.90220	0.08820	0.00000	0.00040	0.46333	2.08100	2.54433
43.5	0.07581	0.00000	0.00031	0.00003	0.03607	0.00371	0.00559	0.03108	0.00009	0.02092	1.92200	0.08330	0.00000	0.00020	0.45795	2.08980	2.54775
44.5	0.07560	0.00000	0.00031	0.00003	0.03488	0.00359	0.00541	0.03100	0.00009	0.02023	1.94550	0.07840	0.00000	0.00010	0.45303	2.10290	2.55593
45.5	0.07500	0.00000	0.00020	0.00002	0.03376	0.00348	0.00523	0.03075	0.00006	0.01958	1.96870	0.07350	0.00000	0.00005	0.44627	2.11600	2.56227
46.5	0.07450	0.00000	0.00020	0.00002	0.03275	0.00337	0.00508	0.03055	0.00006	0.01899	1.99420	0.06860	0.00000	0.00002	0.44060	2.13152	2.57212
47.5	0.07400	0.00000	0.00013	0.00001	0.03181	0.00328	0.00493	0.03034	0.00004	0.01845	2.02310	0.06370	0.00000	0.00000	0.43503	2.15050	2.58553
48.5	0.07350	0.00000	0.00013	0.00001	0.03090	0.00318	0.00479	0.03014	0.00004	0.01792	2.05000	0.05880	0.00000	0.00000	0.42974	2.16760	2.59734
49.5	0.07300	0.00000	0.00009	0.00001	0.03002	0.00309	0.00465	0.02993	0.00002	0.01741	2.07160	0.05390	0.00000	0.00000	0.42442	2.17940	2.60382
50.5	0.07250	0.00000	0.00009	0.00001	0.02914	0.00300	0.00452	0.02973	0.00002	0.01690	2.07720	0.04900	0.00000	0.00000	0.41922	2.17520	2.59442
51.5	0.07200	0.00000	0.00006	0.00001	0.02838	0.00292	0.00440	0.02952	0.00002	0.01646	2.07980	0.04410	0.00000	0.00000	0.41436	2.16800	2.58236
52.5	0.07150	0.00000	0.00006	0.00001	0.02801	0.00288	0.00434	0.02932	0.00002	0.01625	2.07930	0.03920	0.00000	0.00000	0.41088	2.15770	2.56858
53.5	0.07100	0.00000	0.00004	0.00000	0.02789	0.00287	0.00432	0.02911	0.00001	0.01618	2.07930	0.03430	0.00000	0.00000	0.40822	2.14790	2.55612
54.5	0.07050	0.00000	0.00004	0.00000	0.02777	0.00286	0.00430	0.02891	0.00001	0.01611	2.08000	0.02940	0.00000	0.00000	0.40562	2.13880	2.54442
55.5	0.07000	0.00000	0.00003	0.00000	0.02765	0.00285	0.00430	0.02870	0.00001	0.01604	2.07930	0.02450	0.00000	0.00000	0.40305	2.12830	2.53135

Table A3-2: Northern midlatitude VMR profiles of fluorine-containing species, CF_y, F_y and F_{TOT} in ppbv. Trailing zeros are not necessarily significant.

z/km	CF_4	CFC11	CFC12	CFC113	HCFC22	HCFC142b	HFC134a	mPFC	mCFC	mHCFC	HF	COF_2	COClF	SF_6	CF_y	F_y	F_{TOT}
10.5	0.06575	0.24032	0.51511	0.06000	0.17387	0.01153	0.03141	0.02696	0.14423	0.10084	0.03330	0.00000	0.00000	0.00542	2.48199	0.06584	2.54784
11.5	0.06575	0.23793	0.51006	0.06327	0.17102	0.01227	0.03169	0.02696	0.14282	0.09919	0.05083	0.00000	0.00350	0.00544	2.47318	0.08699	2.56017
12.5	0.06575	0.23255	0.49976	0.05967	0.17011	0.01320	0.02855	0.02696	0.13993	0.09866	0.05078	0.01598	0.00720	0.00539	2.42045	0.12227	2.54272
13.5	0.06575	0.22190	0.48355	0.05820	0.17047	0.01378	0.02790	0.02696	0.13539	0.09887	0.07252	0.01964	0.01100	0.00523	2.36790	0.15417	2.52207
14.5	0.06575	0.21461	0.47493	0.05883	0.16722	0.01362	0.02607	0.02696	0.13298	0.09699	0.09963	0.02845	0.01450	0.00514	2.32682	0.20190	2.52871
15.5	0.06575	0.20467	0.47192	0.05109	0.16710	0.01638	0.02690	0.02696	0.13214	0.09692	0.12883	0.03531	0.01830	0.00518	2.29535	0.24886	2.54422
16.5	0.06575	0.19052	0.45695	0.04199	0.16913	0.01530	0.02525	0.02696	0.12795	0.09810	0.18105	0.04572	0.02230	0.00510	2.21623	0.32537	2.54160
17.5	0.06575	0.17006	0.43405	0.04297	0.16087	0.01477	0.02493	0.02696	0.12153	0.09330	0.24644	0.05982	0.02600	0.00489	2.12288	0.42143	2.54432
18.5	0.06575	0.14547	0.40531	0.04013	0.15128	0.01513	0.02345	0.02696	0.11349	0.08774	0.30769	0.07765	0.02950	0.00478	1.99427	0.52117	2.51544
19.5	0.06575	0.11748	0.37425	0.03705	0.14526	0.01496	0.02252	0.02696	0.10479	0.08425	0.38883	0.09674	0.03350	0.00470	1.86664	0.64403	2.51066
20.5	0.06575	0.09574	0.34875	0.03453	0.14058	0.01448	0.02179	0.02696	0.09765	0.08154	0.48493	0.11854	0.03700	0.00462	1.76324	0.78675	2.54999
21.5	0.06726	0.07097	0.31972	0.03165	0.14160	0.01458	0.02195	0.02758	0.08952	0.08213	0.59065	0.13750	0.03920	0.00459	1.67380	0.93239	2.60618
22.5	0.06880	0.05448	0.29172	0.02888	0.13959	0.01438	0.02164	0.02821	0.08168	0.08096	0.67849	0.15629	0.04000	0.00459	1.58508	1.05860	2.64369
23.5	0.06943	0.03800	0.26100	0.02584	0.13347	0.01375	0.02069	0.02847	0.07308	0.07741	0.75969	0.17267	0.03920	0.00446	1.47137	1.17099	2.64235
24.5	0.06861	0.02515	0.22301	0.02208	0.13071	0.01346	0.02026	0.02813	0.06244	0.07581	0.81870	0.18615	0.03700	0.00438	1.34760	1.25427	2.60187
25.5	0.06818	0.01397	0.18687	0.01850	0.12697	0.01308	0.01968	0.02795	0.05232	0.07364	0.89650	0.19728	0.03350	0.00418	1.22869	1.34961	2.57830
26.5	0.06964	0.00916	0.15105	0.01495	0.12215	0.01258	0.01893	0.02855	0.04229	0.07085	0.98900	0.21147	0.02950	0.00416	1.12159	1.46642	2.58801
27.5	0.07074	0.00524	0.11523	0.01141	0.11752	0.01210	0.01822	0.02901	0.03226	0.06816	1.10010	0.21937	0.02500	0.00414	1.01444	1.58868	2.60312
28.5	0.07166	0.00269	0.09219	0.00913	0.11109	0.01144	0.01722	0.02938	0.02581	0.06443	1.21410	0.22105	0.02000	0.00395	0.93466	1.69990	2.63456
29.5	0.07240	0.00084	0.07700	0.00762	0.10273	0.01058	0.01592	0.02968	0.02156	0.05958	1.30080	0.21834	0.01400	0.00381	0.86843	1.77432	2.64275
30.5	0.07229	0.00035	0.06500	0.00644	0.09436	0.00972	0.01463	0.02964	0.01820	0.05473	1.37300	0.20774	0.00700	0.00368	0.80805	1.81757	2.62561
31.5	0.07197	0.00014	0.05600	0.00554	0.08642	0.00890	0.01339	0.02951	0.01568	0.05012	1.42290	0.19580	0.00000	0.00355	0.75616	1.83580	2.59196
32.5	0.07214	0.00005	0.04700	0.00465	0.07944	0.00818	0.01231	0.02958	0.01316	0.04608	1.44430	0.18838	0.00000	0.00340	0.70991	1.84146	2.55137
33.5	0.07223	0.00002	0.03800	0.00376	0.07394	0.00762	0.01146	0.02961	0.01064	0.04289	1.47410	0.18308	0.00000	0.00327	0.66834	1.85988	2.52822
34.5	0.07235	0.00002	0.03000	0.00297	0.06954	0.00716	0.01078	0.02966	0.00840	0.04033	1.50690	0.17823	0.00000	0.00312	0.63323	1.88208	2.51531
35.5	0.07260	0.00000	0.02200	0.00218	0.06551	0.00675	0.01015	0.02977	0.00616	0.03799	1.53720	0.17289	0.00000	0.00295	0.59998	1.90068	2.50066
36.5	0.07297	0.00000	0.01600	0.00158	0.06175	0.00636	0.00957	0.02992	0.00448	0.03582	1.57030	0.17162	0.00000	0.00275	0.57337	1.93004	2.50341
37.5	0.07341	0.00000	0.01200	0.00119	0.05810	0.00598	0.00901	0.03010	0.00336	0.03370	1.60580	0.17287	0.00000	0.00250	0.55253	1.96654	2.51907
38.5	0.07345	0.00000	0.00800	0.00079	0.05452	0.00562	0.00845	0.03012	0.00224	0.03162	1.62990	0.16352	0.00000	0.00225	0.53023	1.97044	2.50067
39.5	0.07393	0.00000	0.00600	0.00059	0.05150	0.00530	0.00798	0.03031	0.00168	0.02987	1.65380	0.16307	0.00000	0.00200	0.51688	1.99194	2.50882
40.5	0.07471	0.00000	0.00500	0.00050	0.04915	0.00506	0.00762	0.03063	0.00140	0.02850	1.68810	0.15400	0.00000	0.00175	0.50973	2.00660	2.51633
41.5	0.07507	0.00000	0.00400	0.00040	0.04702	0.00484	0.00729	0.03078	0.00112	0.02727	1.71560	0.14630	0.00000	0.00150	0.50151	2.01720	2.51871
42.5	0.07535	0.00000	0.00300	0.00030	0.04499	0.00463	0.00697	0.03089	0.00084	0.02610	1.73960	0.13860	0.00000	0.00110	0.49325	2.02340	2.51665
43.5	0.07563	0.00000	0.00200	0.00020	0.04308	0.00444	0.00668	0.03101	0.00056	0.02499	1.74830	0.13090	0.00000	0.00080	0.48543	2.01490	2.50033
44.5	0.07554	0.00000	0.00100	0.00010	0.04134	0.00426	0.00641	0.03097	0.00028	0.02398	1.76260	0.12320	0.00000	0.00040	0.47653	2.01140	2.48793
45.5	0.07500	0.00000	0.00000	0.00000	0.03986	0.00411	0.00618	0.03075	0.00000	0.02312	1.78700	0.11550	0.00000	0.00020	0.46653	2.01920	2.48573
46.5	0.07450	0.00000	0.00000	0.00000	0.03856	0.00397	0.00598	0.03055	0.00000	0.02236	1.80870	0.10780	0.00000	0.00010	0.45987	2.02490	2.48477
47.5	0.07400	0.00000	0.00000	0.00000	0.03729	0.00384	0.00578	0.03034	0.00000	0.02163	1.82830	0.10010	0.00000	0.00005	0.45335	2.02880	2.48215
48.5	0.07350	0.00000	0.00000	0.00000	0.03607	0.00371	0.00559	0.03014	0.00000	0.02092	1.85730	0.09240	0.00000	0.00002	0.44697	2.04222	2.48919
49.5	0.07300	0.00000	0.00000	0.00000	0.03488	0.00359	0.00541	0.02993	0.00000	0.02023	1.89220	0.08470	0.00000	0.00000	0.44075	2.06160	2.50235
50.5	0.07250	0.00000	0.00000	0.00000	0.03376	0.00348	0.00523	0.02973	0.00000	0.01958	1.90930	0.07700	0.00000	0.00000	0.43472	2.06330	2.49802
51.5	0.07200	0.00000	0.00000	0.00000	0.03275	0.00337	0.00508	0.02952	0.00000	0.01899	1.92200	0.06930	0.00000	0.00000	0.42905	2.06060	2.48965
52.5	0.07150	0.00000	0.00000	0.00000	0.03181	0.00328	0.00493	0.02932	0.00000	0.01845	1.93090	0.06160	0.00000	0.00000	0.42367	2.05410	2.47777
53.5	0.07100	0.00000	0.00000	0.00000	0.03090	0.00318	0.00479	0.02911	0.00000	0.01792	1.94100	0.05390	0.00000	0.00000	0.41837	2.04880	2.46717
54.5	0.07050	0.00000	0.00000	0.00000	0.03002	0.00309	0.00465	0.02891	0.00000	0.01741	1.95090	0.04620	0.00000	0.00000	0.41316	2.04330	2.45646
55.5	0.07000	0.00000	0.00000	0.00000	0.02914	0.00300	0.00465	0.02870	0.00000	0.01690	1.96170	0.03850	0.00000	0.00000	0.40851	2.03870	2.44721

Table A3-3: Tropical VMR profiles of fluorine-containing species, CF_y, F_y and F_{TOT} in ppbv. Trailing zeros are not necessarily significant.

z/km	CF_4	CFC11	CFC12	CFC113	HCFC22	HCFC142b	HFC134a	mPFC	mCFC	mHCFC	HF	COF_2	COClF	SF_6	CF_y	F_y	F_{TOT}
10.5	0.06554	0.24337	0.52693	0.04830	0.17789	0.00925	0.03102	0.02687	0.14754	0.10318	0.00000	0.00000	0.00000	0.00562	2.48023	0.03373	2.51396
11.5	0.06554	0.25302	0.53340	0.05533	0.18103	0.00950	0.03083	0.02687	0.14935	0.10500	0.00031	0.00000	0.01000	0.00561	2.53353	0.04396	2.57749
12.5	0.06554	0.25424	0.52557	0.06243	0.18136	0.01209	0.02802	0.02687	0.14716	0.10519	0.00149	0.00000	0.02000	0.00558	2.53303	0.05499	2.58802
13.5	0.06554	0.24845	0.51330	0.06045	0.18109	0.01326	0.02682	0.02687	0.14372	0.10503	0.00175	0.00000	0.03000	0.00524	2.49012	0.06322	2.55334
14.5	0.06554	0.24862	0.50932	0.06104	0.18479	0.01608	0.02910	0.02687	0.14261	0.10718	0.00203	0.00127	0.04000	0.00523	2.50734	0.07595	2.58329
15.5	0.06554	0.25160	0.51702	0.06083	0.18104	0.01965	0.02807	0.02687	0.14477	0.10500	0.00551	0.00138	0.04900	0.00526	2.52061	0.08883	2.60944
16.5	0.06554	0.25328	0.52227	0.05840	0.18841	0.01975	0.03029	0.02687	0.14624	0.10928	0.01195	0.00312	0.05650	0.00541	2.55503	0.10717	2.66220
17.5	0.06554	0.24750	0.51773	0.05126	0.18890	0.01761	0.02928	0.02687	0.14496	0.10956	0.03249	0.00817	0.06300	0.00535	2.51041	0.14394	2.65435
18.5	0.06554	0.23067	0.50173	0.04967	0.17783	0.01600	0.02756	0.02687	0.14048	0.10314	0.06097	0.01787	0.06900	0.00530	2.41371	0.19748	2.61118
19.5	0.06554	0.20690	0.47213	0.04674	0.17095	0.01761	0.02650	0.02687	0.13220	0.09915	0.10706	0.03110	0.07500	0.00505	2.29485	0.27457	2.56942
20.5	0.06554	0.19589	0.45526	0.04507	0.16610	0.01711	0.02575	0.02687	0.12747	0.09634	0.16446	0.04737	0.08200	0.00490	2.22385	0.37059	2.59444
21.5	0.06721	0.17408	0.43853	0.04341	0.16513	0.01701	0.02560	0.02756	0.12279	0.09578	0.21833	0.06351	0.08800	0.00492	2.16301	0.46286	2.62586
22.5	0.06881	0.13365	0.42664	0.04224	0.16771	0.01727	0.02600	0.02821	0.11946	0.09727	0.26535	0.08175	0.09300	0.00492	2.10778	0.55138	2.65916
23.5	0.06954	0.09319	0.40394	0.03999	0.16648	0.01715	0.02580	0.02851	0.11310	0.09656	0.31094	0.09994	0.09700	0.00487	2.00783	0.63702	2.64485
24.5	0.06888	0.06168	0.37038	0.03667	0.16459	0.01695	0.02551	0.02824	0.10371	0.09546	0.35344	0.11944	0.09940	0.00461	1.88051	0.71937	2.59988
25.5	0.06829	0.03427	0.34838	0.03449	0.15731	0.01620	0.02438	0.02800	0.09755	0.09124	0.40541	0.14119	0.10000	0.00445	1.76899	0.81448	2.58347
26.5	0.06983	0.02248	0.33704	0.03337	0.15511	0.01598	0.02404	0.02863	0.09437	0.08996	0.47116	0.16412	0.09870	0.00464	1.72729	0.92593	2.65321
27.5	0.07155	0.01284	0.30161	0.02986	0.15227	0.01568	0.02360	0.02934	0.08445	0.08832	0.54329	0.19005	0.09300	0.00469	1.62427	1.04450	2.66877
28.5	0.07220	0.00659	0.26000	0.02574	0.14918	0.01537	0.02312	0.02960	0.07280	0.08652	0.61428	0.21626	0.08500	0.00437	1.50311	1.15803	2.66114
29.5	0.07258	0.00206	0.22500	0.02228	0.14625	0.01506	0.02267	0.02976	0.06300	0.08483	0.68615	0.23745	0.07200	0.00418	1.40010	1.25815	2.65825
30.5	0.07237	0.00086	0.19000	0.01881	0.14407	0.01484	0.02233	0.02967	0.05320	0.08356	0.75506	0.25420	0.05800	0.00414	1.30035	1.34630	2.64665
31.5	0.07180	0.00034	0.16000	0.01584	0.14229	0.01466	0.02206	0.02944	0.04480	0.08253	0.82059	0.26673	0.04400	0.00395	1.21393	1.42175	2.63568
32.5	0.07162	0.00013	0.13500	0.01337	0.13951	0.01437	0.02162	0.02936	0.03780	0.08092	0.87837	0.27633	0.03000	0.00381	1.13903	1.48387	2.62290
33.5	0.07195	0.00006	0.10500	0.01040	0.13569	0.01398	0.02103	0.02950	0.02940	0.07870	0.92421	0.28158	0.01700	0.00368	1.05009	1.52646	2.57655
34.5	0.07226	0.00006	0.08500	0.00842	0.13152	0.01355	0.02039	0.02962	0.02380	0.07628	0.96162	0.28495	0.00000	0.00355	0.98572	1.55282	2.53854
35.5	0.07231	0.00001	0.06500	0.00644	0.12697	0.01308	0.01968	0.02965	0.01820	0.07364	0.99750	0.28902	0.00000	0.00340	0.91889	1.59594	2.51483
36.5	0.07245	0.00001	0.05000	0.00495	0.12215	0.01258	0.01893	0.02970	0.01400	0.07085	1.04320	0.29288	0.00000	0.00327	0.86439	1.64858	2.51297
37.5	0.07280	0.00000	0.03500	0.00347	0.11752	0.01210	0.01822	0.02985	0.00980	0.06816	1.10280	0.29670	0.00000	0.00312	0.81151	1.71492	2.52643
38.5	0.07327	0.00000	0.02000	0.00198	0.11109	0.01144	0.01722	0.03004	0.00560	0.06443	1.17670	0.29763	0.00000	0.00295	0.75302	1.78966	2.54268
39.5	0.07379	0.00000	0.01000	0.00099	0.10273	0.01058	0.01592	0.03025	0.00280	0.05958	1.25930	0.29876	0.00000	0.00275	0.70105	1.87332	2.57437
40.5	0.07435	0.00000	0.00500	0.00050	0.09436	0.00972	0.01463	0.03048	0.00140	0.05473	1.34770	0.29000	0.00000	0.00250	0.66216	1.94270	2.60486
41.5	0.07508	0.00000	0.00000	0.00000	0.08642	0.00890	0.01339	0.03078	0.00000	0.05012	1.42190	0.27550	0.00000	0.00225	0.62542	1.98640	2.61182
42.5	0.07584	0.00000	0.00000	0.00000	0.07944	0.00818	0.01231	0.03110	0.00000	0.04608	1.47070	0.26100	0.00000	0.00200	0.60506	2.00470	2.60976
43.5	0.07603	0.00000	0.00000	0.00000	0.07394	0.00762	0.01146	0.03117	0.00000	0.04289	1.48970	0.24650	0.00000	0.00175	0.58714	1.99320	2.58034
44.5	0.07575	0.00000	0.00000	0.00000	0.06954	0.00716	0.01078	0.03106	0.00000	0.04033	1.50360	0.23200	0.00000	0.00150	0.57091	1.97660	2.54751
45.5	0.07500	0.00000	0.00000	0.00000	0.06551	0.00675	0.01015	0.03075	0.00000	0.03799	1.53480	0.21750	0.00000	0.00110	0.55387	1.97640	2.53027
46.5	0.07450	0.00000	0.00000	0.00000	0.06175	0.00636	0.00957	0.03055	0.00000	0.03582	1.59410	0.20300	0.00000	0.00080	0.53887	2.00490	2.54377
47.5	0.07400	0.00000	0.00000	0.00000	0.05810	0.00598	0.00901	0.03034	0.00000	0.03370	1.66260	0.18850	0.00000	0.00040	0.52423	2.04200	2.56623
48.5	0.07350	0.00000	0.00000	0.00000	0.05452	0.00562	0.00845	0.03014	0.00000	0.03162	1.71480	0.17400	0.00000	0.00020	0.50982	2.06400	2.57382
49.5	0.07300	0.00000	0.00000	0.00000	0.05150	0.00530	0.00798	0.02993	0.00000	0.02987	1.75530	0.15950	0.00000	0.00010	0.49733	2.07490	2.57223
50.5	0.07250	0.00000	0.00000	0.00000	0.04915	0.00506	0.00762	0.02973	0.00000	0.02850	1.76420	0.14500	0.00000	0.00005	0.48712	2.05450	2.54162
51.5	0.07200	0.00000	0.00000	0.00000	0.04702	0.00484	0.00729	0.02952	0.00000	0.02727	1.77310	0.13050	0.00000	0.00002	0.47766	2.03422	2.51188
52.5	0.07150	0.00000	0.00000	0.00000	0.04499	0.00463	0.00697	0.02932	0.00000	0.02610	1.79760	0.11600	0.00000	0.00000	0.46856	2.02960	2.49816
53.5	0.07100	0.00000	0.00000	0.00000	0.04308	0.00444	0.00668	0.02911	0.00000	0.02499	1.83170	0.10150	0.00000	0.00000	0.45985	2.03470	2.49455
54.5	0.07050	0.00000	0.00000	0.00000	0.04134	0.00426	0.00641	0.02891	0.00000	0.02398	1.86870	0.08700	0.00000	0.00000	0.45172	2.04270	2.49442
55.5	0.07000	0.00000	0.00000	0.00000	0.03986	0.00411	0.00641	0.02870	0.00000	0.02312	1.88130	0.07250	0.00000	0.00000	0.44540	2.02630	2.47170

Table A3-4: Southern midlatitude VMR profiles of fluorine-containing species, CF_y, F_y and F_{TOT} in ppbv. Trailing zeros are not necessarily significant.

z/km	CF_4	CFC11	CFC12	CFC113	HCFC22	HCFC142b	HFC134a	mPFC	mCFC	mHCFC	HF	COF_2	COClF	SF_6	CF_y	F_y	F_{TOT}
10.5	0.06661	0.23217	0.49821	0.06208	0.16167	0.01007	0.03315	0.02731	0.13950	0.09377	0.05637	0.00000	0.00000	0.00524	2.41793	0.08781	2.50574
11.5	0.06661	0.22992	0.49469	0.06135	0.16397	0.01188	0.03194	0.02731	0.13851	0.09510	0.05251	0.00000	0.00350	0.00530	2.41021	0.08779	2.49800
12.5	0.06661	0.22389	0.48497	0.06100	0.16459	0.01321	0.03068	0.02731	0.13579	0.09546	0.06826	0.01875	0.00720	0.00525	2.38016	0.14443	2.52459
13.5	0.06661	0.21465	0.47185	0.05898	0.16342	0.01385	0.02928	0.02731	0.13212	0.09478	0.10079	0.02801	0.01100	0.00516	2.32763	0.19877	2.52639
14.5	0.06661	0.20556	0.46051	0.05328	0.16159	0.01499	0.02955	0.02731	0.12894	0.09372	0.13801	0.03775	0.01450	0.00513	2.27422	0.25881	2.53303
15.5	0.06661	0.19531	0.45390	0.04441	0.16226	0.01441	0.02942	0.02731	0.12709	0.09411	0.18118	0.04709	0.01830	0.00511	2.22233	0.32431	2.54664
16.5	0.06661	0.17917	0.43520	0.03787	0.16342	0.01380	0.02521	0.02731	0.12186	0.09478	0.23525	0.05909	0.02230	0.00501	2.12889	0.40581	2.53469
17.5	0.06661	0.15541	0.40891	0.04048	0.15751	0.01319	0.02441	0.02731	0.11449	0.09136	0.29962	0.07620	0.02600	0.00488	2.03334	0.50729	2.54063
18.5	0.06661	0.12768	0.38042	0.03766	0.15122	0.01350	0.02344	0.02731	0.10652	0.08771	0.37345	0.09618	0.02950	0.00478	1.91268	0.62397	2.53666
19.5	0.06661	0.09947	0.35236	0.03488	0.14862	0.01531	0.02304	0.02731	0.09866	0.08620	0.45743	0.11748	0.03350	0.00472	1.80747	0.75421	2.56168
20.5	0.06661	0.07416	0.32434	0.03211	0.14767	0.01521	0.02289	0.02731	0.09082	0.08565	0.54229	0.13987	0.03700	0.00470	1.70672	0.88722	2.59394
21.5	0.06863	0.05105	0.29444	0.02915	0.14239	0.01467	0.02207	0.02814	0.08244	0.08259	0.62297	0.16289	0.03920	0.00460	1.59748	1.01554	2.61302
22.5	0.06937	0.03920	0.26126	0.02586	0.14160	0.01458	0.02195	0.02844	0.07315	0.08213	0.70238	0.18593	0.04000	0.00450	1.50067	1.14124	2.64191
23.5	0.06942	0.02734	0.22595	0.02237	0.13834	0.01425	0.02144	0.02846	0.06327	0.08024	0.77509	0.20906	0.03920	0.00440	1.38694	1.25884	2.64578
24.5	0.06940	0.01809	0.19220	0.01903	0.13297	0.01370	0.02061	0.02845	0.05382	0.07712	0.84095	0.22835	0.03700	0.00431	1.27235	1.36050	2.63285
25.5	0.06957	0.01005	0.16291	0.01613	0.12697	0.01308	0.01968	0.02852	0.04561	0.07364	0.90278	0.24117	0.03350	0.00420	1.16916	1.44383	2.61299
26.5	0.07021	0.00659	0.13652	0.01352	0.12215	0.01258	0.01893	0.02879	0.03823	0.07085	0.97348	0.25221	0.02950	0.00413	1.08407	1.53218	2.61625
27.5	0.07105	0.00377	0.11091	0.01098	0.11752	0.01210	0.01822	0.02913	0.03105	0.06816	1.04350	0.25922	0.02500	0.00407	1.00320	1.61137	2.61457
28.5	0.07178	0.00193	0.09000	0.00891	0.11109	0.01144	0.01722	0.02943	0.02520	0.06443	1.10810	0.26248	0.02000	0.00395	0.92877	1.67676	2.60552
29.5	0.07213	0.00060	0.07700	0.00762	0.10273	0.01058	0.01592	0.02957	0.02156	0.05958	1.15930	0.26114	0.01400	0.00381	0.86699	1.71842	2.58540
30.5	0.07216	0.00025	0.06500	0.00644	0.09436	0.00972	0.01463	0.02958	0.01820	0.05473	1.19770	0.25318	0.00700	0.00368	0.80736	1.73315	2.54051
31.5	0.07204	0.00010	0.05600	0.00554	0.08642	0.00890	0.01339	0.02954	0.01568	0.05012	1.22750	0.24498	0.00000	0.00355	0.75646	1.73876	2.49522
32.5	0.07205	0.00004	0.04700	0.00465	0.07944	0.00818	0.01231	0.02954	0.01316	0.04608	1.26050	0.23584	0.00000	0.00340	0.70949	1.75258	2.46207
33.5	0.07209	0.00002	0.03800	0.00376	0.07394	0.00762	0.01146	0.02956	0.01064	0.04289	1.30630	0.22770	0.00000	0.00327	0.66773	1.78132	2.44905
34.5	0.07227	0.00002	0.03000	0.00297	0.06954	0.00716	0.01078	0.02963	0.00840	0.04033	1.34440	0.21967	0.00000	0.00312	0.63287	1.80246	2.43533
35.5	0.07254	0.00000	0.02200	0.00218	0.06551	0.00675	0.01015	0.02974	0.00616	0.03799	1.38250	0.21207	0.00000	0.00295	0.59972	1.82434	2.42406
36.5	0.07290	0.00000	0.01600	0.00158	0.06175	0.00636	0.00957	0.02989	0.00448	0.03582	1.42780	0.20680	0.00000	0.00275	0.57305	1.85790	2.43095
37.5	0.07351	0.00000	0.01200	0.00119	0.05810	0.00598	0.00901	0.03014	0.00336	0.03370	1.47630	0.20265	0.00000	0.00250	0.55298	1.89660	2.44958
38.5	0.07420	0.00000	0.00800	0.00079	0.05452	0.00562	0.00845	0.03042	0.00224	0.03162	1.52360	0.19240	0.00000	0.00225	0.53352	1.92190	2.45542
39.5	0.07470	0.00000	0.00600	0.00059	0.05150	0.00530	0.00798	0.03063	0.00168	0.02987	1.56200	0.18860	0.00000	0.00200	0.52029	1.95120	2.47149
40.5	0.07511	0.00000	0.00500	0.00050	0.04915	0.00506	0.00762	0.03079	0.00140	0.02850	1.60400	0.17400	0.00000	0.00175	0.51150	1.96250	2.47400
41.5	0.07528	0.00000	0.00400	0.00040	0.04702	0.00484	0.00729	0.03086	0.00112	0.02727	1.64200	0.16530	0.00000	0.00150	0.50243	1.98160	2.48403
42.5	0.07528	0.00000	0.00300	0.00030	0.04499	0.00463	0.00697	0.03086	0.00084	0.02610	1.67490	0.15660	0.00000	0.00110	0.49294	1.99470	2.48764
43.5	0.07502	0.00000	0.00200	0.00020	0.04308	0.00444	0.00668	0.03076	0.00056	0.02499	1.71690	0.14790	0.00000	0.00080	0.48274	2.01750	2.50024
44.5	0.07479	0.00000	0.00100	0.00010	0.04134	0.00426	0.00641	0.03066	0.00028	0.02398	1.75490	0.13920	0.00000	0.00040	0.47319	2.03570	2.50889
45.5	0.07500	0.00000	0.00000	0.00000	0.03986	0.00411	0.00618	0.03075	0.00000	0.02312	1.77980	0.13050	0.00000	0.00020	0.46653	2.04200	2.50853
46.5	0.07450	0.00000	0.00000	0.00000	0.03856	0.00397	0.00598	0.03055	0.00000	0.02236	1.80940	0.12180	0.00000	0.00010	0.45987	2.05360	2.51347
47.5	0.07400	0.00000	0.00000	0.00000	0.03729	0.00384	0.00578	0.03034	0.00000	0.02163	1.84730	0.11310	0.00000	0.00005	0.45335	2.07380	2.52715
48.5	0.07350	0.00000	0.00000	0.00000	0.03607	0.00371	0.00559	0.03014	0.00000	0.02092	1.86900	0.10440	0.00000	0.00002	0.44697	2.07792	2.52489
49.5	0.07300	0.00000	0.00000	0.00000	0.03488	0.00359	0.00541	0.02993	0.00000	0.02023	1.89720	0.09570	0.00000	0.00000	0.44075	2.08860	2.52935
50.5	0.07250	0.00000	0.00000	0.00000	0.03376	0.00348	0.00523	0.02973	0.00000	0.01958	1.91760	0.08700	0.00000	0.00000	0.43472	2.09160	2.52632
51.5	0.07200	0.00000	0.00000	0.00000	0.03275	0.00337	0.00508	0.02952	0.00000	0.01899	1.93620	0.07830	0.00000	0.00000	0.42905	2.09280	2.52185
52.5	0.07150	0.00000	0.00000	0.00000	0.03181	0.00328	0.00493	0.02932	0.00000	0.01845	1.95180	0.06960	0.00000	0.00000	0.42367	2.09100	2.51467
53.5	0.07100	0.00000	0.00000	0.00000	0.03090	0.00318	0.00479	0.02911	0.00000	0.01792	1.95920	0.06090	0.00000	0.00000	0.41837	2.08100	2.49937
54.5	0.07050	0.00000	0.00000	0.00000	0.03002	0.00309	0.00465	0.02891	0.00000	0.01741	1.96780	0.05220	0.00000	0.00000	0.41316	2.07220	2.48536
55.5	0.07000	0.00000	0.00000	0.00000	0.02914	0.00300	0.00465	0.02870	0.00000	0.01690	1.96400	0.04350	0.00000	0.00000	0.40851	2.05100	2.45951

Table A3-5: Southern high latitude VMR profiles of fluorine-containing species, CF_y, F_y and F_{TOT} in ppbv. Trailing zeros are not necessarily significant.

z/km	CF_4	CFC11	CFC12	CFC113	HCFC22	HCFC142b	HFC134a	mPFC	mCFC	mHCFC	HF	COF_2	COClF	SF_6	CF_y	F_y	F_{TOT}
10.5	0.07036	0.22851	0.48653	0.06459	0.15813	0.01530	0.03291	0.02885	0.13623	0.09172	0.06414	0.00000	0.00000	0.00509	2.41206	0.09466	2.50672
11.5	0.07036	0.21657	0.46535	0.06359	0.16015	0.01703	0.02912	0.02885	0.13030	0.09289	0.08889	0.00000	0.00250	0.00505	2.34235	0.12167	2.46402
12.5	0.07036	0.19661	0.43767	0.06230	0.15352	0.01585	0.02694	0.02885	0.12255	0.08904	0.15931	0.04803	0.00500	0.00494	2.22722	0.29002	2.51724
13.5	0.07036	0.16772	0.40095	0.05724	0.15107	0.01430	0.02322	0.02885	0.11227	0.08762	0.22632	0.07430	0.00750	0.00485	2.07513	0.41154	2.48667
14.5	0.07036	0.13108	0.35936	0.05190	0.13623	0.01459	0.02026	0.02885	0.10062	0.07901	0.39059	0.10257	0.01000	0.00472	1.87807	0.63404	2.51211
15.5	0.07036	0.09478	0.31737	0.03946	0.12925	0.01271	0.02060	0.02885	0.08886	0.07497	0.53805	0.13415	0.01250	0.00457	1.68831	0.84627	2.53459
16.5	0.07036	0.06362	0.26951	0.03262	0.11928	0.01238	0.01871	0.02885	0.07546	0.06918	0.67879	0.16408	0.01500	0.00446	1.49356	1.04871	2.54226
17.5	0.07036	0.03822	0.22331	0.02211	0.11901	0.01233	0.01845	0.02885	0.06253	0.06903	0.80546	0.19264	0.01750	0.00439	1.32946	1.23457	2.56403
18.5	0.07036	0.02247	0.18440	0.01826	0.11733	0.01263	0.01819	0.02885	0.05163	0.06805	0.93230	0.21227	0.01920	0.00436	1.20866	1.40222	2.61088
19.5	0.07036	0.00637	0.15134	0.01498	0.11257	0.01159	0.01745	0.02885	0.04238	0.06529	1.07530	0.22175	0.02000	0.00442	1.09006	1.56529	2.65536
20.5	0.07036	0.00000	0.12301	0.01218	0.10856	0.01118	0.01683	0.02885	0.03444	0.06296	1.19640	0.21959	0.01920	0.00440	0.99703	1.68118	2.67821
21.5	0.06955	0.00000	0.09674	0.00958	0.09701	0.00999	0.01504	0.02851	0.02709	0.05627	1.29680	0.20651	0.01750	0.00428	0.88643	1.75301	2.63943
22.5	0.06888	0.00000	0.07506	0.00743	0.08181	0.00843	0.01268	0.02824	0.02102	0.04745	1.40340	0.19096	0.01500	0.00410	0.77584	1.82494	2.60078
23.5	0.06877	0.00000	0.05720	0.00566	0.07029	0.00749	0.01127	0.02819	0.01602	0.04077	1.48610	0.17592	0.01250	0.00394	0.69207	1.87408	2.56615
24.5	0.06916	0.00000	0.04084	0.00404	0.06888	0.00709	0.01068	0.02836	0.01143	0.03995	1.55340	0.16145	0.01000	0.00376	0.64485	1.90886	2.55371
25.5	0.06984	0.00000	0.02465	0.00244	0.06551	0.00675	0.01015	0.02864	0.00690	0.03799	1.62320	0.14610	0.00750	0.00356	0.59464	1.94427	2.53891
26.5	0.07067	0.00000	0.01386	0.00137	0.06175	0.00636	0.00957	0.02897	0.00388	0.03582	1.69030	0.13127	0.00500	0.00332	0.55768	1.97779	2.53547
27.5	0.07161	0.00000	0.00894	0.00089	0.05810	0.00598	0.00901	0.02936	0.00250	0.03370	1.74110	0.11824	0.00250	0.00310	0.53672	1.99869	2.53541
28.5	0.07225	0.00000	0.00715	0.00071	0.05452	0.00562	0.00845	0.02962	0.00200	0.03162	1.76730	0.10698	0.00000	0.00295	0.52274	1.99896	2.52170
29.5	0.07255	0.00000	0.00537	0.00053	0.05150	0.00530	0.00798	0.02975	0.00150	0.02987	1.77480	0.09612	0.00000	0.00275	0.50920	1.98354	2.49273
30.5	0.07260	0.00000	0.00380	0.00038	0.04915	0.00506	0.00762	0.02977	0.00106	0.02850	1.76510	0.08812	0.00000	0.00250	0.49735	1.95634	2.45369
31.5	0.07256	0.00000	0.00246	0.00024	0.04702	0.00484	0.00729	0.02975	0.00069	0.02727	1.74950	0.08500	0.00000	0.00225	0.48647	1.93299	2.41947
32.5	0.07279	0.00000	0.00111	0.00011	0.04499	0.00463	0.00697	0.02984	0.00031	0.02610	1.73810	0.08829	0.00000	0.00200	0.47711	1.92668	2.40379
33.5	0.07333	0.00000	0.00070	0.00007	0.04308	0.00444	0.00668	0.03007	0.00020	0.02499	1.74100	0.09370	0.00000	0.00175	0.47196	1.93890	2.41086
34.5	0.07389	0.00000	0.00070	0.00007	0.04134	0.00426	0.00641	0.03029	0.00020	0.02398	1.75620	0.10092	0.00000	0.00150	0.46848	1.96704	2.43552
35.5	0.07437	0.00000	0.00040	0.00004	0.03986	0.00411	0.00618	0.03049	0.00011	0.02312	1.77360	0.10987	0.00000	0.00110	0.46479	1.99994	2.46473
36.5	0.07484	0.00000	0.00040	0.00004	0.03856	0.00397	0.00598	0.03068	0.00011	0.02236	1.79100	0.11460	0.00000	0.00080	0.46240	2.02500	2.48740
37.5	0.07543	0.00000	0.00025	0.00002	0.03729	0.00384	0.00578	0.03093	0.00007	0.02163	1.80080	0.11441	0.00000	0.00040	0.46029	2.03202	2.49231
38.5	0.07590	0.00000	0.00025	0.00002	0.03607	0.00371	0.00559	0.03112	0.00007	0.02092	1.81270	0.10586	0.00000	0.00020	0.45819	2.02562	2.48381
39.5	0.07625	0.00000	0.00015	0.00001	0.03488	0.00359	0.00541	0.03126	0.00004	0.02023	1.82040	0.10302	0.00000	0.00010	0.45545	2.02704	2.48249
40.5	0.07659	0.00000	0.00015	0.00001	0.03376	0.00348	0.00523	0.03140	0.00004	0.01958	1.83470	0.09800	0.00000	0.00005	0.45315	2.03100	2.48415
41.5	0.07651	0.00000	0.00009	0.00001	0.03275	0.00337	0.00508	0.03137	0.00003	0.01899	1.83570	0.09310	0.00000	0.00002	0.44916	2.02202	2.47118
42.5	0.07638	0.00000	0.00009	0.00001	0.03181	0.00328	0.00493	0.03132	0.00003	0.01845	1.83940	0.08820	0.00000	0.00000	0.44544	2.01580	2.46124
43.5	0.07627	0.00000	0.00006	0.00001	0.03090	0.00318	0.00479	0.03127	0.00002	0.01792	1.84410	0.08330	0.00000	0.00000	0.44174	2.01070	2.45244
44.5	0.07598	0.00000	0.00006	0.00001	0.03002	0.00309	0.00465	0.03115	0.00002	0.01741	1.85070	0.07840	0.00000	0.00000	0.43749	2.00750	2.44499
45.5	0.07500	0.00000	0.00004	0.00000	0.02914	0.00300	0.00452	0.03075	0.00001	0.01690	1.86310	0.07350	0.00000	0.00000	0.43011	2.01010	2.44021
46.5	0.07450	0.00000	0.00004	0.00000	0.02838	0.00292	0.00440	0.03055	0.00001	0.01646	1.87920	0.06860	0.00000	0.00000	0.42532	2.01640	2.44172
47.5	0.07400	0.00000	0.00002	0.00000	0.02801	0.00288	0.00434	0.03034	0.00001	0.01625	1.89600	0.06370	0.00000	0.00000	0.42180	2.02340	2.44520
48.5	0.07350	0.00000	0.00002	0.00000	0.02789	0.00287	0.00432	0.03014	0.00001	0.01618	1.91750	0.05880	0.00000	0.00000	0.41920	2.03510	2.45430
49.5	0.07300	0.00000	0.00002	0.00000	0.02777	0.00286	0.00430	0.02993	0.00000	0.01611	1.93230	0.05390	0.00000	0.00000	0.41657	2.04010	2.45667
50.5	0.07250	0.00000	0.00002	0.00000	0.02765	0.00285	0.00429	0.02973	0.00000	0.01604	1.93760	0.04900	0.00000	0.00000	0.41395	2.03560	2.44955
51.5	0.07200	0.00000	0.00001	0.00000	0.02753	0.00284	0.00427	0.02952	0.00000	0.01597	1.93780	0.04410	0.00000	0.00000	0.41132	2.02600	2.43732
52.5	0.07150	0.00000	0.00001	0.00000	0.02740	0.00282	0.00425	0.02932	0.00000	0.01589	1.93530	0.03920	0.00000	0.00000	0.40866	2.01370	2.42236
53.5	0.07100	0.00000	0.00001	0.00000	0.02724	0.00281	0.00422	0.02911	0.00000	0.01580	1.93190	0.03430	0.00000	0.00000	0.40592	2.00050	2.40642
54.5	0.07050	0.00000	0.00001	0.00000	0.02709	0.00279	0.00420	0.02891	0.00000	0.01571	1.93500	0.02940	0.00000	0.00000	0.40318	1.99380	2.39698
55.5	0.07000	0.00000	0.00001	0.00000	0.02692	0.00277	0.00420	0.02870	0.00000	0.01562	1.93750	0.02450	0.00000	0.00000	0.40052	1.98650	2.38702